Rational Design, Synthesis and Degradation of Acidic pH-Responsive Block Copolymer Nanoassemblies for Controlled Drug Delivery

Brandon Andrade-Gagnon

A Thesis
In the Department
Of

Chemistry and Biochemistry

Presented in Partial Fulfillment of the Requirements

For the Degree of

Doctor of Philosophy (Chemistry) at Concordia University

Montreal, Quebec, Canada

August 2025

© Brandon Andrade-Gagnon, 2025

CONCORDIA UNIVERSITY SCHOOL OF GRADUATE STUDIES

This is to certify that the thesis prepared Brandon Andrade-Gagnon By: Rational Design, Synthesis and Degradation of Acidic pH-Responsive Block Entitled: Copolymer Nanoassemblies for Controlled Drug Delivery and submitted in partial fulfillment of the requirements for the degree of: Doctor of Philosophy (Chemistry) complies with the regulations of the University and meets the accepted standards with respect to originality and quality. Signed by the final examining committee: Chair Dr. Rafik Naccache **External Examiner** Dr. Xiaosong Wang External to Program Dr. Nhat Truong Nguyen Thesis Supervisor Dr. Jung Kwon Oh Examiner Dr. Louis Cuccia Examiner Dr. Xianming Zhang Approved by Dr. Louis Cuccia, Graduate Program Director 8/25/2025 Dr. Pascale Sicotte, Dean Faculty of Arts and Science

Abstract

Rational Design, Synthesis and Degradation of Acidic pH-Responsive Block Copolymer Nanoassemblies for Controlled Drug Delivery

Brandon Andrade-Gagnon, Ph.D.

Concordia University, 2025

Acidic pH-responsive degradable block copolymer-based nanoassemblies that degrade through the cleavage of acid-labile linkages have gained significant attention due to their biological relevance, particularly in tumor tissues, having acidic environments (pH 4.2-6.9) due to irregular vasculatures of endothelial cells. Although they hold great potential for achieving controlled and enhanced drug release, developing a systematic understanding of the structural factors that influence their pH sensitivity remains a challenge—especially in designing effective acid-degradable, shell-sheddable nanoassemblies. This is particular for acetals and ketals, where their acid-catalyzed hydrolysis could be adjusted with the substituents attached to oxygen atoms as well as central carbon atom in acetal/ketal moieties. The relationship between the location of cleavable linkages and the drug release performance of polymeric micelles is critical in modulating their therapeutic behavior. This not only improves the biodistribution of anticancer drugs but also ensures minimal dosage, enhancing drug efficacy while reducing undesired cytotoxicity to normal tissues.

My PhD research aims at designing and synthesizing single location and dual location acid-degradable block copolymers and their nanoassemblies for controlled drug delivery. My first project (Chapter 3) evaluates single location strategy on acid-degradable shell-sheddable nanoassemblies, where the acid-labile linkage for the block junction was examined by the hydrolysis behaviour at different pH levels relevant to biological environments. The suitable candidate demonstrated that under acidic conditions, the nanoassemblies tend to form large aggregates as a result loosening the core structures, causing destabilization. My second project (Chapter 4) expands my scope of single location strategy to focus on dual location acid-responsive degradation strategy. The dual location nanoassemblies were extensively examined by assessing by the encapsulation of an anticancer drug (Curcumin) and evaluating the controlled drug release, as well as *in vitro* (cell) studies. My third project (Chapter 5) investigates the relationship of sensitivity to acid and stability to radical polymerizations for acetals and ketals.

Overall, my PhD thesis work provides important design principles for the synthesis of well-defined acid-degradable amphiphilic block copolymers (ABPs) with respect to acid-catalyzed hydrolysis rate and stability of acid-labile acetal/ketal, thus eventually, release rate of encapsulated drug molecules from their nanoassemblies in acidic environment.

Acknowledgments

First and foremost, I would like to express my sincere gratitude to my supervisor Dr. Jung Kwon (John) Oh, for giving me the opportunity to work in his research group as well as for his encouragement and patience during my PhD program. I would like to take this time to thank him for his guidance, great support, kind advice, constructive suggestions, and for giving me the freedom to work on my ideas. I would also like to thank my committee members in the Department of Chemistry and Biochemistry at Concordia University, Dr. Louis Cuccia and Dr. Xianming Zhang, for their valuable questions and suggestions in the annual committee meetings. I would like to thank Dr. Nhat Truong Nguyen in the Department of Chemical Materials and Engineering at Concordia (arm-length examiner) and Dr. Xiaosong Wang in the Department of Chemistry at the University of Waterloo (external examiner) for taking their time to read and evaluate my PhD thesis.

Throughout the four years of PhD, I have been fortunate to work multiple internships, with amazing mentors and colleagues. I would like to thank all the current members in Oh research group and my friends in Chemistry Department. I would like to specifically extend my gratitude to Sofia Nieves Casillas-Popova for her help and extensive knowledge on the biological evaluation of various nanoparticles.

I am also grateful to the technical staff who keep our facilities running: Dr. Constantin Yannopoulos at Concordia NMR facility, Dr. Chris Law at Centre for Microscopy and Cellular Imaging (CMCI), and Dr. David Liu in FEMR at McGill University.

I thank Concordia University, Natural Sciences and Engineering Research Council of Canada (NSERC) Discovery, and NSERC CREATE: Polymer Nanoparticles for Drug Delivery (PoND) for funding this research.

Last, but certainly not least, I would like to give a special thanks to my mom for her unlimited encouragement, love, and support during my studies! If not for her, I would not have reached my full potential! This thesis is a representation of all her hard work paying off!

Contribution to Authors

This thesis is an original work by Brandon Andrade-Gagnon under the supervision of Dr. Jung Kwon (John) Oh. The chapters 2, 3, and 5 are reproduced in part or in whole, with permission from the publishers, from the original articles. Brandon Andrade-Gagnon has conducted experimental design, data collection and analysis, and manuscript preparation and revision for all the chapters. The detailed contributions for each chapter are as follows:

Chapter 2: Recent Advances in Synthesis and Shell-Sheddable Disassembly of Acid/Glutathione-Degradable Block Copolymer Nanoassemblies for Drug Delivery

The entire chapter 2 has been published as: Andrade-Gagnon, B & Oh, J. K. *Polym. Chem.*, **2024**,15, 3709-3735.

Contributions: The work was written by Brandon Andrade-Gagnon and edited by Dr. John Oh.

Chapter 3: Design, Synthesis, and Acid-Responsive Disassembly of Shell-Sheddable Block Copolymer Labeled with Benzaldehyde Acetal Junction

The entire chapter 3 has been published as: Andrade-Gagnon, B., Casillas-Popova, S. N., Jazani, A. M., & Oh, J. K. *Macromol. Rapid Commun.*, **2024**, *45*, 2400097.

Contributions: Arman Moini Jazani conducted the synthesis of benzaldehyde hydroxyethyl acetal. Sofia Nieves Casillas-Popova conducted cytotoxicity with HeLa cells for empty micelles.

Chapter 4: Synthesis and Acidic pH-Responsive Disassembly of Dual Shell-Sheddable/Core-Degradable Block Copolymer Nanoassemblies

Contributions: The work was written by Brandon Andrade-Gagnon and edited by Dr. John Oh.

vi

Chapter 5: Stability of Acetals/Ketals under Controlled Radical and Ring Opening Polymerization

The entire chapter 5 has been submitted and accepted into Macromolecular Rapid Communications journal.

Contributions: Sofia Nieves Casillas-Popova conducted ring opening polymerization of lactide with both benzyl acetal and cyclohexyl ketal diol initiators and data analysis.

Table of Contents

List of Figures	xi
List of Tables.	xiv
List of Abbreviations	xv
Chapter 1 : Introduction	1
1.1 Drug Delivery Systems Towards Cancer Treatment	1
1.2 Polymeric Nanocarriers as Potential Drug Delivery Systems	1
1.3 Stimuli-Responsive Degradation Platforms in Drug Delivery Systems	3
1.4 Synthesis of SRD-based ABPs	4
1.5 Objectives and Significance of my PhD Research	5
Chapter 2: Recent Advances in Synthesis and Shell-Sheddable Disassembly of Acid/Glutathi Degradable Block Copolymer Nanoassemblies for Drug Delivery	8
2.2 Single-Location Shell-Sheddable Block Copolymers	9
2.2.1 General Synthetic Approaches	9
2.2.2 Acid-Degradable Systems	11
2.2.2.1 Ketals, Acetals, and Ortho-esters	12
2.2.2.2 Imines and Hydrazones	20
2.2.2.3 Dialkylmaleamidic Amides	23
2.3 Dual-Location Shell-Sheddable/Core-Degradable Block Copolymers	26
2.3.1 General Synthetic Approaches	26
2.3.2 Dual Location Single Acid/GSH Stimulus-Degradable Systems	27
2.3.3 Dual Location Dual Acid/GSH Stimuli-Degradable Systems	31
2.4 Biological Evaluation	34
2.5 Summary and Outlooks	38
Chapter 3 : Design, Synthesis, and Acid-Responsive Disassembly of Shell-Sheddable Block Labeled with Benzaldehyde Acetal Junction	40
3.2 Experimental	42
3.2.1 Instrumentation.	42
3.2.2 Materials	42
3.2.3 Synthesis of Acetal/Ketal-Labeled Diol Precursors	43
3.2.4 Studies of Acid-Catalyzed Hydrolysis of Acetal/Ketal-Labeled Diol Precursors	44
3.2.5 Synthesis of PEG-BzAc-Br ATRP Macroinitiator.	45

3.2.6 ATRP to Synthesize PEG-BzAc-PBM Block Copolymer	45
3.2.7 Determination of Critical Micelle Concentration using a NR probe	46
3.2.8 Aqueous Micellization by Dialysis.	46
3.2.9 Cell Viability	46
3.2.10 Acidic pH-Responsvie Degradation and Disassembly.	47
3.3 Results and Discussion	47
3.3.1 Synthesis of Acid-labile Diol Precursors	47
3.3.2 Studies of Acid-Catalyzed Hydrolysis Kinetics of Acid-labile Diol Precursors	49
3.3.3 Synthesis of PEG-based BzAc-Bearing ATRP Macroinitiator	52
3.3.4 Synthesis of Acid-Degradable BzAc-Labeled Shell-Sheddable ABP	53
3.3.5 Acid-Responsive Degradation of PEG-BzAc-PBM.	55
3.3.6 Aqueous Micellization and Cytotoxicity.	56
3.3.7 Acid-Responsive Disassembly.	58
3.4 Conclusion	59
Chapter 4 : Synthesis and Acidic pH-Responsive Disassembly of Dual Shell-Sheddabl	
Block Copolymer Nanoassemblies	
4.1 Introduction	
4.2 Experimental	
4.2.1 Instrumentation.	
4.2.2 Materials	
4.2.3 ATRP to Synthesize PEG-BzAc-PCIMA ABPs	
4.2.4 Post-Polymerization Modification to Synthesize DLAD ABPs	
4.2.5 Acidic pH-Responsive Degradation Studies.	
4.2.6 Determination of Critical Micelle Concentration using a NR probe	
4.2.7 Aqueous Micellization by Solvent Evaporation Method	
4.2.8 Acidic pH-Responsive Disassembly of DLAD-based Nanoassemblies	
4.2.9 Encapsulation of Cur.	
4.2.10 Acidic pH-Responsvie Release of Cur.	
4.3 Results and Discussion	67
4.3.1 Synthesis of Well-Defined DLAD ABPs.	67
4.3.2 Synthesis of PEG-BzAc-PCIMA BCP	67
4.3.3 Post-Polymerization Modification to Synthesize DLAD ABPs	69
4.3.4 Studies of Acid-Responsive Degradation of DLAD and Precursors	70
4.3.5 Aqueous Micellization and pH-Responsive Disassembly.	73

4.3.6 Loading and pH-Responsive Release of Cur.	75
4.4 Conclusion	77
Chapter 5 : Stability of Acetals/Ketals under Controlled Radical and Ring Opening Polymo	erization
	79
5.1 Introduction	79
5.2 Experimental	81
5.2.1 Instrumentation.	81
5.2.2 Materials	81
5.2.3 Synthesis of Acid-Labile Dibromides	81
5.2.4 Model Studies on Stability of Acetals and Ketals under ATRP Conditions	82
5.2.5 General Procedure for ATRP of Methacrylates	82
5.2.6 General Procedure for ROP of LA	83
5.2.7 Studies of Acid-Catalyzed Degradation.	84
5.3 Results and Discussion	84
5.3.1 Synthesis of Acid-labile Dibromide ATRP Initiators	84
5.3.2 Model Studies on Stability of Acid-Labile Linkages under ATRP Conditions	85
5.3.3 Studies on Stability of Acid-Labile Linkages during ATRP	86
5.3.4 Studies on Stability of Acid-Labile Linkages during ROP	90
5.4 Conclusion	92
Chapter 6 : Conclusion and Future Perspectives	94
6.1 Conclusion	94
6.2 Futures Perspectives	95
6.2.1 Alternative Dual Location Acid-Degradable ABPs	96
6.2.2 Multi-Location SRD-based Nanoassemblies	96
6.2.3 Photo-Induced CRP Methods	98
References	99
Appendix A	119
Appendix B	135
Appendix C	144
Publications	
Oral and Poster Presentations	155

List of Figures

Figure 1.1. Mechanistic approach for formation of micelles by spontaneous emulsification method2
Figure 1.2. Physical, chemical and biochemical SRD material
Figure 1.3. General mechanism for ARGET ATRP polymerization
Figure 2.1. Schematic illustration for two main approaches exploring I) direct polymerization and II) conjugation to synthesize well-defined ShS ABPs with labile linkages
Figure 2.4. Synthesis of acid-cleavable three-armed star block copolymer (PEG-AcA-PCL-AcA-) ₃ via a combination of ROP and CuAAC "Click" reaction
Figure 2.6. Synthesis of BzAc-DOH precursor, PEG-BzAc-Br macroinitiator, and PEG-BzAc-PBM ShS ABP
Figure 2.8. Synthesis of PEG-BzI-PHEI
Figure 2.9. Synthetic approach for the <i>Dlinkm</i> bridged PEG- <i>Dlinkm</i> -R9-PCL25
Figure 2.10. Schematic illustration for four types of DL nanoassemblies exhibiting acid/GSH responses both at core/corona interfaces and in cores, self-assembled from DL single acid-responsive ABP (a), DL single GSH-responsive ABP (b), DL dual GSH (interface)/acid (core)-responsive ABP (c), and DL dual acid (interface)/GSH (core)-responsive ABP (d)
Figure 2.12. Schematic illustration to synthesize PEG-SS-PHMssEt diblock copolymer (a), PLA-SS-PHMssEt-b-POEOMA triblock copolymer (b), and PEG-SS-PLA-SS-PEG triblock copolymer
(c)
Figure 2.14. Cellular uptake for PEG-BzI-PUSS nanoassemblies by CLSM (a), and flow cytometry analysis (b). Samples were incubated at pH = 6.5 and 7.4 for 4 hrs and 24 hrs
HDOH with BzA, CyP, and CyH in the presence of TSA in anhydrous THF at room temperature47

Figure 3.2. ¹ H NMR spectra of BzAc-DOH (a), CyPK-DOH (b), and CyHK-DOH (c) in CDCl ₃ , where
only characteristic peaks are assigned
Figure 3.3. Overlaid ¹ H NMR spectra at pD = 5.0 (a,b,c), schematic illustration of acid-catalyzed
hydrolysis (d,e,f), and evolution of %hydrolysis at pD = 5.0 , 6.8 , and 7.4 (g,h,i) for BzAc-DOH (a,d,g),
CyPK-DOH (b,e,h), and CyHK-DOH (c,f,i) dissolved in 3/1 v/v CD ₃ CN/PB-D ₂ O mixtures50
Figure 3.4. Comparison of %hydrolysis of three diols at $pD = 5.0$ (a), and 6.5 (b)51
Figure 3.5. Synthesis of PEG-BzAc-Br ATRP macroinitiator (a), as well as ¹ H NMR spectra of PEG-
BzAc-OH (b), and PEG-BzAc-Br (c) in CDCl ₃ 53
Figure 3.6. Synthesis by ARGET ATRP (a), GPC diagram compared with that of PEG-BzAc-Br
macroinitiator (b), and ¹ H NMR spectrum in CDCl ₃ of well-defined PEG-BzAc-PBM sheddable block
copolymer bearing acid-labile BzAc at the block junction (c)
Figure 3.7. Schematic illustration of acid-responsive degradation (a), GPC diagram before and after
treatment with acid in THF, compared to PEG-BzAc-Br macroinitiator (b), and ¹ H NMR spectrum in
CDCl ₃ of degraded products formed through acid-catalyzed hydrolysis (c) of PEG-BzAc-PBM sheddable
block copolymer after 24 hrs56
Figure 3.8. Schematic illustration of aqueous micellization through self-assembly of PEG-BzAc-PBM (a),
fluorescence intensity at maximum wavelength for aqueous mixtures consisting of NR with various
amounts of PEG-BzAc-PBM to determine CMC (b), DLS by intensity (c) and TEM images with scale bar
= 200 nm (d) of nanoassemblies at 1 mg mL ⁻¹ 57
Figure 3.9. Schematic illustration of acid-responsive disassembly (a), DLS diagrams by volume incubated
at pH = 7.4 (b), 6.5 (c), and 5.0 (d) for 24 hrs, TEM images with scale bar = 200 nm (e), evolution of z-
average diameter over time incubated at pH = 7.4, 6.5, and 5.0 (f) of ShS nanoassemblies59
Figure 4.1. Our approach to synthesize well-defined DLAD (PEG-BzAc-PBzI) ABPs by ATRP of CIMA
in the presence of PEG-BzAc-Br, forming reactive PEG-BzAc-PCIMA ABPs, followed by its post-
polymerization modification with BzI67
Figure 4.2. Overlaid ¹ H NMR spectra in CDCl ₃ of PEG-BzAc-PCIMA, BzI-OH and DLAD (a), and
overlaid GPC diagrams of PEG-BzAc-Br, PEG-BzAc-PCIMA, and DLAD (b)70
Figure 4.3. Acid-responsive degradation upon cleavage of BzAc and BzI groups of DLAD ABP (a), and
its overlaid GPC diagrams before and after treatment with HCl (acid) in DMF, compared with PEG-
BzAc-Br macroinitiator (b)71
Figure 4.4. Schemes for aicd-responsive degradation (a,b), and %degradation at pD = 5.0, 6.5, and 7.4
(c,d) for PEG-BzAc-Br (a,c) and BzI-OH (b,d)72
Figure 4.5. Schematic illustration of aqueous micellization through self-assembly of DLAD (a),
fluorescence intensity at maximum wavelength for aqueous mixtures consisting of NR with various
amounts of DLAD to determine CMC (b), DLS by intensity (c), and TEM images with different
magnification nanoassemblies at 6 mg mL ⁻¹ (scale bar = 50 nm (left) and 100 nm (right)) (d)74
Figure 4.6. Schematic illustration of acid-responsive disassembly (a), overlaid DLS by intensity incubated
at pH = 7.4 , 6.5 , and 5.0 after 72 hrs (b), evolution of z-average diameter over time incubated at pH = 7.4 ,
6.5, and 5.0 (c) and TEM images with scale bar = 50 nm (left) and 100 nm (right) of dual location
nanoassemblies (d)75
Figure 4.7. Cur-loaded micelles measured by DLS by intensity (a), TEM images with scale bar = 50 nm
(left) and 100 nm (right) (b), schematic illustration of acid-responsive disassembly for release of Cur (c)
and %Cur release from Cur-NPs being incubated at pH = 7.4, 6.5, and 5.0 (d)77

Figure 5.1. Chemical structures and acid-catalyzed hydrolysis rate of acetals and ketals of interest in this
work80
Figure 5.2. Synthesis of aicd-labile dibromides. BzAc-DBr (a), and CyHK-DBr (b), by a facile coupling
reaction of BzAc-DOH and CyHK-DOH with Br-iBuBr in the presence of Et ₃ N (a base)84
Figure 5.3. ¹ H NMR spectra of BzAc-DBr (a) and CyHK-DBr (b) in CDCl ₃ 85
Figure 5.4. Degradation to corresponding benzaldehyde and two Br-OH species bearing terminal
hydroxyl groups (a,c), and overlaid ¹ H NMR spectra incubated with HCl (0.24M) in DMSO-d ₆ (b,d) for
BzAc-DBr (a,b) and CyHK-DBr (c,d)86
Figure 5.5. Synthesis by ATRP of BM in the presence of BzAc-DBr and acid-responsive degradation
upon cleavage of BzAc groups of PBM-BzAc-PBM (ATRP-1) (a) and its overlaid GPC diagrams before
and after treatment with HCl (acid) in DMF (b)
Figure 5.6 Synthesis by ATRP of BM in the presence of CyHK-DBr in an attempt to synthesize PBM-
CyHK-PBM and its acid-responsive degradation upon cleavage of CyHK groups (a) and its overlaid GPC
diagrams before and after treatment with HCl (acid) in DMF (b)89
Figure 5.7. ROP of LA initiated with BzAc-DOH (ROP-1) in an attempt to synthesize PLA-BzAc-PLA
and its acid-responsive degradation upon cleavage of BzAc groups (a), ¹ H NMR spectrum in DMSO-d ₆
(b), and overlaid GPC diagrams before and after treatment with HCl (acid) in DMF (c)91
Figure 5.8. ROP of LA initiated with CyHK-DOH (ROP-2) in an attempt to synthesize PLA-CyHK-PLA
and its acid-responsive degradation upon cleavage of CyHK groups (a), and overlaid GPC diagrams
before and after treatment with HCl (acid) in DMF (b)92
Figure 6.1 Proposed synthetic pathway to optimize dual location acid-degradable ABPs using dimethyl
ketal linkages as pendant chains96
Figure 6.2. Proposed synthetic pathway for multi-location ABPs using BzAc and SS linkages at the block
junction, and Azo and ThK linkages as pendant chains97
Figure 6.3. Proposed synthetic pathway for photoRAFT to synthesize a well-defined PEG-BzAc-PBzI-
UV ABP98

List of Tables

Table 3.1. Summary of acid-catalyzed hydrolysis rates as times when a half concentration of	acetal/ketal
linkages is cleaved (t _{1/2}) for acid-labile diol precursors	51
Table 3.2. Characteristics and properties of PEG-BzAc-Br and PEG-BzAc-PBM ABP	55
Table 4.1. Characteristics and properties of PEG-BzAc-PCIMA under different initial mole anisole. ^{a)}	
Table 5.1. Characteristics and properties of polymers prepared by ATRP of BM or OEOMA	initiated with
BzAc-DBr or CyHK-DBr in anisole. ^{a)}	87
Table 5.2. Characteristics and properties of polymers prepared by ROP of LA initiated with	BzAc-DOH
or CyHK-DOH in toluene. ^{a)}	90

LIST OF ABBREVIATIONS

ABP Amphiphilic block copolymer

ARGET Activators regenerated by electron transfer

ATRP Atom transfer radical polymerization

BM Benzyl methacrylate

Br-iBuBr Bromoisobutyryl bromide

BzAc Benzyl acetal

BzI-OH Benzoic imine

CDCl₃ Deuterated chloroform

CDI Carbonyl diimidazole

CHCl₃ Chloroform

CMC Critical micelle concentration

CRP Controlled radical polymerization

Cur Curcumin

DCM Dichloromethane

DDS Drug delivery system

DLS Dynamic light scattering

DMAP 4-(Dimethylamino)pyridine

DMF N,N-dimethyl formamide

DMSO Dimethyl sulfoxide

DMSO-d₆ Deuterated dimethyl sulfoxide

DP Degree of polymerization

EPR Enhanced permeability and retention effect

Et₃N Triethylamine

EtOAc Ethyl acetate

GPC Gel-permeation chromatography

HEMA 2-Hydroxyethyl methacrylate

Hex Hexane

HR-MS High resolution mass spectrometry

M_n Number average molecular weight

M_w Average molecular weight

MWCO Molecular weight cut off

NMR Nuclear magnetic resonance

NR Nile red

OEOMA Oligo (ethylene glycol) monomethyl ether methacrylate

PBS Phosphate buffer solution

PEG Poly(ethylene glycol)

PES Polyethersulfone

PTFE Polytetrafluoroethylene

RAFT Reversible addition fragmentation chain transfer

ROP Ring opening polymerization

SRD Stimuli-responsive degradation

Sn(EH)₂ Tin(II)ethyl hexanoate

TSA P-toluene sulfonic acid monohydrate

TEM Transmission electronic microscopy

THF Tetrahydrofuran

TPMA Tris(2-pyridylmethyl)amine

UV/Vis Ultraviolet/visible

Chapter 1: Introduction

1.1 Drug Delivery Systems Towards Cancer Treatment

Nanomedicine is an important area in nanotechnology, focused on the diagnosis, prevention and treatment of diseases to specific medical intervention at the molecular level. A major goal in nanomedicine is site-specific drug delivery, which aims to achieve selective targeting of cancer cells. This approach involves using carriers that conjugate with or encapsulate drugs to deliver them directly to predetermined or targeted cells in a controlled manner. As a result, therapeutic agents are concentrated at the intended site while minimizing exposure to healthy cells, thereby reducing side effects and enhancing efficacy. 1-4 Conventional therapeutics, particularly those with low molecular weights, tend to distribute indiscriminately throughout the body. They can penetrate various compartments and affect numerous cell types and subcellular structures. This form of indiscriminate distribution leads to not only the occurrence of side effects but also the need for higher doses of drugs to elicit a satisfactory pharmacological response. Overall, conventional therapeutics suffer from major drawbacks, including limited water solubility, low bioavailability, toxicity, and premature degradation. 5-7

To address these challenges, the development of advanced drug delivery systems has become a priority. These systems are designed to improve pharmacological performance, allowing for lower drug doses and reduced side effects.⁶ In this context, research to develop novel drug delivery systems is of interest, as they provide advantages of (i) an increase in the drug's hydrophilicity, (ii) prevention of premature drug degradation, (iii) enhancement in cellular uptake, and (iv) reduction in toxicity. Additionally, many of these systems exploit the enhanced permeability and retention (EPR) effect—where leaky tumor vasculature and inefficient lymphatic drainage allow for greater drug accumulation at tumor sites.^{8, 9}

1.2 Polymeric Nanocarriers as Potential Drug Delivery Systems

Synthetic polymers have played a pivotal role in advancing drug delivery systems for cancer therapy. One of the earliest approaches involved the use of polymeric micelles capable of encapsulating drug molecules, thereby enhancing their solubility and protecting them from enzymatic degradation. Since then, a wide range of polymeric micelles has been developed, with variations in polymer structure and preparation methods tailored to achieve specific properties and controlled release profiles for optimized delivery. These micelles are typically

formed via the self-assembly of amphiphilic block copolymers (ABPs) in aqueous solutions. ^{13, 14} ABPs, composed of covalently—and more recently, non-covalently—linked macromolecular segments, serve as a key platform for constructing soft-matter-based core—shell nanoparticles with valuable properties and functionalities. In aqueous environments, ABPs spontaneously self-assemble to reduce energetically unfavorable interactions between hydrophobic segments and water (Figure 1.1). The packing behavior of these ABPs, and the resulting nanostructure morphology, is primarily governed by their amphiphilic shape. This shape is determined by the relative size of the hydrophilic and hydrophobic blocks under equilibrium self-assembly conditions, which dictates the curvature at the hydrophilic—hydrophobic interface. Additional factors such as polymer concentration, solvent composition, and temperature also significantly influence the final morphology. ^{15, 16}

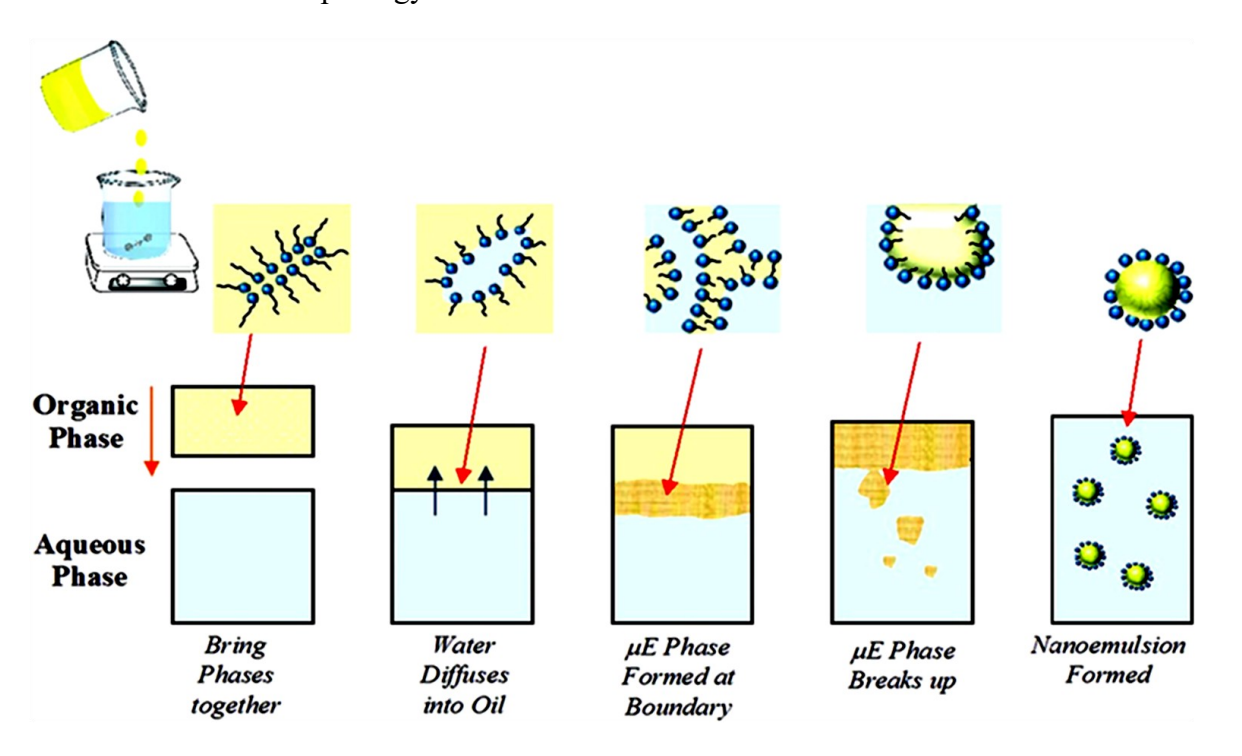


Figure 1.1. Mechanistic approach for formation of micelles by spontaneous emulsification method. When the organic phase and aqueous phase (water) are brought into contact, a bicontinuous microemulsion (μE) is formed at the boundary, which breaks up and forms tiny oil droplets. ¹⁷ Copyright 2016 Wiley.

1.3 Stimuli-Responsive Degradation (SRD) Platforms in Drug Delivery Systems (DDS):

Conventional ABP-based nanoassemblies, though they provide preferential accumulation in tumors due to passive targeting, they suffer adverse effects as a result of nonspecific biodistribution and uncontrolled drug release. 18, 19 To address these challenges, stimuliresponsive degradation (SRD) polymers have been engineered with built-in, environmentsensitive features. ABPs exhibiting stimuli-responsive degradation (SRD)—through cleavage of labile covalent bonds or molecular conformational changes triggered by endogenous (internal) or exogenous (external) stimuli—have been widely used as building blocks for constructing selfassembled nanoassemblies.²⁰ These systems serve as platforms for drug delivery, offering controlled drug release profiles. ²¹⁻²³ Following endocytosis into cancer cells via the EPR effect, these SRD-enabled nanoassemblies disassemble through various mechanisms, such as shifts in the hydrophilic/hydrophobic balance or degradation of polymer backbones. This disassembly is typically initiated by stimuli like acidic pH, light, and redox conditions, including reductive, oxidative, or enzymatic reactions (Figure 1.2). As a result, encapsulated drugs are selectively released within tumor tissues or cancer cells. Such controlled drug release enhances the biodistribution of anticancer agents, allows for lower dosing, and reduces off-target cytotoxicity commonly associated with small molecule drugs.²⁴⁻³⁰

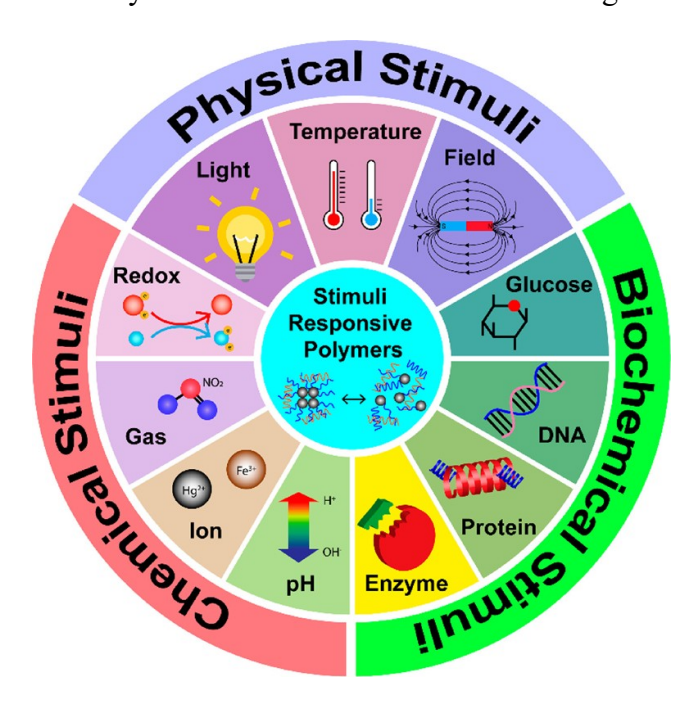


Figure 1.2. Physical, chemical, and biochemical SRD material.³¹ Copyright 2021 American Chemical Society.

Among various stimuli, changes in acidity are particularly noteworthy, as the extracellular environment of tumor tissues is slightly acidic (pH = 6.5–6.9), while endosomes and lysosomes within cells are even more acidic (pH = 4.5–5.5), in contrast to the neutral pH of normal tissues (pH = 7.4).³²⁻³⁹ Among the various acid-labile linkages, acetals and ketals hold significant promise, as their acid-catalyzed hydrolysis rates can be finely tuned by modifying the substituents attached to the oxygen atoms and the central carbon atom within the acetal/ketal structure.⁴⁰ Most of the SRD-based nanoassemblies have been designed with cleavable-labile linkages positioned at the interfaces of hydrophobic cores and hydrophilic coronas. The position of these cleavable linkages plays a critical role in the design and function of nanomaterials, as it directly influences the disassembly mechanism of micelles. While initial efforts focused on incorporating cleavable linkages at a single site, this approach has limitations. More recent studies are exploring dual or multiple linkage sites to better understand how their placement affects drug release profiles and enhances other therapeutic properties of polymeric micelles, such as tumor penetration and cellular uptake.^{29, 41, 42}

1.4 Synthesis of SRD-based ABPs

Over the past 25 years, the development of SRD-based ABPs has made considerable strides, largely driven by advancements in controlled radical polymerization (CRP), also referred to as reversible deactivation radical polymerization (RDRP) by the International Union of Pure and Applied Chemistry (IUPAC). This type of polymerization represents approximately 50% of all polymers formed in the industry. 43 There are three main radical methods that can apply proper control to its polymerization, including nitroxide mediated polymerization (NMP), atom transfer radical polymerization (ATRP) and reversible addition fragmentation chain transfer (RAFT) polymerization. 44-49 In NMP and ATRP, the equilibrium is established by a reversible termination mechanism of the propagating chain, in which the balance strongly favors the dormant species. The RAFT polymerization proceeds through a degenerative chain transfer process, where the reproduced species are balanced with the dormant species. More versatile and simpler approaches involve ATRP and RAFT polymerization. However, ATRP is not commonly approached as it is a radical pseudo-living polymerization, catalyzed by a transition metal, which is also called an activator. The initiation occurs through a transfer of single electrons from the metal to the halogen in the covalent bond, which leads to the homolysis to give the radical, oxidizing the metal complex by a (+1), causing an attachment of the free halide. One particular

type of ATRP commonly used is activators regenerated by electron transfer (ARGET) ATRP, in which minimal concentration of copper species is applied, and the reaction initially has an inactive copper species, as well as a reducing agent to re-activate the copper species for radicals to form (Figure 1.3).^{46, 48, 50}

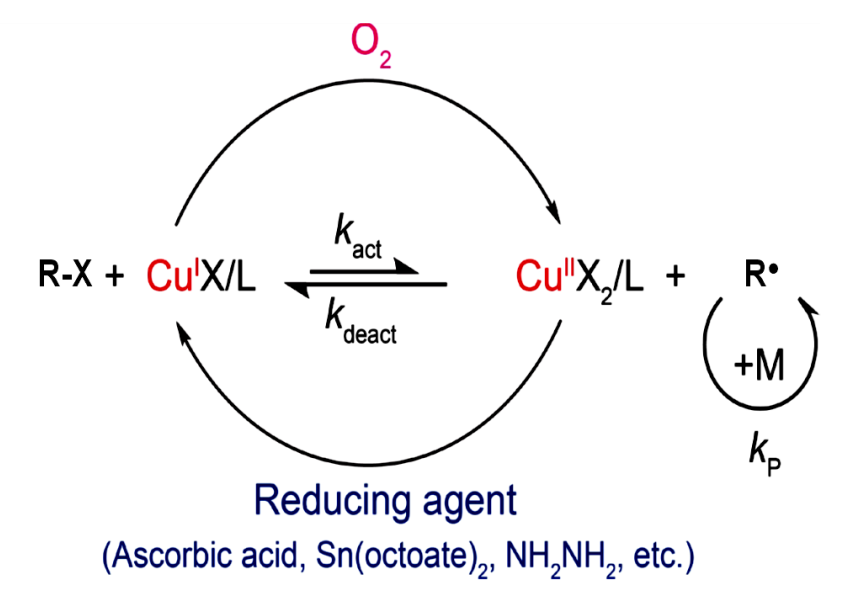


Figure 1.3 General mechanism for ARGET ATRP polymerization. Note: R^* = radical species, X = halogen species, L = ligand, k_{act} = rate constant of activation, k_{deact} = reversible deactivation rate constant, and k_p = propagating chain rate constant. Opening 2023 Wiley.

1.5 Objectives and Significance of my PhD Research:

The overall objective of my PhD thesis is to design and develop robust strategies that allows for the synthesis of acid-degradable block copolymer nanoassemblies, aiming to solve the critical challenges, such as PEG dilemma, controlled drug release, and enhanced drug efficiency for tumor-targeting drug delivery. These copolymers were designed to have acid-labile benzyl acetal (BzAc) groups at the junction of the hydrophilic and hydrophobic blocks, thus at the interfaces of cores and coronas in their nanoassemblies. The synthesized copolymers were characterized for aqueous micellization driven by self-assembly, acidic pH-responsive degradation and disassembly, drug loading and release, as well as biological activities towards cancer cells. Furthermore, we studied the stability of acid-labile linkages under radical polymerization methods to understand the relationship of sensitivity to acid and stability to controlled polymerizations to acid-labile linkages. This could provide important design principles for the

synthesis of well-defined acid-degradable ABPs with respect to acid-catalyzed hydrolysis rates, thus eventually, release rate of encapsulated drug molecules from their nanoassemblies in acidic environment.

This thesis consists of six chapters, namely preface (Chapter 1), review literature encapsulating the recent advances of shell-sheddable acid-degradable ABPs (Chapter 2), three research projects (Chapters 3-5), conclusion and future works (Chapter 6).

Chapter 2 describes the literature overview of SRD-based shell-sheddable (ShS) ABP nanoassemblies for controlled drug delivery. This review highlights the recent advances in synthetic strategies for single-location ShS ABP nanoassemblies and advanced strategies for dual-location ShS/core-degradable ABP nanoassemblies, focusing on their acidic pH and GSH-responsive degradation. Furthermore, the benefits and drawbacks of these nanoassemblies in biological aspects and outlooks for effective tumor targeting drug delivery are also investigated.

Chapter 3 describes the synthesis and acid-responsive degradation through acid-catalyzed hydrolysis of three acetal and ketal diols and identified benzaldehyde acetal (BzAc) to be a suitable candidate for junction acid-labile linkage. The suitable candidacy was used to explore the synthesis and aqueous micellization, utilizing ARGET ATRP to form well-defined PEG-based block copolymer bearing BzAc linkage covalently attached to a polymethacrylate block for the formation of colloidally-stable nanoassemblies with BzAc groups at core/corona interfaces. The acid-catalyzed hydrolysis and disassembly of the formed nanoassemblies confirm that the approach with the choice of BzAc linkage as the block junction is promising in the development of acid-degradable ShS nanoassemblies and further dual-acid/stimulus-degradable nanoassemblies as advanced drug delivery nanocarriers.

Chapter 4 describes the initially adopted synthetic route using an initiator introduced in chapter 3 to utilize AGET ATRP, followed by post-polymerization modification to synthesize a dual location acidic pH degradable block copolymer (PEG-BzAc-PBzI). This block copolymer is labeled with an acid-labile benzyl acetal linkage at the block junction and acid-labile benzoic imine pendant groups in the hydrophobic block. This chapter focuses on the investigation of self-assembly, dual acidic pH, and release of Curcumin from the nanoassemblies. In addition, studies of their anticancer cell activity and cellular internalization are also investigated to emphasize the

synergistic and accelerated release of encapsulated Curcumin, compared to single reduction at the core and acidic pH at the interface.

Chapter 5 investigates the relationship of sensitivity to acid and stability to radical polymerizations for acetals and ketals. The ATRP and ROP polymerization methods are applied to both benzyl acetal and cyclohexyl ketal as the acetal and ketal candidates, respectively. Despite comprehensive studies on their acid-catalyzed hydrolysis rate with substituents attached to oxygen atoms, the stability of the groups under ATRP and tin-catalyzed ROP conditions have been rarely studied. This work could provide important design principles for the synthesis of well-defined acid-degradable ABPs with respect to acid-catalyzed hydrolysis rates, thus eventually, release rate of encapsulated drug molecules from their nanoassemblies in acidic environment.

Chapter 6 describes the summary and conclusion of the research conducted during the program and proposed future works.

Chapter 2: Recent Advances in Synthesis and Shell-Sheddable Disassembly of Acid/Glutathione-Degradable Block Copolymer Nanoassemblies for Drug Delivery

2.1. Introduction

Development of smart nanoassemblies based on amphiphilic block copolymers (ABPs) exhibiting stimuli-responsive degradation (SRD) through chemical transitions has been explored as a promising platform for controlled drug delivery targeting tumors. 52-59 These SRD-exhibiting ABPs have been designed through the incorporation of labile covalent linkages, which can be cleaved in response to stimuli when needed. SRD causes the disintegration or destabilization of nanoassemblies, leading to controlled/enhanced release of encapsulated therapeutics in targeted tissues (e.g. tumor tissues). 60, 61 Endogenous triggers, including acidic pH, GSH, enzymes, and reactive oxygen species, are those found in biological environments of the body, which can attain biodegradation. 62-70 In particular, acidic pH is the most promising as the extracellular compartment of tumor tissues is slightly acidic at pH = 6.5-6.9 and further endosomes and lysosomes in cancer cells are more acidic at pH = 4.5–5.5, compared to normal tissues (pH = 7.4).⁷¹⁻⁷³ GSH is a tripeptide consisting of cysteine reside with a pendant thiol group. GSH exists at a millimolar concentration (0.5-10 mM) in intracellular compartments, while at a micromolar concentration (2-20 µM) in extracellular compartments and plasmas. Moreover, its concentration is known to be 4-5 times greater than that of normal tissues.⁷⁴⁻⁷⁸ Thus, the cellular GSH as a biological reducing agent provides a reducing environment.

Because of these features, the design and synthesis of well-defined ABPs and their nanoassemblies degradable in acidic environments⁷⁹⁻⁸³ and in the presence of GSH⁸⁴⁻⁸⁶ have been extensively investigated. Depending on where the degradation (e.g. response to acidic pH or GSH) occurs, these nanoassemblies could be sorted to be core-degradable and ShS.^{30, 87} Core-degradable nanoassemblies have been mainly fabricated through self-assembly of SRD-ABPs labeled with cleavable linkages on hydrophobic backbones or in pendant chains. These nanoassemblies could be dissociated via the breakdown of main chains upon the cleave of the linkages in the cores. Contrastingly, ShS nanoassemblies have been assembled with SRD-ABPs having cleavable linkages at the junction of hydrophilic and hydrophobic blocks. They could be

disintegrated by shedding hydrophilic coronas from hydrophobic cores upon the cleavage of the linkage at core/corona interfaces. Such detachment of corona, mostly poly(ethylene glycol) (PEG), could achieve enhanced release of encapsulated drugs. PEGylated nanoassemblies have prolonged circulation lifetimes because PEG corona minimizes undesired protein absorption in serum; however, they have limited ability for entry to cells (e.g. endocytosis or cellular uptake) because PEG is neutral and thus less interact with anionic phosphates on cell membranes. This so-called "PEG dilemma" could be overcome by PEG detachment after extravasation to tumor tissues during blood circulation. 88-91 Further to the single location (SL) ShS nanoassemblies where the degradation occurs only at core/corona interface, dual location (DL) nanoassemblies degrade in both interface and core. These DL nanoassemblies have been recently explored to overcome the drawbacks such as undesired large aggregation as well as controlled/enhanced and programed degradation and drug release profile on demands.

This review describes the recent advance in ShS-ABPs and their nanoassemblies with a focus on synthetic strategies for acid- and GSH-responsive degradation. These strategies are summarized by direct polymerization and conjugation approaches for SL ShS ABPs and DL ShS/core-degradable ABPs. In addition, advanced strategies allow for the synthesis of dual acid/GSH-degradable junction ShS ABPs which contain both acid-labile and disulfide linkages at the block junction and thus at core/corona interfaces of nanoassemblies. These strategies could correlate the benefits and drawbacks on the number and location of linkages towards enhanced drug release. This review also discusses biological aspects and outlooks of these ShS ABP-based nanoassemblies for tumor-targeting controlled drug delivery.

2.2. Single-Location Shell-Sheddable Block Copolymers

2.2.1. General Synthetic Approaches

Figure 2.1 shows the schematic illustration of two main approaches to synthesize ShS ABPs bearing labile linkages at the block junctions. Approach I involves direct polymerization mostly exploring ring opening polymerization (ROP)⁹²⁻⁹⁶ or controlled radical polymerization (CRP) techniques, ⁹⁷⁻¹⁰⁰ particularly atom transfer radical polymerization (ATRP)¹⁰¹⁻¹⁰⁴ and reversible addition fragmentation chain transfer (RAFT) polymerization. ¹⁰⁵⁻¹¹⁰ As depicted in Figure 2.1, these direct polymerization techniques require the synthesis of hydrophilic macroinitiators for ROP and ATRP or macro-agents for RAFT polymerization. The synthesized macroinitiators or

macro-agents are used for chain extension with hydrophobic polymer blocks in a living manner, thus yielding well-defined PEG-based ABPs with determined molecular weights and narrow molecular weight distribution. This approach presents relatively easy purification with no need to separate excess homopolymers. Furthermore, this approach allows for the variation of hydrophobic block lengths with the choice of the initial mole ratio of monomer to macroinitiator (or macro-agent). This design principle could be advantageous in that the content of hydrophilic PEG corona in nanoassemblies is optimized, which significantly influences their morphology and colloidal stability in biological environments as well as loading and release kinetics of drug molecules. However, this approach could present the potential instability of labile linkages under polymerization conditions.

Approach II involves the conjugation of hydrophilic and hydrophobic homopolymers bearing reactive functional groups. The reactive precursor polymers are synthesized mostly by ROP or CRP techniques, followed by post-polymerization modification. Thus, this approach examines the combination of ROP or CRP with conjugation reaction. "Click-type" reactions are preferably investigated for high efficiency conjugation reactions of both reactive polymers under mild conditions. As illustrated in Figure 2.1, Method A explores the facile coupling reactions of reactive functional groups through the formation of ester or amide bonds. One of two reactive (co)polymers are required to be labeled with designated labile linkages. Method B involves *in situ* formation of labile linkages at the block junction, typically including acetal/ketal and imine formation as well as thiol-disulfide exchange reaction. While allowing for the synthesis of broad spectra of ShS-ABPs, approach II requires tedious purification steps to remove excess (unreacted) homopolymers, and thus to obtain pure ABPs.

Both approaches allow for the synthesis of a variety of well-defined ShS-ABPs with linear and non-linear (branched) architectures. Linear architectures are mostly studied, mainly because they have less synthetic challenges and facilitate diverse structures and specifically-tailored properties. Non-linear copolymers have been reported to provide enhanced colloidal stability, high drug loading, and performance improvements. 118-122

Approach I) Direct Polymerization ROP or CRP Monomer (X: labile group; : initiating or mediating species) Approach II) Conjugation Method A Coupling Method B In-Situ

Figure 2.1. Schematic illustration for two main approaches exploring I) direct polymerization and II) conjugation to synthesize well-defined ShS-ABPs with labile linkages at the junctions of hydrophilic (typically PEG) and hydrophobic blocks.

(, , , R1, & R2: Reactive groups)

2.2.2. Acid-Degradable Systems

Ketal, acetal, orthoester, imine, hydrazone, and 2,3-dialkylmaleamidic amide are the typical acid-labile linkages that have been studied for the synthesis of acid-degradable ShS-ABPs. As illustrated in Figure 2.2, these linkages can be cleaved to the corresponding degraded products through acid-catalyzed hydrolysis. Such cleavage results in shedding PEG coronas from hydrophobic cores, causing the disintegration of nanoassemblies, leading to the enhanced release of encapsulated drug molecules.

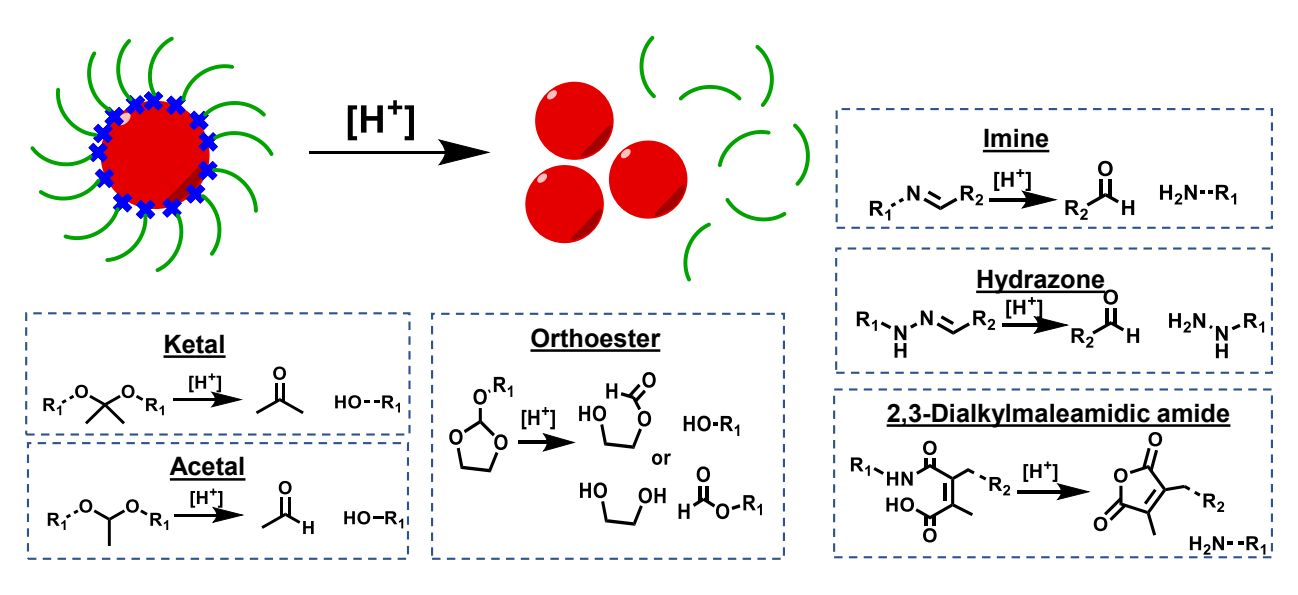


Figure 2.2. Schematic illustration of typical acid-labile linkages including ketal, acetal, orthoester, imine, hydrazone and 2,3-dialkylmaleamidic amide that have been explored for the synthesis of acid-degradable ShS-ABPs.

2.2.2.1 Ketals, Acetals, and Ortho-esters

Ketal groups have been incorporated into the synthesis of acid-degradable ShS-ABPs consisting of hydrophilic PEG and hydrophobic polycaprolactone (PCL) blocks, mainly by direct polymerization through a ROP technique. Stepanek et al. synthesized a PEG bearing acid-labile dimethyl ketal (DMK) linkage (PEG-DMK-OH) by a click-type azido-alkyne reaction of an alkyne-labeled PEG (PEG-alkyne) with a derivative bearing an internal ketal group and a terminal azido group (HO-Et-DMK-N₃) in the presence of a copper (Cu)(I) catalyst. The formed PEG-DMK-OH was utilized as a macro-initiator for the ROP of caprolactone (CL) in the presence of a tin-based catalyst, yielding PEG-DMK-PCL diblock copolymers. 123, 124 Further to linear ABPs, non-linear diblock copolymers bearing a cyclic ketal (CK) linkage at the junction of PEG and PCL blocks were synthesized. Qian at el. reported the synthesis of Y-shaped ABPs consisting of a PEG block and two PCL blocks as hydrophobic arms with CK linkage at the block junction. As illustrated in Figure 2.3, a PEG bearing D-Ketal group (mPEG-Ketal -2OH) was first synthesized with three steps through the conjugation of PEG with α,α '-dichloro-mxylene and subsequently with a cyclic ketal derivative bearing terminal hydroxy and alkene group, followed by the oxidation of the alkene group with OsO₄. The purified mPEG-Ketal-2OH was then used as a macroinitiator for ROP of CL with tin (II) octanoate, a typical catalyst for

ROP of CL, yielding well-defined mPEG-Ketal-(PCL)₂ ABPs with different PCL block lengths. ¹²⁵ The formed linear and Y-shaped ABPs self-assembled to form colloidally-stable nanoassemblies with ketal linkages at the interfaces of PCL cores and PEG corona. In acidic pH = 5.0, PEG corona was shed from PCL cores through acid-catalyzed hydrolysis of acid-labile ketal linkages, which caused the disintegration of the nanoassemblies. Such degradation enabled the enhanced release of encapsulated anticancer drugs such as doxorubicin (Dox) or paclitaxel (PTX). Both drug-loaded nanoassemblies exhibit in vitro cytotoxicity and cellular uptake with a HeLa cell line, as well as showed enhanced blood circulation time and good tumor-targeting efficiency, based on in vivo studies with a mouse model.

Figure 2.3. Synthesis of well-defined Y-shaped PEG-CK-(PCL)₂ ABP. ¹²⁵ Note that "CK" denotes "Ketal" in the Figure and this Figure was redrawn by ourselves for better quality. Copyright 2018 Elsevier.

Acetal groups have been incorporated through both conjugation and direct polymerization approaches to synthesize acid-degradable ShS ABPs with acetaldehyde acetal (AcA) junction linkage. Conjugation approach has been investigated mainly through a click-type coppercatalyzed azide-alkyne (CuAAC) reaction mostly with AcA linkage. Ni et al. reported the synthesis of a linear ABA-type triblock copolymer consisting of a PEG central block and PCL terminal blocks with AcA junction linkage (e.g. PCL-AcA-PEG-AcA-PCL). A PEG-based diazide bearing methyl acetal groups (N₃-AcA-PEG-AcA-N₃) was synthesized by the reaction of HO-PEG-OH with chloroethyl vinyl ether, followed by the azidation of terminal chloro group to the corresponding azido group. The formed diazide precursor was conjugated with PCL

containing propargyl group (propargyl-PCL), synthesized by ROP of CL, yielding PCL-AcA-PEG-AcA-PCL triblock copolymer. ¹²⁶ The formed ABA triblock copolymer formed flower-type nanoassemblies with a loop-shaped PEG corona. In addition to linear architecture, a three-arm star architecture consisting of PEG-AcA-PCL diblock copolymer (e.g. (PEG-AcA-PCL-AcA-)₃) was synthesized by the reaction of triprop-2-ynyl benzene-1,3,5-tricarboxylate (a tri-functional alkyne) with PEG-AcA-PCL-AcA-N₃ (Figure 2.4). The azido precursor was synthesized by the reaction of PEG-AcA-N₃ with propargyl-PCL-AcA-Cl which was initially synthesized by the reaction of propargyl-PCL with chloroethyl vinyl ether. ¹²⁷ A feature of the formed star block copolymer could be the design with AcA linkages located at both the junction of PEG and PCL blocks in the arms and the junction of PCL block and star center. In an acidic environment, the block copolymer allows for detachment of PEG corona as well as degradation of hydrophobic star PCL block to the corresponding PCL and small molecule star species. Such dual location could facilitate the degradation of cores of ShS nanoassemblies, along with the detachment of PEG coronas in tumoral and endo/lysosomal pHs.

The azido-alkyne click reaction with AcA junction linkage has been further examined to synthesize a variety of AcA-labeled ShS ABPs with different architectures. Typical ABPs include polyester grafted with AcA-labeled PEG (e.g. polyester-g-AcA-PEG),¹²⁸ H40 hyperbranched polyester star of PCL-AcA-PEG (e.g. H40-star-PCL-AcA-PEG),¹²⁹ and hydrophilic vinyl copolymers conjugated with AcA-labeled PCL (e.g. vinyl copolymer-AcA-PCL).^{130, 131}

(A) OH + CI
$$\xrightarrow{CI}$$
 \xrightarrow{DMAP} \xrightarrow{O} \xrightarrow{O} \xrightarrow{O} \xrightarrow{O} \xrightarrow{O} \xrightarrow{CI} \xrightarrow{CI} \xrightarrow{O} \xrightarrow{CI} \xrightarrow{O} \xrightarrow{CI} \xrightarrow{O} \xrightarrow

Figure 2.4. Synthesis of acid-cleavable three-armed star-block copolymer (PEG-AcA-PCL-AcA-)₃ via a combination of ROP and CuAAC "Click" reaction. ¹³² Copyright 2015 Royal Society of Chemistry.

Direct polymerization approach has been investigated through ROP technique for propylene oxide¹³³ and D,L-lactide (LA).^{134, 135} This approach is required for the synthesis of an acetal-bearing PEG macroinitiator for ROP. Yang et al. synthesized an AcA-bearing PEG (PEG-AcA-OH) by a facile coupling reaction of PEG-OH with butyl vinyl acetate, followed by the deprotection of acetate group by a base-catalyzed hydrolysis. The formed PEG-AcA-OH initiated ROP of LA, yielding PEG-AcA-PLA.¹³⁴ Oh et al. reported the synthesis of three PEG precursors labelled with benzoic cyclic acetal (BzCA) group (PEG-BzCA-OH) with spacers exhibiting different inductive effects between PEG and BzCA linkage (Figure 2.5a). The order of

increasing acid-catalyzed hydrolysis was found to be ether > ester oxygen > ester carbonyl, which is attributed to the stability of the benzylic carbocation. Particularly, PEG-BzCA-OH with ether space (e.g. PEG-x-1) was synthesized in three steps, as depicted in Figure 2.5b, which includes 1) the mesylation of PEG, 2) the reaction of the formed PEG-Ms with 4-hydroxybenzaldehyde, and 3) the reaction of the formed PEG-et-Bz-CHO with 1,1,1-tris(hydroxymethyl)ethane in the presence of HCl. The synthesized PEG-x-1 was stable under a tin-catalyzed condition for ROP of LA, enabling the synthesis of well-controlled acid-degradable PEG-BzCA-PLA ABP. In acidic pH, the junction BzCA linkage was cleaved, causing the degradation of the copolymer (Figure 2.5c). 136 Recently, Ajiro et al. synthesized a vanillinderived BzCA (VBzCA) bearing PEG (PEG-VBzCA-OH) with multi steps, including a coupling reaction of vanillin with a diol bearing PEG. The phenylic OH group in the PEG-VBzCA-OH successfully initiated the ROP of L-LA and D-LA, yielding PEG-VBzCA-PLLA and PEG-VBzCA-PDLA whose PLA blocks have different stereo orientations. These block copolymers formed supramolecular aggregates through stereo-complexation. Furthermore, they exhibit enhanced aggregation rates in the composites with titanium oxide nanoparticles. 135

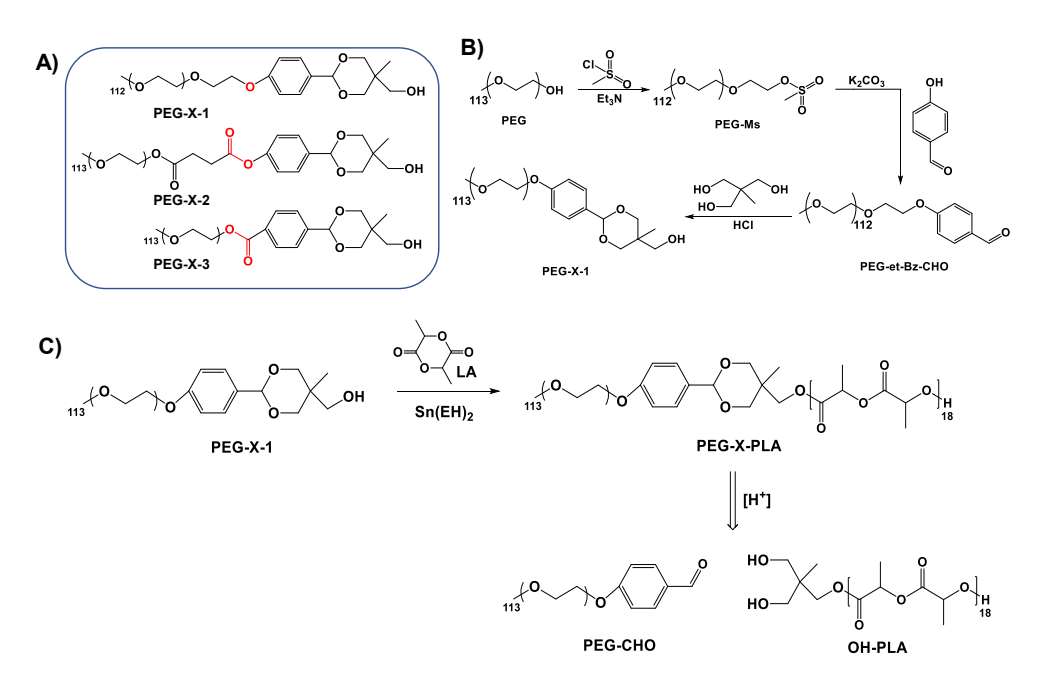


Figure 2.5. Chemical structures of three precursors labeled with different spacers, including ether, ester oxygen, and ester carbonyl, between PEG and BzCA groups (a), synthesis of PEG-X-1 labelled with an ether spacer (b), synthesis by ROP of LA initiated with PEG-X-1 under a tincatalyzed condition and acid-catalyzed degradation of PEG-BzCA-PLA block copolymer (c). Copyright 2023 Wiley.

CRP techniques have also been employed to the synthesis of acid-degradable ShS ABPs with hydrophobic polymethacrylate blocks, thus PEG-based polymethacrylate ABPs. This approach explores a general strategy with the synthesis of new PEG-based precursors bearing an acid-labile linkage as macro-initiators for ATRP or as macro-agents for RAFT polymerization and nitroxide-mediated polymerization (NMP).

An example includes the synthesis of PEG-RAFT macro-agent labeled with an ester carbonyl-based BzCA linkage (PEG-BzCA-RAFT) by a facile carbodiimide coupling reaction of a PEG-BzCA-OH with commercially-available 4-(cyanopentanoic acid)-4-dithiobenzoate. The formed macro-agent was used for RAFT polymerization of a cholesterol-bearing methacrylate (ChMA), thus forming PEG-BzCA-PChMA ABP. Upon further modification with RNA after aminolysis of a terminal phenylthiodithio group, the copolymer was explored for gene delivery exhibiting the enhanced release of therapeutic RNA upon the cleavage of junction BzCA linkages in an endo/lysosomal pH condition. 137 The other example includes the synthesis of an AcA-functionalized PEG-based nitroxide labeled with 2,2,6,6-tetramethylpiperidine-1-oxyl (TEMPO) (PEG-AcA-TEMPO) through three steps. They include i) the reaction of PEG with 2chloroethyl vinyl ether, ii) azidation to PEG-AcA-N₃, and iii) its reaction with TEMPO adducts of an alkyne-bearing styrene. The PEG-AcA-TEMPO was used for NMP of styrene, yielding well-defined PEG-AcA-polystyrene ABP. The formed copolymer was studied for self-assembly and acid-degradation to fabricate nanoporous thin films in solid state. 138 Recent example involves the synthesis of a PEG-based bromine macroinitiator bearing a benzaldehyde acetal (BzAc) group (thus forming PEG-BzAc-Br). As illustrated in Figure 2.6, BzAc-labeled diol (BzAc-DOH) was synthesized by the reaction of benzaldehyde with 1,6-hexanediol under acidic condition. The synthesized BzAc-DOH reacted with a carbonylimidazole-activated PEG (PEG-CI), yielding PEG-BzAc-CI, followed by esterification. As a proof-of-concept, the PEG-BzAc-Br initiated ATRP of benzyl methacrylate (BM) to synthesize well-defined PEG-BzAc-PBM ShS-ABP. BzAc linkages have slow acid-catalyzed hydrolysis rate at tumoral pH = 6.5, while rapid hydrolysis at endo/lysosomal pH = 5.0. The copolymer self-assembled to form welldefined nanoassemblies with BzAc linkages at core/corona interfaces and disassembled in acidic condition.¹³⁹

Figure 2.6. Synthesis of BzAc-DOH precursor, PEG-BzAc-Br macroinitiator, and PEG-BzAc-PBM ShS.¹³⁹ Copyright 2024 Wiley.

An interesting strategy includes the synthesis of PCL-based polymethacrylate ABPs with sheddable PEG pendants. This strategy centers on the synthesis of an acid-labile methacrylate bearing AcA group conjugated with PEG, thus MA-AcA-PEG. A double-head initiator bearing both hydroxyl and bromo terminal groups initiated the ROP of CL, yielding hydrophobic PCL block, and the ATRP of MA-AcA-PEG, yielding hydrophilic P(MA-AcA-PEG) block, thus forming well-defined PCL-b-P(MA-AcA-PEG) block copolymer. Different from conventional ShS ABPs having acid-labile AcA linkages at the junction of hydrophilic and hydrophobic blocks, the formed PCL-b-P(MA-AcA-PEG) ABPs were designed with AcA linkages in pendant chains of hydrophilic blocks. When being self-assembled in water, the block copolymer formed nanoassemblies with AcA linkages in hydrophilic coronas. In an acidic pH, the block copolymer degraded to the corresponding PEG and PCL-b-poly(2-hydroxyethyl methacrylate) block copolymer upon the cleavage of AcA linkages, which causes the detachment of PEG from coronas.¹⁴⁰

Furthermore, a BzCA-bearing multifunctional molecule labeled with both RAFT species (as RAFT agent) and bromide (as ATRP initiator) (RAFT-BzCA-Br) was synthesized by the condensation of 2-bromoisobutyrate group derived benzaldehyde with glycerol, followed by a carbodiimide coupling reaction with a carboxylated RAFT agent. The formed dual-head RAFT-BzCA-Br initiator/agent enabled the synthesis of a well-defined block copolymer with BzCA

junction under both ATRP and RAFT polymerization conditions. Although the feasibility was demonstrated with common vinyl monomers including t-butyl acrylate and styrene, the strategy is anticipated to the synthesis of ShS ABPs with both hydrophilic and hydrophobic polymethacrylate blocks.¹⁴¹

Orthoester (ORT) groups contain an extra alcoholic unit compared to acetals and ketals. As illustrated in Figure 2.2, their acid-catalyzed hydrolysis differs into two separate approaches to create the corresponding alcohols and formates or esters depending on hydrophobic substituents on orthoester (ORT) bonds. Li et al. synthesized a well-defined PEG-based ShS linear ABP consisting of cationic poly(dimethyl aminoethyl methacrylate) (PDMAEMA) block with ORT linkage at block junction, thus forming PEG-ORT-PDMAEMA. As illustrated in Figure 2.7, PEG-based bromide bearing ORT group (PEG-ORT-Br, P5) was synthesized and used as an acid-labile macroinitiator for ATRP of DMAEMA in the presence of Cu(I)Br and tris(2-aminoethyl)amine. The formed copolymer enabled to form micelleplexes with genes and exhibit enhanced release of genes upon the cleavage of ORT linkages in endosomal acidic pH = 5.0, suggesting the potential for controlled/enhanced gene delivery. 142 Recently, Tang et al. reported the synthesis of an ORT-labeled ShS graft copolymer with PEG side chains. The copolymer was synthesized through a carbodiimidazole-mediated coupling reaction of ORTbearing PEG with polyurethane backbones. The release of encapsulated Dox was investigated. The results demonstrate the enhanced release of Dox at pH = 6.5, compared to pH = 7.4, confirming the disintegration of the nanoassemblies at extracellular pH of tumor tissues. 90, 143

$$H_2N \longrightarrow OH$$
 $F_3C \longrightarrow N \longrightarrow OH$
 $F_3C \longrightarrow N$

Figure 2.7. Synthesis of acid-degradable PEG-ORT-PDMAEMA ABPs. ¹⁴² Copyright 2008 American Chemical Society.

2.2.2.2. Imines and Hydrazone

Imine (C=N) bonds, also known as Schiff base, is generally formed through reactions between an aldehyde group (-CHO) and a primary amine group (-NH₂). Typically, benzoic imine (BzI) groups have been incorporated into the block junction of ShS ABPs, through conjugation or direct polymerization method, as conventional imines are known to be less stable under physiological conditions.¹⁴⁴

To explore conjugation method, both *in-situ* and facile coupling approaches were investigated. In regard to *in-situ* imine formation approach, Tian et al. designed a triblock copolymer for the encapsulation and enhanced drug release of PTX and curcumin. Initially, a PEG bearing benzaldehyde (PEG-CHO) was synthesized through the esterification of PEG with p-formylbenzoic acid. Separately, the hydrophobic poly(γ-benzyl-L-aspartate)-*b*-poly(1-vinylimidazole) (PBLA-b-PVIm) was synthesized by ROP of γ-benzyl-L-aspartate in the presence of PVIm as a macroinitiator. PVIm was synthesized by free radical polymerization of VIm with an azo-type radical initiator and 2-aminoethanethiol as a chain transfer agent. Lastly, the reaction of PEG-CHO and PBLA-b-PVIm bearing a terminal amine group through *in-situ* formation of BzI bond by Schiff base reaction yielded a well-defined PEG-BzI-PBLA-b-PVIm triblock copolymer.¹⁴⁵ In other reports, PEG-CHO was used for *in-situ* BzI formation with 1-

octadecylamine (C18) through Schiff base reaction to synthesize PEG-BzI-C18 for the encapsulation and enhanced release of zoledronic acid for osteoporosis and cancer bone metastasis. ¹⁴⁶ Further, PEG-CHO was conjugated with an oxime-labeled PLA labeled with terminal hydroxylamine group (called oxime-tethered PCL, OPCL) to synthesize PEG-oxime-PCL-oxime-PEG ABA-type triblock copolymer. ¹⁴⁷

More complex polymeric nanocarriers were developed by Dimitrov et al., where a well-defined lactobionic acid (LBA)-PEG-BzI-PLA-b-PDMAEMA-triphenylphosphonium triblock copolymer was synthesized and investigated with curcumin, exhibiting enhanced release at pH = 7.0 under physiological conditions, making it inefficient for tumor-targeting. ¹⁴⁸ In addition to linear ABPs, bottlebrush ABPs provided *in situ* imine formation at the block junction with hydrophobic pendants chains of polypeptides, ¹⁴⁹ polyesters, ¹⁵⁰ and polymethacrylates. ¹⁵¹ For facile coupling approach, Lui et al. synthesized a PEG amine bearing BzI linkage (PEG-BzI-NH₂) by reaction of PEG-CHO with diaminopropane. A hydrophobic polymer, poly(amino ester) (PAE), was synthesized by a Michael-type step-growth polymerization of hexane-1,6-dioldiacrylate and 3-aminopropanol. Two reactive polymers were subjected to Michael-addition reaction, followed by the conjugation with cholesterol (Chol) to synthesize PEG-BzI-PAE-g-Chol triblock copolymer, where acid-labile BzI is located at the hydrophilic/hydrophobic block junction. ¹⁵²

For direct polymerization method, Wei et al. studied the enzyme-mediated ROP of CL in the presence of lipase Novozyme-435, initiated with PEG-BzI-NH₂ as the macroinitiator, yielding a well-defined PEG-BzI-PCL ShS ABP. ¹⁵³ In addition, Huang et al. studied RAFT polymerization to synthesize a PEG-based ShS ABP bearing BzI at the block junction. As shown in Figure 2.8, 2-([2-4-(2-methylpropil)phenyl]propionyl]oxy) ethyl methacrylate (HEI) was synthesized through the esterification of ibuoprofen with 2-hydroxyethyl methacrylate (HEMA). A PEG bromide bearing a BzI (labeled as PEG-CBA-Br) was synthesized by the reaction of PEG-BzI-OH (labeled PEG-CBA-OH) with 2-bromoisobutyryl bromide and then used for ATRP of HEI, yielding PEG-BzI-PHEI ABP. ¹⁵⁴

Figure 2.8. Synthesis of PEG-BzI-PHEI ABP.¹⁵⁴ Copyright 2017 Royal Society of Chemistry. (Note: PEG-BzI-OH for PEG-CBA-OH and PEG-BzI-PHEI for MPEG-PHEI are labeled in the text).

Hydrazones (HYD) can substantially improve the resistance to hydrolysis because of their decreased electrophilicity by mesomeric effect. ¹⁵⁵⁻¹⁵⁹ Both direct polymerization and conjugation methods have been explored. For the direct polymerization method, ROP technique has been typically investigated to incorporate HYD linkages into the design of acid-degradable ShS ABPs. Kurcok et al. reported the synthesis of well-defined ABPs, where initially, a PEG-levulinic acid (LEV) conjugate bearing HYD linkage (thus, PEG-HYD-LEV) was first synthesized by the carbamate formation of PEG-OH with a phenyl chloroformate, followed by the formation of

hydrazone group. The synthesized PEG-HYD-LEV was used as a macroinitiator for anionic ROP of 3-hydroxybutyrate (HB), yielding PEG-HYD-PHB ABP. The copolymer was examined for the encapsulation of Dox and enhanced release of encapsulated Dox at pH= $5.0.^{160}$ Song et al., on the other hand, reported on the ROP of LA using a PEG-HYD-phenol macroinitiator in the presence of tin (II) 2-ethylhexanoate (Sn(Oct)₂) catalyst, yielding well-defined PEG-HYD-PLA. The formed copolymer exhibits enhanced release of both Dox and PTX at pH = 4.0 and moderate release at pH = $5.0.^{161}$ Aside from direct ROP methods, the conjugation method was studied for PEG-HYD derivatives with PCL for cartilage repair treatments 162 and poly(lactic- 163 glycolic acid) (PLGA) for oral insulin delivery. 163

2.2.2.3. Dialkylmaleamidic Amides

Dimethylmaleamidic acid (DMMA) group is sensitive to tumoral pH at 6.5-6.9 and undergoes acid-controlled transition through the cleavage of amide bond to the corresponding amine group, followed by the protonation to be converted to the corresponding cationic ammonium salt. Such charge reversal has been conducted to overcome PEG dilemma. However, due to the lack of additional functionality, DMMA group has been mainly used to modify the side groups of acid-degradable copolymers. ¹⁶⁴⁻¹⁶⁷

Replacing the conventional methyl group of DMMA with higher functional groups, ^{168, 169} Wang and coworkers have explored the strategies that allow for the synthesis of acid-degradable ShS ABPs labeled with methylpropylmaleamidic acid group (*Dlinkm*) at the block junction through both conjugation and direct ROP approaches for acid-responsive enhanced drug and gene delivery. ^{170, 171} The strategies center on the modification of PEG with 2-propionic-3-methylmaleic anhydride (CDM) to synthesize PEG-CDM. To investigate direct ROP approach, PEG-CDM reacted with 6-amino-1-hexanol to yield an acid-degradable PEG-*Dlinkm*-OH, which was used as a macroinitiator for ROP of LA to synthesize PEG-*Dlinkm*-PLA. In tumoral pH, the *Dlinkm* linkage was cleaved to generate PEG and PLA degraded products, which was confirmed with the change in chemical structures by ¹H-NMR analysis and average size and size distributions of nanoassemblies by DLS analysis. ¹⁷² Further studies demonstrate that PEG-*Dlinkm*-PLA is capable of meeting the requirements of several stages for gene delivery, including prolonged blood circulation, enhanced accumulation and penetration in the tumor, facilitated

cellular internalization through detachment of PEG shells and rapid release of the active drug in the tumor cells.¹⁷³

In another strategy exploring the conjugation approach, as illustrated in Figure 2.9, the PEG-CDM precursor reacted with a PCL-based poly(alginate) (PCL-R9) through amidation, to yield PEG-Dlink_m-R9-PCL. PCL-R9 was synthesized by multiple steps including 1) ROP of CL to synthesize Boc-protected PCL, 2) deprotection of Boc group to amino-terminated PCL, 3) *N*-hydroxysuccinimide (NHS)-mediated conjugation with Fmoc-R9-NHS, and deprotection of Fmoc group. The copolymer formed micelleplex delivery system with siRNA, which features i) PEG corona, which is stable in the circulatory system and protects nanovectors from reticuloendothelial system clearance; ii) a tumoral pH-responsive linkage breakage, which induces PEG detachment at tumor sites and thereby facilitates cell targeting; and iii) a cell-penetration peptide, which is exposed upon the removal of PEG and further enhances cellular uptake.¹⁷⁴

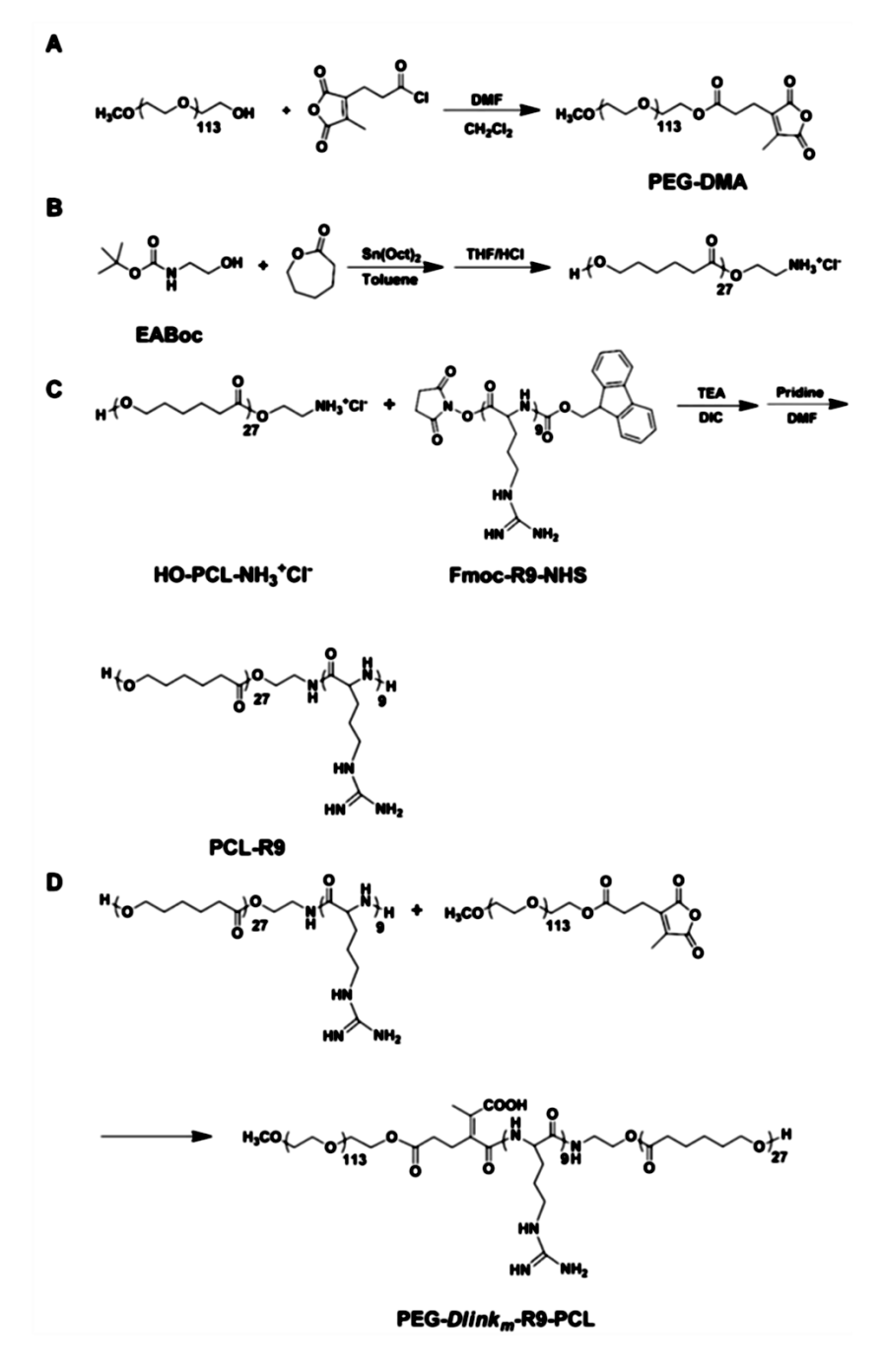


Figure 2.9. Synthetic approach for the *Dlink_m* bridged PEG-*Dlink_m*-R9-PCL.¹⁷⁵ Copyright 2016 American Chemical Society.

2.3. Dual-Location Shell-Sheddable/Core-Degradable Block Copolymers

2.3.1. General Synthetic Approaches

While single location ShS-ABPs are designed with either acid-labile or SS/SeSe linkage at the block junction, dual location ShS/core-degradable ABPs (DL-ABPs) have been synthesized with either acid-labile or SS linkage at the block junction and in the hydrophobic block.

Nanoassemblies fabricated from DL-ABPs are featured with cleavable linkages at both cores and core/corona interfaces, thus attaining DL ShS/core-degradable nanoassemblies. These DL-ABP nanoassemblies could circumvent the challenge for single location ShS ABP nanoassemblies that involves their tendency to form aggregates upon the detachment of coronas upon the cleavage of the labile linkages at the interfaces. This section focuses on acid- and GSH-responsive degradable DL-ABPs and their nanoassemblies.

As illustrated in Figure 2.10, four different designs are discussed, including i) acid response both at interface and in core (called DL acid-responsive ABP), ii) GSH response both at interface and in core (DL GSH-responsive ABP), iii) GSH response at interface/acid response in core (DL dual GSH (interface)/acid (core)-responsive ABP), and iv) acid response at interface/GSH response in core (DL dual acid (interface)/GSH (core)-responsive ABP).

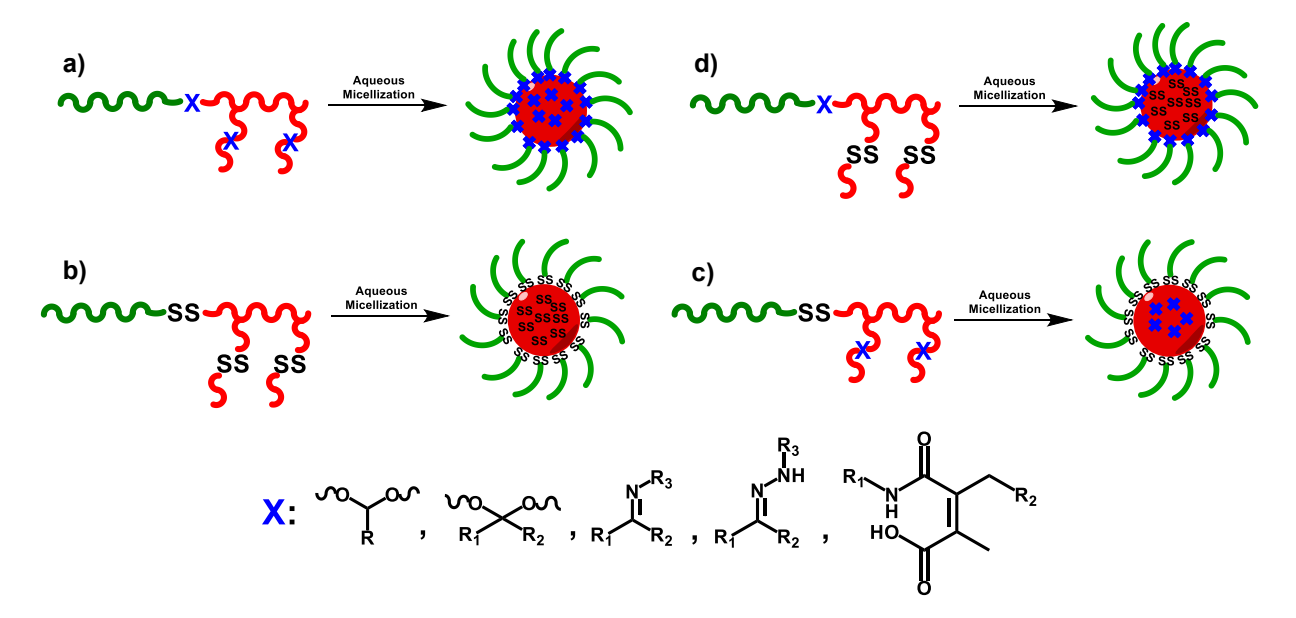


Figure 2.10. Schematic illustration of four types of DL nanoassemblies exhibiting acid/GSH responses both at core/corona interfaces and in cores, self-assembled from DL single acid-responsive ABP (a), DL single GSH-responsive ABP (b), DL dual GSH (interface)/acid (core)-responsive ABP (c), and DL dual acid (interface)/GSH (core)-responsive ABP (d).

2.3.2. Dual Location Single Acid/GSH Stimulus-Degradable Systems

For the development of dual location acid-responsive ABPs, a novel strategy was explored to synthesize dual location single acid-degradable nanoassemblies labeled with AcA groups both at core/corona interfaces and in hydrophobic cores. As illustrated in Figure 2.11a, the strategy investigated the direct polymerization through ATRP of a methacrylate bearing a pendant AcA group (called ACMA) in the presence of an AcA-bearing PEG-based Br (PEG-AcA-Br) as an acid-labile macroinitiator. PEG-AcA-Br was synthesized by the reaction of ethylene glycol vinyl ether with 2-bromoisobuytryl bromide under basic condition, followed by direct acetalization with PEG in the presence of pyridinium p-toluenesulfonate as an acid catalyst. The synthesized block copolymer, PEG-AcA-PACMA bearing AcA group both at the block junction and in the hydrophobic block (P1) self-assembled to form colloidally-stable nanoassemblies having AcA groups in dual locations as at core/corona interfaces and in hydrophobic cores. Further, a methacrylate bearing pendant imidazole group (called CIMA) was introduced to the hydrophobic block, thus forming a hydrophobic random copolymer block of ACMA and CIMA, thus forming PEG-AcA-P(ACMA-co-CIMA) ABP (P2). Interestingly, P2 improved the encapsulation of Dox through π - π interaction and enhanced the acid-catalyzed hydrolysis of acetal linkages. In addition, the presence of the imidazole pendants induced the occurrence of core-crosslinking that compensates the kinetics of acetal hydrolysis and drug release.³³

Another strategy allows for the synthesis of a PEG-based DL acid-responsive ABP that bears AcA group at the block junction and pendant boronate ester bonds in hydrophobic block (Figure 2.11b). Bortezomib (BTZ), an anticancer drug containing a phenylboronic acid group, was conjugated to the hydrophobic block through the formation of boronate ester linkage between boronic acid and catechol groups. In acidic pH, PEG coronas were detached upon the cleavage of junction AcA groups and BTZ drugs were released upon the cleavage of boronate ester bonds.¹⁷⁶

Figure 2.11. Schematic illustration of PEG-AcA-PACMA (noted as P1) and PEG-AcA-P(ACMA-co-CIMA (noted as P2) by direct polymerization through ATRP in the presence of PEG-AcA-Br macroinitiator (a).³³ Copyright 2021 Wiley; and a PEG-based DL acid-responsive ABP bearing AcA at the block junction and pendant boronate bonds in hydrophobic block (b).¹⁷⁶ Copyright 2018 American Chemical Society.

For the synthesis of DL-GSH-responsive ABPs, Oh and his team reported three strategies exploring direct polymerization through ROP and ATRP techniques.⁸⁷ Strategy I enabled the synthesis of a well-defined PEG-based ABP composed of PEG conjugated through SS with a polymethacrylate block bearing pendant SS groups (PHMssEt), thus forming PEG-SS-PHMssEt

diblock copolymer (Figure 2.12a). ATRP was examined for HMssEt in the presence of PEG-SS-Br macroinitiator. The block copolymer was designed as a proof-of-concept to provide accelerated release of encapsulated drugs upon GSH-responsive degradation through the cleavage of SS linkages at dual locations.⁴²

Strategy II explores the synthesis of a PLA-based ABC-type triblock copolymer consisting of PHMssEt middle block and POEOMA block, thus PLA-SS-PHMssEt-b-POEOMA (Figure 2.12b). The strategy includes the ROP of LA in the presence of HO-SS-Br dual-head initiator to synthesize PLA-SS-OH as the first step, the ATRP of HMssEt to synthesize PLA-SS-PHMssEt-Br as the second step, and the ATRP of OEOMA to synthesize the triblock copolymer. Its nanoassemblies consists of multiple pendant SS linkages in a hydrophobic interlayer as well as single disulfides at interfaces of the interlayer and PLA cores, which exhibit enhanced colloidal stability as well as rapid GSH-responsive destabilization.¹⁷⁷

Strategy III allows for the synthesis of an ABA-type triblock copolymer composed of hydrophobic PLA middle block and hydrophilic PEG terminal blocks. A SS linkage is labeled both in the center of PLA middle block and at the junction of PLA and PEG block, thus forming PEG-SS-PLA-SS-PEG triblock copolymer (Figure 2.12c). The strategy explores a combination of ROP, facile coupling reactions, and ATRP. The reductive response to GSH as a cellular trigger resulted in the cleavage of the SS linkages at the interface shedding hydrophilic coronas as well as the disulfides in the PLA core causing disintegration of PLA cores. Such dual disulfide degradation process led to a synergistically enhanced release of encapsulated anticancer drugs in cellular environments. ¹⁷⁸

Figure 2.12. Schematic illustration to synthesize PEG-SS-PHMssEt diblock copolymer (a); PLA-SS-PHMssEt-b-POEOMA triblock copolymer (b).⁴² Copyright 2013 Royal Society of Chemistry; and PEG-SS-PLA-SS-PLA-SS-PEG (c) triblock copolymer.¹⁷⁸ Copyright 2015 American Chemical Society.

2.3.3. Dual Location Dual Acid/GSH Stimuli-Degradable Systems

For DL dual GSH (interface)/acid (core)-responsive ABPs, a few strategies have been reported. One strategy investigates the combination of ROP of LA, ATRP of OEOMA, and their coupling reaction to synthesize an ABA-type triblock copolymer composed of PLA and PEG. The block copolymer is labeled with DMK linkage in the middle of PLA block and SS linkage at the junction of PLA and PEG blocks, thus PEG-SS-PLA-DMK-PLA-SS-PEG.¹⁷⁹ Another strategy includes the synthesis of a PEG-based diblock copolymer with a polycarbonate block having pendant cyclic acetal linkages by ROP of cyclic acetal-bearing carbonate monomer.¹⁸⁰ Other examples include the synthesis of ABPs with PCL,¹⁸¹ vinyl polymer,¹⁸² and prodrugs.^{183, 184} These ABPs self-assembled nanoassemblies with SS located at the interfaces and acid-labile linkages in the cores. Both linkages were cleaved in response to GSH and in acidic pH.

In contrast, numerous strategies have been reported to synthesize a variety of novel DL dual acid (interface)/GSH (core)-responsive ABPs mostly through direct polymerization approach. Strategy I studies the combination of RAFT polymerization and ROP techniques to synthesize PCL-based grafted or star-shaped copolymers bearing AcA groups at the block junction and SS group in the middle of hydrophobic block. 185-187 Strategy II allows for the synthesis of polyurethane-based linear block copolymer with BzI^{188} and HYD^{189} linkages at the block junctions. Strategy III studies the fabrication of core-crosslinked nanogels through the formation of SS crosslinks by the oxidation of pendant thiol groups in polypeptide block copolymers. As illustrated in Figure 2.13a, this strategy involves the ROP of nitrobenzyl-bearing α-amino acid Ncarboxyanhydride initiated with DMMA-labeled PEG amine to form PEG-DMMA-poly(nitrobenzylbearing α-amino acid N-carboxyanhydride). Following photo-cleavage reaction to generate pendant thiol groups allowed for the synthesis of a PEG-DMMA-polycysteine block copolymer. The block copolymer self-assembled to form nanoassemblies composed of pendant thiol groups in the cores and DMMA at the interfaces. The oxidation of thiol groups allowed for the fabrication of core-crosslinked nanogels with sheddable PEG corona composed of junction DMMA groups and SS-crosslinked cores. 190 Similar strategy to fabricate DL dual acid/GSH-degradable core-disulfide crosslinked nanogels through oxidation was conducted with a BzI block junction. 191

Strategy IV studies CRP techniques for HMssEt (a methacrylate bearing pendant SS group) with the design and synthesis of acid-degradable PEG-based precursors bearing acid-labile

linkages. As depicted in Figure 2.13b, a novel PEG-DMK-RAFT macro-agent was synthesized by multiple steps and used for RAFT polymerization of HMssEt, yielding PEG-DMK-PHMssEt diblock copolymer.²¹ Interestingly, ATRP of HMssEt in the presence of PEG-DMK-Br was not successful because of the unexpected cleavage of DMK linkage under ATRP condition.¹⁹² However, PEG-AcA-Br successfully initiated the ATRP of a mixture of OEOMA and HMssEt to synthesize well-defined PEG-AcA-P(OEOMA-co-HMssEt) double hydrophilic diblock copolymer (Figure 2.13c).⁴¹ For Strategy V, carbonylimidazole chemistry has been conducted to synthesize polydisulfide having SS on the backbones, which was further conjugated with a PEG bearing BzCA (benzylic cyclic acetal) (e.g. PEG-BzCA-OH) to synthesize PEG-BzCA-polydisulfide-BzCA-PEG triblock copolymer (Figure 2.13d).¹⁹³

Other strategies include the conjugation of two reactive polymers through *in situ* formation of HYD or BzI groups for acid-labile block junctions. A CHO-bearing PEG was synthesized and used for conjugation with a reactive polyurethane labeled with multiple SS bonds on the backbones bearing pendant amine groups (to form BzI junction)¹⁹⁴ and a reactive PCL labeled with a SS bond in the middle of the central block bearing terminal hydrazine groups (to form HYD junction).¹⁹⁵ Dextran was conjugated with a long chain alkyl (C18) group through disulfide bond and then with a PEG through hydrazone bond after oxidation. As a result, this yielded a PEG-grafted dextran labeled with SS in the hydrophobic block and HYD at the block junction.¹⁹⁶

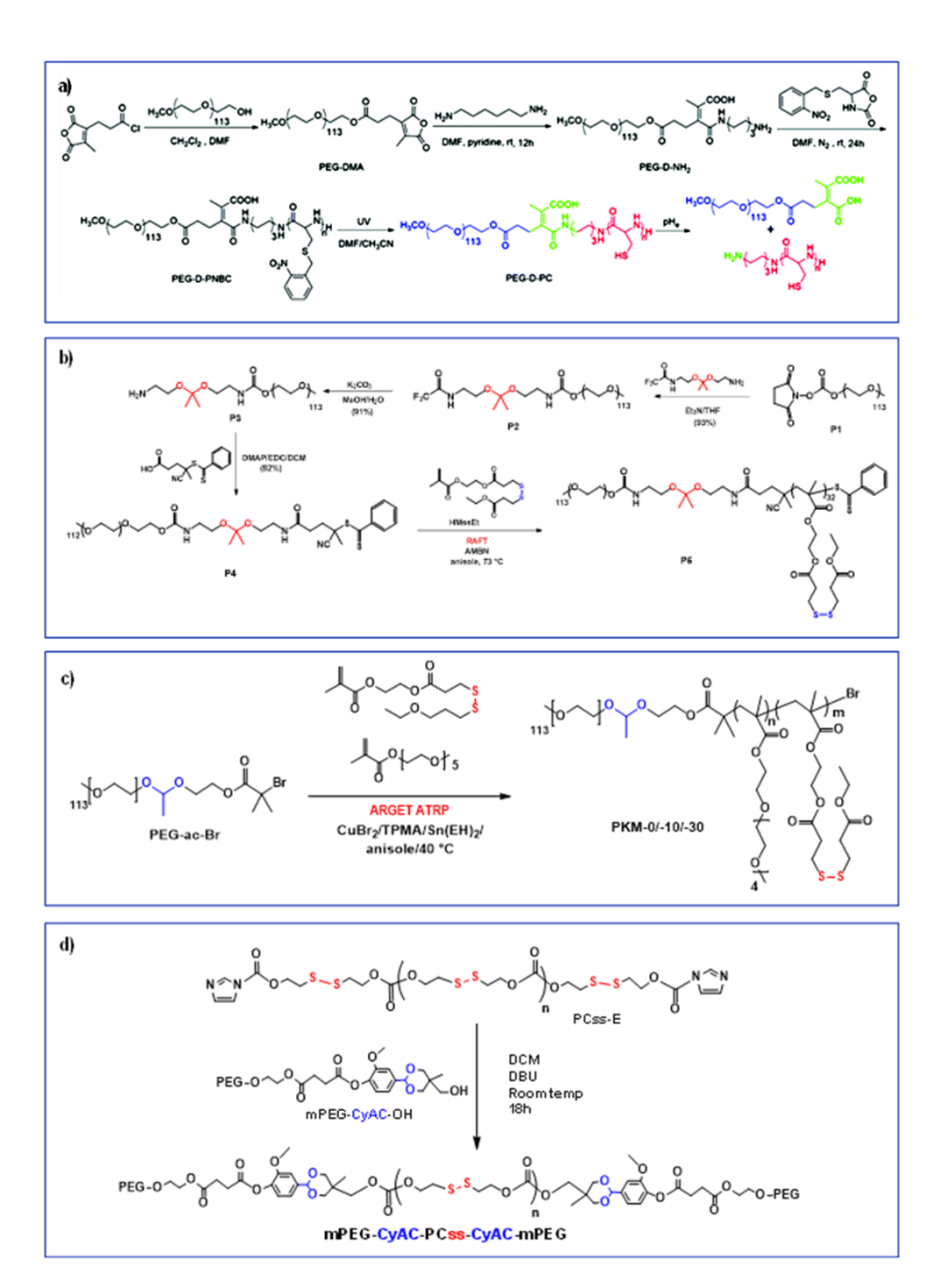


Figure 2.13. Schematic illustration to synthesize PEG-Dlink-polycystein (a). ¹⁹⁰ Copyright 2018 Royal Society of Chemistry; PEG-DMK-PHMssEt (b). ²¹ Copyright 2019 Royal Society of Chemistry; PEG-AcA-P(OEOMA-co-HMssEt) (c). ⁴¹ Copyright 2020 American Chemical Society; and PEG-BzCA-polydisulfide-BzCA-PEB triblock copolymer (d). ¹⁹³ Copyright 2020 Elsevier.

2.4. Biological Evaluation

Drug-loaded ABP-based nanoassemblies designed with SRD are required to be internalized into cells through endocytosis (or entry to cells). Depending on their endocytic pathways, these nanoassemblies can be entrapped in either endosomes/lysosomes or cytosol inside cells. This is critical because the nanoassemblies must escape endosomal/lysosomal pathway for the cargo to be active. These nanoassemblies have been examined for their biological evaluation in vitro (cells), and in vivo (animal models) as the drug release efficiency is not fully understood. For in vitro evaluation, cytotoxicity test is one of the standard practices to measure the toxicity of the nanoassemblies for target substance. 197 Typically, colorimetric assay using tetrazolium salts such as 3-[4,5-dimethylthiazol-2-yl]-2,5 diphenyl tetrazolium bromide (MTT) or 3-(4,5dimethylthiazol-2-yl)-5-(3-carboxymethoxyphenyl)-2-(4-sulfophenyl)-2H-tetrazolium (MTS) has been employed to determine the capability of mitochondria of live cells to reduce tetrazolium salts to deeply coloured formazan dye as to determine the change in their UV/Vis absorption or fluorescence. 198-205 Alternatively, live/dead cell assay with fluorescent microscopy has also been used to measure membrane integrity indicative of cytotoxicity, in addition to metabolic-based assays for determining live, proliferating, cytotoxic and apoptotic cells. 206-208 Most of ShS nanoassemblies based on naturally-occurring and synthetic ABPs have been designed to not be cytotoxic (e.g. biocompatible) up to certain concentrations.

Cellular uptake is another practice for *in vitro* evaluation, commonly by flow cytometry and confocal laser scanning microscopy (CLSM). Flow cytometry determines the amount of nanocarriers translocated by scanning a laser beam and fluorescent intensity responses occur to discover the ratio of dead cells to marker cells. CLSM helps visualize the nanocarriers localization by using a laser light through a standard light microscope and excite a specimen through a narrow focus plane, leading to fluorescent imaging. 209-214 As an example, ShS nanoassemblies based on PEG-based polyurethane ABP labeled with junction BzI were incubated with HeLa cancer cells. The nanoassemblies loaded with Dox were prepared with and without folic acid cell-targeting ligand to folate receptor over-expressed on cancer-cell surfaces to confirm the benefit of active targeting of folic acid (FA)-conjugated ShS nanoassemblies through specific ligand-receptor interaction. As seen in Figure 2.14, both CLSM and flow cytometry analysis suggest that both Dox-loaded nanoassemblies conjugated with and without FA ligands have strong fluorescence intensity, meaning excellent cellular uptake, when they

were incubated in mild acidic condition at pH = 6.5 (tumoral pH). Additionally, the conjugation with FA appeared to have better cellular uptake through active targeting. Overall, these results confirms that cellular uptake could be enhanced through the detachment of PEG corona upon the cleavage of BzI linkages at tumoral pH = 6.5 and additionally ligand-receptor interaction through active targeting platform.²¹⁵

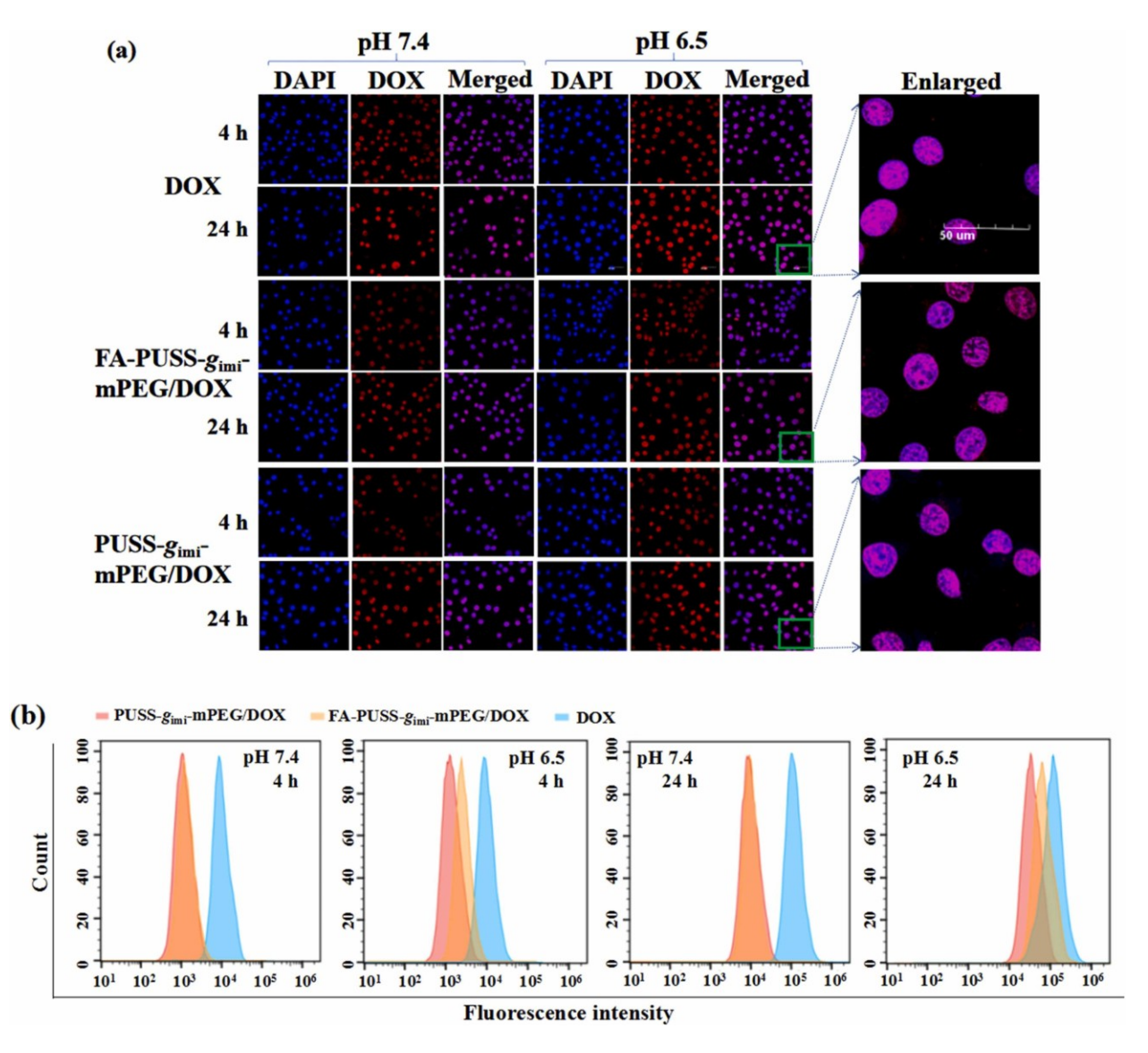


Figure 2.14. Cellular uptake for PEG-BzI-PUSS nanoassemblies by CLSM (a) and flow cytometry analysis (b). Samples were incubated at pH = 6.5 and 7.4 for 4 hrs and 24 hrs. ²¹⁵ Copyright 2023 Elsevier.

In vivo evaluation through animal studies, particularly mouse models, provide important information on carcinogenicity, pulmonary, gastrointestinal, immunological, neurological, and

cardiovascular toxicities of the nanoassemblies.²¹⁶⁻²²⁴ Generally, after the nanoassemblies are distributed into various organs, they can remain in the same structure or become modified or metabolized for an unknown amount of time before leaving to other organs or be excreted. To evaluate for these parameters, biodistributions of the mice are measured through bioluminescence of implanted tumor cells in the mice for in vivo imaging and the bioluminescence of the isolated organs of the liver, spleen, brain, heart and kidney through ex vivo imaging. There have been few reports for single location 134, 145, 152, 225 and dual location 226-229 ShS nanoassemblies that have provided explicit differences between free Dox and Dox-loaded micelles. One example is an ABP composed of PEG-BzI-poly(β -amino ester) grafted with cholesterol (PEG-BzI-PAE-g-Chol), where tumor volumes were treated and measured with injections of PBS, free Dox, PEG-BzI-PAE-g-Chol (Polymer), and PEG-BzI-PAE-g-Chol/Dox (Dox-PMs). As shown in Figure 2.15a, tumor suppression occurred with Dox-PMs compared to free Dox. Figure 2.15 b&c provide mean tumor weight after 30 days, illustrating Dox-PMs provided a significant difference. Figure 2.15d demonstrated little to no body weight difference in mice after 14-day post-injection, providing stability and consistency in results. Figure 2.15e shows histological examinations of each major organ under a microscope, where no signs of metastasis occur in Dox-PMs, indicating biocompatibility and biosafety for enhanced drug release. 152 However, even with successful biological studies, there are major hurdles for getting approval. One particular example is the lack of specific regulatory guidelines, where there are inconsistent and insufficient standardized testing protocols to evaluate the *in vitro* and *in vivo* properties of nanomedicines at the early stage. This leads to a high risk of failure in clinical trials, impeding the clinical translation of nanoparticle-based drug delivery system. 230-237

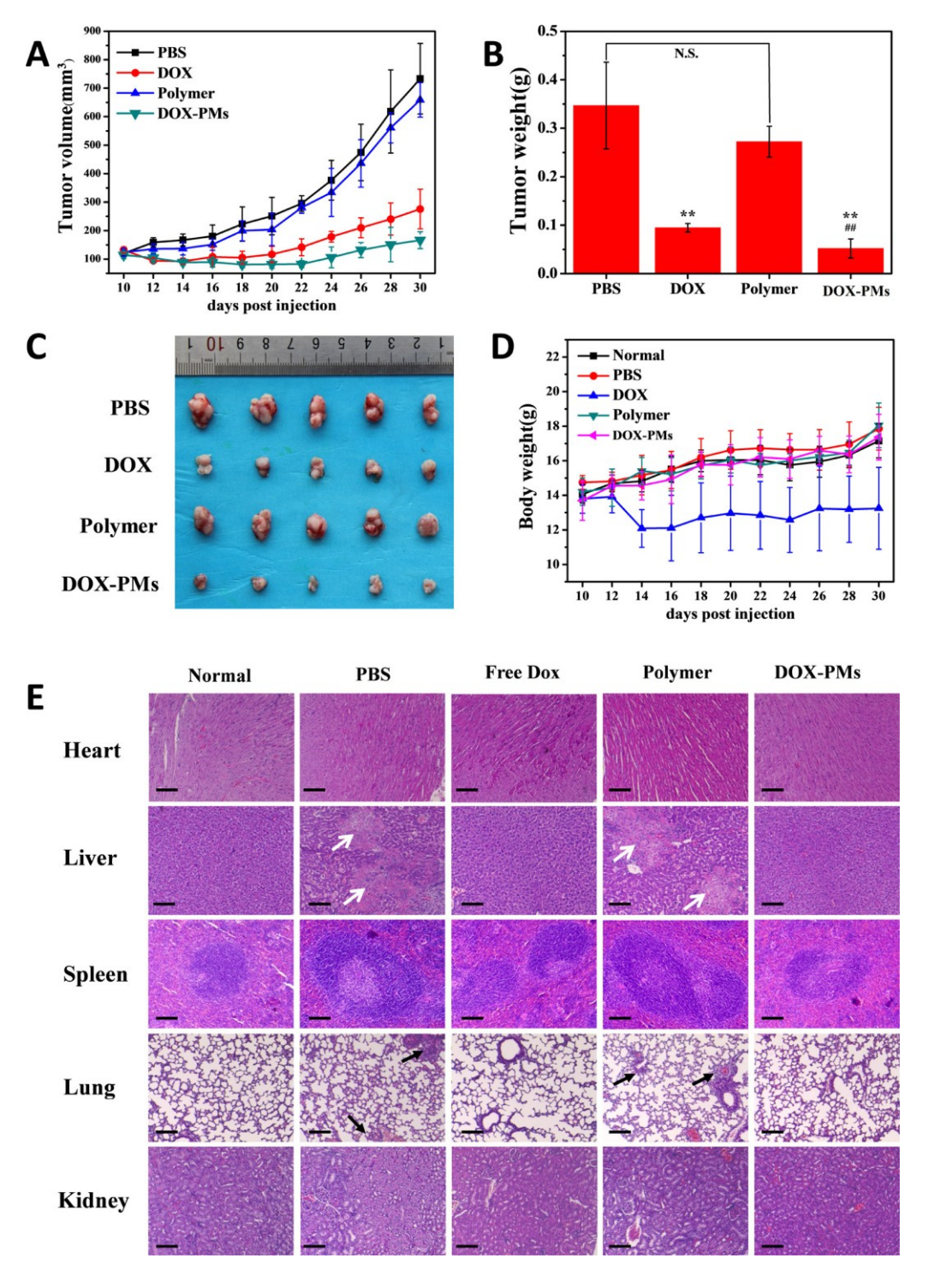


Figure 2.15. In vivo (mouse model) studies for polymer to measure tumor volume (a), tumor weight after 30 day (b,c), body weight change after post-injection (d), and histological images of major organs (e). ¹⁵² Copyright 2019 American Chemical Society.

2.5. Summary and Outlooks

Recent advances in the development of well-defined ShS ABPs and their nanoassemblies are summarized with the focus on acid- and GSH-responsive degradation. These ABPs have been designed with acid-labile linkages such as acetal, ketal, orthoester, imine, hydrazone, and dialkylmaleamidic amide (acid-responsive degradation) or SS/SeSe groups (GSH-responsive degradation) at the junction of hydrophilic and hydrophobic blocks; consequently these linkages are located at the core/corona interfaces in their self-assembled nanoassemblies. In response to acidic pH or GSH as endogenous stimulus found in tumor tissues or cancer cells, the linkages could be cleaved, causing the disintegration of ShS nanoassemblies, leading to the enhanced release of encapsulated drug molecules in cancer cells or the improvement of PEG dilemma in tumoral tissue environment. Numerous strategies have been developed to allow for the synthesis of single location ShS-ABPs that are labeled with either acid-labile or SS/SeSe group at the block junction. Most strategies have utilized either direct polymerization approach through controlled polymerization techniques such as CRP and ROP or conjugation approach through well-known coupling and *in situ* reaction. The strategies have proven to be robust as a means to synthesize well-defined ShS ABPs with a variety of chemical structures and compositions of particularly hydrophobic blocks, along with PEG as a common hydrophilic block.

Despite these advances, the current designs of single location ShS-ABPs present several challenges to be addressed for various aspects of effective tumor-targeting drug delivery. PEG has been mainly employed as a hydrophilic block of acid-degradable ABPs, thus attaining corona (or shell) of ShS nanoassemblies. The detachment of PEG corona upon the cleavage of acid-labile linkages at the interfaces aims to overcome PEG dilemma as to enhance the ability of nanoassemblies for endocytosis in the tumoral pH at 6.5-6.9. Despite significant advance in the synthesis of acid-degradable ShS ABPs with various acid-labile linkages, the choice of the junction acid-labile linkage appears to be lack of rationale. Efforts could be made to investigate a library of acid-labile linkages as suitable junction candidates that meet pH requirements. Moreover, they should not interfere with controlled polymerization mechanisms. Another aspect involves the occurrence of large aggregation of hydrophobic cores upon the detachment of PEG coronas. DL ShS/core-degradable nanoassemblies have been designed to have both the detachment of hydrophilic PEG corona and the degradation of cores in response to acidic pH and

GSH. Despite these advances, more robust strategies to synthesize DL nanoassemblies that can meet the requirements have to be developed.

A few ABP-based nanoassemblies have reached clinical studies such as PEG-b-PLA²³⁸⁻²⁴⁰, PEG-modified polyglutamate²⁴¹⁻²⁴³, and PEG-b-poly(aspartic acid).^{9, 244-246} It is anticipated that nano-formulations based on SRD-exhibiting nanoassemblies designed with chemical transition (e.g. the cleavage of acid-labile or disulfide bonds) can be in clinical studies for next-generation drug delivery.

Chapter 3: Design, Synthesis, and Acid-Responsive Disassembly of Shell-Sheddable Block Copolymer Labeled with Benzaldehyde Acetal Junction

3.1 Introduction

Colloidally-stable nanoassemblies based on amphiphilic block copolymers (ABPs) composed of hydrophilic and hydrophobic blocks have been considered as effective nanoplatforms enabling the encapsulation and targeted delivery of hydrophobic biomolecules in pharmaceutical science. 247-250 Particularly, well-defined ABPs exhibiting stimuli-responsive degradation through chemical transition have been designed with labile linkages that can be cleaved in response to stimuli. 55, 251-261 Acidic pH is the most promising endogenous stimulus found in biological environments, typically tumor tissues and cancer cells. Compared with normal tissues (pH = 7.4), an extracellular compartment of tumor tissues is slightly acidic (pH = 6.5-6.9) and endosomes and lysosomes in cancer cells is even more acidic (pH = 4.5-5.5). $^{262-264}$ Given these features, acid-degradable ABPs and their nanoassemblies have been designed with various acid-labile linkages such as acetal, ketal, orthoester, imine, oxime, hydrazone, 2,3dialkylmaleamidic amide, boronic ester, and β-thiopropionate groups.^{36, 265-270} When being exposed to an acidic environment, the nanoassemblies degrade upon the cleavage of the acidlabile linkages, exhibiting the controlled/enhanced release of encapsulated drug molecules. Such controlled drug release can improve biodistribution, ensure minimal dosage, and minimize undesired cytotoxicity to healthy tissues common to small molecule drugs.²⁷¹⁻²⁷³

Various strategies have been reported to synthesize acid-degradable ABPs and their nanoassemblies with different locations of acid-labile linkages. ²⁷⁴⁻²⁸⁴ A promising strategy involves the acid-labile linkages positioned at the junction of hydrophilic and hydrophobic blocks of ABPs, and thus located at the interfaces of hydrophobic cores and hydrophilic coronas of nanoassemblies. These acid-degradable shell-sheddable nanoassemblies have been commonly designed with poly(ethylene glycol) (PEG) as corona (or shell) and thus provide colloidal stability in aqueous solutions and prevent undesired protein absorption during blood circulation. While being stable at physiological pH = 7.4, the nanoassemblies could enable to shed PEG corona upon the cleavage of junction acid-labile linkages at the core/corona interfaces in the tumoral pH at 6.5-6.9. Such detachment of PEG corona could not only address PEG dilemma

and facilitate entry to cells but also enhance therapeutic activity of encapsulated drug molecules. 91, 285-287

Various acid-labile linkages, including mainly ketal as dimethyl ketal, $^{179, 192, 288}$ acyclic acetal as acetaldehyde acetal $^{128, 132, 289-297}$ and cyclic acetal $^{193, 298-300}$ as well as benzoic imine, $^{301-303}$ hydrazone, 304 and 2,3-dialkylmaleamidic amide $^{190, 305}$ have been explored for the development of acid-degradable shell-sheddable ABPs. Despite these advances, the choice of such junction acid-labile linkages seemed to be intuitional and lack of rationale. Dimethyl ketal, benzoic imine, and 2,3-dialkylmaleamidic amide linkages are cleaved rapidly at pH = 6.5 and to a significant extent even at pH = 7.4. In contrast, acetaldehyde acetal and cyclic benzylic acetal linkages have very slow hydrolysis rate at pH = 6.5 and even at pH = 5.0. Thus, it is highly desired to design the appropriate candidate of junction acid-labile linkage meeting its criteria including slow cleavage (acid-catalyzed hydrolysis) at tumoral pH, while rapid cleavage at endo/lysosomal pH and no significant cleavage at physiological pH.

Acetal/ketal chemistry is promising in that the cleavage rates of acetal/ketal groups through acid-catalyzed hydrolysis could be adjusted with the substituents attached to oxygen atoms as well as central carbon atom in acetal/ketal moieties. Their tunable hydrolysis rates are attributed to the stability of the corresponding carbocation intermediates generated through the protonation of an oxygen atom and subsequent elimination of the corresponding alcohol species. The substituents greatly influence the stability of the carbocations through steric, resonance, and induction effects, and ultimately the cleavage rate (hydrolysis rate) of acetal/ketal groups. 40, 136, 306-310 We envisioned to establish the design principle of acetal/ketal linkages for the development of effective acid-degradable shell-sheddable ABPs that meet the requirements for tumor-targeting drug delivery.

In this work, we investigated three candidates of acetal/ketals bearing benzaldehyde acetal (BzAc), cyclopentyl ketal (CyPK), and cyclohexyl ketal (CyHK) groups as suitable candidates for junction acid-labile linkages. Their diol precursors were synthesized to systematically investigate their structure-driven acid-catalyzed hydrolysis rates at acidic pHs of 6.5 (tumoral pH) and 5.0 (endo/lysosomal pH), compared with pH of 7.4 (physiological pH). The suitability of BzAc as the junction acid-labile group for acid-degradable shell-sheddable nanoassemblies are demonstrated with the synthesis of a well-defined block copolymer labeled with BzAc group

at the junction of PEG and poly(benzyl methacrylate) (PBM) blocks, thus forming PEG-BzAc-PBM diblock copolymer, followed by aqueous micellization and acid-responsive disassembly.

3.2 Experimental

3.2.1 Instrumentations. ¹H NMR spectra were recorded using a 300 MHz Bruker spectrometer and a 500 MHz Varian spectrometer. The CDCl₃ singlet at 7.26 ppm, DMSO-d₆ quintet at 2.5 ppm, CD₃CN singlet at 1.94 ppm, and D₂O singlet at 4.79 ppm were selected as the reference standards. Spectral features are tabulated in the following order: chemical shift (ppm); multiplicity (s - singlet, d - doublet, t - triplet, m - complex multiple); number of protons; position of protons. Molecular weight and molecular weight distribution were determined by gel permeation chromatography (GPC). A Malvern GPCmax was equipped with a 1260 Infinity Isocratic Pump and a Refractive Index Detector. A Waters Styragel GPC Column (5 μm, 7.8 mm x 300 mm, ranging at 2 K – 4 M/mol) was used with THF at a flow rate of 1.0 mL min⁻¹. Linear poly(methyl methacrylate) standards from Fluka were used for calibration. Aliquots of the polymer samples were dissolved in THF and the clear solutions were filtered using a PTFE disk filter with 0.40 µm pores to remove any of insoluble species. A drop of anisole was added as a flow rate marker. Fluorescence spectra on a Varian Cary Eclipse fluorescence spectrometer were recorded using a 1 cm wide quartz cuvette. The size and size distribution of aqueous nanoassemblies in hydrodynamic diameter were measured by dynamic light scattering (DLS) at a fixed scattering angle of 175° at 25 °C with a Malvern Instruments Nano S ZEN1600 equipped with a 633 nm He-Ne gas laser.

Transmission Electron Microscopy (TEM) images were obtained using a Talos L120C TEM operated at 80 kV electrons. To prepare the specimens, aqueous dispersions of nanoassemblies (5 μL) were dropped on a copper grid with carbon coating (300 mesh size). After 3 min, the droplets were blotted off the grids using filter paper and dried at room temperature in a desiccator before measurements. The average diameter was calculated with >50 nanoassemblies in TEM images using ImageJ software.

3.2.2 Materials. Benzaldehyde (BzA, natural, 98%), benzaldehyde dimethyl acetal (99%), cyclopentanone (CyP), cyclohexanone (CyH), 1,6-hexanediol (HDOH, 97%), triethylamine (Et₃N, 99.5%), p-toluene sulfonic acid monohydrate (TSA, >98%), 1,1'-carbonyldiimidazole (CDI, 97%), 1,8-diazabicyclo[5.4.0]undec-7-ene (DBU, 98%), 2-bromoisobutyryl bromide (Br-

iBuBr, 98%), methoxy-terminated poly(ethylene glycol) (PEG, MW = 5000 g/mol), benzyl methacrylate (BM, 96%), and Nile Red (NR) from Sigma-Aldrich or Alfa Aesar as well as tris(2-pyridylmethyl) amine (TPMA) from TCI Chemicals were purchased and used without further purification unless otherwise noted. Dialysis tubing made of cellulose membranes with molecular weight cut-off (MWCO) of 12-14 kDa was purchased from Spectra/Por. Anhydrous tetrahydrofuran (THF) was obtained from a solvent purification system using aluminum oxide columns. A PEG activated with CDI (PEG-CI, a precursor for the synthesis of PEG-BzAA-Br ATRP macroinitiator) was synthesized as described elsewhere.³¹¹

3.2.3 Synthesis of Acetal/Ketal-Labeled Diol Precursors. Three acid-labile diols bearing BzAc, CyPK, and CyHK linkages were synthesized through direct acetalization/ketalization. All reactions were conducted with use of air- and moisture-free techniques and reagent-grade solvents.

BzAc-DOH. In a 100 mL round bottom flask dried at 70 °C overnight, HDOH (13.4 g, 113 mmol) and TSA (0.54 g, 3 mmol) were mixed with anhydrous THF (50 mL) containing 5 Å molecular sieves (25 g) dried in an oven at 180 °C for 5 hours. BzA (3 g, 28 mmol) was added and the mixture was stirred at room temperature for 24 hours. After the removal of molecular sieves by filtration, the resulting mixture was quenched with Et₃N (1 mL). Solvent was removed by rotary evaporation and the residues were re-dissolved in ethyl acetate. Crude was extracted with an aqueous 2.5% sodium bicarbonate solution (2 x 50 mL) and the organic layer was dried with magnesium sulfate. The product was collected as the second of the total two bands off a silica gel column using an eluent of 1/1 v/v hexane/ethyl acetate mixture, and then dried in vacuum oven for 24 hrs. Colorless oil residue with yield = 5.7 g (62%); R_f = 0.17 on (1/1 v/v hexane/ethyl acetate). ¹H-NMR (CDCl3, ppm): 7.46-7.30 (m, 5H, Ar-H), 5.50 (s, 1H, CH-O₂), 3.66-3.60 (q, 4H, CH₂-OH), 3.56-3.42 (m, 4H, CH₂-CH₂-O), 1.65-1.55 (m, 8H, CH₂), 1.40-1.38 (m, 8H, CH₂). ¹³C NMR (CDCl₃, ppm): 138.99, 128.25, 128.13, 126.66, 101.57, 65.37, 62.55, 32.65, 32.60, 29.70, 26.13, 26.10, 25.59, 25.56, 25.52. Mass calculated for C₁₉O₄H₃₁Na⁺: 347.2193 and found: 347.2192.

CyPK-DOH. Similar procedure was used, except for the use of HDOH (16.9 g, 143 mmol), TSA (0.68 g, 4 mmol), cyclopentanone (3 g, 36 mmol), and 5 Å molecular sieves (25 g). The product was collected as the second of the total two bands off a silica gel column using an eluent of 3/2 v/v hexane/ethyl acetate mixture, and then dried in vacuum oven for 24 hrs. Colorless oil residue with yield = 5.5 g (51%); $R_f = 0.10$ on (3/2 v/v hexane/ethyl acetate). 1 H-NMR (CDCl3, ppm): 3.65-3.63 (m, 4H, **CH2**-OH), 3.42-3.37 (m, 4H, CH2-**CH2**-O), 1.75-1.55 (m, 16H, **CH2**), 1.42-1.36 (m, 8H, **CH2**-cyclopentyl). 13 C NMR (CDCl₃, ppm): 111.54, 62.43, 62.32, 61.62, 34.67, 32.59, 32.52, 29.98, 26.28, 26.17, 25.65, 25.49, 22.85. Mass calculated for $C_{17}O_4H_{33}Na^+$: 325.2349 and found: 325.2350.

CyHK-DOH. Similar procedure was used, except for the use of HDOH (14.4 g, 122 mmol), TSA (0.58 g, 3 mmol), cyclopentanone (3 g, 31 mmol), and 5 Å molecular sieves (25 g). The product was collected as the second of the total two bands off a silica gel column using an eluent of 3/2 v/v hexane/ethyl acetate mixture, and then dried in vacuum oven for 24 hrs. Colorless oil residue with yield = 3.87 g (40%); $R_f = 0.22$ on (3/2 v/v hexane/ethyl acetate). ¹H-NMR (CDCl3, ppm): 3.66-3.62 (t, 4H, CH₂-OH), 3.38-3.35 (t, 4H, CH₂-CH₂-O), 1.64-1.48 (m, 16H, CH₂), 1.39-1.37 (m, 8H, CH₂-cyclohexyl). ¹³C NMR (CDCl₃, ppm): 99.87, 62.51, 62.39, 59.47, 33.73, 32.64, 32.55, 30.07, 26.27, 25.69, 25.65, 25.51, 23.00 ppm. Mass calculated for $C_{18}O_4H_{35}Na^+$: 339.2506 and found: 339.2504.

3.2.4 Studies of Acid-Catalyzed Hydrolysis of Acetal/Ketal-Labeled Diol Precursors. 0.2 M Aqueous phosphate buffered saline (PBS) solutions in D_2O at potential of deuterium (pD) = 5.0, 6.5, and 7.4 were prepared by mixing aqueous stock solutions of NaH_2PO_4 (0.2 M) with Na_2HPO_4 (0.2 M) in D_2O at different volume ratios. pH values were measured using a pH meter with a glass electrode standardized with aqueous buffer solutions (pH = 4, 7 and 10). pD values were calculated using the equation of pD = pH (measured) + 0.41.

To study hydrolysis, the solutions of diol precursors (whose moles were adjusted to 10 μ mol) dissolved in CD₃CN (0.3 mL) were mixed with the as-prepared 0.2 M aqueous PBS solutions in D₂O (PB-D₂O, 0.1 mL) at pD = 5.0, 6.5 and 7.4. The resultant mixtures were analyzed by ¹H NMR at 25 °C for given periods of time.

3.2.5 Synthesis of PEG-BzAc-Br ATRP Macroinitiator. A two-step procedure with PEG-CI was employed. In the first step to synthesize PEG-BzAA-OH precursor, a solution containing BzAc-DOH (2.53 g, 7.80 mmol) and DBU (0.20 g, 1.30 mmol) dissolved in dichloromethane (DCM, 30 mL) was mixed with a solution of PEG-CI (6.60 g, 1.30 mmol) dissolved in DCM (30 mL) at room temperature for 2 days. The resulting mixture was washed with aqueous PBS solution (pH = 7.4) two times and then dried over magnesium sulfate. After solvent was removed by rotary evaporation, the product was precipitated from anhydrous diethyl ether (50 mL), isolated by vacuum filtration, and dried in a vacuum oven at room temperature for 12 hours, yielding 4.9 g (70%).

In the second step, a solution containing the dried PEG-BzAc-OH (3.26 g, 0.59 mmol) and Et₃N (0.84 g, 8.30 mmol) dissolved in DCM (40 mL) was mixed with Br-iBuBr (0.55 g, 2.37 mmol) dissolved in DCM (3 mL) in an ice bath. The resulting mixture was stirred at room temperature for 24 hours. The formed solids (Et₃N-HBr adducts) were removed by vacuum filtration. The solution was washed with PBS (pH = 7.4) two times and then dried over magnesium sulfate. Solvent was removed by rotary evaporation. The product was then precipitated from anhydrous diethyl ether (50 mL), isolated by vacuum filtration, and dried in a vacuum oven at room temperature for 12 hours, yielding 3.2 g (>98%).

3.2.6 ATRP to Synthesize PEG-BzAc-PBM Block Copolymer. PEG-BzAc-Br (0.26 g, 46.5 μmol), BM (0.82 g, 4.65 mmol), [Cu(II)Br/TPMA]Br (1.19 mg, 2.30 μmol), TPMA (2.01 mg, 6.98 μmol), and anisole (3.3 g) were mixed in a 10 mL Schlenk flask. The mixture was deoxygenated by purging under nitrogen for 1 hour. A nitrogen pre-purged solution of Sn(II)(EH)₂ (7.54 mg, 18.6 μmol) dissolved in anisole (0.5 g) was injected into the Schlenk flask to initiate polymerization, and then placed in an oil bath at 40 °C. Polymerization was stopped after 3 hours by cooling the reaction mixture in an ice bath and exposing it to air.

The as-synthesized products were purified by precipitation from hexane three times to ensure the removal of remaining monomers. The precipitates were isolated and dried in a vacuum oven at room temperature overnight.

- 3.2.7 Determination of Critical Micelle Concentration (CMC) using a NR probe. A stock solution of NR in THF at 1 mg mL $^{-1}$ and stock solutions of PEG-BzAc-PBM in THF at 1 mg mL $^{-1}$ and 0.1 µg ml $^{-1}$ were first prepared. The same volume of the stock solution of NR (0.5 mL, thus, 0.5 mg NR) was mixed with various volumes of the stock solutions of PEG-BzAc-PBM. Water (0.5 mL) was then dropwise added to the resulting organic solutions of NR and PEG-BzAc-PBM at room temperature. The resulting dispersions were stirred overnight to remove THF and then were subjected to further addition of water to keep concentration consistent. The solutions were centrifuged at 2500 rpm for 5 minutes, followed by filtration using a PES filter with 0.45 µm pores to remove excess NR. A series of NR-loaded micelles at various concentrations of PEG-BzAc-PBM ranging from 10^{-6} to 0.1 mg mL $^{-1}$ were formed. From their fluorescence spectra recorded with $\lambda_{ex} = 350$ nm, the fluorescence intensity at maximum wavelength was recorded.
- 3.2.8 Aqueous Micellization by Dialysis. PBS (pH = 7.4, 20 mL) was added dropwise to an organic solution of PEG-BzAc-PBM dissolved in DMSO (2.0 mL) using a syringe pump equipped with a plastic syringe (20 mL, 20 mm diameter) at an addition rate of 0.2 mL min⁻¹. The resulting dispersion was dialyzed against PBS solution (3 L) twice for 24 h, yielding aqueous micellar dispersion at 1 mg mL⁻¹.
- 3.2.9 Cell Viability. HeLa cells were cultured at $5x10^4$ cell/mL per well into a 96-well plate in $100~\mu L$ in Dulbecco's modified Eagle's medium (DMEM) supplemented with 10% fetal bovine serum and 1% antibiotics (50~U/mL penicillin and 50~U/mL streptomycin) at $37~^{\circ}C$, 5% CO₂, and 90- 95% humidity. After 48 h, the cells were washed with sterile PBS solution and exposed for 24 h to micellar dispersions prepared in $20~\mu L$ of PBS solution and $80~\mu L$ of DMEM media at concentrations ranging from $14\text{-}560~\mu g/mL$. According to the manufacturer's protocol, $10~\mu L$ of a 1.4~mg/mL solution of 3-(4,5-dimethylthiazol-2-yl)-2,5-diphenyltetrazolium bromide (MTT) was added to each well to assess cell viability using the Cell Proliferation Assay Kit (MTT, Promega). After 3~h incubation, culture media was carefully removed from the wells and replaced with DMSO to dissolve formed insoluble formazan salts. Absorbance of the samples were recorded at $\lambda = 570~nm$ using a Perkin-Elmer EnSight plate reader. Each concentration was repeated six times. Cell viability was calculated as the percent ratio of absorbance of mixtures with micelles to control (cells only).

3.2.10 Acidic pH-Responsive Degradation and Disassembly. Aliquots of the purified, dried PEG-BzAc-PBM (10 mg) was dissolved in CDCl₃ (1 mL) containing DCl (20 μ L) to examine its degradation by 1 H NMR and GPC analysis. Aliquots of aqueous nanoassemblies of PEG-BzAc-PBM (1 mL, 1 mg mL $^{-1}$) were mixed with aqueous PBS (3 mL) and their pHs were adjusted to be 6.5 and 5.3, along with at pH = 7.4 as a control to examine their disassembly by DLS analysis.

3.3 Results and Discussion

3.3.1 Synthesis of Acid-labile Diol Precursors. Our experiments began with the synthesis of three diol precursors bearing acetal/ketal groups. As depicted in Figure 3.1, the approach explores the in situ formation of acetal and ketal linkages through coupling reaction (called direct acetalization/ketalization) of HDOH with BzA for BzAc-DOH, CyP for CyPK-DOH, and CyH for CyHK-DOH in the presence of TSA as an acid catalyst in anhydrous condition at room temperature. After neutralization with Et₃N, the formed products were purified by column chromatography saturated with 1% Et₃N. The use of Et₃N is critical to prevent the undesired cleavage of acetal and ketal bonds in silica column. NMR spectroscopy was used for structural analysis of three diol precursors.

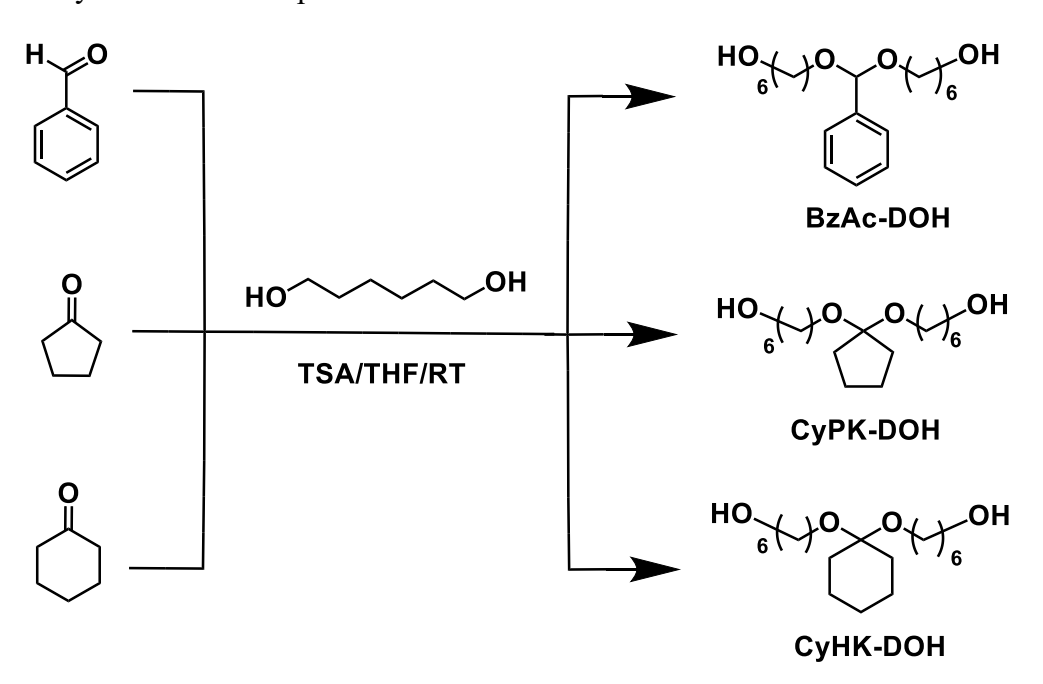


Figure 3.1. Synthesis of three diol precursors bearing acetal/ketal groups through coupling reaction of HDOH with BzA, CyP, and CyH in the presence of TSA in anhydrous THF at room temperature (RT).

For the synthesis of BzAc-DOH, its ¹H NMR spectrum in Figure 3.2a shows the typical peaks at 7.30-7.50 ppm (a) corresponding to aromatic protons, 5.50 ppm (b) corresponding to methine proton in acetal group, and 3.60 ppm (c) corresponding to methylene protons adjacent to terminal hydroxy group. For CyPK-DOH and CyHK-DOH, their ¹H NMR spectra (Figure 3.2b and 3.2c) show the typical peaks at 3.70 ppm (a) corresponding to methylene protons adjacent to terminal hydroxy units and 3.40 ppm (b) corresponding to methylene protons adjacent to oxygen atoms of ketal units. The integral ratios of these peaks are quantitative to their numbers of protons present in the precursor products. Combined with ¹³C NMR analysis (Figure A1-A3) and high-resolution MS results, ¹H NMR analysis confirms the successful synthesis of BzAc-DOH, CyPK-DOH, and CyHK-DOH. The isolated yield was as high as 40-62%.

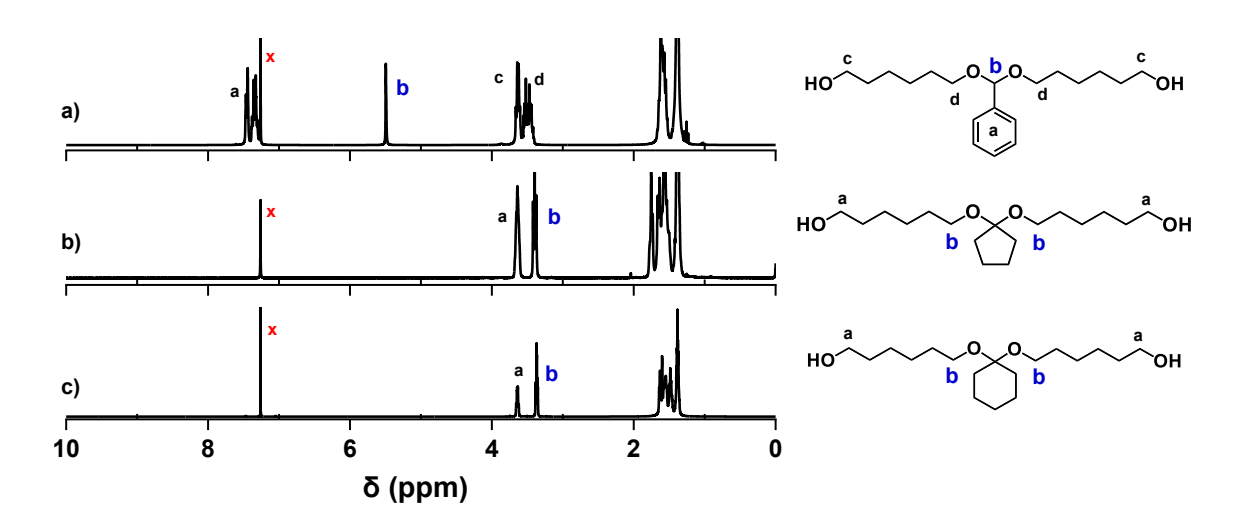


Figure 3.2. ¹H NMR spectra of BzAc-DOH (a), CyPK-DOH (b), and CyHK-DOH (c) in CDCl₃, where only characteristics peaks are assigned. X denotes a trace of CHCl₃ containing CDCl₃.

In a separate experiment, an alternative approach utilizing transacetalization was examined to synthesize BzAc-DOH. As depicted in Figure A4, the approach involves the reaction of HDOH with benzaldehyde dimethyl acetal (BzAc-DMA) in the presence of a catalytic amount of TSA in an anhydrous condition. After neutralization with Et₃N and purification through column chromatography, ¹H NMR analysis confirms the synthesis of the target product of BzAc-DOH at 48% of isolated yield (Figure A4).

An interesting result was observed when glycol was used instead of HDOH in an attempt to synthesize benzaldehyde dihydroxyethyl acetal (BzAc-DHEOH), a family of BzAc-DOH

(benzaldehyde dihydroxyhexyl acetal). ¹H NMR analysis confirms the formation of a cyclic acetal instead of BzAc-DHEOH, an aliphatic acetal diol (Figure A5). The successful approach to synthesize BzAc-DHEOH is illustrated in Figure A6 and the detailed synthetic procedures are summarized in supporting information. The approach involves two-step synthesis consisting of the transacetalization of BzAc-DMA with 2-hydroxyethyl acetate to synthesize BzAc-DEAc, followed by its base-catalyzed hydrolysis with NaOH. ¹H NMR analysis confirms the successful synthesis of BzAc-DMA (Figure A7), BzAc-DEAc (Figure A8), and BzAc-DHEOH (Figure A9).

3.3.2 Studies of Acid-Catalyzed Hydrolysis Kinetics of Acid-labile Diol Precursors.

Given the success in the synthesis and structural analysis of three acid-labile diol precursors, their acid-responsive degradation kinetics through acid-catalyzed hydrolysis was investigated in acidic conditions. ^{1}H NMR spectroscopy was employed for the purified precursors dissolved in a mixture of 3/1 v/v CD₃CN/PB-D₂O at acidic pDs = 5.0 (endo/lysosomal pH) and 6.5 (tumoral pH), compared with pD = 7.4 (physiological pH) as a control at 25 °C. Their ^{1}H NMR spectra were recorded over incubation time as shown in Figure 3.3 at pD = 5.0 and Figure A10-A15 at pD = 6.5 and 7.4.

For BzAc-DOH, the new peak at 10 ppm (a) corresponding to aldehyde proton appeared and its integral increased over incubation time, whereas the integral of the acetal methine peak at 5.40 ppm (b) decreased (Figure 3.3a). For CyPK-DOH and CyHK-DOH, the new peaks at 2.10 (a) and 2.40 ppm (b) corresponding to methylene protons adjacent to ketone groups appeared and their integrals increased over incubation time, whereas the integral of the methylene protons adjacent to oxygen atom of ketal units at 3.40 ppm (b) decreased (Figure 3.3b and 3.3c). Such changes are attributed to the generation of BzA as a consequence of the cleavage of the acetal linkage for BzAc-DOH or CyP or CyH as a result of the cleavage of ketal linkages for CyPK-DOH and CyHK-DOH in an acidic condition (Figure 3.3d-3.3f). Their integral ratios were used to determine %hydrolysis of BzAc, CyPK, and CyHK linkages.

Figure 3.3g-3.3i shows their percent hydrolysis at different pDs over incubation time. For BzAc-DOH, its %hydrolysis increased over incubation time at three pDs. Acid-catalyzed hydrolysis rate is much faster when being incubated in acidic conditions (i.e. pD = 6.5 and 5.0), compared with physiological pD = 7.4. Furthermore, the rate is faster at pD = 5.0 than pD = 6.5,

which is plausibly attributed to higher concentration of protons. For CyPK-DOH and CyHK-DOH, the trend of acid-catalyzed hydrolysis is similar in that their %hydrolysis increased over time and the rates in acidic pDs are faster than that at pD = 7.4.

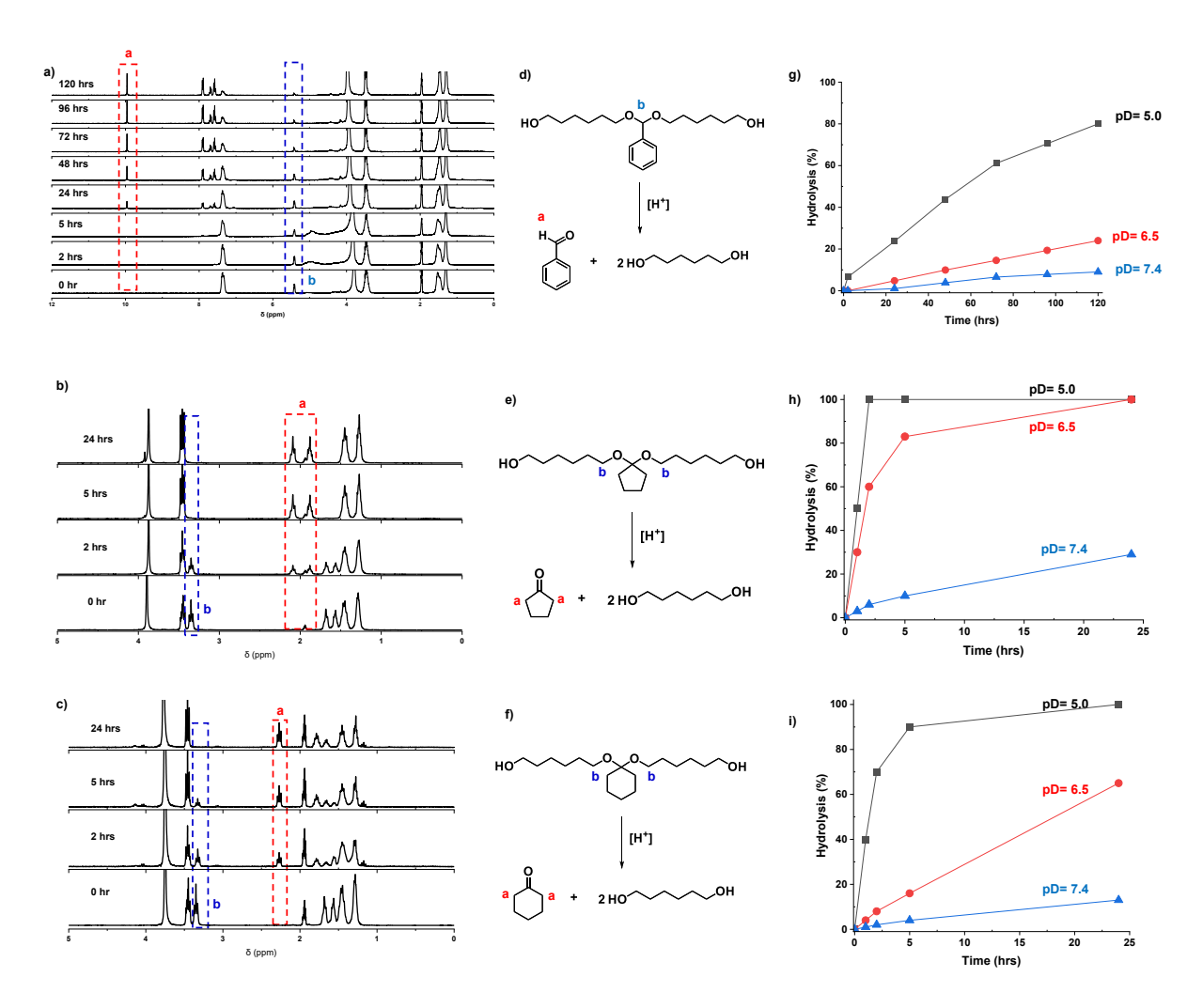


Figure 3.3. Overlaid ¹H NMR spectra at pD = 5.0 as an example (a, b, c), schematic illustration of acid-catalyzed hydrolysis (d, e, f), and evolution of %hydrolysis at pD = 5.0, 6.8, and 7.4 (g, h, i) for BzAc-DOH (a, d, g), CyPK-DOH (b, e, h), and CyHK-DOH (c, f, i) dissolved in a 3/1 v/v CD₃CN/PB-D₂O mixtures.

For further quantitative analysis of acid-catalyzed hydrolysis of three acid-labile diol precursors, their times when a half concentration of acetal/ketal linkages is cleaved ($t_{1/2}$) were determined from the plots in Figure 3.4 and summarized in Table 3.1. Their percent hydrolysis is compared at pD = 6.5 and 5.0 in Figure 3.4. For BzAc-DOH, $t_{1/2}$ was 2 days at pD = 5.0 and 10 days at pD = 6.5, while it was 1 hr at pD = 5.0 and 2 hrs at pD = 6.5 for CyPK-DOH and 2 hr at

pD = 5.0 and 5 hrs at pD = 6.5 for CyHK-DOH. These results confirm that the rate for BzAc-DOH at pD = 6.5 appears to be slower compared with those for CyPK-DOH and CyHK-DOH. Different from BzAc-DOH, the rate for two ketal precursors at pD = 6.5 appears to be as fast as at pD = 5.0. Our results are consistent with the order of hydrolysis rate published in literature, which is CyPK > CyHK > BzAc group in the mixture of 3/1 v/v CD₃CN/PB-D₂O at the same volume ratio as our experiment, even though their relative hydrolysis rates are somewhat different.

Given such promising results, we can conclude that the benzylic acetal precursor is the only candidate that can be considered for the junction point between the hydrophilic and hydrophobic blocks as this is the determining factor towards the efficient degradability of the nanoparticles for the best drug release profile.

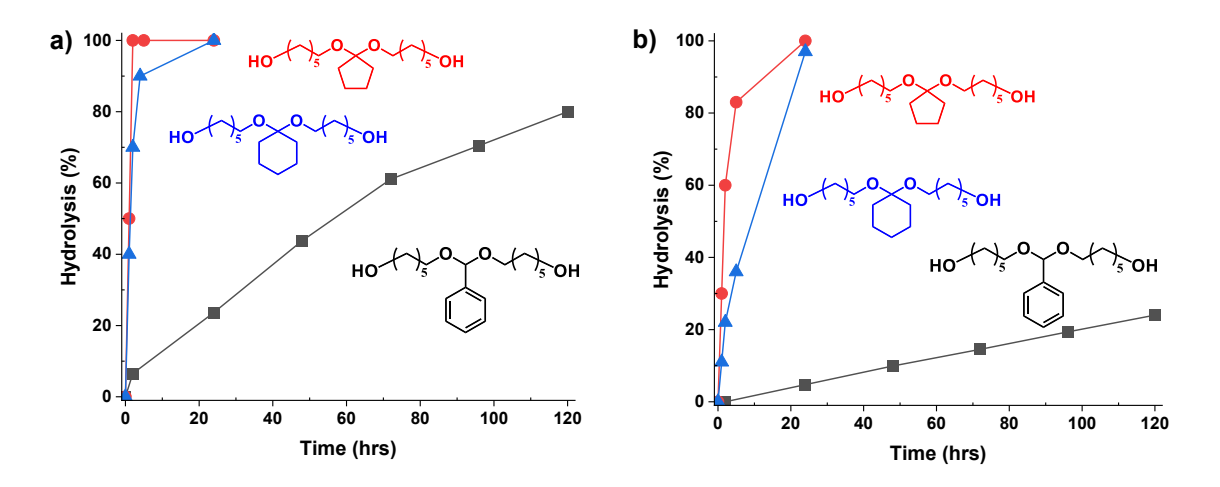


Figure 3.4. Comparison of %hydrolysis of three diols at pD = 5.0 (a) and 6.5 (b). The plots are built from the data shown in Figure 3.3.

Table 3.1. Summary of acid-catalyzed hydrolysis rates as times when a half concentration of acetal/ketal linkages is cleaved ($t_{1/2}$) for acid-labile diol precursors.

Diol Precursor	pD = 5.0	pD = 6.5	pD = 7.4
BzAc-DOH	65	>248 ^{a)}	>617 a)
CyPK-DOH	0.5	5	42
CyHK-DOH	2	11	46

a) Predicted using mathematical models that are fit to their data up to 120 hrs.

3.3.3 Synthesis of PEG-based BzAc-Bearing ATRP Macroinitiator. Given that BzAc group is the promising candidate of the acid-labile junction group of hydrophilic and hydrophobic blocks, we investigated the proof-of-concept synthesis of an acid-degradable PEG-based amphiphilic sheddable block copolymer. As the first step, the synthesis of a PEG-based BzAc-labeled bromine (PEG-BzAc-Br) as a macroinitiator for atom transfer radical polymerization (ATRP)^{312, 313} was explored.

As depicted in Figure 3.5a, the approach involves a two-step process. The first step is the coupling reaction of BzAc-DOH with PEG-CI in the presence of DBU as a base catalyst to synthesize a PEG-BzAc-OH precursor. After being purified by precipitation from diethyl ether, the white solid product at a yield of 70% was characterized by ¹H NMR analysis. Figure 3.5b shows the characteristic peaks at 7.30-7.50 ppm (aromatic protons, a), 5.50 ppm (methine proton in acetal moiety, b), and 3.35 ppm (methoxy protons in PEG moiety, c), along with 1.37-1.59 ppm (methylene protons in BzAc moiety, d). The integral ratio of the peaks (a/b/c) is quantitative to be 5/1/3, consistent with the number of their protons (Figure A16). Furthermore, no peaks at 8.50-7.00 ppm corresponding aromatic protons in CI species are shown. These results confirm that mono-substituted PEG-BzAc-OH could be the major product (>98% efficiency) and undesired dimer (PEG-BzAc-PEG) could be negligible.

The second step is the coupling reaction of the purified PEG-BzAc-OH with iBuBr in the presence of Et₃N. Excess iBuBr was used to maximize the coupling efficiency of the esterification. The product was purified by precipitation from diethyl ether at >95% yield. Its ¹H NMR spectrum in Figure 3.5c shows the new peak at 1.90 ppm (methyl protons of bromine species, e), along with 5.50 ppm (methine proton in acetal moiety, b) and 3.20 ppm (methoxy protons in PEG moiety, c). Their integral ratio is quantitative to the number of protons present in the product (Figure A17), suggesting >98% efficiency of the esterification. These results confirm the synthesis of well-defined PEG-BzAc-Br ATRP macroinitiator.

The synthesized PEG-BzAc-Br was examined for its acid-responsive degradation, for comparison with BzAc-DOH, its corresponding diol precursor, using ¹H NMR spectroscopy in 3/1 v/v CD₃CN/PB-D₂O mixtures at pD = 5.0, 6.5, and 7.4 (Figures A18-A20). Similar to BzAc-DOH, %hydrolysis was determined as the integral ratio of aldehyde proton at 9.8 ppm to acetal methine proton at 5.4 ppm. As seen in Figure A21, percent hydrolysis rates of PEG-BzAc-Br

appeared to be similar to those of BzAc-DOH precursor at pDs. These results suggest that relatively long PEG chains have no significant effect on acid-catalyzed hydrolysis of BzAc group.

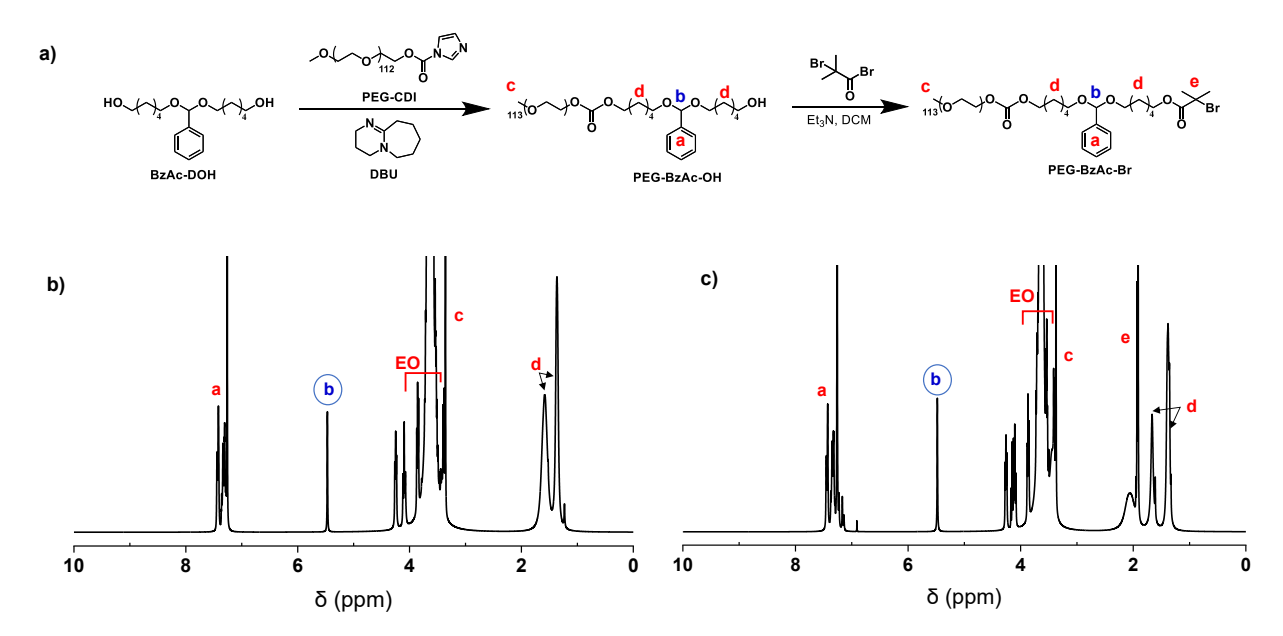


Figure 3.5. Synthesis of PEG-BzAc-Br ATRP macroinitiator (a) as well as ¹H NMR spectra of PEG-BzAc-OH (b) and PEG-BzAc-Br (c) in CDCl₃.

3.3.4 Synthesis of Acid-Degradable BzAc-Labeled Shell-Sheddable ABP. Given such promising results, we have synthesized a well-defined acid-degradable shell-sheddable ABP bearing BzAc linkage at the junction of hydrophilic and hydrophobic blocks. Figure 3.6a shows our approach utilizing Activator ReGenerated by Electron Transfer process for ATRP (ARGET ATRP).³¹⁴ BM was chosen to form a hydrophobic polymethacrylate block in consideration that phenyl pendants could enhance the loading capacity of drug molecules that contain aromatic species such as doxorubicin through π - π stacking.³¹⁵⁻³¹⁷

ARGET ATRP was conducted for BM with oxidatively-stable Cu(II)Br₂/TPMA complexes in the presence of PEG-BzAc-Br macroinitiator at 40 °C in anisole. The initial mole ratio of [BM]₀/[PEG-BzAc-Br]₀ was set to be 100/1, corresponding to the target degree of polymerization at complete monomer conversion to be 100. A reason is our intention to obtain the desired portion of PEG to be 30-40 wt% in the block copolymer and its nanoassemblies at monomer conversion of 50-60%.

After purification by precipitation from hexane at 45% monomer conversion, the formed copolymer was characterized by GPC for molecular analysis and 1 H NMR for structural analysis and determination of degree of polymerization (DP). Its GPC trace in Figure 3.6b shows the clear shift of molecular weight distribution to higher molecular weight with no significant trace of PEG-BzAc-Br macroinitiator. The formed copolymer had the number average molecular weight (M_n)= 15 kg/mol with narrow molecular weight distribution as M_w/M_n = 1.33. 1 H NMR in Figure 3.6c shows the presence of PEG block at 3.40-3.60 ppm (EO) and polyBM block at 0.70-0.90 ppm for methyl protons (c). With their integral ratio, along with the DP of PEG block to be 113, the DP of polyBM block was determined to be 51 (DP = 45 based on 45% monomer conversion). More promisingly, the peak at 5.50 ppm corresponding to methine proton (a) is presented, which indicates the junction BzAc group remained intact during ATRP. These results, as summarized in Table 3.2, confirm the synthesis of well-controlled shell-sheddable ABP with a benzaldehyde acetal linkage at the block junction, thus PEG113-BzAc-PBM51.

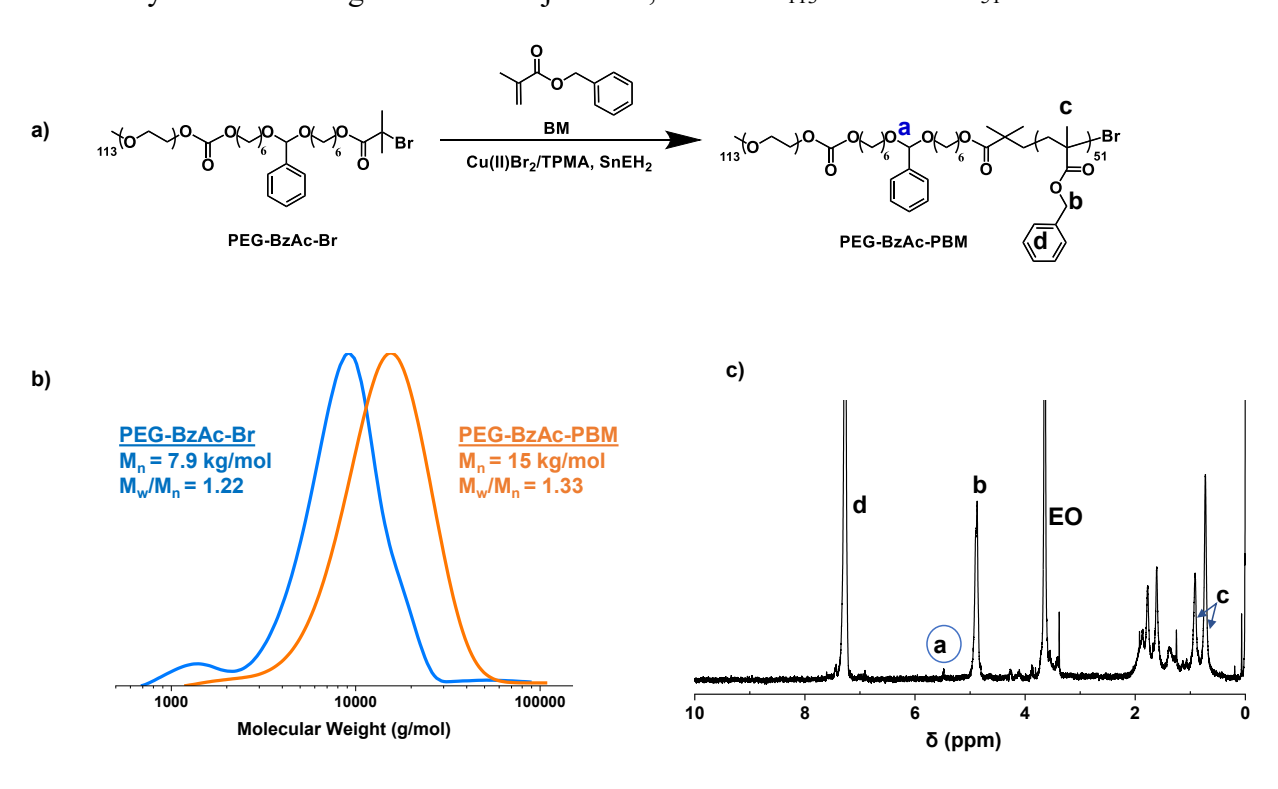


Figure 3.6. Synthesis by ARGET ATRP (a), GPC diagram compared with that of PEG-BzAc-Br macroinitiator (b), and ¹H NMR spectrum in CDCl₃ of well-defined PEG-BzAc-PBM sheddable block copolymer bearing acid-labile BzAc at the block junction (c). Conditions for ATRP: [BM]₀/[PEG-BzAc-Br]₀/[Cu(II)Br₂/TPMA]₀/[TPMA]₀ = 100/1/0.05/0.15 in anisole at 40 °C, BM/anisole = 0.25 wt/wt.

Table 3.2. Characteristics and properties of PEG-BzAc-Br macroinitiator and PEG-BzAc-PBM ABP.

Recipe	[BM] ₀ /[PEG- BzAc-Br] ₀	Time (hrs)	DP b)	M _n c) (kg/mol)	Đ c)
PEG-BzAc-Br	-	-	-	7.9	1.22
PEG-BzAc-PBMa)	100/1	3	51	15	1.33

a) Conditions for ATRP: [BM]₀/[PEG-BzAc-Br]₀/[Cu(II)Br₂/TPMA]₀/[TPMA]₀ = 100/1/0.05/0.15 in anisole at 40 °C, BM/anisole = 0.25 wt/wt; b) Determined by ¹H-NMR; c) GPC with PMMA standards

3.3.5 Acid-Responsive Degradation of PEG-BzAc-PBM. Figure 3.7a illustrates the degradation of PEG-BzAc-PBM upon the cleavage of the junction BzAc linkage through acidcatalyzed hydrolysis to the corresponding degraded products (PEG-OH, HO-PBM, and BzA) when being exposed to acidic pH. Acid-responsive degradation of the copolymer was investigated in THF (a homogeneous solution) using GPC technique to follow any changes of its molecular weights and distributions. As seen in Figure 3.7b, the GPC diagram of the degraded products was shifted to low molecular weight region, with the decrease in the molecular weight from $M_n = 15$ to 5 kg mol⁻¹. Furthermore, molecular weight distribution became bimodal with a shoulder in lower molecular weight region, which corresponds to the degraded PEG-OH. The distribution in higher molecular weight region could correspond to HO-PBM. Our further investigation to acid-responsive cleavage of the benzacetate acetal linkages was conducted using ¹H NMR spectroscopy. An aliquot of PEG-BzAc-PBM at a concentration of 20 mg/mL was incubated with DCl in an NMR tube for 24 hours. Figure 3.7c shows the appearance of the new peak at 10 ppm presenting an aldehyde proton of BzAc and the disappearance of the peak at 5.50 ppm corresponding to methine proton in BzAc moiety. These results obtained from combined GPC and NMR analysis confirm the cleavage of BzAc linkage in PEG-BzAc-PBM at acidic pH.

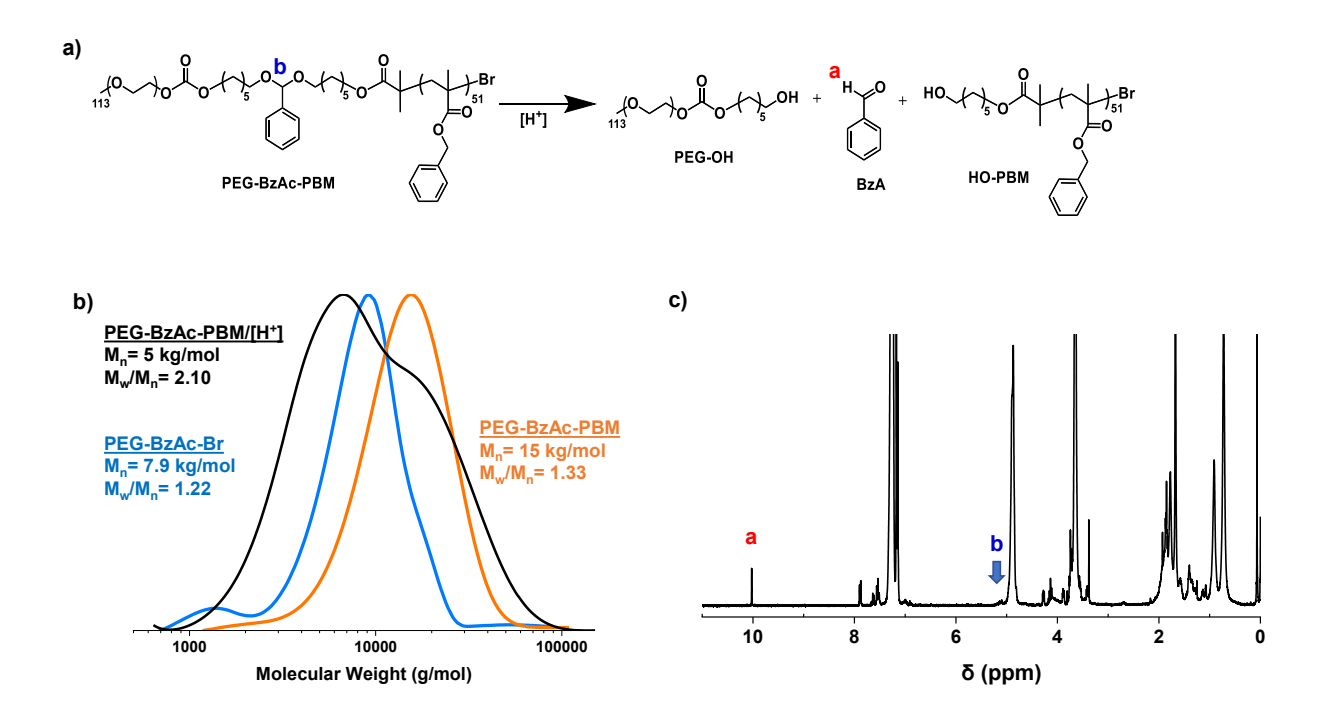


Figure 3.7. Schematic illustration of acid-responsive degradation (a), GPC diagram before and after treatment with acid in THF, compared to PEG-BzAc-Br initiator (b), and ¹H NMR spectrum in CDCl₃ of degraded products formed through acid-catalyzed hydrolysis (c) of PEG-BzAc-PBM sheddable block copolymer after 24 hours.

3.3.6 Aqueous Micellization and Cytotoxicity. The formed PEG-BzAc-PBM block copolymer consists of both hydrophilic PEG and hydrophobic PBM blocks with a BzAc at the block junction, thus undergoing self-assembly to form colloidal nanoassemblies in aqueous environments (Figure 3.8a). Given the amphiphilicity, its CMC was determined using a fluorescence spectroscopic technique with a NR probe. 42 Figure 3.8b shows the maximum fluorescence intensity of NR over an increasing concentration of PEG-BzAc-PBM, which is constructed from their fluorescence spectra (Figure A22). At its lower concentration, the NR fluorescence intensity remained low because of the existence of most NR molecules in aqueous solution. Upon increasing the concentration of PEG-BzAc-PBM, the fluorescence intensity increased as a consequence of the encapsulation of NR molecules in nanoassemblies. Their linear progressions allow for the determination of CMC of PEG-BzAc-PBM to be 50 μg mL⁻¹.

Given its CMC, the copolymer was examined for aqueous micellization using a dialysis method with DMSO at 1 mg mL⁻¹, above its CMC. DLS analysis confirms the formation of

nanoassemblies with the average diameter = 147 nm and monomodal distribution (Figure 3.8c). TEM analysis shows that the morphology of these nanoassemblies is spherical (Figure 3.8d and Figure A23). Their average diameter was 78.2 ± 25.3 nm (Figure A24), which appears to be smaller than that determined by DLS, because of nanoassemblies being in dried state for TEM measurements. Interestingly, solvent evaporation method with THF yielded nanoassemblies with multimodal distribution at the same concentration.

The formed nanoassemblies fabricated through dialysis method were examined for cell viability. Various concentrations of nanoassemblies were incubated with HeLa cells for 24 hrs. A MTT assay based on colorimetric analysis was employed to determine the viability of HeLa cells. As seen in Figure A25, the viability was >85% in the presence of the nanoassemblies at the concentrations up to 560 µg/mL, suggesting that PEG-BzAc-PBM is noncytotoxic.

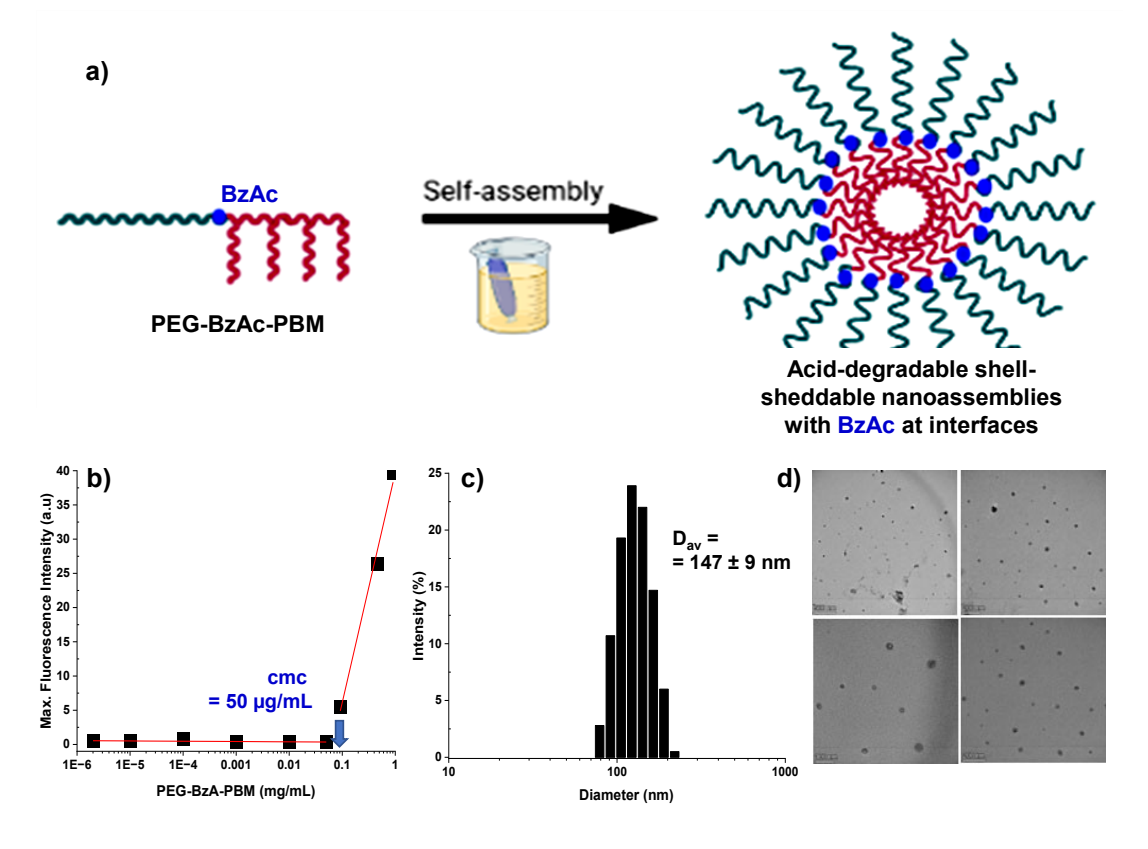


Figure 3.8. Schematic illustration of aqueous micellization through self-assembly of PEG-BzAc-PBM (a), fluorescence intensity at maximum wavelength for aqueous mixtures consisting of NR with various amounts of PEG-BzAc-PBM to determine CMC (b), DLS by intensity (c) and TEM image with scale bar = 200 nm (d) of nanoassemblies at 1 mg mL⁻¹.

3.3.7 Acid-Responsive Disassembly. We then investigated acid-responsive disassembly of shell-sheddable aqueous nanoassemblies (Figure 3.9a). As seen in Figure 3.9b-3.9d, their size distribution was kept unchanged at pH = 7.4. When being incubated at acidic pHs = 6.5 and 5.0, their size distributions were shifted to large size region with increasing average diameters. Furthermore, large precipitates observed in the bottom of vials. Given our acid-catalyzed hydrolysis of PEG-BzAc-PBM copolymer in THF, such increases in size and size distribution of nanoassemblies could be attributed to the detachment of PEG corona chains from the cores as a consequence of the cleavage of benzaldehyde acetal linkages at the interface of core/corona. Such detachment could cause the disintegration of the nanoassemblies. The hydrophobic cores generated from the detachment of PEG corona could be agglomerated, increasing the shift of the size distribution in their DLS diagram. The agglomeration was confirmed by TEM analysis (Figure 3.9e). Our quantitative analysis to acid-responsive disassembly was furthered confirmed with the evolution of their z-average diameter (by intensity) over incubation time (Figure 3.9f). The diameter increased abruptly at pH = 5.0, while it increased gradually at pH = 6.5. After longer period of time, the particles remained aggregated, with little change in size. While these results are not beneficial for drug delivery applications, they are greatly promising in the support for our choice of benzaldehyde acetal linkage as a good candidate as acid-labile linkage for the junction of shell-sheddable block copolymers. This is a first step in understanding the fundamental aspects of how the choice of stimuli can greatly affect how the nanoassemblies break down and that one single stimulus is not sufficient for drug release. The need for dual/multi-stimuli is necessary, where choosing the fundamental stimuli within the hydrophobic core to avoid any agglomeration, will allow an enhanced drug release for biological applications. In addition, it is known that the benzaldehyde as a cleavage product is non-toxic as it is a natural compound biosynthesized by vegetables and is a product of the metabolism of plants. It also contains antibacterial activity against Staphylococcus aureus and toxic action against fruit flies. 318-320

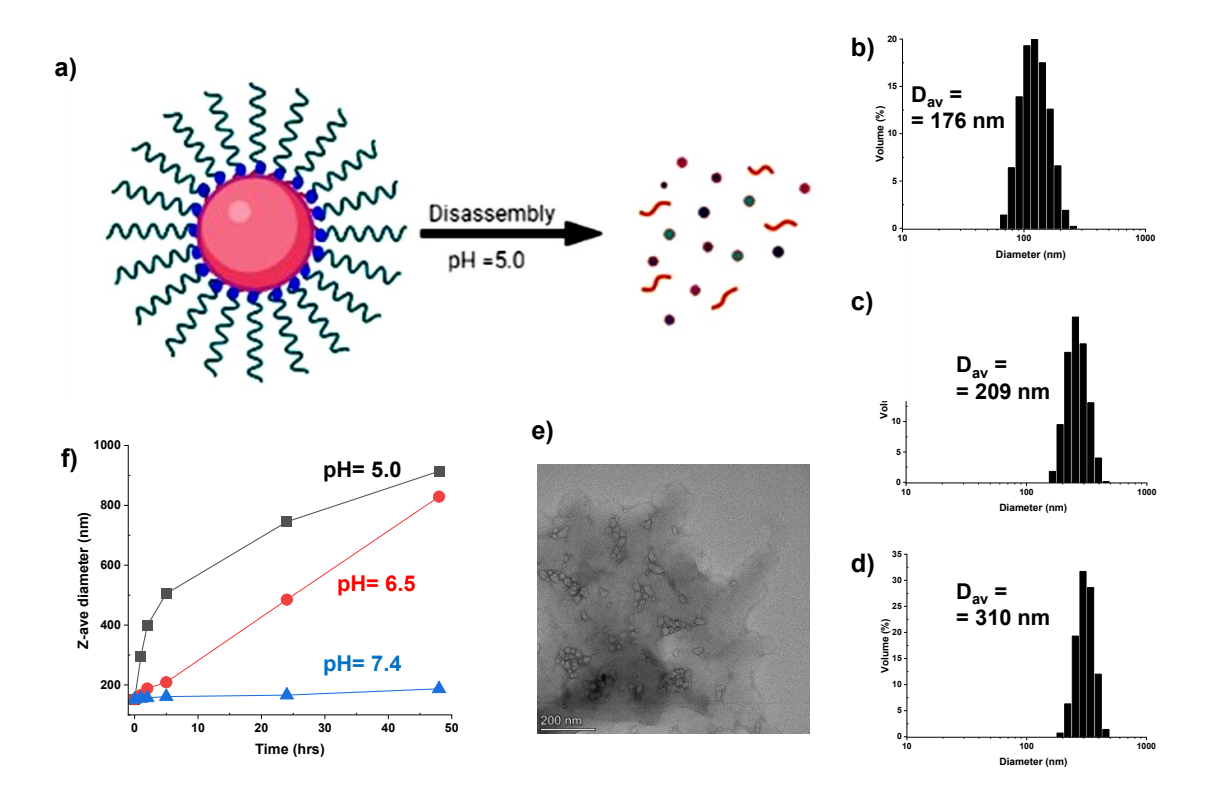


Figure 3.9. Schematic illustration of acid-responsive disassembly (a), DLS diagrams by volume incubated at pH = 7.4 (b), 6.5 (c), and 5.0 (d) for 24 hrs, TEM image with scale bar = 200 nm (e), evolution of z-average diameter over time incubated at pH = 7.4, 6.5, and 5.0 (f) of shell-sheddable nanoassemblies.

3.4 Conclusion

Three diol precursors bearing BzAc, CyHK, and CyPK groups were synthesized to investigate their acid-catalyzed hydrolysis at various pHs: 5.0 (endo/lysosomal pH), 6.5 (tumoral pH), and 7.4 (physiological pH). Our ¹H NMR analysis confirms the order of increasing acid-catalyzed hydrolysis to be CyPK>CyHK>BzAc at pH = 5.0, which would be attributed to their inductive and/or resonance effect. More importantly, BzAc had slow hydrolysis with t_{1/2} > 240 hr at pH = 6.5 and relatively rapid hydrolysis with t_{1/2} = 60 hr at pH = 5.0, suggesting that BzAc group could be suitable for the junction acid-labile group of acid-degradable shell-sheddable ABPs. With such promising results, a well-defined block copolymer labeled with BzAc group at the junction of PEG and PBM blocks was synthesized by ATRP in the presence of PEG-BzAc-Br macroinitiator. The formed block copolymer self-assembled to form aqueous colloidally-stable nanoassemblies with BzAc groups at the core/corona interfaces. The formed

nanoassemblies turned to be noncytotoxic up to $560~\mu g/mL$. Furthermore, they disassembled in acidic pHs; promisingly their response turned to be slower at pH = 6.5, but faster at pH = 5.0, while being stable at pH = 7.4, based on our DLS and TEM analysis. These results confirm that our approach with the choice of BzAc linkage as the block junction is promising in the development of acid-degradable shell-sheddable nanoassemblies and further dual acid/stimulus-degradable nanoassemblies as advanced drug delivery nanocarriers.

Chapter 4: Synthesis and Acidic pH-Responsive Disassembly of Dual Shell-Sheddable/Core-Degradable Block Copolymer Nanoassemblies

4.1 Introduction

Development of well-defined amphiphilic block copolymers (ABPs) and their nanoassemblies designed to degrade in acidic environments has been extensively explored as a promising platform for tumor-targeting drug delivery. Such efforts have been made because acidic pH is an endogenous stimulus found in biological environments, particularly tumoral extracellular compartments at pH = 6.5-6.9 and endosomes and lysosomes at pH = 4.5–5.5.^{71, 72, 321} A prevailing approach to synthesize acid-responsive degradable ABPs involves the incorporation of acid-labile linkages, typically acetal, ketal, benzoic imine, and 2,3-dialkylmaleamidic amide groups. These linkages have been positioned in a single location, as in hydrophobic cores (called core-degradable nanoassemblies) and at the interfaces of cores and coronas (called shell-sheddable nanoassemblies). ^{124, 135, 146, 152, 153, 322-325}

To address these issues, dual-location acid-responsive degradation strategy with the synthesis of acid-degradable nanoassemblies labeled with acid-labile linkages in both core and core/corona interface has been proposed. In acidic environments, they could be disintegrated through both the detachment of hydrophilic coronas upon the cleavage of the linkage at the interfaces as well as the change in hydrophobic/hydrophilic balance upon the cleavage of the linkage in hydrophobic cores simultaneously. ^{32, 36, 136, 294, 326-330} Such acid response in dual locations could accelerate the release of encapsulated hydrophobic drug molecules in acidic sites. Recently, we have demonstrated the versatility of dual location acid-responsive degradation strategy with the synthesis of well-defined PEG-based ABPs bearing acetaldehyde acetal (AcA) both at the block junction and in hydrophobic polymethacrylate block. Although their nanoassemblies exhibited synergistic responses to acidic pH both in core and at interface, they turned slowly degrade even at pH = 5, which is attributed to the slow acid-catalyzed hydrolysis of AcA group. ³³

Benzaldehyde acetal (BzAc) turned to exhibit optimal hydrolysis profiles in targeted pH ranges (e.g. pH = 5.0-6.5) and was identified to be a suitable candidate for junction acid-labile linkage: slow degradation at tumoral pH = 6.5 and rapid disassembly at endo/lysosomal pH = 6.5

5.0, while colloidal stability at physiological pH =7.4.¹³⁹ We envisioned that the suitability of BzAc for junction acid-labile group could refine the features of dual-location acid-degradation strategy. Furthermore, the strategy could be versatile with the choice of acid-labile groups in a hydrophobic block, enabling the tunable acid-catalyzed degradation of acid-degradable nanoassemblies.

In this work, we synthesized a well-defined poly(ethylene glycol) (PEG)-based ABP labeled with BzAc at the block junction and benzoic imine (BzI) pendants in the hydrophobic polymethacrylate block, thus forming PEG-BzAc-PBzI (called DLAD). Our synthetic approach explores the post-polymerization modification through a facile carbonylimidazole-hydroxy coupling reaction. Their nanoassemblies consisting of hydrophobic BzI cores at BzAc interfaces with PEG coronas underwent acid-responsive degradation through the detachment of PEG corona and the disruption of hydrophobic cores upon the cleavage of both BzAc and BzI groups in acidic pHs. They enabled to encapsulate curcumin anticancer drug and further exhibited the enhanced release of curcumin at pH = 5, while its slower release at pH = 6.5. Our work demonstrates that dual core/interface location acid-degradable nanoassemblies are advanced designs for effective tumor-targeting drug delivery with enhanced drug release.

4.2 Experimental

4.2.1 Instrumentations. ¹H NMR spectra were recorded using a 300 MHz Bruker spectrometer and a 500 MHz Varian spectrometer. The CDCl₃ singlet at 7.26 ppm, , CD₃CN singlet at 1.94 ppm, and D₂O singlet at 4.79 ppm were selected as the reference standards. Spectral features are tabulated in the following order: chemical shift (ppm); multiplicity (s - singlet, d - doublet, t - triplet, m - complex multiple); number of protons; position of protons. Monomer conversion was determined by ¹H NMR spectroscopy. Molecular weight and molecular weight distribution were determined by gel permeation chromatography (GPC). An Agilent GPC was equipped with a 1260 Infinity Isocratic Pump and a RI detector. Two Agilent PLgel mixed-C and mixed-D columns were used with DMF containing 0.1 mol% LiBr at 50 °C at a flow rate of 1.0 mL min⁻¹. Linear poly(methyl methacrylate) standards from Fluka were used for calibration. Aliquots of the polymer samples were dissolved in DMF with 0.1% lithium bromide and the clear solutions were filtered using a PTFE disk filter with 0.40 μm pores to remove any of insoluble species. A drop of anisole was added as a flow rate marker. The size and

size distribution of aqueous nanoassemblies in hydrodynamic diameter were measured by dynamic light scattering (DLS) at a fixed scattering angle of 175° at 25 °C with a Malvern Instruments Nano S ZEN1600 equipped with a 633 nm He-Ne gas laser. UV/vis spectra on an Agilent Cary 60 UV/vis spectrometer were recorded using a 1 cm wide quartz cuvette.

Transmission Electron Microscopy (TEM) images were obtained using a Thermo Scientific Talos F200X G2 (S)TEM located at the Facility for Electron Microscopy Research at McGill University. To prepare the specimens, aqueous dispersions of nanoassemblies (5 μL) were dropped on a copper grid with carbon coating (300 mesh size). After 3 min, the droplets were blotted off the grids using filter paper and dried at room temperature in a desiccator before measurements. The average diameter was calculated with >50 nanoassemblies in TEM images using ImageJ software.

4.2.2 Materials. Benzaldehyde (BzA, 98%), 1,1'-carbonyldiimidazole (CDI, 97%), 2-hydroxyethyl methacrylate (HEMA, 99%), 4-amino benzyl alcohol (98%), Curcumin (Cur) and Nile Red (NR) from Sigma-Aldrich or Alfa Aesar as well as tris(2-pyridylmethyl) amine (TPMA) from TCI Chemicals were purchased and used without further purification unless otherwise noted. Dialysis tubing made of cellulose membranes with molecular weight cut-off (MWCO) of 12-14 kDa was purchased from Spectra/Por. Anhydrous tetrahydrofuran (THF) was obtained from a solvent purification system using aluminum oxide columns. A PEG-based bromine macroinitiator bearing BzAc group (PEG-BzAc-Br), 139 carbonyl imidazole-bearing methacrylate (CIMA), 292 and benzoic imine (BzI-OH) were synthesized as described in our previous publications.

4.2.3 ATRP to Synthesize PEG-BzAc-PCIMA ABPs. PEG-BzAc-Br, CIMA, [Cu(II)Br/TPMA]Br, TPMA, and anisole (4.5 g) were mixed in a 10 mL Schlenk flask. The mixture was deoxygenated by purging under nitrogen for 1 hour. A nitrogen pre-purged solution of Sn(II)(EH)₂ dissolved in anisole (0.5 g) was injected into the Schlenk flask to initiate polymerization, and then placed in an oil bath at 40 °C. Polymerization was stopped after 40 min by cooling the reaction mixture in an ice bath and exposing it to air.

PBPM-50: PEG-BzAc-Br (0.48 g, 89.1 μmol), CIMA (1.00 g, 4.46 mmol), [Cu(II)Br/TPMA]Br (4.58 mg, 8.91 μmol), TPMA (6.47 mg, 22.2 μmol), Sn(II)(EH)₂ (7.23 mg, 17.8 μmol).

PBPM-100: PEG-BzAc-Br (0.24 g, 44.2 μ mol), CIMA (1.55 g, 4.42 mmol), [Cu(II)Br/TPMA]Br (4.58 mg, 8.91 μ mol), TPMA (6.47 mg, 22.2 μ mol), Sn(II)(EH)₂ (7.23 mg, 17.8 μ mol).

PBPM-200: PEG-BzAc-Br (0.12 g, 22.5 μmol), CIMA (1.00 g, 4.46 mmol), [Cu(II)Br/TPMA]Br (4.58 mg, 8.91 μmol), TPMA (6.47 mg, 22.2 μmol), Sn(II)(EH)₂ (7.23 mg, 17.8 μmol).

The as-synthesized copolymers were purified by passing through a basic alumina oxide column to remove tin and copper species, followed by precipitation from hexane three times to remove the residue CIMA monomers. The precipitates were isolated and dried in a vacuum oven at room temperature overnight.

To investigate kinetics, aliquots were taken periodically to analyze monomer conversion by ¹H NMR spectroscopy and molecular weight and its distribution by GPC.

4.2.4 Post-Polymerization Modification to Synthesize DLAD ABPs. The purified, dried PEG-BzAc-PCIMA (PBPM-100, 1.90 g, 70 μmol) was mixed with BzI-OH (1.42 g, 6.9 mmol) and DBU (0.53 g, 3.5 mmol) in DCM (10 mL) under stirring for 24 hours. The formed polymer was purified by precipitation from cold diethyl ether and dried in a vacuum oven set at 70 °C for 24 hrs.

4.2.5 Acidic pH-Responsive Degradation Studies. For PEG-BzAc-Br and BzI-OH, 0.2 M aqueous phosphate buffered saline (PBS) solutions in D₂O at potential of deuterium (pD) = 5.0, 6.5, and 7.4 were prepared by mixing aqueous stock solutions of NaH₂PO₄ (0.2 M) with Na₂HPO₄ (0.2 M) in D₂O at different volume ratios. pH values were measured using a pH meter with a glass electrode standardized with aqueous buffer solutions (pH = 4, 7 and 10). pD values were calculated using the equation of pD = pH (measured) + 0.41. To study hydrolysis, solutions of PEG-BzAc-Br (10 mg) and BzI-OH (10 mg) dissolved in CD₃CN (0.3 mL) were mixed with the as-prepared, 0.2 M aqueous PBS solutions in D₂O (PB-D₂O, 0.1 mL) at pD = 5.0, 6.5 and 7.4. The resultant mixtures were analyzed by ¹H NMR spectroscopy at 25 °C for given periods of time.

For DLAD, its aliquots (10 mg) were dissolved in CDCl₃ (1 mL) containing DCl (20 μ L) and their ¹H NMR spectra were recorded at given time intervals. Similarly, aliquots of DLAD

(10 mg) were dissolved in DMF (0.1% LiBr, 2 mL) containing HCl (20 μ L) and their GPC traces were recorded at given time intervals.

- 4.2.6 Determination of Critical Micelle Concentration (CMC) using a NR probe. A stock solution of NR in THF at 1 mg mL⁻¹ and two stock solutions of DLAD in THF at 1 mg mL⁻¹ and 0.1 μ g ml⁻¹ were prepared. The same volume of the stock solution of NR (0.5 mL, thus, 0.5 mg NR) was mixed with the various volumes of the stock solutions of DLAD. Water (0.5 mL) was then dropwise added to the resulting organic solutions of NR and DLAD at room temperature. The resulting dispersions were stirred overnight to remove THF in a fume hood. After water was added to keep their concentrations consistent, the resulting dispersions were subjected to centrifugation (2500 rpm for 5 min, followed by filtration using a disk-type PES filter with 0.45 μ m pores to remove excess NR. A series of NR-loaded nanoassemblies at various concentrations of DLAD ranging from 10⁻⁶ to 0.1 mg mL⁻¹ were prepared and their emission spectra upon excitation at $\lambda_{ex} = 350$ nm were recorded.
- **4.2.7 Aqueous Micellization by Solvent Evaporation Method.** Deionized water (pH = 7.4, 10 mL) was added dropwise to an organic solution of DLAD in acetone (2.0 mL) using a syringe pump equipped with a plastic syringe (20 mL, 20 mm diameter) at an addition rate of 0.2 mL min⁻¹. The resulting dispersion was heated at 30 °C to evaporate acetone for 24 hrs, yielding aqueous dispersion of nanoassemblies at 6 mg mL⁻¹.
- **4.2.8** Acidic pH-Responsive Disassembly of DLAD-based Nanoassemblies. Aliquots of aqueous nanoassemblies of DLAD (1 mL, 1 mg mL $^{-1}$) were mixed with aqueous acetate buffer (3 mL) to adjust their pHs to be 5.3 and 6.5 as well as PBS (3 mL, pH = 7.4). Their mixtures were analyzed by DLS technique.
- **4.2.9 Encapsulation of Cur.** Typically, Cur (5.5 mg) and DLAD (50 mg) were dissolved in acetone (2 mL). Water (10 mL, pH = 7.4) was drop-wise added under a magnetic stirring in a fume hood for 24 hrs to remove acetone. The resulting dispersions were subjected to a centrifugation (10,000 rpm and 10 minutes) and the supernatant was removed from the free Curcumin. The dispersions were passed through a disk-type PES filter (0.45 μ m pore, xx diameter), yielding aqueous Cur-loaded nanoassemblies (Cur-NPs) at 6 mg mL⁻¹.

For quantitative analysis, aqueous Cur solutions (10 mL) were prepared as Cur (55 μ g) being dissolved in PBS at pH = 7.4 and Cur (55 μ g) in acetate buffer solution at pH = 5.3.

Aliquots (1 mL) of the resultant transparent solutions were diluted with ethanol (4 mL) to prepare a series of solutions of Cur at various concentrations. Their UV-Vis spectra were recorded to determine the extinction coefficient of Cur in a mixture of water/ethanol (1/4 v/v).

To determine encapsulation efficiency (EE%) and loading content (LC%) of Cur using a UV/vis spectroscopy, an aliquot of aqueous Cur-NPs (2 mL) was mixed with ethanol (8 mL) to form transparent solutions. After being passed through a disk-type PTFE filter (0.25 μ m pore size), their UV/vis spectra were recorded. The EE% and LC% were determined by the following equations:

1)
$$EE\% = \frac{\text{Weight of Curcumin encapsulated in micelles}}{\text{Weight of feeding Curcumin}} * 100\%$$

2)
$$LC\% = \frac{Weight\ of\ Curcumin\ encapsulated\ in\ micelles}{Weight\ of\ micelles + encapsulated\ Curcumin} * 100\%$$

To get an insight to the effect of the weight ratio of Cur/DLAD on the loading and efficiency of Cur, a series of aqueous Cur-NPs with the varying wt ratios of Cur/DLAD were prepared from the mixtures of a given amount of Cur (5.5 mg) with varying amounts of DLAD (275 mg, 92 mg, 50 mg, 27.5 mg, 18.3 mg, 13.8 mg, 10 mg). Their UV/vis spectra were recorded. The detailed characteristics and properties are summarized in Table B1.

4.2.10 Acidic pH-Responsive Release of Cur. Aliquots of Cur-NP dispersion (6 mg mL⁻¹, 2 mL) were transferred into a dialysis tubing (MWCO = 12 000 g mol⁻¹) and immersed in aqueous PBS solution (40 mL) at pH = 7.4 and aqueous acetate buffer solution (40 mL) at pH = 5.3 and pH = 6.5. Aliquots (4 mL) were taken and mixed with ethanol (16 mL, thus water/ethanol = 1/4 v/v). Their UV-Vis spectra were recorded. The equal volume of fresh buffer solution was added to keep the same volume of outer buffer solution.

4.3 Results and Discussion

4.3.1 Synthesis of Well-Defined DLAD ABPs. Figure 4.1 depicts our approach with two steps, including i) an ATRP of CIMA in the presence of PEG-BzAc-Br, forming reactive PEG-BzAc-PCIMA ABPs, and ii) its post-polymerization modification with BzI-OH.

Figure 4.1. Our approach to synthesize well-defined DLAD PEG-BzAc-PBzI ABPs by ATRP of CIMA in the presence of PEG-BzAc-Br, forming reactive PEG-BzAc-PCIMA ABPs, followed by its post-polymerization modification with BzI.

4.3.2 Synthesis of PEG-BzAc-PCIMA BCP. An Activators Generated by Electron Transfer (AGET) for ATRP (called AGET ATRP) was examined for CIMA in the presence of an acid-degradable PEG-BzAc-Br macroinitiator, catalyzed by Cu(II)/TPMA complexes at 40 °C in anisole. As an initial thrust, the initial mole ratio of [CIMA]₀/[PEG-BzAc-Br]₀ was set to be 100/1, which corresponds to the target degree of polymerization (DP) of PCIMA block to be 100 at complete monomer conversion (PBPM-100). As-synthesized copolymer was purified by precipitation from hexane, when monomer conversion reached 90% in 40 min.

 1 H NMR in Figure 4.2a shows the characteristic peaks at 8.2-7.0 ppm (a) corresponding to aromatic imidazole protons, and peaks at 0.8-1.0 ppm (b) corresponding to methyl protons in PCIMA block, along with peaks at 3.40-3.60 ppm (EO) presenting PEG block. With the integral ratio of the peaks [(d/3)/(EO/4)] with the DP = 113 for PEG block, the DP of the PCIMA block

was determined to be 96, thus forming PEG₁₁₃-BzAc-PCIMA₉₆ ABP. The formed PBPM-100 had its molecular weight by number average (M_n) = 35.6 kg/mol with molecular weight distribution as narrow as its dispersion (D)= 1.22 by GPC analysis (Figure 4.2b). Its GPC trace clearly shifted to higher molecular weight region with a negligible trace of PEG-BzAc-Br macroinitiator, indicating the successful chain extension of PEG-BzAc-Br with PCIMA block.

Given the synthesis of PBPM-100, the initial mole ratio of [CIMA] $_0$ /[PEG-BzAc-Br] $_0$ was varied with 50/1 (PBPM-50) and 200/1 (PBPM-200) to see the feasibility of our approach to synthesize well-defined PEG-BzAc-PCIMA ABPs with different DPs of PCIMA blocks. Similar to PBPM-100, the purified copolymers were characterized using 1 H NMR spectroscopy for PBPM-50 and PBPM-200 (Figure B1) and their overlaid GPC trace (Figure B2). Table 4.1 summarizes their characteristics and properties. Monomer conversion reached 90% in 60 min for BA-P50, while 42% in 180 min for BA-P200. The plausible reason for slow polymerization with PBPM-200 could be due to the lower concentration of initiators and Cu complex in the recipe. The DP of PCIMA block was 73 for PBPM-50 and 80 for PBPM-200. Molecular weight determined by GPC was M_n = 29.4 kg/mol for PBPM-50 and M_n = 36.1 kg/mol for PBPM-200, with D= 1.09-1.22.

Table 4.1. Characteristics and properties of PEG-BzAc-PCIMA under different initial mole ratios in anisole.^{a)}

Recipe	[CIMA] ₀ /[PEG- BzAc-Br] ₀	Time (min)	Conv. b) (%)	DP b)	M _n ,Theo ^{c)} (kg/mol)	$M_{n,GPC}^{d)}$ (kg/mol)	∌ d)
PBPM-50	50/1	60	90	73	21.9	29.4	1.09
PBPM-100	100/1	40	90	96	25.4	35.6	1.22
PBPM-200	200/1	100	42	80	23.4	36.1	1.12

a) Conditions: $[CIMA]_0/[PEG-BzAc-Br]/[Cu(II)Br_2/TPMA]/[TPMA] = (50, 100 \text{ or } 200)/1/0.2/0.5 \text{ in anisole at } 40 \,^{\circ}\text{C}, CIMA/anisole = 0.40/1 \text{ wt/wt; b) determined by } ^{1}\text{H NMR; c)} M_n = DP x conv. + MW of PEG-BzAc-Br; and d) determined by GPC with PMMA standards.$

In a separate experiment, kinetics for ARGET ATRP of CIMA in the presence of PEG-BzAc-Br was investigated with a choice of PBPM-100 as a typical example. As shown in Figure B3, the polymerization is first order, suggesting the constant concentration of active centers during polymerization, up to 90% conversion. Molecular weight increased linearly with conversion and dispersity was as low as 1.20. Moreover, GPC diagram evolved to higher

molecular wight region over conversion. These results suggest that the ARGET ATRP of CIMA in the presence of PEG-BzAc-Br proceeded in a controlled manner.

4.3.3 Post-Polymerization Modification to Synthesize DLAD ABPs. Post-polymerization modification of PEG-BzAc-PCIMA was explored through a CDI-mediated coupling reaction with a diol precursor bearing a conjugated benzoic imine (BzI-OH) to synthesize PEG-BzAc-PBzI (DLAD) ABPs. The mole equivalent ratio of OH to pendant CI was set to be 1/1 to facilitate the purification step due to the sensitivity of imine bonds even in a neutral environment. As compared with ¹H NMR spectra of PEG-BzAc-PCIMA and BzI-OH precursors, Figure 4.2a shows the appearance of the characteristic peaks at 5.5-4.0 ppm (f, g, h), while disappearance of aromatic imidazole protons at 8.2-7.0 ppm. Their integrals are quantitative to the number of their protons. GPC trace of the copolymer shifted to higher molecular weight region with an increasing M_n from 35.6 to 42.6 kg/mol (Figure 4.2b). These results confirms the successful conjugation of PEG-BzAc-PCIMA with BzI-OH, yielding PEG-BzAc-PBzI (DLAD) ABP.

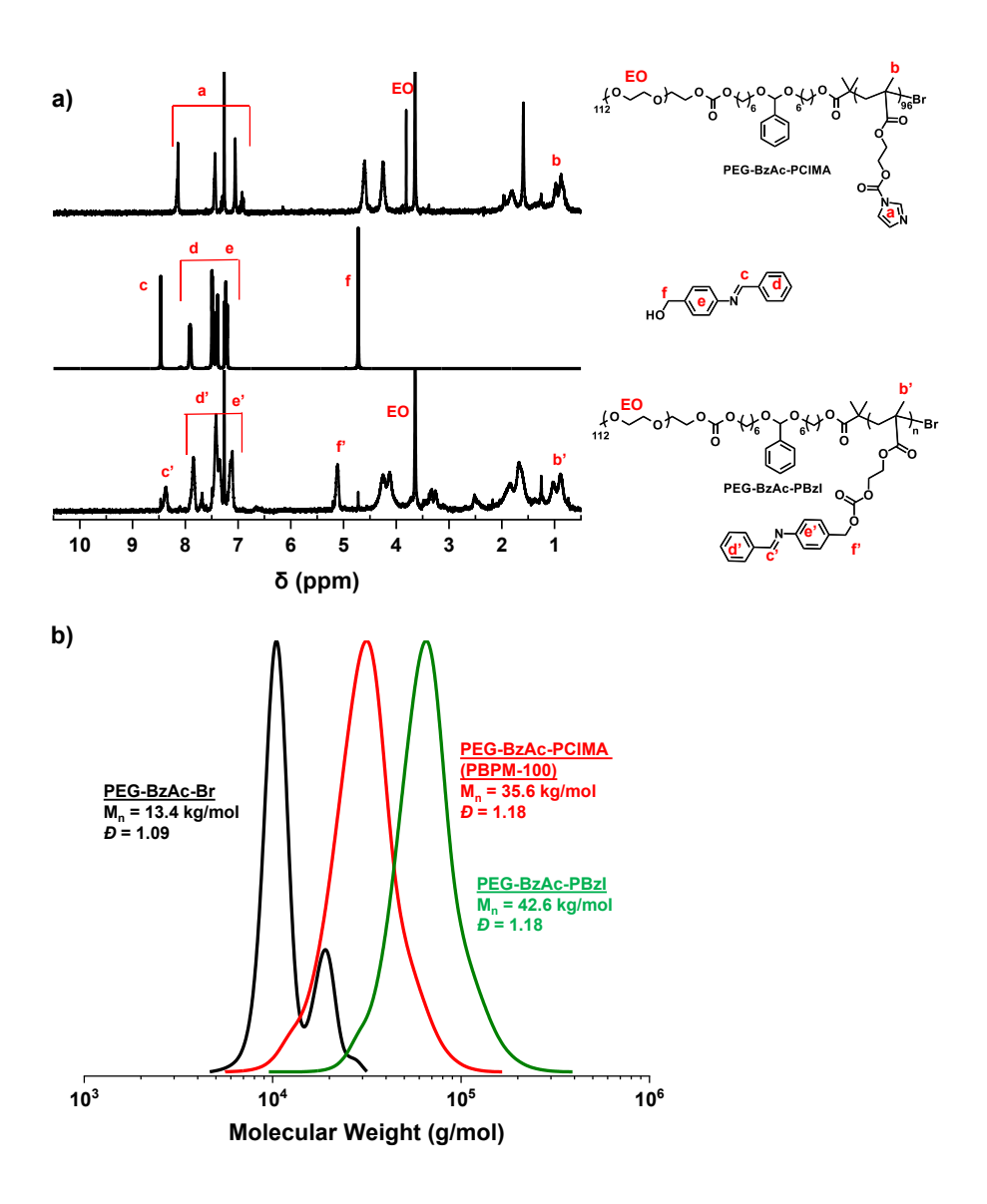


Figure 4.2. Overlaid ¹H NMR spectra in CDCl₃ of PEG-BzAc-PCIMA, BzI-OH, and DLAD (a) and overlaid GPC diagrams of PEG-BzAc-Br, PEG-BzAc-PCIMA, and DLAD (b).

4.3.4 Studies of Acid-Responsive Degradation of DLAD and Precursors. Figure 4.3a depicts the acid-responsive degradation of DLAD to its degraded products including PEG-OH, benzaldehyde, and HO-PM upon the cleavage of both junction BzAc and pendant BzI groups through acid-catalyzed hydrolysis. GPC technique was first examined for the qualitative analysis of the acid-degradation of DLAD in the presence of HCl (an acid) in DMF. As seen in Figure 4.3b, its GPC trace shifted to lower molecular weight region with the decrease in its molecular weight from $M_n = 42.6$ to 18.0 kg/mol. The molecular weight distribution of the degraded

products (e.g. PEG-Br and OH-PM) became bimodal. A shoulder in lower molecular weight region could correspond to the degraded PEG-OH, while the main peak could be the HO-PM. Our deconvolution method allowed us to estimate the wt% of the degraded PEG-OH to be 14%, which is somewhat close to the theoretical wt% calculated from the recipe to be 18%. These GPC results suggest the significant cleavage of BzAc and BzI linkages of DLAD in the presence of acid. Given the promising GPC analysis, ¹H NMR spectroscopy was examined in an attempt to quantitatively analyze acid-responsive degradation of DLAD incubated with HCl in a mixture of CH₃CN/D₂O. As seen in overlaid ¹H NMR spectra in Figure B4, our ¹H NMR analysis did not appear to be straightforward because the characteristic peaks corresponding to imine protons of BzI pendants and aromatic protons in BzAc moieties are not clearly identified.

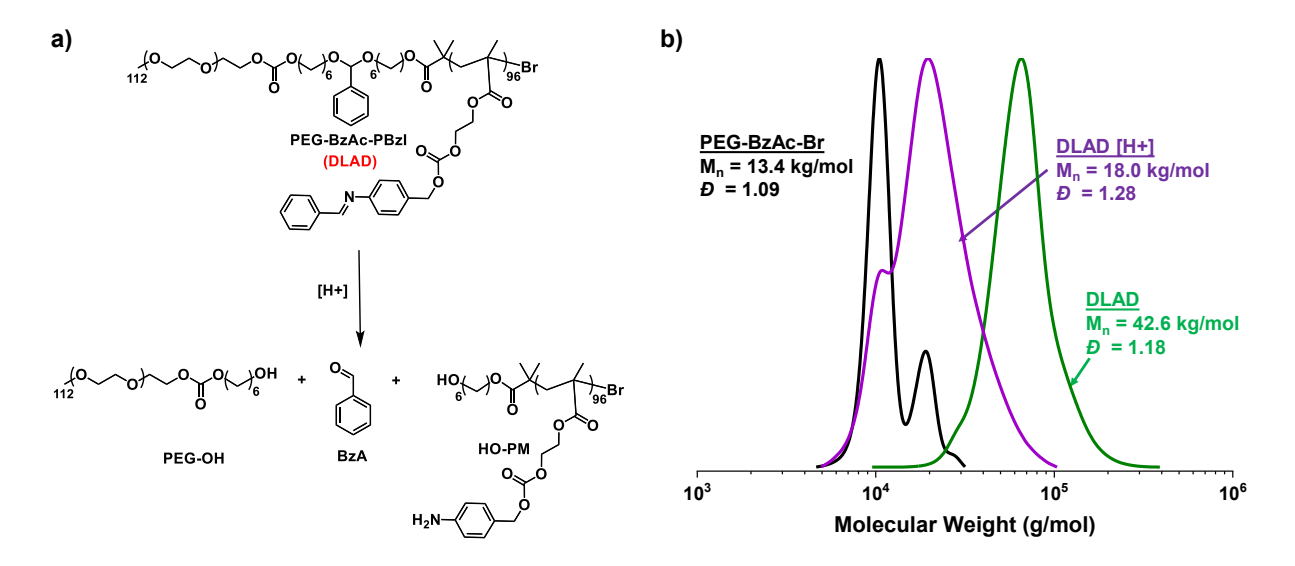


Figure 4.3. Acid-responsive degradation upon the cleavage of BzAc and BzI groups of DLAD ABP (a) and its overlaid GPC diagrams before and after treatment with HCl (acid) in DMF, compared with PEG-BzAc-Br macroinitiator (b).

In additional experiments, acid-responsive degradation of its precursors including PEG-BzAc-Br and BzI-OH was investigated using ¹H NMR spectroscopy. As depicted in Figure 4.4a and 4.4b, PEG-BzAc-Br degrades to corresponding PEG-OH, OH-Br, and benzaldehyde, while BzI-OH to 4-aminobenzyl alcohol (OH-aniline) and benzaldehyde. Figure B5-B10 shows overlaid ¹H NMR spectra of PEG-BzAc-Br and BzI-OH incubated at acidic pDs = 5.0 (endo/lysosomal pH) and 6.5 (tumoral pH), compared with pD = 7.4 (physiological pH) as a control at 25 °C. For quantitative analysis, the characteristic peaks of the precursors and their

degraded products could be used to calculate their %cleavage (e.g. %degradation or %hydrolysis). Typical peaks include machine proton (1H) in PEG-BzAc-Br precursor and benzyl protons (2H) of BzI-OH, along with aldehyde proton (1H) in benzaldehyde (a degraded product). Figure 4.4c and 4.4d show %cleavage over incubation time. For both PEG-BzAc-Br and BzI-OH, %cleavage increased over the incubation time at three pHs with its increasing order of pD = 5.0 > 6.5 > 7.4. As expected, %cleavage was greater for BzI-OH than PEG-BzAc-Br, confirming that acid-catalyzed hydrolysis is faster for BzI than BzAc bond. For example, $t_{1/2}$ which is the time for a half hydrolysis was 30 minutes for BzI, which is much greater than that for PEG-BzAc-Br (30 hrs) at pD = 5.0. Moreover, the cleavage of BzAc appeared be slower at pD = 6.5 and even much slower at pD = 7.4.

These results could imply that BzAc group at the block junction of DLAD and thus core/corona interfaces at DLAD-based nanoassemblies could slowly degrade at pH = 6.5 (e.g in tumoral extracellular compartment), while being stable at physiological pH = 7.4 (e.g. during blood circulation). BzI groups in hydrophobic cores, along with BzAc groups, degrade faster at pH = 5.0 (in endo/lysosomes after endocytosis to cancer cells).

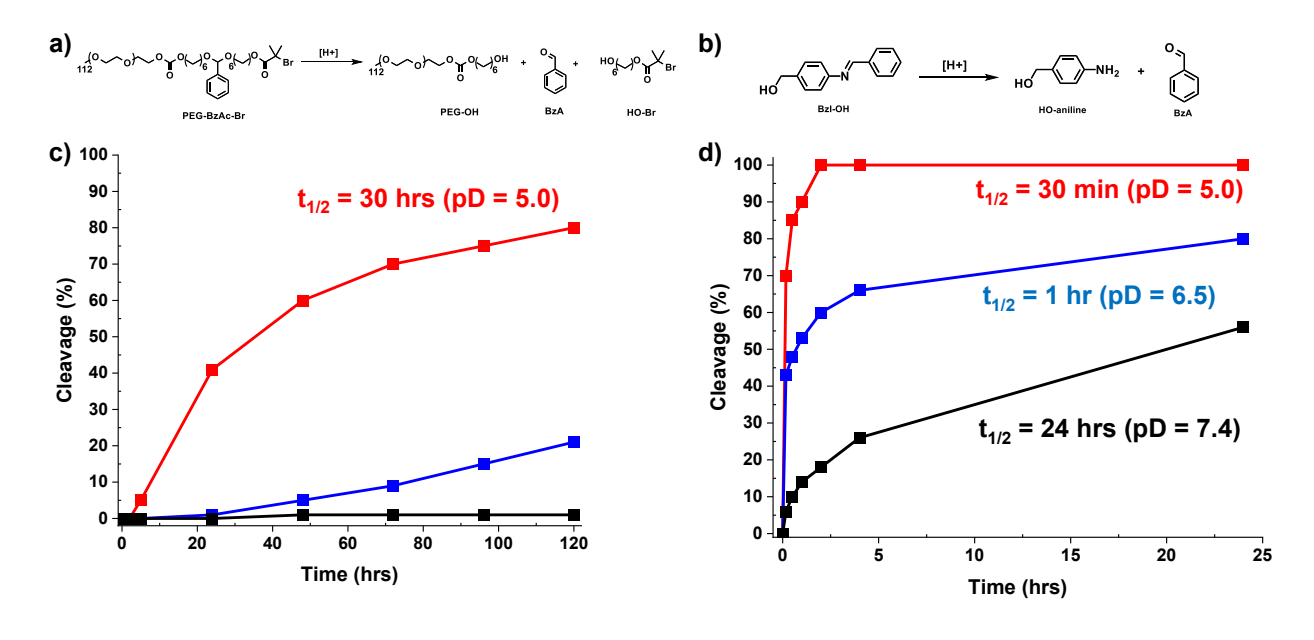


Figure 4.4. Schemes for acid-responsive degradation (a, b) and %degradation at pD = 5.0, 6.5, and 7.4 (c, d) for PEG-BzAc-Br (a, c) and BzI-OH (b, d).

4.3.5 Aqueous Micellization and pH-Responsive Disassembly. The formed DLAD ABP consists of both hydrophilic PEG and hydrophobic PBzI blocks with a BzAc at the block junction. Given the amphiphilicity, the ABP self-assembled in aqueous solution form colloidal nanoassemblies (Figure 4.5a). Its CMC was determined using a fluorescence spectroscopic technique with an NR probe. From the emission spectra for a series of mixtures consisting of the given amount of NR and the different amounts of DLAD (Figure B11), the maximum fluorescence intensity of NR over an increasing concentration of DLAD was constructed (Figure 4.5b). At its lower concentration, the NR fluorescence intensity remained low because of the existence of most NR molecules in aqueous solution. Upon increasing the concentration of DLAD, the fluorescence intensity increased as a consequence of the encapsulation of NR molecules in nanoassemblies. Their linear progressions allow for the determination of the CMC of DLAD to be 30 μg mL⁻¹. Given its CMC, the copolymer was examined for aqueous micellization using a solvent evaporation method with acetone, typically, at 6 mg mL⁻¹ above its CMC. The resulting nanoassemblies had an average diameter of 53.1 nm with monomodal distribution, by DLS analysis (Figure 4.5c). They turned to be spherical with average diameter was 27.7 ± 4.0 nm by TEM analysis (Figure 4.5d). The diameter by TEM analysis appeared to be smaller than that determined by DLS, because of their being in a dried state for TEM measurements.

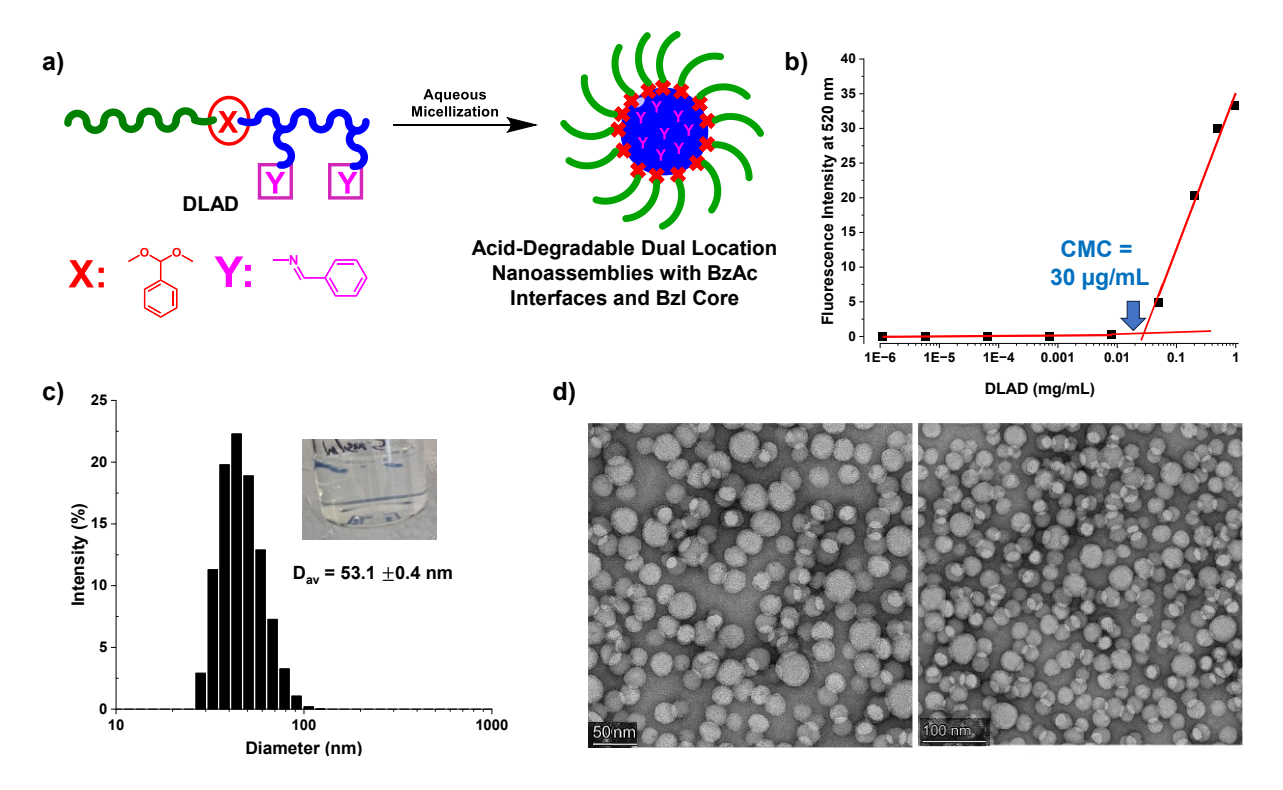


Figure 4.5. Schematic illustration of aqueous micellization through self-assembly of DLAD (a), fluorescence intensity at maximum wavelength for aqueous mixtures consisting of NR with various amounts of DLAD to determine CMC (b), DLS by intensity (c) and TEM images with different magnification nanoassemblies at 6 mg mL⁻¹ (scale bar = 50 nm (left) and 100 nm (right)) (d).

The formed DLAD-based nanoassemblies consist of acid-labile BzAc groups at the core/corona interfaces and BzI groups in the hydrophobic cores. As illustrated in Figure 4.6a, the nanoassemblies could degrade through the detachment of PEG coronas as well as the degradation of cores upon the cleavage of these acid-labile groups in acidic pHs. When being incubated in acidic pHs = 5.0 and 6.5, their size distributions became bimodal or multimodal with the population of aggregates (diameter > $0.7 \mu m$) (Figure 4.6b and Figure B12). The changes in size distributions were qualitatively analyzed with the evolution of their z-average diameter (by intensity) over incubation time (Figure 4.6c). At neutral pH, no change in z-average diameter was observed, which indicates that nanoassemblies are stable. At mild acidic pH = 6.5, the diameter increased from 54 nm to ≈ 75 nm in early 40 hrs and then did not appear to be significantly changed. At more acidic pH = 5.0, the diameter increased to ≈ 150 nm in 250 hrs and then abruptly increased to 400 nm. Such increases in size and size distribution of

nanoassemblies in acidic pHs could be attributed to acid-catalyzed hydrolysis of BzAc and BzI groups, leading to the detachment of PEG corona and degradation of cores. Such aggregation was confirmed by TEM analysis (Figure 4.6d).

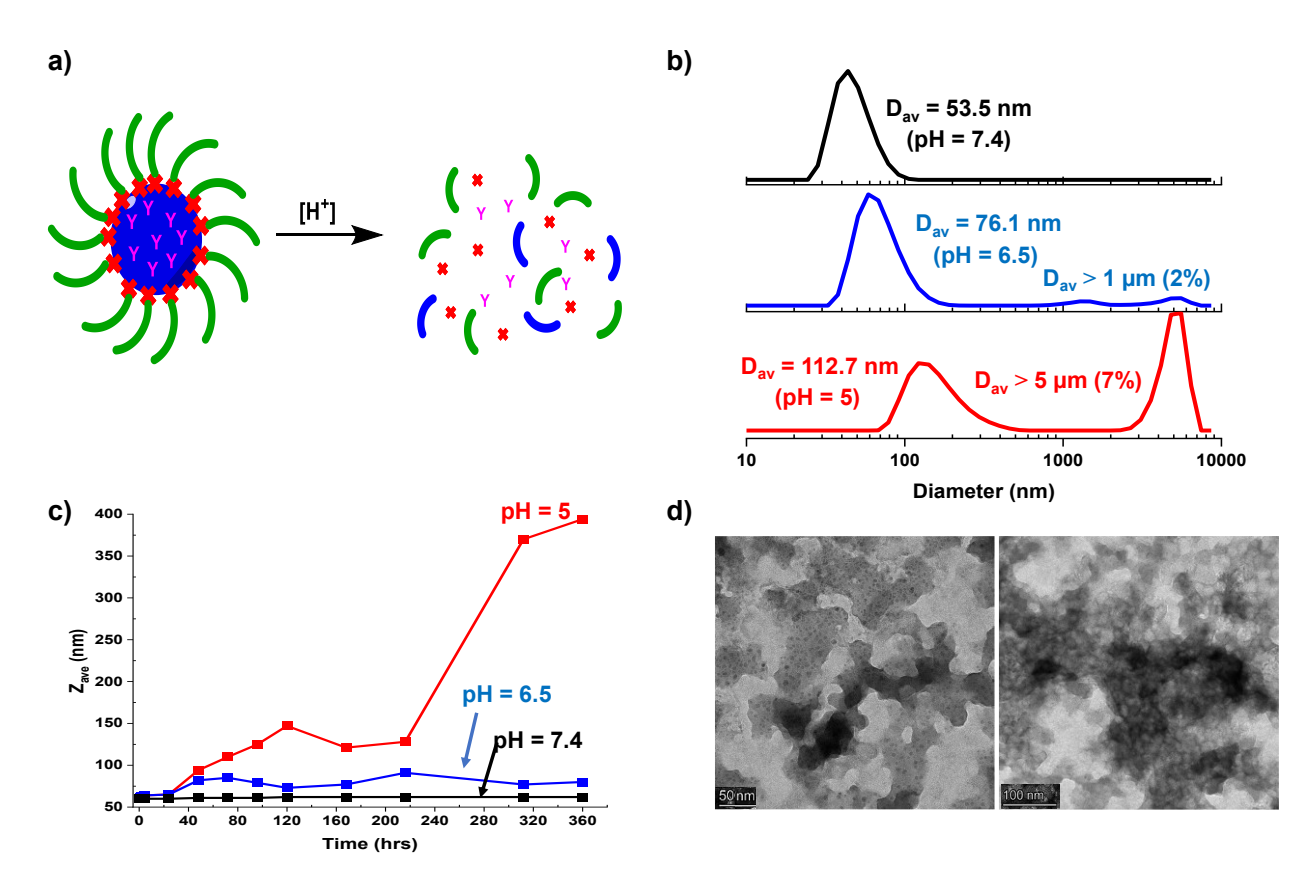


Figure 4.6. Schematic illustration of acid-responsive disassembly (a), overlaid DLS by intensity incubated at pH = 7.4, 6.5, and 5.0 after 72 hrs (b) evolution of z-average diameter over time incubated at pH = 7.4, 6.5, and 5.0 (c), and TEM images with scale bar = 50 nm (left) and 100 nm (right) of dual location nanoassemblies (d).

4.3.6 Loading and pH-Responsive Release of Cur. Cur is clinically used as a non-toxic anticancer drug. A solvent evaporation method with acetone, followed by centrifugation to remove free Cur, was examined to fabricate Cur-loaded DLAD nanoassemblies (Cur-NPs). With a typical wt/wt ratio of Cur/DLAD to be 2/1, aqueous dispersion of Cur-NPs in an orange color was fabricated at 6 mg mL⁻¹. They had an average diameter of 74.1 \pm 1.3 nm with monomodal distribution, by DLS (Figure 4.7a) and 41.8 \pm 4.2 nm with spherical morphology, by TEM analysis (Figure 4.7b). Next, LC% and EE% of Cur was determined using UV/vis spectroscopy. With their UV/vis spectrum and the pre-determined extinction coefficient of Cur (ϵ = 55,000 M⁻

¹cm⁻¹) in water/ethanol (1/4 v/v) (Figure B13), the LC% to be 2.0 wt% and EE% to be 99% were determined.

To get an insight into the effect of the amount of Cur on its LC% and EE%, a series of mixtures consisting of a given amount of DLAD (50 mg) with various amounts of Cur were prepared using the similar protocol (Figure B14 for their UV/vis spectra). When Cur/DLAD wt/wt ratio increased from 2/1 to 55/1 (e.g. decrease in the amount of Cur in the recipe), EE% decreased from 99% to 13%. Interestingly, LC% increased from 2.0 to 9.1% up to 11/1 ratio and then appeared to slightly decrease to 6.6% upon further increase in ratio.

Given our promising results on Cur loading, we investigated in vitro release of Cur from Cur-NPs using UV-Vis spectroscopy. For this method, aliquots of Cur-NPs in a dialysis tubing (MWCO = 12 kDa) were placed in outer buffer solution under different = 5.3, 6,5 (acidic), and 7.4 (control). Upon the degradation of Cur-NPs, as illustrated in Figure 4.7c, Cur could be released and diffused out of the dialysis bag into outer buffer solutions. Aliquots (4 mL) of outer buffer were taken at given times and mixed with ethanol (16 mL) to record their UV spectra (Figure B15). For the quantitative analysis, the extinction coefficient of Cur was used to determine the amount of Cur released from Cur-NPs at given time intervals. Figure 4.7d shows the %Cur release over incubation time at pH = 7.4, 6.5 and 5.0, where each was examined in triplicates to analyze the standard deviation of our %Cur release. At neutral pH (pH = 7.4), there is little to no release of Cur, remaining at a plateau of 1% after 5 days. At extracellular pH = 6.5, the release of Cur was enhanced to a 45%, whereas at intracellular pH = 5.0, the release was accelerated to 85% after 5 days. Such rapid Cur release could be attributed to the degradation of Cur-NPs through both PEG detachment and core polarity change upon the cleavage of both BzAc and BzI linkages located both at interfaces and in cores, respectively. These results suggest beneficial advantages for dual location pH-responsive nanoassemblies.

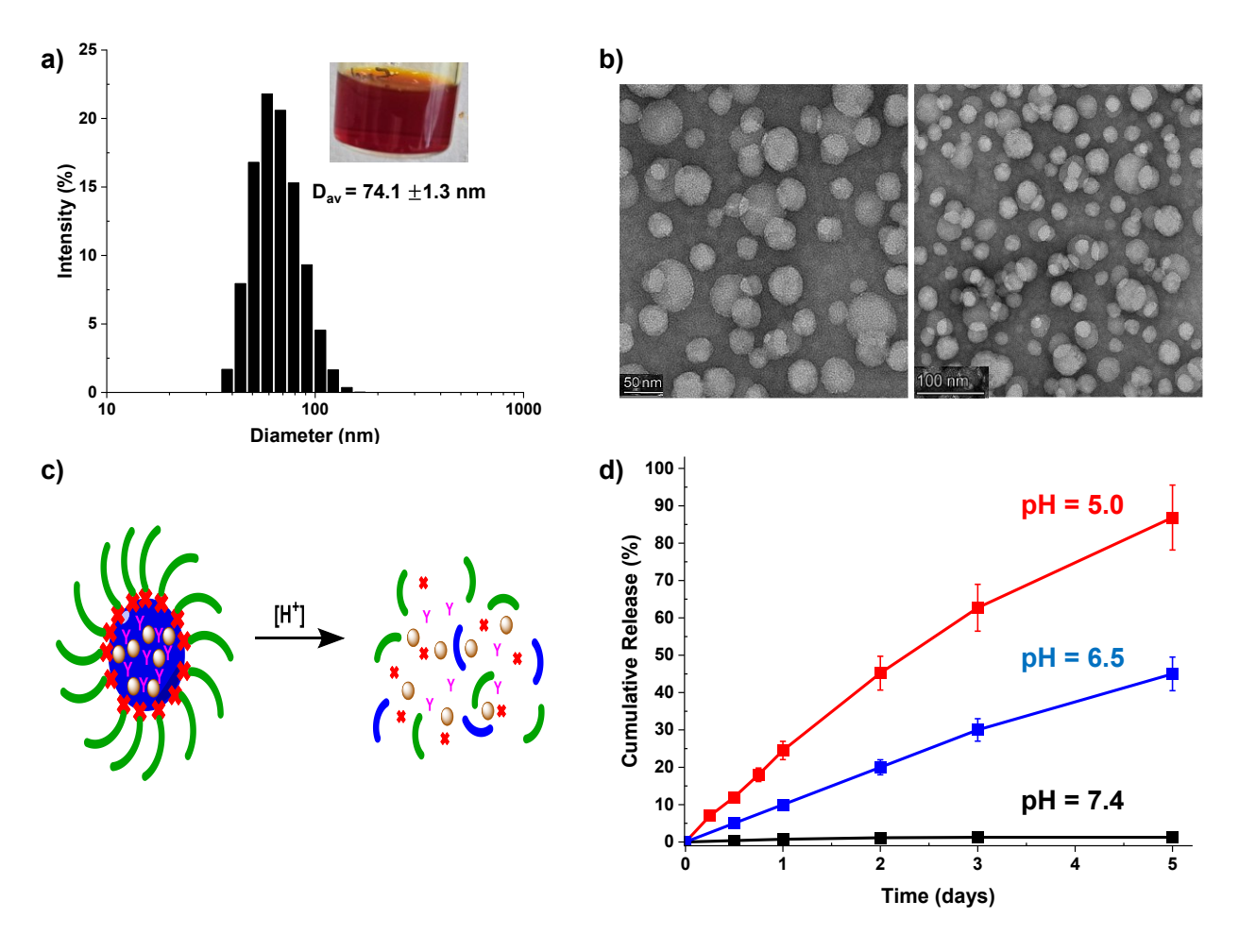


Figure 4.7. Cur-loaded micelles measured by DLS by intensity (a), TEM images with scale bar = 50 nm (left) and 100 nm (right) (b), schematic illustration of acid-responsive disassembly for release of Cur (c) and %Cur release from Cur-NPs being incubated at pH = 7.4, 6.5 and 5.0 (d).

4.4 Conclusion

A dual location acid-degradable ABP labeled with BzAc linkage at the block junction and BzI hydrophobic blocks was synthesized by AGET ATRP, followed by post-polymerization modification. At above CMC of 30 μ g mL⁻¹, ABP self-assembled to form aqueous colloidally-stable nanoassemblies with BzAc groups at the core/corona interfaces and BzI groups within the hydrophobic core. Their acid-responsive degradation was driven by the tunable acid-catalyzed hydrolysis of BzAc and BzI linkages, and the disassembly of the nanoassemblies indicated promisingly their response to be slower at pH = 6.5, but faster at pH = 5.0, while being stable at pH = 7.4, based on our DLS and TEM analysis.

These nanoassemblies could encapsulate Cur anticancer drugs to form Cur-NPs with diameter = 74 nm which had an encapsulation efficiency as high as 91% and a loading content of 9.1% when the weight ratio of Cur/DLAD was designed to be 11/1. Owing to dual response to acidic pH at both the core and the interface, they exhibit the synergistic and accelerated release of encapsulated Cur at endo/lysosomal pH, and moderate Cur release at extracellular pH, while no release occurred at physiological pH. These results emphasizes the promise of dual location acid-responsive degradation nanoassemblies in delivering therapeutic agents with high efficiency for advanced drug delivery.

Chapter 5: Stability of Acetals/Ketals under Controlled Radical and Ring Opening Polymerization

5.1 Introduction

The development of well-defined amphiphilic block copolymer (ABP)-based nanoassemblies designed to degrade through chemical transition in response to endogenous triggers found in cells and tissues has been explored for advanced polymeric drug delivery platforms. $^{29, 55, 251-255, 257-261, 330, 332-334}$ In particular, acid-degradable nanoassemblies have been widely developed as acidic pH is the most promising endogenous trigger found in tumor environments. $^{36, 265-267, 269, 270, 335}$ Compared to normal tissues at pH = 7.4, extracellular compartments of tumor tissues are slightly acidic at pH = 6.5–6.9 and endosomes and lysosomes are more acidic at pH = 4.5–5.5. $^{71, 72, 321}$ Most acid-degradable ABPs have been designed with acid-labile acetal, ketal, orthoester, imine, oxime, hydrazone, 2,3-dialkylmaleamidic amide, boronic ester, and β -thiopropionate groups. $^{82, 190, 275-279, 282, 283, 330, 336-339}$

Particular interest focuses on acetals and ketals because of their ability to tune acid-catalyzed hydrolysis rate with substituents on both the oxygen atoms and the central carbon in their structures. The nature of the substituents strongly affects the stability of the intermediate carbocation generated from the elimination of protonated alcohol in acidic condition - and thus overall acid-catalyzed hydrolysis rate - through steric, resonance, and inductive effects. $^{136, 307, 340}$, 341 Along with the report on acid-catalyzed hydrolysis rates at pH = 5 for acetals and ketals with various substituents, 342 recent report also describes the increasing order of acid-catalyzed hydrolysis to be benzyl acetal (BzAc) < cyclohexyl ketal (CyHK) < cyclopentyl ketal (CyPK) at pH = $5.0.^{139}$ Compared with the three candidates, acid-catalyzed hydrolysis is slower for acetaldehyde acetal (AcA), while faster for dimethyl ketal (DMK). Their chemical structures are shown in Figure 5.1.

Figure 5.1. Chemical structures and acid-catalyzed hydrolysis rate of acetals and ketals of interest in this work.

A general approach to synthesize acid-degradable poly(ethylene glycol)-based ABPs utilizes controlled polymerization techniques, particularly atom transfer radical polymerization (ATRP) of methacrylate monomers and ring opening polymerization (ROP) of cyclic monomers. Most reports describe the synthesis of acid-degradable ABPs bearing acetaldehyde acetal (AcA) groups by ATRP, suggesting that AcA is stable under the ATRP condition. 33, 292, 294, 343-345 Interestingly, our recent report describes the instability (cleavage) of dimethyl ketal (DMK) linkage under ATRP condition, thus not allowing for the synthesis of acid-degradable ABPs labeled with DMK group at the block junction by ATRP. 192 It can be implicated that the sensitivity of acetals and ketals to acidity is likely related to the stability to ATRP condition. In contrast, reports describe the instability of both AcA²⁹³ and DMK¹⁷⁹ under a tin-catalyzed ROP condition, suggesting that no relationship of sensitivity to acid with stability to ROP condition.

Given limited studies addressing the relationship of sensitivity to acid and stability to controlled polymerization, we investigated the stability of acid-labile groups under ATRP and ROP conditions with the choice of BzAc as a typical acetal and CyHK as a typical ketal. Their dibromide ATRP initiators synthesized here were examined for model studies and ATRP of two methacrylate monomers on their stability under ATRP condition. Further, their diol precursors were examined for ROP of lactide (LA) on their stability under a tin-catalyzed ROP condition.

5.2 Experimental

- **5.2.1 Instrumentations.** ¹H NMR spectra were recorded using a 300 MHz Bruker spectrometer. The CDCl₃ singlet at 7.26 ppm and DMSO-d₆ quintet at 2.5 ppm were selected as the reference standards. Spectral features are tabulated in the following order: chemical shift (ppm); multiplicity (s singlet, d doublet, t triplet, m complex multiplet); number of protons; position of protons. Monomer conversion was determined by ¹H NMR spectroscopy with the integral ratio of the methyl group on backbone of polymethacrylate to the methacrylate group of methacrylate monomer. Molecular weight and molecular weight distribution were determined by gel permeation chromatography (GPC). An Agilent GPC was equipped with a 1260 Infinity Isocratic Pump and a RI detector. Two Agilent PLgel mixed-C and mixed-D columns were used with DMF containing 0.1 mol% lithium bromide at 50 °C at a flow rate of 1.0 mL min⁻¹. Linear poly(methyl methacrylate) standards from Fluka were used for calibration. Aliquots of the polymer samples were dissolved in DMF with 0.1% lithium bromide and the clear solutions were filtered using a disk-type PTFE filter (manufactured by MilliporeSigma) with 0.45 μm pores to remove any insoluble species. A drop of anisole was added as a flow rate marker.
- **5.2.2 Materials**. Triethylamine (Et₃N, 99.5%), 2-bromoisobutyryl bromide (Br-iBuBr, 98%), benzyl methacrylate (BM, 96%), oligo(ethylene glycol) methyl ether methacrylate (OEOMA, M_W = 300 g/mol), copper (II) bromide (Cu(II)Br₂, 99%), D,L-lactide (LA, 99%), and tin (II) ethylhexanoate (Sn(EH)₂, 95%) from Sigma-Aldrich or Alfa Aesar as well as tris(2-pyridylmethyl) amine (TPMA) from TCI Chemicals were purchased and used without further purification. Anhydrous anisole and anhydrous toluene were purchased from Sigma-Aldrich and used after treated with 3 Å molecular sieves.

Diols bearing acid-labile benzyl acetal (BzAc-DOH) and cyclohexyl ketal (CyHK-DOH) were synthesized as described in our previous publications. 139

5.2.3 Synthesis of Acid-Labile Dibromides. Br-iBuBr dissolved in DCM (8 mL) was added dropwise to an organic solution containing diol bearing acid-labile group and Et₃N in DCM (20 mL) in an ice bath. The resulting mixture was stirred at 0 °C for 3 hrs. After the formed solids (Et₃N-HBr adducts) were removed by vacuum filtration, the mixture was washed with phosphate buffer saline (PBS) solution (pH = 7.4) twice and then dried over magnesium

sulfate. Solvents were removed by rotary evaporation. The product was collected as the second of the total two bands off a silica gel column using an eluent of 3/2 v/v hexane/ethyl acetate mixture and then dried in vacuum oven for 24 hrs.

BzAc-DBr: BzAc-DOH (1.5 g, 4.63 mmol), Et₃N (5.6 g, 55.4 mmol), and Br-iBuBr (3.2 g, 13.9 mmol). $R_f = 0.4$ with 3/2 v/v hexane/ethyl acetate mixture. Yield = 45%. ¹H NMR (CDCl₃, ppm): 7.46-7.30 (m, 5H, Ar-H), 5.50 (s, 1H, CH-O₂), 4.20 (t, 4H, CH₂-COCBr), 3.5 (t, 4H, CH₂-CH₂-O), 1.94 (s, 12H, C(CH₃)₂Br), 1.65-1.55 (m, 8H, CH₂), 1.40-1.38 (m, 8H, CH₂).

CyHK-DBr: CyHK-DOH (2.0 g, 6.31 mmol), Et₃N (7.7 g, 75.8 mmol), Br-iBuBr (5.8 g, 25.2 mmol). $R_f = 0.6$ with 3/2 v/v hexane/ethyl acetate mixture. Yield = 53%. ¹H NMR (CDCl₃, ppm): 4.20 (t, 4H, CH₂-COCBr), 3.40 (t, 4H, CH₂-CH₂-O), 1.94 (s, 12H, C(CH₃)₂Br), 1.64-1.48 (m, 16H, CH₂), 1.39-1.37 (m, 8H, CH₂-cyclohexyl).

- **5.2.4** Model Studies on Stability of Acetals and Ketals under ATRP Conditions.

 Aliquots of BzAc-DBr and CyHK-DBr (30 mg) were mixed with Cu(II)Br₂ (2 mg) in DMSO-d₆ (1 mL) for ¹H NMR spectroscopy.
- **5.2.5** General Procedure for ATRP of Methacrylates. BzAc-DBr or CyHK-DBr, BM or OEOMA, [Cu(II)Br/TPMA]Br, TPMA, and anisole (7.2 g) were mixed in a 10 mL Schlenk flask. The mixture was deoxygenated by purging under nitrogen for 1 hour. A nitrogen prepurged solution of Sn(EH)₂ dissolved in anisole (0.8 g) was injected into the Schlenk flask to initiate polymerization, and then placed in an oil bath at 40 °C. Polymerization was stopped after 3 hrs by cooling the reaction mixture in an ice bath and exposing it to air. Below are the detailed recipes which are also summarized in Table C1.

ATRP-1 (PBM-BzAc-PBM): BzAc-DBr (0.14 g, 23.2 μmol), BM (2.05 g, 11.6 mmol), [Cu(II)Br/TPMA]Br (2.98 mg, 5.81 μmol), TPMA (5.06 mg, 17.4 μmol), Sn(EH)₂ (18.8 mg, 46.5 μmol).

ATRP-2 (POEOMA-BzAc-POEOMA): BzAc-DBr (91 mg, 0.14 mmol), OEOMA (2.2 g, 7.3 mmol), [Cu(II)Br/TPMA]Br (1.88 mg, 3.67 μmol), TPMA (3.19 mg, 11.0 μmol), Sn(EH)₂ (11.8 mg, 29.3 μmol).

ATRP-3 (PBM-BzAc-PBM): BzAc-DBr (0.15 g, 25.0 μ mol), BM (2.20 g, 12.5 mmol), [Cu(II)Br/TPMA]Br (12.8 mg, 25.0 μ mol), TPMA (18.1 mg, 62.4 μ mol), Sn(EH)₂ (20.2 mg, 49.9 μ mol).

ATRP-4 (POEOMA-BzAc-POEOMA): BzAc-DBr (82.9 mg, 0.13 mmol), OEOMA (2.00 g, 6.7 mmol), [Cu(II)Br/TPMA]Br (6.84 mg, 13.3 μmol), TPMA (9.67 mg, 33.3 μmol), Sn(EH)₂ (10.8 mg, 26.7 μmol).

ATRP-5 (PBM-CyHK-PBM): CyHK-DBr (0.15 g, 23.9 μ mol), BM (2.10 g, 11.9 mmol), [Cu(II)Br/TPMA]Br (3.06 mg, 5.96 μ mol), TPMA (5.19 mg, 17.8 μ mol), Sn(EH)₂ (19.3 mg, 47.6 μ mol).

ATRP-6 (POEOMA-CyHK-POEOMA): CyHK-DBr (0.11 g, 18.0 μmol), OEOMA (2.7 g, 9.0 mmol), [Cu(II)Br/TPMA]Br (2.30 mg, 4.50 μmol), TPMA (3.91 mg, 13.5 μmol), Sn(EH)₂ (14.6 mg, 36.0 μmol).

The as-synthesized polymers were purified by passing through a basic alumina oxide column to remove copper species, followed by precipitation from hexane three times to remove residue monomers. The precipitates were isolated and dried in a vacuum oven at room temperature for 13 hrs.

To investigate kinetics, aliquots were taken periodically to analyze monomer conversion by ¹H NMR spectroscopy and molecular weight and its distribution by GPC.

5.2.6 General Procedure for ROP of LA. BzAc-DOH or CyHK-DOH, LA, Sn(EH)₂ and toluene (10 mL) were mixed in a 15 mL Schlenk flask. The mixture was deoxygenated by purging under nitrogen for 1 hr, and then placed in an oil-bath at 120 °C. Polymerization was stopped after 18 hrs by cooling the reaction mixture in an ice bath and exposing it to air. Below are the detailed recipes which are also summarized in Table C2.

ROP-1 (PLA-BzAc-PLA): BzAc-DOH (0.21 g, 0.63 mmol), LA (5.0 g, 43.8 mmol), Sn(EH)₂ (20.3 mg, 0.10 mmol).

ROP-2 (PLA-CyHK-PLA): CyHK-DOH (0.20 g, 0.60 mmol), LA (5.0 g, 43.8 mmol), Sn(II)(EH)₂ (20.3 mg, 0.10 mmol).

The as-synthesized PLAs were purified by precipitation from methanol three times to remove the residue LA monomers. The precipitates were isolated and dried in a vacuum oven at room temperature overnight.

5.2.7 Studies of Acid-Catalyzed Degradation. Aliquots of polymers (30 mg) were incubated with HCl (20 μL) in DMSO-d₆ for ¹H NMR and in DMF for GPC analysis.

5.3 Results and Discussion

5.3.1 Synthesis of Acid-labile Dibromide ATRP initiators. Figure 5.2 depicts our approach to synthesize BzAc-DBr and CyHK-DBr. The approach explores a facile coupling reaction of corresponding acid-labile diol precursors with Br-iBuBr in the presence of Et₃N as a base.

a)
$$Br \rightarrow Br$$

$$Br \rightarrow G$$

$$Et_3N, DCM$$

$$BzAc-DBr$$

$$Br \rightarrow G$$

$$CyHK-DOH$$

$$Et_3N, DCM$$

$$CyHK-DBr$$

Figure 5.2. Synthesis of acid-labile dibromides, BzAc-DBr (a) and CyHK-DBr (b), by a facile coupling reaction of BzAc-DOH and CyHK-DOH with Br-iBuBr in the presence of Et₃N (a base).

For BzAc-DBr, ¹H NMR spectrum in Figure 5.3a shows the characteristic peaks at 5.5 ppm (b) corresponding to methine proton in acetal moiety (red), 4.2 ppm (c) corresponding to methylene protons adjacent to ester group (blue), and 1.9 ppm (e) corresponding to methyl protons of Br moiety (green). For CyHK-DBr in Figure 5.3b shows the ¹H NMR with the peaks at 4.2 ppm (b) corresponding to ester bonds, and at 1.9 ppm (c) corresponding to methyl protons of Br moiety. Our ¹H NMR analysis confirm the synthesis of BzAc-DBr and CyHK-DBr.

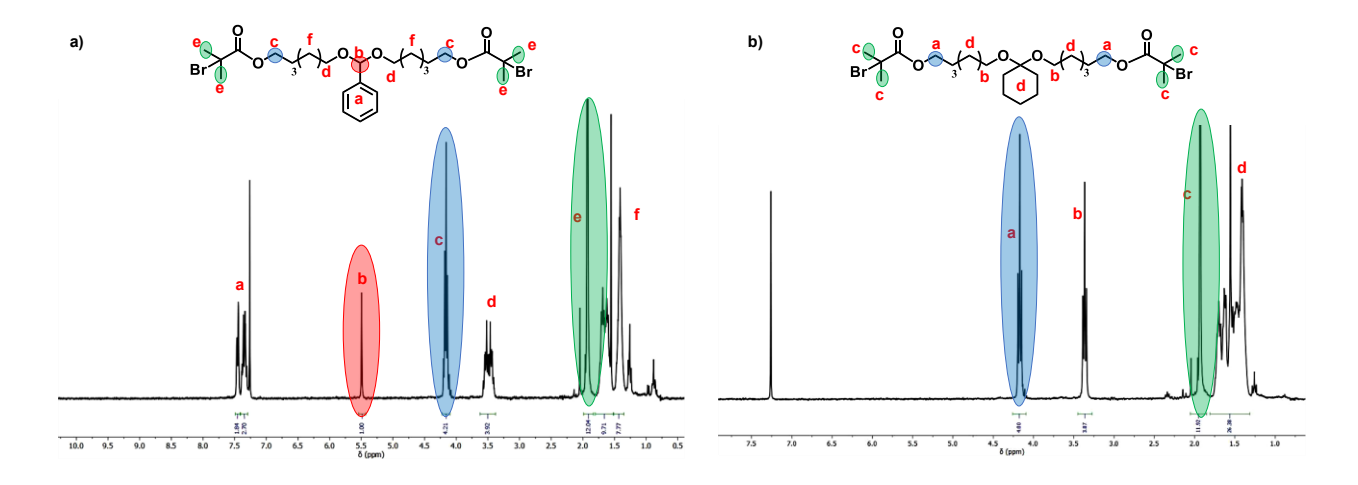


Figure 5.3. ¹H NMR spectra of BzAc-DBr (a) and CyHK-DBr (b) in CDCl₃.

5.3.2 Model Studies on Stability of Acid-Labile Linkages under ATRP Conditions. To examine if acid-labile linkages can be cleaved under ATRP condition, ¹H NMR spectroscopy was used for the mixture of dibromide with Cu(II)Br₂ in DMSO-d₆. Their amounts were designed to mimic the characteristics of practical ATRP (e.g. [DBr]₀/[Cu(II)Br₂]₀ = 1/0.05.

For BzAc-DBr, Figure 5.4a illustrates its degradation to corresponding benzaldehyde (BzA) and two bromine species with a hydroxy terminal group (Br-OH) upon the cleavage of BzAc linkage. Figure 5.4b shows overlaid ¹H NMR spectra of BzAc-DBr incubated with HCl (0.24 M). The peak at 5.4 ppm (a) corresponding to methine proton in BzAc moieties did not appear to significantly decrease. Consequently, the peak at 10 ppm (b) corresponding to benzaldehyde proton barely appeared up to 3 hr incubation. Using their integral ratio, the %cleavage of BzAc group was determined to be less than 1 % in 3 hr incubation, suggesting that BzAc group is stable under ATRP condition.

For CyHK-DBr, Figure 5.4c shows its degradation to corresponding cyclohexanone and two Br-OH species upon the cleavage of CyHK linkage. As shown in Figure 5.4d, the peak at 3.3 ppm (a) corresponding to methylene protons in CyHK moieties decreased. As a consequence, the peak at 2.2 ppm (b) corresponding to methylene protons in cyclohexanone increased. Their integral ratio allows to determine %degradation to be 35 % in 3 hr incubation, implicating the instability of CyHK linkagee under ATRP condition. This result is consistent with the instability of DMK group under similar ATRP condition. 192

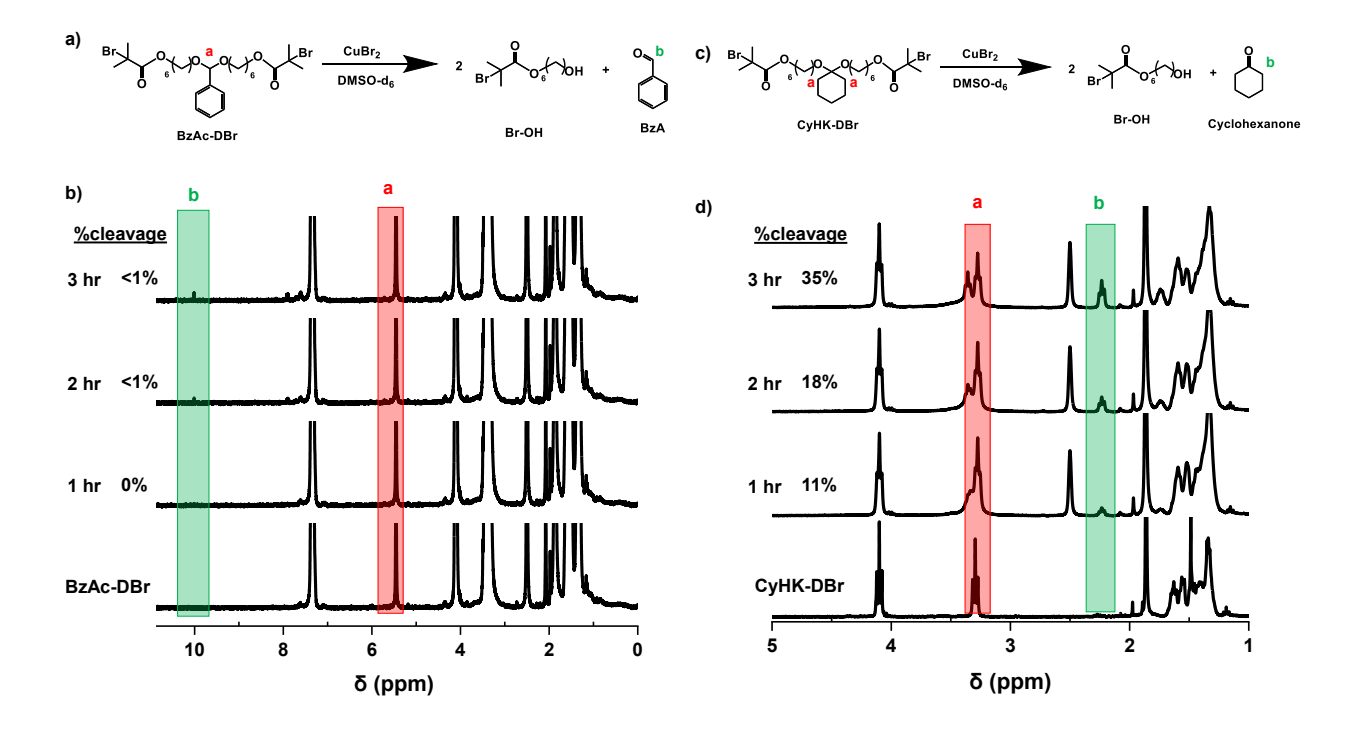


Figure 5.4. Degradation to corresponding benzaldehyde and two Br-OH species bearing terminal hydroxyl groups (a,c) and overlaid ¹H NMR spectra incubated with HCl (0.24 M) in DMSO-d₆ (b,d) for BzAc-DBr (a,b) and CyHK-DBr (c,d).

5.3.3 Studies on Stability of Acid-Labile Linkages during ATRP. The newly synthesized acid-labile dibromides, BzAc-DBr and CyHK-DBr, were examined for ATRP of BM and OEOMA in anisole at 40 °C, yielding PBM-BzAc-PBM and POEOMA-BzAc-POEOMA. For most ATRP, initial mole ratio was set to be [DBr]₀/[Cu(II)Br₂/TPMA]₀/[TPMA]₀/[Sn(EH)₂]₀ = 1/0.05/0.15/0.4, which is a typical condition for an Activators ReGenerated by Electron Transfer (ARGET) process for ATRP (called ARGET ATRP). [BM or OEOMA]₀/[DBr]₀ was set to be 50/1, equivalent to the target degree of polymerization (DP) = 50 at complete monomer conversion (e.g. DP of each PBM or POEOMA to be 25). After being purified by precipitation from hexane, the polymers were characterized for chemical structure by ¹H NMR spectroscopy and molecular weight and its distribution by GPC. Table 5.1 summarizes their characteristics and properties. Their acid-catalyzed hydrolysis was investigated for the qualitative and quantitative analysis to the stability of BzAc and CyHK groups during ATRP.

Table 5.1. Characteristics and properties of polymers prepared by ATRP of BM or OEOMA initiated with BzAc-DBr or CyHK-DBr in anisole.^{a)}

Recipe	Monomer	DBr	[DBr] ₀ /[Cu(II)] ₀	Time	Conv. b)	$\mathbf{M_n}^{c)}$	Đ c)
				(hrs)	(%)	(kg/mol)	
ATRP-1	BM	BzAc-DBr	1/0.05	3	62	6.5	1.18
ATRP-2	OEOMA	BzAc-DBr	1/0.05	3	73	9.6	1.16
ATRP-3	BM	BzAc-DBr	1/0.2	3	52	7.4	1.2
ATRP-4	OEOMA	BzAc-DBr	1/0.2	3	63	11.2	1.16
ATRP-5	BM	CyHK-DBr	1/0.05	3	55	5.8	1.16
ATRP-6	OEOMA	CyHK-DBr	1/0.05	3	42	8.4	1.13

a) [Monomer] $_0$ /[DBr] $_0$ = 50/1 in anisole at 40 °C; b) determined by 1 H NMR; and c) determined by GPC.

BzAc. Figure 5.5a illustrates the ATRP of BM in the presence of BzAc-DBr, to synthesize PBM-BzAc-PBM (ATRP-1). ¹H NMR spectrum in Figure C1 shows the peaks at 7.3 ppm (a), 5.2 ppm (b) and 0.8-1.0 ppm (c), all of which present PBM. However, the peak corresponding to the methine proton in BzAc moieties was not clearly seen. Moreover, the peaks corresponding to the aromatic protons of BzAc moieties overlapped with the aromatic protons in PBM. Consequently, ¹H NMR analysis did not appear to be straightforward for quantitative analysis to the stability of BzAc groups. GPC analysis in Figure 5.5b confirms that the polymer had a molecular weight by number average molecular weight $(M_n) = 6.5 \text{ kg/mol}$ with molecular weight distribution as narrow as D = 1.16. When the polymer was treated with HCl, its GPC trace clearly shifted to low molecular weight region, with a significant decrease in molecular weight to $M_n = 4.6 \text{ kg/mol}$ with D = 1.10. Such a decrease in molecular weight could be attributed to the degradation of PBM-BzAc-PBM to corresponding two PBM-OH and benzaldehyde as degraded products upon the cleavage of BzAc through acid-catalyzed hydrolysis (Figure 5.5a). ATRP of OEOMA in the presence of BzAc-DBr yielded POEOMA-BzAc-POEOMA (ATRP-2) with molecular weight as the $M_n = 9.6$ kg/mol (Figure C2). Similarly, the molecular weight significantly decreased to $M_n = 6.9$ kg/mol when the polymer was mixed with HCl. These results obtained by GPC analysis, along with our model studies with BzAc-DBr by ¹H NMR analysis, suggest that a majority of BzAC groups appear to be intact (not cleaved) during ATRP, thus forming well-defined BzAc-bearing polymers.

Kinetic studies were conducted for the ATRP in the presence of BzAc-DBr. As seen in Figure C3 for BM and Figure C4 for OEOMA, monomer conversion linearly increased with time, suggesting that the polymerization is first-order with the constant concentration of active centers during polymerization. Molecular weight increased linearly with conversion and molecular weight distribution (D) was narrow as $M_w/M_n < 1.2$.

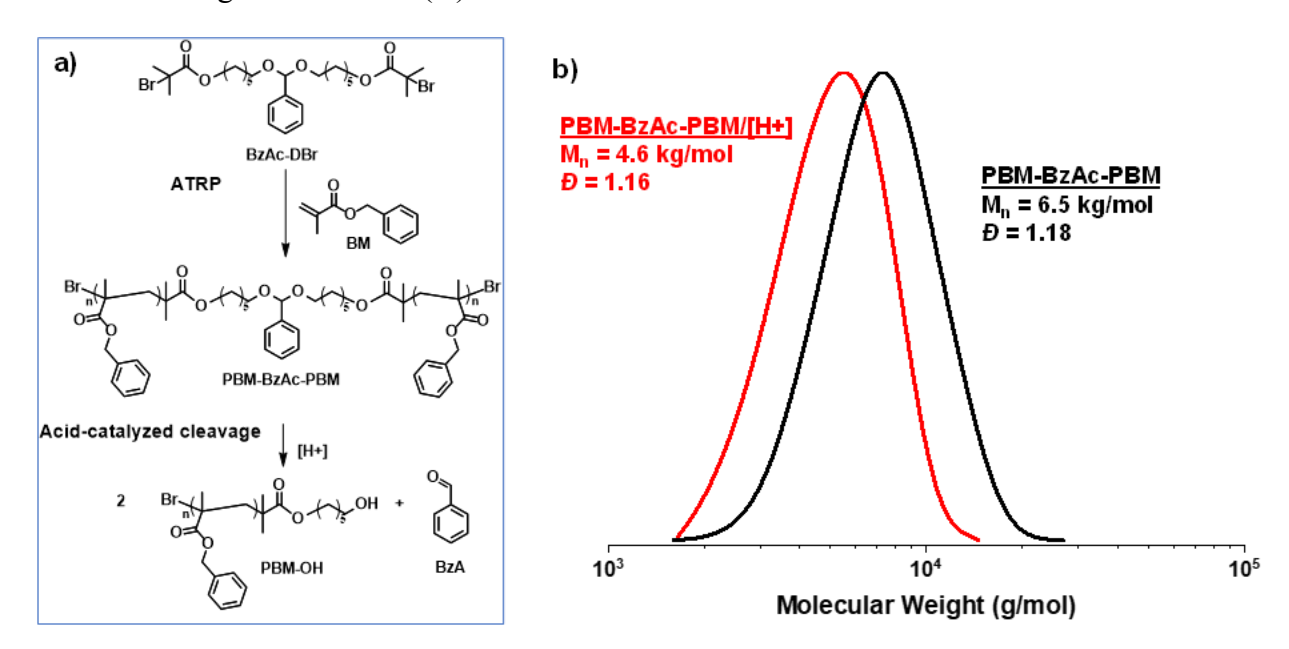


Figure 5.5. Synthesis by ATRP of BM in the presence of BzAc-DBr and acid-responsive degradation upon the cleavage of BzAc groups of PBM-BzAc-PBM (ATRP-1) (a) and its overlaid GPC diagrams before and after treatment with HCl (acid) in DMF (b). Conditions for ATRP: $[BM]_0/[BzAc-DBr]_0/[Cu(II)Br_2/TPMA]_0/[TPMA]_0/[Sn(EH)_2]_0 = 50/1/0.05/0.15/0.4$ in anisole at 40 °C, BM/anisole = 0.25/1 wt/wt.

Further to get insight into the stability of BzAc with the increasing amount of Cu catalyst for ATRP of BM (ATRP-3), the amount of Cu catalyst as the initial mole ratio of [BzAc-DBr] $_0$ /[Cu(II)Br $_2$ /TPMA] $_0$ increased from 1/0.05 to 1/0.2, which is a typical condition for an Activators Generated by Electron Transfer (AGET) process for ATRP (called AGET ATRP). As compared in Figure C5, the molecular weight of PBM-BzAc-PBM (ATRP-3) had the M_n =7.4 kg/mol, which decreased to M_n = 4.7 kg/mol upon the treatment with HCl. Similar results were observed for ATRP of OEOMA (ATRP-4) where the molecular weight of POEOMA-BzAc-POEOMA decreased from M_n = 11.2 kg/mol to M_n = 6.9 kg/mol upon the treatment with HCl (Figure C6). These results suggest that BzAc bonds appeared to be stable during ATRP with the

increasing amount of Cu catalyst, suggesting no significant effect of Cu catalyst on the stability of BzAc groups on ATRP.

CyHK. ATRP of BM was examined in the presence of CyHK-DBr in an attempt to synthesize PBM-CyHK-PBM (ATRP-5) (Figure 5.6a). 1 H NMR spectrum shows the peaks at 7.3 ppm (a), 5.0 ppm (b), and 0.8-1.0 ppm (c), which present PBM; however, the characteristic peaks corresponding to the protons in cyclohexyl ketal moiety were not seen (Figure C7). GPC analysis confirms that the polymer had the $M_n = 5.8$ kg/mol with D = 1.16 (Figure 5.6b). Upon the treatment with HCl, its GPC trace slightly changed and thus its molecular weight slightly decreased to $M_n = 5.2$ kg/mol. For the ATRP of OEOMA in the presence of CyHK-DBr (ATRP-6), similar results were observed before and after treatment with HCl (Figure C8). The plausible reason that the GPC traces of the polymers remained unchanged after treatment with HCl could be attributed to the cleavage of CyHK groups during ATRP. Such cleavage could occur randomly on not only CyHK-DOH but also PBM-CyHK-PBM polymers (not found), eventually to be expected to form PBM-OH (a degraded polymer shown in Figure 5.6a) (see Figure C9 for plausible mechanism).

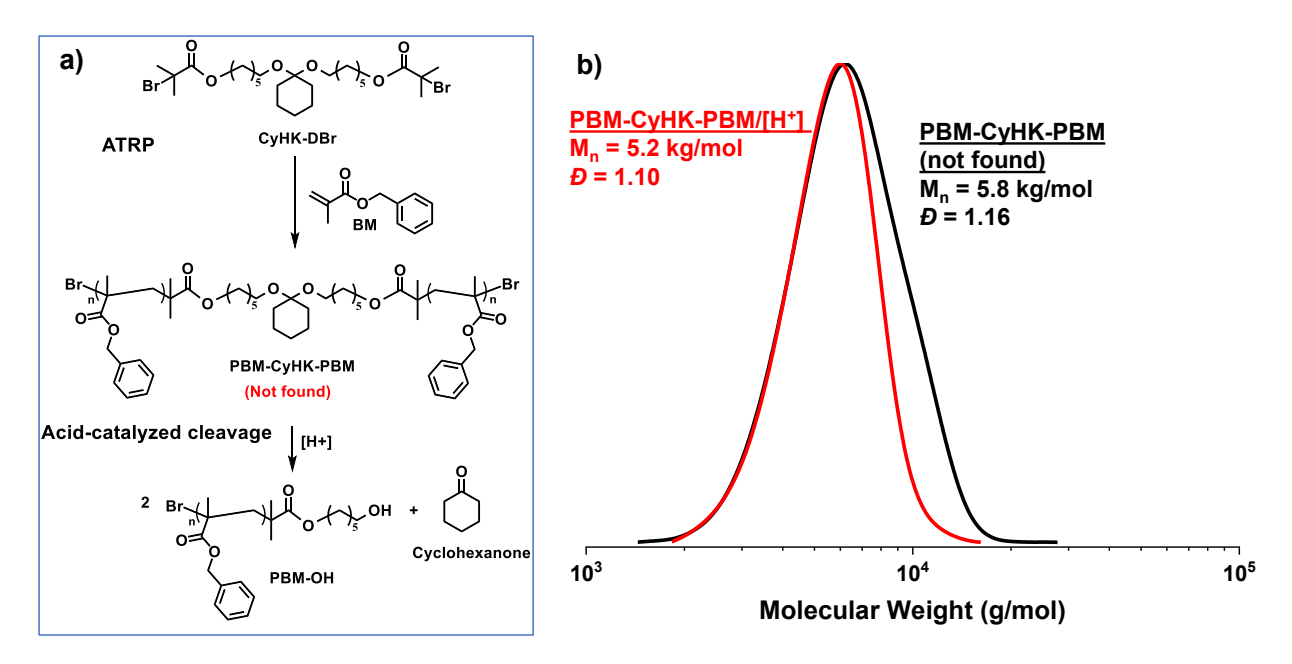


Figure 5.6. ATRP of BM in the presence of CyHK-DBr in an attempt to synthesize PBM-CyHK-PBM and its acid-responsive degradation upon the cleavage of CyHK groups (a) and overlaid GPC diagrams before and after treatment with HCl (acid) in DMF (b). Conditions for ATRP: [BM]₀/[CyHK-DBr]₀/[Cu(II)Br₂/TPMA]₀/[TPMA]₀/[Sn(EH)₂]₀ = 50/1/0.05/0.15/0.4 in anisole at 40 °C, BM/anisole = 0.25/1 wt/wt.

5.3.4 Studies on Stability of Acid-Labile Linkages during ROP. Acid-labile diols, BzAc-DOH and CyHK-DOH, were examined for ROP of LA under a tin-catalyzed condition with toluene at 120 °C, in an attempt to synthesize PLA-BzAc-PLA and PLA-CyHK-PLA. Initial mole ratio of [LA]₀/[DOH]₀/[Sn(EH)₂]₀ = 70/1/0.4 was designed with the target DP of PLA to be 70 (e.g. DP of each PLA to be 35) upon complete conversion. After being purified by precipitation from MeOH, the polymers were characterized for chemical structure by ¹H NMR spectroscopy and molecular weight and its distribution by GPC. Table 5.2 summarizes their characteristics and properties. Their acid-catalyzed hydrolysis was investigated for the qualitative and quantitative analysis to the stability of BzAc and CyHK groups during ROP.

Table 5.2. Characteristics and properties of polymers prepared by ROP of LA initiated with BzAc-DOH or CyHK-DOH in toluene.^{a)}

Recipe	DOH	[DOH] ₀ /[Sn(EH) ₂] ₀	Time (hrs)	M _n b) (kg/mol)	∌ b)
ROP-1	BzAc-DOH	1/0.4	18	12.7	1.14
ROP-2	CyHK-DOH	1/0.4	18	11.4	1.27

a) $[LA]_0/[DOH]_0 = 70/1$ in toluene at 120 °C and b) determined by GPC.

BzAc. For ROP-1 conducted with BzAc-DOH (Figure 5.7a), 1 H-NMR spectrum of the purified PLA-BzAc-PLA in Figure 5.7b shows the peaks at 4.1 ppm (c) and 1.3-1.4 ppm (e), present in PLA. Importantly, the peaks at 7.4 ppm (a) corresponds to aromatic protons (5Hs) in BzAc moiety and the peaks at 4.5-4.0 ppm (c,d) is equivalent to the protons (6Hs) in two PLAs. Their integral ratio indicates that only 54 % of BzAc groups could be intact, thus forming PLA-BzAc-PLA, while 46% of BzAc groups appeared to be cleaved during ROP. GPC analysis confirms that the formed polymer had its $M_n = 12.7$ kg/mol with D = 1.14 (Figure 5.7c). After the treatment with HCl (0.24 M), its molecular weight decreased to $M_n = 9.7$ kg/mol with D = 1.16, suggesting BzAc bonds appeared to be stable to some extent during ROP of LA.

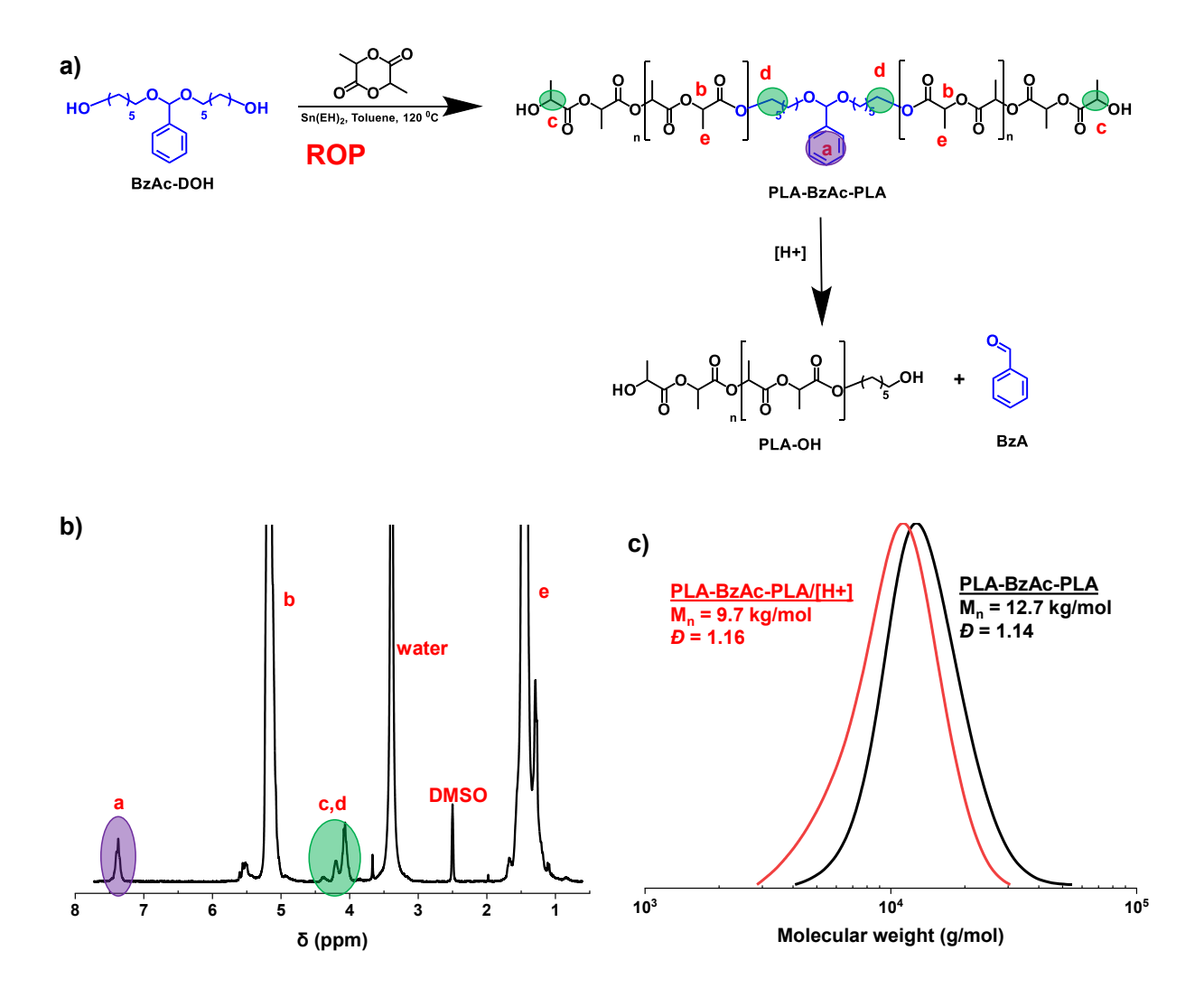


Figure 5.7. ROP of LA initiated with BzAc-DOH (ROP-1) in an attempt to synthesize PLA-BzAc-PLA and its acid-responsive degradation upon the cleavage of BzAc groups (a), 1 H NMR spectrum in DMSO-d₆ (b), and overlaid GPC diagrams before and after treatment with HCl (acid) in DMF (c). Conditions for ROP: [LA]₀/[BzAc-DOH]₀/[Sn(EH)₂]₀ = 70/1/0.4 in toluene at 120 °C, LA/toluene = 0.4/1 wt/wt.

CyHK. For ROP-2 conducted with CyHK-DOH (Figure 5.8a), 1 H NMR analysis was not straightforward because the characteristic peaks corresponding to methylene protons in CyHK moiety and in cyclohexanone were not seen in 1 H NMR spectrum (Figure C10). GPC analysis confirms that the formed polymer had the $M_n = 11.4$ kg/mol with D = 1.11 which did not change when it was treated with HCl (Figure 5.8b). This result confirms the significant cleavage of CyHK bonds during ROP with a tin catalyst. Similar to ATRP for BM or OEOMA with CyHK-DBr, the plausible reason that the GPC traces of the polymers remained unchanged after

treatment with HCl could be attributed to the cleavage of CyHK groups during ROP with a tin catalyst. Such cleavage could be more complicated than ATRP because there will be more polylactide products generated from various initiating species (bearing OH groups) upon the cleavage of CyHK groups during ROP (see Figure C11 for plausible mechanism).

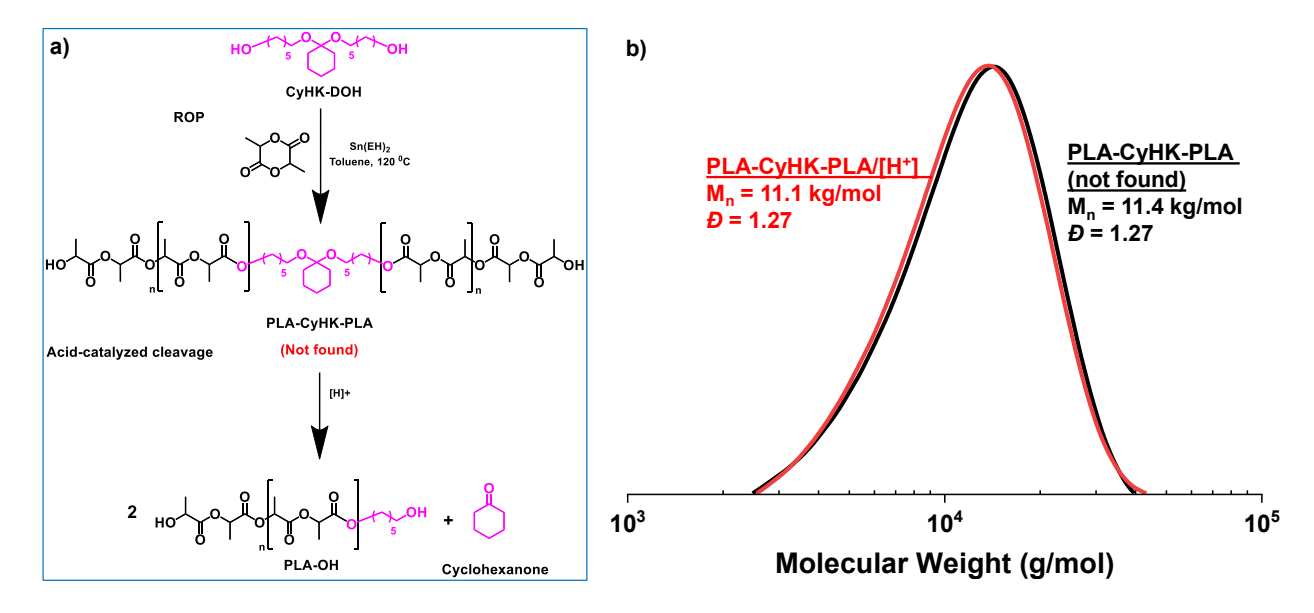


Figure 5.8. ROP of LA initiated with CyHK-DOH (ROP-2) in an attempt to synthesize PLA-CyHK-PLA and its acid-responsive degradation upon the cleavage of CyHK groups (a) and GPC diagrams before and after treatment with HCl (acid) in DMF solvent (b). Conditions for ROP: $[LA]_0/[CyHK-DOH]_0/[Sn(EH)_2]_0 = 70/1/0.4$ in toluene at 120 °C, LA/toluene = 0.4/1 wt/wt.

5.4 Conclusion

In this work, we investigated the stability of acetal and ketal groups with BzAc and CyHK under ATRP and tin-catalyzed ROP conditions. Their dibromide ATRP initiators, BzAc-DBr and CyHK-DBr, were synthesized by a facile coupling reaction. BzAc-DBr appeared to be stable under ATRP condition and successfully initiated ATRP of both BM and OEOMA, forming well-defined, acid-degradable BzAc-labeled polymethacrylates. CyHK-DBr, similar to DMK, was cleaved under ATRP condition. Expectedly, both BzAc and CyHK turned to be cleaved either partially or completely during ROP. Combined findings reported in literature, our results could suggest i) most ketal groups are not stable under ATRP condition, ii) acetaldehyde acetal and benzacetal groups are stable under ATRP, and iii) most acetal and ketal groups are not stable under a tin-catalyzed ROP condition. For acetals, cyclic acetals are expected to be stable, while

methoxy substituted benzacetals could be further investigated since their acid-catalyzed hydrolysis rates are faster than that of benzacetal group. Overall, our results could give an insight into important design principles for the synthesis of well-defined acid-degradable ABPs with respect to acid-catalyzed hydrolysis rate of acetals and ketals, thus eventually, release rate of encapsulated drug molecules from their nanoassemblies in acidic environment, and their stability under controlled polymerization techniques.

Chapter 6: Conclusion and Future Perspectives

6.1 Conclusion

The current designs of acid-degradable ABPs present several challenges, such as detachment of PEG corona from nanoassemblies, where the choice of the junction acid-labile linkage leads to variable outcomes. The rationale behind the choice of acid-labile linkage is lacking as most do not consider the possible interference of the linkage with the controlled polymerization mechanism.

My PhD research aimed to understand and rationally design new-generation acid-degradable ABPs and their nanoassemblies and characterize their properties for the applications in intracellular drug delivery. In this dissertation, I report new synthetic strategies to prepare benzyl acetal and cyclohexyl ketal linkages through direct acetalization/ketalization, as well as using CRP and post-polymerization modification to prepare ABPs with acid-labile linkages at dual locations (e.g. at the block junction and/or pendant chain of the hydrophobic block). The successful dual acidic degradation, disassembly, and drug release from the block copolymer-based nanoassemblies were confirmed by several analytical methods, such as NMR, GPC, DLS, UV/vis, and TEM. Moreover, I demonstrated the relationship of acid-labile linkages based their sensitivity to acid with their stability to controlled polymerization methods.

In chapter 3, three diol precursors bearing BzAc, CyHK, and CyPK groups were synthesized to investigate their acid-catalyzed hydrolysis at various pHs: 5.0 (endo/lysosomal pH), 6.5 (tumoral pH), and 7.4 (physiological pH). Our systematic analysis confirms that the slow hydrolysis of BzAc was suitable for the junction acid-labile group of acid-degradable shell-sheddable ABPs. A well-defined block copolymer labeled with BzAc groups at the junction of was synthesized by ARGET ATRP in the presence of PEG-BzAc-Br macroinitiator and a benzyl methacrylate monomer. The formed block copolymer self-assembled to form aqueous colloidally-stable nanoassemblies with BzAc groups at the core/corona interfaces. Under acidic conditions, DLS and TEM analysis confirms disassembly with fast degradation at pH = 5.0, slow degradation at pH = 6.5, while being stable at pH = 7.4. The choice of BzAc linkage as the block junction is promising in the development of acid-degradable nanoassemblies for advanced drug delivery nanocarriers.

In chapter 4, a dual location acid-degradable ABP labeled with BzAc linkage at the block junction and BzI hydrophobic blocks was synthesized by AGET ATRP, followed by post-polymerization modification. These ABPs self-assembled to form aqueous colloidally-stable nanoassemblies with BzAc groups at the core/corona interfaces and BzI groups within the hydrophobic core. The formation of Cur-loaded nanoassemblies provided an optimized encapsulation efficiency of 91% and a loading content of 9.1% when the weight ratio of Cur/DLAD was 11/1. The degradation of the block copolymers induced by acidic cleavage of the acetal linkages at interfaces and the imine cleavage of pendant chain in the core led to the disassembly and accelerated Cur release. These results emphasizes the promise of dual location nanoassemblies in delivering therapeutic agents for advanced drug delivery.

In chapter 5, the stability of BzAc and CyHK linkages under ATRP and tin-catalyzed ROP conditions was investigated. For ATRP, their dibromide initiators, BzAc-DBr and CyHK-DBr, were synthesized by a facile coupling reaction. BzAc-DBr appeared to be stable under ATRP condition and successfully initiated ATRP of both BM and OEOMA, forming well-defined, acid-degradable BzAc-labeled polymethacrylates. CyHK-DBr, on the other hand, was cleaved under ATRP condition. Expectedly, both BzAc and CyHK turned to be cleaved either partially or completely during ROP. The results could suggest i) most ketal groups are not stable under ATRP condition, ii) most acetal groups are stable under ATRP, and iii) most acetal and ketal groups are not stable under a tin-catalyzed ROP condition. Overall, these results could give an insight into important design principles for the synthesis of well-defined acid-degradable ABPs with respect to acid-catalyzed hydrolysis rate of acetals and ketals, thus eventually, release rate of encapsulated drug molecules from their nanoassemblies in acidic environment, and their stability under controlled polymerization techniques.

6.2 Future Perspectives

Although there is a better understanding as the appropriate method to incorporate acid labile linkages to form acid-degradable ABPs, and that a dual location acid-degradable ABP has been developed, there still exist some challenges that necessitate future research. The future direction for this dissertation should be viewed from three perspectives: 7.2.1) alternative dual location acid-degradable ABPs, 7.2.2) multi-location SRD-based nanoassemblies and 7.2.3) photo-induced CRP methods.

6.2.1 Alternative Dual Location Acid-Degradable ABPs

Since there have been few reports on dual location acid-degradable ABPs, a comprehensive investigation on the structural diversity, synthetic accessibility, and degradation kinetics of these systems are a necessity. Considering we obtained to optimal candidate for the block junction, exploration of different acid-labile linkages within the pendant chain should be investigated. Two acid-labile linkages should be explored: (i) ketal, and (ii) hydrazone, as they are known to cleave quicker than BzAc linkage. Figure 6.1 provides the proposed route for a ketal linkage within the pendant chain. Additionally, the impact of dual-location degradation on nanoassembly disintegration pathways, drug release profiles, and polymer clearance kinetics must be thoroughly investigated using model drug systems and advanced characterization techniques. In addition, in vivo studies will further validate the value and robustness of our system.

Figure 6.1. Proposed synthetic pathway to optimize dual location acid-degradable ABPs using dimethyl ketal linkages as pendant chains.

6.2.2 Multi-Location SRD-Based Nanoassemblies

Building upon the concept of dual location nanoassemblies, the development of multilocation of multi-stimuli (both internal and external stimuli) systems offer an exciting path for enhancing the functional complexity of SRD-based nanoassemblies. By incorporating multiple stimuli units—strategically distributed across the polymer backbone, block junctions, pendant side-chains, and chain ends—it may be possible to design nanoassemblies with programmable degradation profiles that respond to multiple stimuli as a result of the complexity of each type of cancer cell (slightly acidic environment, high concentrations of glutathione, low oxygen levels...), where each type behaves differently. Such a system could allow for sequential release of different therapeutic agents, improved endosomal escape, or structural rearrangement. Figure 6.2 provides a proposed route to synthesize a well-defined ABP, composed of BzAc and disulfide (SS) linkages at the block junction, and azobenzene (Azo) and thioketal (ThK) in the pendant chains. The BzAc linkage represents the pH-stimuli, the SS linkage represents the glutathione (GSH)-stimuli, which are internal-based stimuli, while the Azo linkage represents the light-responsive stimuli, which is an external-based stimuli. The ThK linkage represents the reactive oxygen species (ROS), which is considered to be both an internal and external-based stimuli.

The synthesis of multi-location degradable ABPs will require the use of orthogonal protection strategies and precision polymerization techniques, such as sequential ATRP or click chemistry, to control the positioning and density. Importantly, this approach will also necessitate a careful balance between structural stability during circulation (pH 7.4) and sufficient sensitivity to various stimuli of choice. Advanced analytical techniques, including NMR, GPC, DLS, DSC, TGA, and TEM, along with real-time drug release assays, will be essential in evaluating how these systems respond to acid triggers and how degradation kinetics correlate with therapeutic efficacy.

Figure 6.2. Proposed synthetic pathway for multi-location ABPs using BzAc and SS linkages at the block junction, and Azo and ThK linkages as pendant chains.

6.2.3 Photo-Induced CRP Methods

Although thermally-induced CRP methods such as RAFT, ATRP, and NMP have enabled the controlled synthesis of ABPs with well-defined architectures, light-mediated CRP techniques introduce several advantages, such as no need for harsh solvents or high temperatures, which is more environmentally friendly and reduces potential side reactions, making it more sustainable option. In addition, the ability to use different wavelengths of light (UV, visible light) allows for selective activation of photoinitiators or photoinitiated species. This can be used to create polymer materials, with a large variety of monomers, to form gradient structures or multifunctional properties. 346-350 Light-induced polymerization methods, including photoinduced electron transfer-RAFT (PET-RAFT) and light-mediated ATRP, offer spatiotemporal control, oxygen tolerance, and the ability to operate under mild, aqueous, and ambient conditions conditions that are highly compatible with acid-labile functionalities that may otherwise degrade during thermal or harsh chemical synthesis. 351-356 This opens avenues for producing complex polymer architectures such as multiblock copolymers, star polymers, or brush polymers containing multiple cleavable segments. Furthermore, integrating light-based control into stimuli-responsive systems may enable dual-responsive nanoassemblies that degrade upon both pH change and light exposure, which could be particularly useful in targeted photodynamic or site-specific therapies. Figure 6.3 provides a proposed route through photoRAFT to synthesize a dual location acid-degradable ABP, using Eosin Y as the photocatalyst under UV light, to overcome the need of post-polymerization modification.

Figure 6.3. Proposed synthetic pathway for photoRAFT to synthesize a well-defined PEG-BzAc-PBzI-UV ABP.

References

- 1. Tibbitt, M. W.; Dahlman, J. E.; Langer, R., Emerging frontiers in drug delivery. *Journal of the American Chemical Society* **2016**, *138* (3), 704-717.
- 2. Schacher, F. H.; Rupar, P. A.; Manners, I., Functional block copolymers: nanostructured materials with emerging applications. *Angewandte Chemie International Edition* **2012**, *51* (32), 7898-7921.
- 3. Jain, V.; Jain, S.; Mahajan, S., Nanomedicines based drug delivery systems for anti-cancer targeting and treatment. *Current Drug Delivery* **2015**, *12* (2), 177-191.
- 4. Anselmo, A. C.; Mitragotri, S., An overview of clinical and commercial impact of drug delivery systems. *Journal of Controlled Release* **2014**, *190* (1), 15-28.
- 5. Farokhzad, O. C.; Langer, R., Impact of nanotechnology on drug delivery. *ACS Nano* **2009**, *3* (1), 16-20.
- 6. Vilar, G.; Tulla-Puche, J.; Albericio, F., Polymers and drug delivery systems. *Current Drug Delivery* **2012**, *9* (4), 367-394.
- 7. Li, C.; Wang, J.; Wang, Y.; Gao, H.; Wei, G.; Huang, Y.; Yu, H.; Gan, Y.; Wang, Y.; Mei, L., Recent progress in drug delivery. *Acta Pharmaceutica Sinica B* **2019**, *9* (6), 1145-1162.
- 8. Lee, W. L.; Liles, W. C., Endothelial activation, dysfunction and permeability during severe infections. *Current Opinion in Hematology* **2011**, *18* (3), 191-196.
- 9. Cabral, H.; Kataoka, K., Progress of drug-loaded polymeric micelles into clinical studies. *Journal of Controlled Release* **2014**, *190*, 465-476.
- 10. Kamaly, N.; Xiao, Z.; Valencia, P. M.; Radovic-Moreno, A. F.; Farokhzad, O. C., Targeted polymeric therapeutic nanoparticles: design, development and clinical translation. *Chemical Society Reviews* **2012**, *41* (7), 2971-3010.
- 11. Elsabahy, M.; Wooley, K. L., Design of polymeric nanoparticles for biomedical delivery applications. *Chemical Society Reviews* **2012**, *41* (7), 2545-2561.
- 12. Morachis, J. M.; Mahmoud, E. A.; Almutairi, A., Physical and chemical strategies for therapeutic delivery by using polymeric nanoparticles. *Pharmacological Reviews* **2012**, *64* (3), 505-519.
- 13. Tritschler, U.; Pearce, S.; Gwyther, J.; Whittell, G. R.; Manners, I., 50th anniversary perspective: Functional nanoparticles from the solution self-assembly of block copolymers. *Macromolecules* **2017**, *50* (9), 3439-3463.
- 14. Imran, M.; Shah, M. R., Amphiphilic block copolymers—based micelles for drug delivery. In *Design and Development of New Nanocarriers*, Elsevier: 2018; pp 365-400.
- 15. Blanazs, A.; Armes, S. P.; Ryan, A. J., Self-assembled block copolymer aggregates: from micelles to vesicles and their biological applications. *Macromol Rapid Commun* **2009**, *30* (4-5), 267-277.
- 16. Mai, Y.; Eisenberg, A., Self-assembly of block copolymers. *Chemical Society Reviews* **2012**, *41* (18), 5969-5985.
- 17. Komaiko, J. S.; McClements, D. J., Formation of food-grade nanoemulsions using low-energy preparation methods: A review of available methods. *Comprehensive Reviews in Food Science and Food Safety* **2016**, *15* (2), 331-352.
- 18. Uhrich, K. E.; Cannizzaro, S. M.; Langer, R. S.; Shakesheff, K. M., Polymeric systems for controlled drug release. *Chemical Reviews* **1999**, *99* (11), 3181-3198.
- 19. Fredenberg, S.; Wahlgren, M.; Reslow, M.; Axelsson, A., The mechanisms of drug release in poly (lactic-co-glycolic acid)-based drug delivery systems—A review. *International Journal of Pharmaceutics* **2011**, *415* (1-2), 34-52.
- 20. Hu, X.; Oh, J. K., Direct Polymerization Approach to Synthesize Acid-Degradable Block Copolymers Bearing Imine Pendants for Tunable pH-Sensitivity and Enhanced Release. *Macromolecular Rapid Communications* **2020**, *41* (22), 2000394.

- 21. Jazani, A. M.; Arezi, N.; Shetty, C.; Hong, S. H.; Li, H.; Wang, X.; Oh, J. K., Tumor-targeting intracellular drug delivery based on dual acid/reduction-degradable nanoassemblies with ketal interface and disulfide core locations. *Polymer Chemistry* **2019**, *10* (22), 2840-2853.
- 22. Liang, J.; Yang, B.; Zhou, X.; Han, Q.; Zou, J.; Cheng, L., Stimuli-responsive drug delivery systems for head and neck cancer therapy. *Drug Delivery* **2021**, *28* (1), 272-284.
- 23. Liu, X.; Yang, Y.; Urban, M. W., Stimuli-responsive polymeric nanoparticles. *Macromolecular Rapid Communications* **2017**, *38* (13), 1700030.
- 24. Chan, Y.; Bulmus, V.; Zareie, M. H.; Byrne, F. L.; Barner, L.; Kavallaris, M., Acid-cleavable polymeric core–shell particles for delivery of hydrophobic drugs. *Journal of Controlled Release* **2006**, *115* (2), 197-207.
- 25. Barua, S.; Mitragotri, S., Challenges associated with penetration of nanoparticles across cell and tissue barriers: a review of current status and future prospects. *Nano Today* **2014**, *9* (2), 223-243.
- 26. Hong, S. H.; Larocque, K.; Jaunky, D. B.; Piekny, A.; Oh, J. K., Dual disassembly and biological evaluation of enzyme/oxidation-responsive polyester-based nanoparticulates for tumor-targeting delivery. *Colloids and Surfaces B: Biointerfaces* **2018**, *172* (1), 608-617.
- 27. Lee, J. H.; Yeo, Y., Controlled drug release from pharmaceutical nanocarriers. *Chemical Engineering Science* **2015**, *125*, 75-84.
- 28. Oh, J. K., Disassembly and tumor-targeting drug delivery of reduction-responsive degradable block copolymer nanoassemblies. *Polymer Chemistry* **2019**, *10* (13), 1554-1568.
- 29. Bawa, K. K.; Oh, J. K., Stimulus-Responsive Degradable Polylactide-Based Block Copolymer Nanoassemblies for Controlled/Enhanced Drug Delivery. *Molecular Pharmaceutics* **2017**, *14* (8), 2460-2474.
- 30. Zhang, Q.; Ko, N. R.; Oh, J. K., Recent advances in stimuli-responsive degradable block copolymer micelles: synthesis and controlled drug delivery applications. *Chemical Communications* **2012**, *48* (61), 7542-7552.
- 31. Sun, X.; Agate, S.; Salem, K. S.; Lucia, L.; Pal, L., Hydrogel-based sensor networks: Compositions, properties, and applications—A review. *ACS Applied Bio Materials* **2020**, *4* (1), 140-162.
- 32. Andrade-Gagnon, B.; Bélanger-Bouliga, M.; Trang Nguyen, P.; Nguyen, T. H. D.; Bourgault, S.; Nazemi, A., Degradable Spirocyclic Polyacetal-Based Core-Amphiphilic Assemblies for Encapsulation and Release of Hydrophobic Cargo. *Nanomaterials* **2021**, *11* (1), 161.
- 33. Jazani, A. M.; Shetty, C.; Movasat, H.; Bawa, K. K.; Oh, J. K., Imidazole-Mediated Dual Location Disassembly of Acid-Degradable Intracellular Drug Delivery Block Copolymer Nanoassemblies. *Macromolecular Rapid Communications* **2021**, *42* (16), 2100262.
- 34. Maji, R.; Omolo, C. A.; Agrawal, N.; Maduray, K.; Hassan, D.; Mokhtar, C.; Mackhraj, I.; Govender, T., pH-responsive lipid–dendrimer hybrid nanoparticles: An approach to target and eliminate intracellular pathogens. *Molecular Pharmaceutics* **2019**, *16* (11), 4594-4609.
- 35. Raza, A.; Rasheed, T.; Nabeel, F.; Hayat, U.; Bilal, M.; Iqbal, H. M., Endogenous and exogenous stimuli-responsive drug delivery systems for programmed site-specific release. *Molecules* **2019**, *24* (6), 1117.
- 36. Hu, X.; Jazani, A. M.; Oh, J. K., Recent advances in development of imine-based acid-degradable polymeric nanoassemblies for intracellular drug delivery. *Polymer* **2021**, *230*, 124024.
- 37. Deirram, N.; Zhang, C.; Kermaniyan, S. S.; Johnston, A. P.; Such, G. K., pH-responsive polymer nanoparticles for drug delivery. *Macromolecular Rapid Communications* **2019**, *40* (10), 1800917.
- 38. Binauld, S.; Stenzel, M. H., Acid-degradable polymers for drug delivery: a decade of innovation. *Chemical Communications* **2013**, *49* (21), 2082-2102.
- 39. AlSawaftah, N. M.; Awad, N. S.; Pitt, W. G.; Husseini, G. A., pH-responsive nanocarriers in cancer therapy. *Polymers* **2022**, *14* (5), 936.

- 40. Liu, B.; Thayumanavan, S., Substituent effects on the pH sensitivity of acetals and ketals and their correlation with encapsulation stability in polymeric nanogels. *Journal of the American Chemical Society* **2017**, *139* (6), 2306-2317.
- 41. Maruya-Li, K.; Shetty, C.; Moini Jazani, A.; Arezi, N.; Oh, J. K., Dual Reduction/Acid-Responsive Disassembly and Thermoresponsive Tunability of Degradable Double Hydrophilic Block Copolymer. *ACS Omega* **2020**, *5* (7), 3734-3742.
- 42. Chan, N.; Khorsand, B.; Aleksanian, S.; Oh, J. K., A dual location stimuli-responsive degradation strategy of block copolymer nanocarriers for accelerated release. *Chemical Communications* **2013**, *49* (68), 7534-7536.
- 43. Chatgilialoglu, C.; Ferreri, C.; Matyjaszewski, K., Radicals and dormant species in biology and polymer chemistry. *ChemPlusChem* **2016**, *81* (1), 11-29.
- 44. Gurnani, P.; Perrier, S., Controlled radical polymerization in dispersed systems for biological applications. *Progress in Polymer Science* **2020**, *102*, 101209.
- 45. Grubbs, R. B., Nitroxide-mediated radical polymerization: limitations and versatility. *Polymer Reviews* **2011**, *51* (2), 104-137.
- 46. Pan, X.; Fantin, M.; Yuan, F.; Matyjaszewski, K., Externally controlled atom transfer radical polymerization. *Chemical Society Reviews* **2018**, *47* (14), 5457-5490.
- 47. Rodrigues, P. R.; Vieira, R. P., Advances in atom-transfer radical polymerization for drug delivery applications. *European Polymer Journal* **2019**, *115* (1), 45-58.
- 48. Magenau, A. J.; Bortolamei, N.; Frick, E.; Park, S.; Gennaro, A.; Matyjaszewski, K., Investigation of electrochemically mediated atom transfer radical polymerization. *Macromolecules* **2013**, *46* (11), 4346-4353.
- 49. Keddie, D. J., A guide to the synthesis of block copolymers using reversible-addition fragmentation chain transfer (RAFT) polymerization. *Chemical Society Reviews* **2014**, *43* (2), 496-505.
- 50. Rodrigues, P. R.; Vieira, R. P., Advances in atom-transfer radical polymerization for drug delivery applications. *European Polymer Journal* **2019**, *115*, 45-58.
- 51. Wang, R.; Wei, Q.; Sheng, W.; Yu, B.; Zhou, F.; Li, B., Driving polymer brushes from synthesis to functioning. *Angewandte Chemie* **2023**, *135* (27), e202219312.
- 52. Wei, H.; Zhuo, R.-X.; Zhang, X.-Z., Design and development of polymeric micelles with cleavable links for intracellular drug delivery. *Progress in Polymer Science* **2013**, *38* (3), 503-535.
- 53. Rijcken, C. J. F.; Soga, O.; Hennink, W. E.; van Nostrum, C. F., Triggered destabilization of polymeric micelles and vesicles by changing polymers polarity: An attractive tool for drug delivery. *Journal of Controlled Release* **2007**, *120* (3), 131-148.
- 54. Alvarez-Lorenzo, C.; Concheiro, A., Smart drug delivery systems: from fundamentals to the clinic. *Chemical Communication* **2014**, *50* (58), 7743-7765.
- 55. Loomis, K.; McNeeley, K.; Bellamkonda, R. V., Nanoparticles with targeting, triggered release, and imaging functionality for cancer applications. *Soft Matter* **2011**, *7* (3), 839-856.
- 56. Mura, S.; Nicolas, J.; Couvreur, P., Stimuli-responsive nanocarriers for drug delivery. *Nature Materials* **2013**, *12* (11), 991-1003.
- 57. Delplace, V.; Nicolas, J., Degradable vinyl polymers for biomedical applications. *Nature Chemistry* **2015**, *7* (10), 771-784.
- 58. Beach, M. A.; Nayanathara, U.; Gao, Y.; Zhang, C.; Xiong, Y.; Wang, Y.; Such, G. K., Polymeric Nanoparticles for Drug Delivery. *Chemical Reviews* **2024**, *124* (9).
- 59. Liu, H.; Lu, H. H.; Alp, Y.; Wu, R.; Thayumanavan, S., Structural Determinants of Stimuli-Responsiveness in Amphiphilic Macromolecular Nano-assemblies. *Progress in Polymer Science* **2024**, *148* (1).
- 60. Wang, Y.; Xu, H.; Zhang, X., Tuning the Amphiphilicity of Building Blocks: Controlled Self-Assembly and Disassembly for Functional Supramolecular Materials. *Advanced Materials* **2009**, 21 (28), 2849-2864.

- 61. Jackson, A. W.; Fulton, D. A., Making polymeric nanoparticles stimuli-responsive with dynamic covalent bonds. *Polymer Chemistry* **2013**, *4* (1), 31-45.
- 62. Deng, C.; Jiang, Y.; Cheng, R.; Meng, F.; Zhong, Z., Biodegradable polymeric micelles for targeted and controlled anticancer drug delivery: promises, progress and prospects. *Nano Today* **2012**, *7* (5), 467-480.
- 63. Ding, Y.; Kang, Y.; Zhang, X., Enzyme-responsive polymer assemblies constructed through covalent synthesis and supramolecular strategy. *Chemical Communications* **2015**, *51* (6), 996-1003.
- 64. Segal, M.; Avinery, R.; Buzhor, M.; Shaharabani, R.; Harnoy, A. J.; Tirosh, E.; Beck, R.; Amir, R. J., Molecular Precision and Enzymatic Degradation: From Readily to Undegradable Polymeric Micelles by Minor Structural Changes. *Journal of American Chemical Society* **2017**, *139* (2), 803-810.
- 65. Deng, Z.; Hu, J.; Liu, S., Reactive Oxygen, Nitrogen, and Sulfur Species (RONSS)-Responsive Polymersomes for Triggered Drug Release. *Macromolecular Rapid Communications* **2017**, *38* (11), n/a.
- 66. Zhang, W.; Hu, X.; Shen, Q.; Xing, D., Mitochondria-specific drug release and reactive oxygen species burst induced by polyprodrug nanoreactors can enhance chemotherapy. *Nature Communications* **2019**, *10* (1), 1704.
- 67. Shi, J.; Ma, B.; Zhang, Y.; Yong, H.; Li, Z.; A, S.; Huang, X.; Zhou, D., Targeted Delivery of Anticancer Therapeutics with Polymers by Harnessing Tumor Microenvironment Acidity. *Chemistry of Materials* **2023**, *35* (17), 6573-6590.
- 68. Cook, A. B.; Decuzzi, P., Harnessing Endogenous Stimuli for Responsive Materials in Theranostics. *ACS Nano* **2021**, *15* (2), 2068-2098.
- 69. Sharma, A.; Arambula, J. F.; Koo, S.; Kumar, R.; Singh, H.; Sessler, J. L.; Kim, J. S., Hypoxia-targeted drug delivery. *Chemical Society Reviews* **2019**, *48* (3), 771-813.
- 70. Song, Y.; Ding, Y.; Dong, C. M., Stimuli-responsive polypeptide nanoassemblies: Recent progress and applications in cancer nanomedicine. *Wiley Interdisciplinary Reviews:*Nanomedicine and Nanobiotechnology **2022**, 14 (2), e1742.
- 71. Tannock, I. F.; Rotin, D., Acid pH in tumors and its potential for therapeutic exploitation. *Cancer Research* **1989**, *49* (16), 4373-4384.
- 72. Watson, P.; Jones, A. T.; Stephens, D. J., Intracellular trafficking pathways and drug delivery: fluorescence imaging of living and fixed cells. *Advanced Drug Delivery Reviews* **2005**, *57* (1), 43-61.
- 73. Bazban-Shotorbani, S.; Hasani-Sadrabadi, M. M.; Karkhaneh, A.; Serpooshan, V.; Jacob, K. I.; Moshaverinia, A.; Mahmoudi, M., Revisiting structure-property relationship of pH-responsive polymers for drug delivery applications. *Journal of Controlled Release* **2017**, *253* (1), 46-63.
- 74. Russo, A.; DeGraff, W.; Friedman, N.; Mitchell, J. B., Selective modulation of glutathione levels in human normal versus tumor cells and subsequent differential response to chemotherapy drugs. *Cancer Research* **1986**, *46* (6), 2845-8.
- 75. Saito, G.; Swanson, J. A.; Lee, K.-D., Drug delivery strategy utilizing conjugation via reversible disulfide linkages: role and site of cellular reducing activities. *Advanced Drug Delivery Reviews* **2003**, *55* (2), 199-215.
- 76. Ottaviano, F. G.; Handy, D. E.; Joseph Loscalzo, J., Redox Regulation in the Extracellular Environment. *Circulation Journal* **2008**, *72* (1), 1-16.
- 77. Li, Y.; Chen, M.; Yao, B.; Lu, X.; Zhang, X.; He, P.; Vasilatos, S. N.; Ren, X.; Bian, W.; Yao, C., Transferrin receptor-targeted redox/pH-sensitive podophyllotoxin prodrug micelles for multidrug-resistant breast cancer therapy. *Journal of Materials Chemistry B: Materials for Biology and Medicine* **2019**, 7 (38), 5814-5824.
- 78. Hwang, C.; Sinskey, A. J.; Lodish, H. F., Oxidized redox state of glutathione in the endoplasmic reticulum. *Science (Washington, D C, 1883-)* **1992,** *257* (5076), 1496-502.

- 79. Kocak, G.; Tuncer, C.; Butun, V., pH-Responsive polymers. *Polymer Chemistry* **2017**, *8* (1), 144-176.
- 80. Binauld, S.; Stenzel, M. H., Acid-degradable polymers for drug delivery: a decade of innovation. *Chemical Communications* **2013**, *49* (21), 2082-2102.
- 81. Qu, X.; Yang, Z., Benzoic-Imine-Based Physiological-pH-Responsive Materials for Biomedical Applications. *Chemistry -An Asian Journal* **2016**, *11* (19), 2633-2641.
- 82. Jazani, A. M.; Oh, J. K., Development and disassembly of single and multiple acid-cleavable block copolymer nanoassemblies for drug delivery. *Polymer Chemistry* **2020**, *11* (17), 2934-2954.
- 83. Gannimani, R.; Walvekar, P.; Naidu, V. R.; Aminabhavi, T. M.; Govender, T., Acetal containing polymers as pH-responsive nano-drug delivery systems. *Journal of Controled Release* **2020**, *328* (1), 736-761.
- 84. Cheng, R.; Feng, F.; Meng, F.; Deng, C.; Feijen, J.; Zhong, Z., Glutathione-responsive nanovehicles as a promising platform for targeted intracellular drug and gene delivery. *Journal of Controlled Release* **2011**, *152* (1), 2-12.
- 85. Quinn, J. F.; Whittaker, M. R.; Davis, T. P., Glutathione responsive polymers and their application in drug delivery systems. *Polymer Chemistry* **2017**, *8* (1), 97-126.
- 86. Hsu, P.-H.; Almutairi, A., Recent progress of redox-responsive polymeric nanomaterials for controlled release. *Journal of Materials Chemistry B* **2021**, *9* (9), 2179-2188.
- 87. Chan, N.; Ko, N. R.; An, S. Y.; Khorsand, B.; Oh, J. K., Dual location reduction-responsive degradable nanocarriers: A new strategy for intracellular anticancer drug delivery with accelerated release. In *Controlled Radical Polymerization: Materials*, ACS Publications: 2015; pp 273-291.
- 88. Zalba, S.; Ten Hagen, T. L. M.; Burgui, C.; Garrido, M. J., Stealth nanoparticles in oncology: Facing the PEG dilemma. *Journal of Controlled Release* **2022**, *351* (1), 22-36.
- 89. Fang, Y.; Xue, J.; Gao, S.; Lu, A.; Yang, D.; Jiang, H.; He, Y.; Shi, K., Cleavable PEGylation: a strategy for overcoming the "PEG dilemma" in efficient drug delivery. *Drug Delivery* **2017**, *24* (sup1), 22-32.
- 90. Kong, L.; Campbell, F.; Kros, A., DePEGylation strategies to increase cancer nanomedicine efficacy. *Nanoscale Horizons* **2019**, *4* (2), 378-387.
- 91. Jin, Q.; Deng, Y.; Chen, X.; Ji, J., Rational Design of Cancer Nanomedicine for Simultaneous Stealth Surface and Enhanced Cellular Uptake. *ACS Nano* **2019**, *13* (2), 954-977.
- 92. Pesenti, T.; Nicolas, J., 100th anniversary of macromolecular science viewpoint: Degradable polymers from radical ring-opening polymerization: Latest advances, new directions, and ongoing challenges. *ACS Macro Letters* **2020**, *9* (12), 1812-1835.
- 93. Tardy, A.; Nicolas, J.; Gigmes, D.; Lefay, C.; Guillaneuf, Y., Radical ring-opening polymerization: Scope, limitations, and application to (bio) degradable materials. *Chemical Reviews* **2017**, *117* (3), 1319-1406.
- 94. Albertsson, A.-C.; Varma, I. K., Recent developments in ring opening polymerization of lactones for biomedical applications. *Biomacromolecules* **2003**, *4* (6), 1466-1486.
- 95. Jérôme, C.; Lecomte, P., Recent advances in the synthesis of aliphatic polyesters by ring-opening polymerization. *Advanced Drug Delivery Reviews* **2008**, *60* (9), 1056-1076.
- 96. Wu, J.; Yu, T.-L.; Chen, C.-T.; Lin, C.-C., Recent developments in main group metal complexes catalyzed/initiated polymerization of lactides and related cyclic esters. *Coordination Chemistry Reviews* **2006**, *250* (5-6), 602-626.
- 97. Jones, G. R.; Wang, H. S.; Parkatzidis, K.; Whitfield, R.; Truong, N. P.; Anastasaki, A., Reversed Controlled Polymerization (RCP): Depolymerization from Well-Defined Polymers to Monomers. *Journal of American Chemical Society* **2023**, *145* (18), 9898-9915.
- 98. Braunecker, W. A.; Matyjaszewski, K., Controlled/living radical polymerization: Features, developments, and perspectives. *Progress in Polymer Science* **2007**, *32* (1), 93-146.

- 99. De Neve, J.; Haven, J. J.; Maes, L.; Junkers, T., Sequence-definition from controlled polymerization: the next generation of materials. *Polymer Chemistry* **2018**, *9* (38), 4692-4705.
- 100. Corrigan, N.; Jung, K.; Moad, G.; Hawker, C. J.; Matyjaszewski, K.; Boyer, C., Reversible-deactivation radical polymerization (Controlled/living radical polymerization): From discovery to materials design and applications. *Progress in Polymer Science* **2020**, *111* (1), 101311.
- 101. Matyjaszewski, K.; Xia, J., Atom transfer radical polymerization. *Chemical Reviews* **2001**, *101* (9), 2921-2990.
- 102. Szewczyk-Łagodzińska, M.; Plichta, A.; Dębowski, M.; Kowalczyk, S.; Iuliano, A.; Florjańczyk, Z., Recent Advances in the Application of ATRP in the Synthesis of Drug Delivery Systems. *Polymers* **2023**, *15* (5), 1234.
- 103. Kreutzer, J., Atom-transfer radical polymerization: New method breathes life into ATRP. *Nature Reviews Chemistry* **2018**, *2* (2), 0111.
- 104. Matyjaszewski, K., Atom transfer radical polymerization (ATRP): current status and future perspectives. *Macromolecules* **2012**, *45* (10), 4015-4039.
- 105. Perrier, S., 50th Anniversary Perspective: RAFT Polymerization ☐ A User Guide. *Macromolecules* **2017**, *50* (19), 7433-7447.
- 106. Barner-Kowollik, C.; Perrier, S., The future of reversible addition fragmentation chain transfer polymerization. *Journal of Polymer Science Part A: Polymer Chemistry* **2008**, *46* (17), 5715-5723.
- 107. Chernikova, E.; Sivtsov, E., Reversible addition-fragmentation chain-transfer polymerization: Fundamentals and use in practice. *Polymer Science, Series B* **2017**, *59* (1), 117-146.
- 108. Barner-Kowollik, C., Handbook of RAFT polymerization. John Wiley & Sons: 2008.
- 109. Nothling, M. D.; Fu, Q.; Reyhani, A.; Allison-Logan, S.; Jung, K.; Zhu, J.; Kamigaito, M.; Boyer, C.; Qiao, G. G., Progress and perspectives beyond traditional RAFT polymerization. *Advanced Science* **2020**, *7* (20), 2001656.
- 110. Moad, G.; Rizzardo, E., *RAFT Polymerization: Methods, Synthesis, and Applications*. John Wiley & Sons: 2021.
- 111. Bates, F. S.; Fredrickson, G. H., Block copolymers—designer soft materials. *Physics today* **1999**, 52 (2), 32-38.
- 112. Hadjichristidis, N.; Pitsikalis, M.; Iatrou, H., Synthesis of block copolymers. *Block Copolymers I* **2005**, 1-124.
- 113. Hadjichristidis, N.; Iatrou, H.; Pitsikalis, M.; Mays, J., Macromolecular architectures by living and controlled/living polymerizations. *Progress in Polymer Science* **2006**, *31* (12), 1068-1132.
- 114. Cabral, H.; Miyata, K.; Osada, K.; Kataoka, K., Block copolymer micelles in nanomedicine applications. *Chemical Reviews* **2018**, *118* (14), 6844-6892.
- 115. Zhang, Y.; Cao, M.; Han, G.; Guo, T.; Ying, T.; Zhang, W., Topology affecting block copolymer nanoassemblies: linear block copolymers versus star block copolymers under PISA conditions. *Macromolecules* **2018**, *51* (14), 5440-5449.
- 116. Deng, Z.; Liu, S., Emerging trends in solution self-assembly of block copolymers. *Polymers* **2020**, *207* (1), 122914.
- 117. Li, X.; Iocozzia, J.; Chen, Y.; Zhao, S.; Cui, X.; Wang, W.; Yu, H.; Lin, S.; Lin, Z., From precision synthesis of block copolymers to properties and applications of nanoparticles.

 Angewandte Chemie International Edition 2018, 57 (8), 2046-2070.
- 118. Hadjichristidis, N.; Pitsikalis, M.; Iatrou, H.; Pispas, S., The strength of the macromonomer strategy for complex macromolecular architecture: Molecular characterization, properties and applications of polymacromonomers. *Macromolecular Rapid Communications* **2003**, *24* (17), 979-1013.
- 119. Kainthan, R. K.; Janzen, J.; Levin, E.; Devine, D. V.; Brooks, D. E., Biocompatibility testing of branched and linear polyglycidol. *Biomacromolecules* **2006**, *7* (3), 703-709.

- 120. Vazaios, A.; Touris, A.; Echeverria, M.; Zorba, G.; Pitsikalis, M., Micellization behaviour of linear and nonlinear block copolymers based on poly (n-hexyl isocyanate) in selective solvents. *Polymers* **2020**, *12* (8), 1678.
- 121. Ji, X.; Li, W., Effect of chain architectures on the domain spacing of block copolymers with equivalent segregation degrees. *Physical Chemistry Chemical Physics* **2020**, *22* (32), 17824-17832.
- 122. Abdullah, C. S.; Ray, P.; Alam, S.; Kale, N.; Aishwarya, R.; Morshed, M.; Dutta, D.; Hudziak, C.; Banerjee, S. K.; Mallik, S., Chemical architecture of block copolymers differentially abrogate cardiotoxicity and maintain the anticancer efficacy of doxorubicin. *Molecular Pharmaceutics* **2020**, *17* (12), 4676-4690.
- 123. Petrova, S.; Jager, E.; Konefal, R.; Jager, A.; Venturini, C. G.; Spevacek, J.; Pavlova, E.; Stepanek, P., Novel poly(ethylene oxide monomethyl ether)-b-poly(ε-caprolactone) diblock copolymers containing a pH-acid labile ketal group as a block linkage. *Polymer Chemistry* **2014**, *5* (12), 3884-3893.
- 124. Petrova, S. L.; Jäger, E.; Jäger, A.; Höcherl, A.; Konefał, R.; Zhigunov, A.; Pavlova, E.; Janoušková, O.; Hrubý, M., Development of an Acid-Labile Ketal Linked Amphiphilic Block Copolymer Nanoparticles for pH-Triggered Release of Paclitaxel. *Polymers* **2021**, *13* (9), 1465.
- 125. Zhang, Y.; Lu, Y.; Cao, M.; Chen, P.; Yang, B.; Miao, J.; Xia, R.; Qian, J., Y-shaped copolymers of poly (ethylene glycol)-poly (ε-caprolactone) with ketal bond as the branchpoint for drug delivery. *Materials Science and Engineering: C* 2018, 93, 554-564.
- 126. Wang, H.; He, J.; Zhang, M.; Tao, Y.; Li, F.; Tam, K. C.; Ni, P., Biocompatible and acid-cleavable poly (ε-caprolactone)-acetal-poly (ethylene glycol)-acetal-poly (ε-caprolactone) triblock copolymers: synthesis, characterization and pH-triggered doxorubicin delivery. *Journal of Materials Chemistry B* **2013**, *I* (48), 6596-6607.
- Hu, J.; He, J.; Zhang, M.; Ni, P., Precise modular synthesis and a structure-property study of acid-cleavable star-block copolymers for pH-triggered drug delivery. *Polymer Chemistry* **2015**, *6* (9), 1553-1566.
- 128. Wu, W. X.; Wang, N.; Liu, B. Y.; Deng, Q. F.; Yu, X. Q., Lipase-catalyzed synthesis of azido-functionalized aliphatic polyesters towards acid-degradable amphiphilic graft copolymers. *Soft Matter* **2014**, *10* (8), 1199-213.
- 129. Zhang, S.; Xu, J.; Chen, H.; Song, Z.; Wu, Y.; Dai, X.; Kong, J., Acid-Cleavable Unimolecular Micelles from Amphiphilic Star Copolymers for Triggered Release of Anticancer Drugs. *Macromolecular Bioscience* **2017**, *17* (3), 1600258.
- 130. Hao, Y.; He, J.; Li, S.; Liu, J.; Zhang, M.; Ni, P., Synthesis of an acid-cleavable and fluorescent amphiphilic block copolymer as a combined delivery vector of DNA and doxorubicin. *Journal of Materials Chemistry B* **2014**, *2* (27), 4237-4249.
- 131. Patil, S. S.; Wadgaonkar, P. P., Temperature and pH dual stimuli responsive PCL-b-PNIPAAm block copolymer assemblies and the cargo release studies. *Journal of Polymer Science, Part A: Polymer Chemistry* **2017**, *55* (8), 1383-1396.
- Hu, J.; He, J.; Zhang, M.; Ni, P., Precise modular synthesis and a structure-property study of acid-cleavable star-block copolymers for pH-triggered drug delivery. *Polymer Chemistry* **2015**, *6* (9), 1553-1566.
- 133. Worm, M.; Kang, B.; Dingels, C.; Wurm, F. R.; Frey, H., Acid-labile amphiphilic PEO-b-PPO-b-PEO copolymers: degradable poloxamer analogs. *Macromolecular Rapid Communications* **2016**, *37* (9), 775-780.
- 134. Xiao, L.; Huang, L.; Moingeon, F.; Gauthier, M.; Yang, G., pH-responsive poly (ethylene glycol)-block-polylactide micelles for tumor-targeted drug delivery. *Biomacromolecules* **2017**, *18* (9), 2711-2722.
- 135. Sarisuta, K.; Iwami, M.; Martín-Vaca, B.; Chanthaset, N.; Ajiro, H., pH Effect on Particle Aggregation of Vanillin End-Capped Polylactides Bearing a Hydrophilic Group Connected by a Cyclic Acetal Moiety. *Langmuir* **2023**, *39* (11), 3994-4004.

- 136. Bawa, K. K.; Shetty, C.; Arezi, N.; Oh, J. K., Synthesis and Structure-Driven Acid-Catalyzed Degradation of Benzoic Cyclic Acetal-Labeled PEG Precursors toward Shell-Sheddable PLA Block Copolymer Synthesis. *Macromolecular Chemistry and Physics* **2023**, *224* (16).
- 137. Huang, X.; Sevimli, S. I.; Bulmus, V., pH-labile sheddable block copolymers by RAFT polymerization: Synthesis and potential use as siRNA conjugates. *European Polymer Journal* **2013**, *49* (10), 2895-2905.
- 138. Satoh, K.; Poelma, J. E.; Campos, L. M.; Stahl, B.; Hawker, C. J., A facile synthesis of clickable and acid-cleavable PEO for acid-degradable block copolymers. *Polymer Chemistry* **2012**, *3* (7), 1890-1898.
- 139. Andrade-Gagnon, B.; Casillas-Popova, S. N.; Jazani, A. M.; Oh, J. K., Design Synthesis, and Acid-Responsive Disassembly of Shell-Sheddable Block Copolymer Labeled with Benzaldehyde Acetal Junction. *Macromolecular Rapid Communications* **2024**, *45* (12), 2400097.
- 140. Zheng, L.; Zhang, X.; Wang, Y.; Liu, F.; Peng, J.; Zhao, X.; Yang, H.; Ma, L.; Wang, B.; Chang, C., Fabrication of acidic pH-cleavable polymer for anticancer drug delivery using a dual functional monomer. *Biomacromolecules* **2018**, *19* (9), 3874-3882.
- 141. Sui, X.; Zhang, Z.; Guan, S.; Xu, Y.; Li, C.; Lv, Y.; Chen, A.; Yang, L.; Gao, L., A facile strategy for the synthesis of block copolymers bearing an acid-cleavable junction. *Polymer Chemistry* **2015**, *6* (14), 2777-2782.
- 142. Lin, S.; Du, F.; Wang, Y.; Ji, S.; Liang, D.; Yu, L.; Li, Z., An acid-labile block copolymer of PDMAEMA and PEG as potential carrier for intelligent gene delivery systems. *Biomacromolecules* **2008**, *9* (1), 109-115.
- 143. Yan, G.; Zhang, P.; Wang, J.; Wang, X.; Tang, R., Dynamic micelles with detachable PEGylation at tumoral extracellular pH for enhanced chemotherapy. *Asian Journal of Pharmaceutical Sciences* **2020**, *15* (6), 728-738.
- 144. Musikavanhu, B.; Liang, Y.; Xue, Z.; Feng, L.; Zhao, L., Strategies for Improving Selectivity and Sensitivity of Schiff Base Fluorescent Chemosensors for Toxic and Heavy Metals. *Molecules* **2023**, *28* (19), 6960.
- 145. Yang, Z.; Sun, N.; Cheng, R.; Zhao, C.; Liu, Z.; Liu, J.; Tian, Z., pH multistage responsive micellar system with charge-switch and PEG layer detachment for co-delivery of paclitaxel and curcumin to synergistically eliminate breast cancer stem cells. *Biomaterials* **2017**, 147, 53-67.
- 146. Chou, Y.-H.; Liu, Y.-L.; Hsu, T.-C.; Yow, J.-L.; Tzang, B.-S.; Chiang, W.-H., Tumor acidity-responsive polymeric nanoparticles to promote intracellular delivery of zoledronic acid by PEG detachment and positive charge exposure for enhanced antitumor potency. *Journal of Materials Chemistry B* **2022**, *10* (23), 4363-4374.
- 147. Jin, Y.; Song, L.; Su, Y.; Zhu, L.; Pang, Y.; Qiu, F.; Tong, G.; Yan, D.; Zhu, B.; Zhu, X., Oxime linkage: a robust tool for the design of pH-sensitive polymeric drug carriers. *Biomacromolecules* **2011**, *12* (10), 3460-3468.
- 148. Babikova, D.; Kalinova, R.; Momekova, D.; Ugrinova, I.; Momekov, G.; Dimitrov, I., Multifunctional polymer nanocarrier for efficient targeted cellular and subcellular anticancer drug delivery. *ACS Biomaterials Science & Engineering* **2019**, *5* (5), 2271-2283.
- 149. Gu, J.; Cheng, W.-P.; Liu, J.; Lo, S.-Y.; Smith, D.; Qu, X.; Yang, Z., pH-triggered reversible "stealth" polycationic micelles. *Biomacromolecules* **2008**, *9* (1), 255-262.
- 150. Wu, S.; Zheng, L.; Li, C.; Xiao, Y.; Huo, S.; Zhang, B., Grafted copolymer micelles with pH triggered charge reversibility for efficient doxorubicin delivery. *Journal of Polymer Science A: Polymer Chemistry* **2017**, *55* (12), 2036-2046.
- 151. Yang, X.; An, J.; Luo, Z.; Yang, R.; Yan, S.; Liu, D.-E.; Fu, H.; Gao, H., A cyanine-based polymeric nanoplatform with microenvironment-driven cascaded responsiveness for imaging-guided chemo-photothermal combination anticancer therapy. *Journal of Materials Chemistry B* **2020**, 8 (10), 2115-2122.

- 152. Xu, M.; Zhang, C. Y.; Wu, J.; Zhou, H.; Bai, R.; Shen, Z.; Deng, F.; Liu, Y.; Liu, J., PEG-detachable polymeric micelles self-assembled from amphiphilic copolymers for tumor-acidity-triggered drug delivery and controlled release. *ACS Applied Materials & Interfaces* **2019**, *11* (6), 5701-5713.
- 153. Song, C.; Yang, F.; Ji, R.; Lv, Y.; Wei, Z., Construction of a drug delivery system via pH-responsive polymeric nanomicelles containing ferrocene for DOX release and enhancement of therapeutic effects. *ACS Omega* **2021**, *6* (42), 28242-28253.
- 154. Zeng, Z.; Wei, Z.; Ma, L.; Xu, Y.; Xing, Z.; Niu, H.; Wang, H.; Huang, W., pH-Responsive nanoparticles based on ibuprofen prodrug as drug carriers for inhibition of primary tumor growth and metastasis. *Journal of Materials Chemistry B* **2017**, *5* (33), 6860-6868.
- 155. Kalia, J.; Raines, R. T., Hydrolytic stability of hydrazones and oximes. *Angewandte Chemie International Edition* **2008**, *47* (39), 7523-7526.
- 156. Angelova, V. T.; Vassilev, N. G.; Nikolova-Mladenova, B.; Vitas, J.; Malbaša, R.; Momekov, G.; Djukic, M.; Saso, L., Antiproliferative and antioxidative effects of novel hydrazone derivatives bearing coumarin and chromene moiety. *Medicinal Chemistry Research* **2016**, *25*, 2082-2092.
- 157. Nguyen, R.; Huc, I., Optimizing the reversibility of hydrazone formation for dynamic combinatorial chemistry. *Chemical Communications* **2003**, *8* (1), 942-943.
- 158. Hannachi, D.; Khelfaoui, N.; Zaidi, M.; Yahiaoui, D.; Lakehal, S.; Morell, C.; Chermette, H., The effect of resonance-assisted hydrogen bond on the second-order nonlinear optical properties of pyridine hydrazone photoswitches: a quantum chemistry investigation. *New Journal of Chemistry* **2023**, *47* (39), 18359-18373.
- 159. Sonawane, S. J.; Kalhapure, R. S.; Govender, T., Hydrazone linkages in pH responsive drug delivery systems. *European Journal of Pharmaceutical Sciences* **2017**, *99* (1), 45-65.
- 160. Domiński, A.; Domińska, M.; Skonieczna, M.; Pastuch-Gawołek, G.; Kurcok, P., Shell-Sheddable Micelles Based on Poly (ethylene glycol)-hydrazone-poly [R, S]-3-hydroxybutyrate Copolymer Loaded with 8-Hydroxyquinoline Glycoconjugates as a Dual Tumor-Targeting Drug Delivery System. *Pharmaceutics* **2022**, *14* (2), 290.
- 161. Xu, J.; Luan, S.; Qin, B.; Wang, Y.; Wang, K.; Qi, P.; Song, S., Backbone-hydrazone-containing biodegradable copolymeric micelles for anticancer drug delivery. *Journal of Nanoparticle Research* **2016**, *18*, 1-15.
- 162. Su, W.-T.; Huang, C.-C.; Liu, H.-W., Evaluation and Preparation of a Designed Kartogenin Drug Delivery System (DDS) of Hydrazone-Linkage-Based pH Responsive mPEG-Hz-b-PCL Nanomicelles for Treatment of Osteoarthritis. *Frontiers in Bioengineering and Biotechnology* **2022**, *10* (1), 816664.
- 163. Li, J.; Qiang, H.; Yang, W.; Xu, Y.; Feng, T.; Cai, H.; Wang, S.; Liu, Z.; Zhang, Z.; Zhang, J., Oral insulin delivery by epithelium microenvironment-adaptive nanoparticles. *Journal of Controlled Release* **2022**, *341* (1), 31-43.
- 164. Du, J. Z.; Sun, T. M.; Song, W. J.; Wu, J.; Wang, J., A tumor-acidity-activated charge-conversional nanogel as an intelligent vehicle for promoted tumoral-cell uptake and drug delivery. *Angewandte Chemie International Edition in English* **2010**, *49* (21), 3621-6.
- 165. Deng, H.; Liu, J.; Zhao, X.; Zhang, Y.; Liu, J.; Xu, S.; Deng, L.; Dong, A.; Zhang, J., PEG-b-PCL Copolymer Micelles with the Ability of pH-Controlled Negative-to-Positive Charge Reversal for Intracellular Delivery of Doxorubicin. *Biomacromolecules* **2014**, *15* (11), 4281-4292.
- 166. Miao, Y.; Qiu, Y.; Yang, W.; Guo, Y.; Hou, H.; Liu, Z.; Zhao, X., Charge reversible and biodegradable nanocarriers showing dual pH-/reduction-sensitive disintegration for rapid site-specific drug delivery. *Colloids Surfaces B Biointerfaces* **2018**, *169* (1), 313-320.
- 167. Fan, M.; Zeng, Y.; Ruan, H.; Zhang, Z.; Gong, T.; Sun, X., Ternary Nanoparticles with a Sheddable Shell Efficiently Deliver MicroRNA-34a against CD44-Positive Melanoma. *Molecular Pharmaceutics* **2017**, *14* (9), 3152-3163.

- 168. Takemoto, H.; Miyata, K.; Hattori, S.; Ishii, T.; Suma, T.; Uchida, S.; Nishiyama, N.; Kataoka, K., Acidic pH-responsive siRNA conjugate for reversible carrier stability and accelerated endosomal escape with reduced IFNalpha-associated immune response. *Angewandte Chemie International Edition in English* **2013**, *52* (24), 6218-21.
- 169. Maier, K.; Wagner, E., Acid-labile traceless click linker for protein transduction. *Journal of American Chemical Society* **2012**, *134* (24), 10169-73.
- 170. Du, J.-Z.; Li, H.-J.; Wang, J., Tumor-Acidity-Cleavable Maleic Acid Amide for Smart Nanoparticles To Overcome Delivery Barriers in Cancer Nanomedicine. *Accounts of Chemical Research* **2018**, *51* (11), 2848-2856.
- 171. Du, J. Z.; Mao, C. Q.; Yuan, Y. Y.; Yang, X. Z.; Wang, J., Tumor extracellular acidity-activated nanoparticles as drug delivery systems for enhanced cancer therapy. *Biotechnology Advances* **2014**, *32* (4), 789-803.
- 172. Sun, C.-Y.; Liu, Y.; Du, J.-Z.; Cao, Z.-T.; Xu, C.-F.; Wang, J., Facile Generation of TumorpH-Labile Linkage-Bridged Block Copolymers for Chemotherapeutic Delivery. *Angewandte Chemie International Edition* **2016**, *55* (3), 1010-1014.
- 173. Xu, C. F.; Zhang, H. B.; Sun, C. Y.; Liu, Y.; Shen, S.; Yang, X. Z.; Zhu, Y. H.; Wang, J., Tumor acidity-sensitive linkage-bridged block copolymer for therapeutic siRNA delivery. *Biomaterials* **2016**, *88*, 48-59.
- 174. Sun, C.-Y.; Shen, S.; Xu, C.-F.; Li, H.-J.; Liu, Y.; Cao, Z.-T.; Yang, X.-Z.; Xia, J.-X.; Wang, J., Tumor Acidity-Sensitive Polymeric Vector for Active Targeted siRNA Delivery. *Journal of American Chemical Society* **2015**, *137* (48), 15217-15224.
- 175. Sun, C.-Y.; Shen, S.; Xu, C.-F.; Li, H.-J.; Liu, Y.; Cao, Z.-T.; Yang, X.-Z.; Xia, J.-X.; Wang, J., Tumor Acidity-Sensitive Polymeric Vector for Active Targeted siRNA Delivery. *Journal of American Chemical Society* **2015**, *137* (48), 15217-15224.
- 176. Liu, S.; Ono, R. J.; Yang, C.; Gao, S.; Ming Tan, J. Y.; Hedrick, J. L.; Yang, Y. Y., Dual pHresponsive shell-cleavable polycarbonate micellar nanoparticles for in vivo anticancer drug delivery. *ACS Applied Materials & Interfaces* **2018**, *10* (23), 19355-19364.
- 177. Chan, N.; An, S. Y.; Oh, J. K., Dual location disulfide degradable interlayer-crosslinked micelles with extended sheddable coronas exhibiting enhanced colloidal stability and rapid release. *Polymer Chemistry* **2014**, *5* (5), 1637-1649.
- 178. Ko, N. R.; Oh, J. K., Glutathione-Triggered Disassembly of Dual Disulfide Located Degradable Nanocarriers of Polylactide-Based Block Copolymers for Rapid Drug Release. *Biomacromolecules* **2014**, *15* (8), 3180-3189.
- 179. Bawa, K. K.; Jazani, A. M.; Shetty, C.; Oh, J. K., PLA-Based Triblock Copolymer Micelles Exhibiting Dual Acidic pH/Reduction Responses at Dual Core and Core/Corona Interface Locations. *Macromolecular Rapid Communications* **2018**, *39* (24), 1800477.
- 180. Chen, W.; Zhong, P.; Meng, F.; Cheng, R.; Deng, C.; Feijen, J.; Zhong, Z., Redox and pHresponsive degradable micelles for dually activated intracellular anticancer drug release. *Journal of Controlled Release* **2013**, *169* (3), 171-179.
- 181. Wang, Y.; Zhang, L.; Zhang, X.; Wei, X.; Tang, Z.; Zhou, S., Precise Polymerization of a Highly Tumor Microenvironment-Responsive Nanoplatform for Strongly Enhanced Intracellular Drug Release. *ACS Applied Materials and Interfaces* **2016**, *8* (9), 5833-5846.
- 182. Klaikherd, A.; Nagamani, C.; Thayumanavan, S., Multi-Stimuli Sensitive Amphiphilic Block Copolymer Assemblies. *Journal of American Chemical Society* **2009**, *131* (13), 4830-4838.
- 183. Li, B.; Shan, M.; Di, X.; Gong, C.; Zhang, L.; Wang, Y.; Wu, G., A dual pH- and reduction-responsive anticancer drug delivery system based on PEG–SS–poly(amino acid) block copolymer. *RSC Advances* **2017**, *7* (48), 30242-30249.
- 184. Yin, T.; Wang, Y.; Chu, X.; Fu, Y.; Wang, L.; Zhou, J.; Tang, X.; Liu, J.; Huo, M., Free Adriamycin-Loaded pH/Reduction Dual-Responsive Hyaluronic Acid-Adriamycin Prodrug Micelles for Efficient Cancer Therapy. *ACS Applied Materials and Interfaces* **2018**, *10* (42), 35693-35704.

- 185. Shao, W.; Miao, K.; Liu, H.; Ye, C.; Du, J.; Zhao, Y., Acid and reduction dually cleavable amphiphilic comb-like copolymer micelles for controlled drug delivery. *Polymer Chemistry* **2013**, *4* (11), 3398-3410.
- 186. Liu, H.; Li, C.; Tang, D.; An, X.; Guo, Y.; Zhao, Y., Multi-responsive graft copolymer micelles comprising acetal and disulfide linkages for stimuli-triggered drug delivery. *Journal of Materials Chemistry B* **2015**, *3* (19), 3959-3971.
- 187. Miao, K.; Shao, W.; Liu, H.; Zhao, Y., Synthesis and properties of a dually cleavable graft copolymer comprising pendant acetal linkages. *Polymer Chemistry* **2014**, *5* (4), 1191-1201.
- 188. Song, N.; Ding, M.; Pan, Z.; Li, J.; Zhou, L.; Tan, H.; Fu, Q., Construction of targeting-clickable and tumor-cleavable polyurethane nanomicelles for multifunctional intracellular drug delivery. *Biomacromolecules* **2013**, *14* (12), 4407-4419.
- 189. Ding, M.; Li, J.; He, X.; Song, N.; Tan, H.; Zhang, Y.; Zhou, L.; Gu, Q.; Deng, H.; Fu, Q., Molecular Engineered Super-Nanodevices: Smart and Safe Delivery of Potent Drugs into Tumors. *Advanced Materials* **2012**, *24* (27), 3639-3645.
- 190. Ding, Y.; Du, C.; Qian, J.; Zhou, L.; Su, Y.; Zhang, R.; Dong, C.-M., Tumor pH and intracellular reduction responsive polypeptide nanomedicine with a sheddable PEG corona and a disulfide-cross-linked core. *Polymer Chemistry* **2018**, *9* (25), 3488-3498.
- 191. Su, Z.; Xu, Y.; Wang, Y.; Shi, W.; Han, S.; Shuai, X., A pH and reduction dual-sensitive polymeric nanomicelle for tumor microenvironment triggered cellular uptake and controlled intracellular drug release. *Biomaterials Science* **2019**, *7* (9), 3821-3831.
- 192. Jazani, A. M.; Oh, J. K., Dual Location, Dual Acidic pH/Reduction-Responsive Degradable Block Copolymer: Synthesis and Investigation of Ketal Linkage Instability under ATRP Conditions. *Macromolecules* **2017**, *50* (23), 9427-9436.
- 193. Arezi, N.; Oh, J. K., Carbonylimidazole-hydroxyl coupling chemistry: Synthesis and block copolymerization of fully bio-reducible poly(carbonate-disulfide)s. *Polymers* **2020**, *206* (1), 122793.
- 194. Tao, W.; Wang, J.; Zhou, Y.; Liu, Z.; Chen, H.; Zhao, Z.; Yan, H.; Liao, X., Acid/reduction dual-sensitive amphiphilic graft polyurethane with folic acid and detachable poly(ethylene glycol) as anticancer drug delivery carrier. *Colloids Surfaces B Biointerfaces* **2023**, *222* (1), 113084.
- 195. Cao, Y.; Zhao, J.; Zhang, Y.; Liu, J.; Liu, J.; Dong, A.; Deng, L., pH/redox dual-sensitive nanoparticles based on the PCL/PEG triblock copolymer for enhanced intracellular doxorubicin release. *RSC Advances* **2015**, *5* (36), 28060-28069.
- 196. Wang, S.; Wang, H.; Liu, Z.; Wang, L.; Wang, X.; Su, L.; Chang, J., Smart pH- and reduction-dual-responsive folate-PEG-coated polymeric lipid vesicles for tumor-triggered targeted drug delivery. *Nanoscale* **2014**, *6* (13), 7635-42.
- 197. Cooper Jr, J.; Mintz, B.; Palumbo, S.; Li, W., Assays for determining cell differentiation in biomaterials. In *Characterization of Biomaterials*, Elsevier: 2013; pp 101-137.
- 198. Gonnabathula, P.; Mekala, N.; Relangi, P. K., Nanotoxicology: Evaluating Toxic Potential of Drug Nanoparticles. In *Nanotechnology in Biology and Medicine*, CRC Press: 2019; pp 235-243.
- 199. Oh, J. K., Polylactide (PLA)-based amphiphilic block copolymers: synthesis, self-assembly, and biomedical applications. *Soft Matter* **2011**, *7* (11), 5096-5108.
- 200. Jung, J.; Lee, I.-H.; Lee, E.; Park, J.; Jon, S., pH-Sensitive Polymer Nanospheres for Use as a Potential Drug Delivery Vehicle. *Biomacromolecules* **2007**, *8* (11), 3401-3407.
- 201. Massoumi, B.; Abbasian, M.; Jahanban-Esfahlan, R.; Motamedi, S.; Samadian, H.; Rezaei, A.; Derakhshankhah, H.; Farnudiyan-Habibi, A.; Jaymand, M., PEGylated hollow pH-responsive polymeric nanocapsules for controlled drug delivery. *Polymer International* **2020**, *69* (5), 519-527.
- 202. Pinyakit, Y.; Palaga, T.; Kiatkamjornwong, S.; Hoven, V. P., Sequential post-polymerization modification of a pentafluorophenyl ester-containing homopolymer: a convenient route to effective pH-responsive nanocarriers for anticancer drugs. *Journal of Materials Chemistry B* **2020**, *8* (3), 454-464.

- 203. Markopoulou, P.; Panagiotou, N.; Li, A.; Bueno-Perez, R.; Madden, D.; Buchanan, S.; Fairen-Jimenez, D.; Shiels, P. G.; Forgan, R. S., Identifying differing intracellular cargo release mechanisms by monitoring in vitro drug delivery from MOFs in real time. *Cell Reports Physical Science* **2020**, *1* (11).
- 204. Mohtar, N.; Parumasivam, T.; Gazzali, A. M.; Tan, C. S.; Tan, M. L.; Othman, R.; Fazalul Rahiman, S. S.; Wahab, H. A., Advanced nanoparticle-based drug delivery systems and their cellular evaluation for non-small cell lung cancer treatment. *Cancers* **2021**, *13* (14), 3539.
- 205. Maghsoudnia, N.; Eftekhari, R. B.; Sohi, A. N.; Zamzami, A.; Dorkoosh, F. A., Application of nano-based systems for drug delivery and targeting: a review. *Journal of Nanoparticle Research* **2020,** 22 (1), 1-41.
- 206. Riss, T. L.; Moravec, R. A.; Niles, A. L., Cytotoxicity testing: measuring viable cells, dead cells, and detecting mechanism of cell death. *Mammalian Cell Viability: Methods and Protocols* **2011**, 103-114.
- 207. Riss, T.; Niles, A.; Moravec, R.; Karassina, N.; Vidugiriene, J., Cytotoxicity assays: in vitro methods to measure dead cells. **2019**.
- 208. Aslantürk, Ö. S., In vitro cytotoxicity and cell viability assays: principles, advantages, and disadvantages. *Genotoxicity-A predictable risk to our actual world* **2018**, *2* (1), 64-80.
- 209. Jain, A. K.; Thareja, S., In vitro and in vivo characterization of pharmaceutical nanocarriers used for drug delivery. *Artificial Cells, Nanomedicine, and Biotechnology* **2019**, *47* (1), 524-539.
- 210. Adan, A.; Alizada, G.; Kiraz, Y.; Baran, Y.; Nalbant, A., Flow cytometry: basic principles and applications. *Critical Reviews in Biotechnology* **2017**, *37* (2), 163-176.
- 211. Petersen, S.; Fahr, A.; Bunjes, H., Flow cytometry as a new approach to investigate drug transfer between lipid particles. *Molecular Pharmaceutics* **2010**, *7* (2), 350-363.
- 212. Ducat, E.; Evrard, B.; Peulen, O.; Piel, G., Cellular uptake of liposomes monitored by confocal microscopy and flow cytometry. *Journal of Drug Delivery Science and Technology* **2011**, *21* (6), 469-477.
- 213. Cook, M. T.; Saratoon, T.; Tzortzis, G.; Edwards, A.; Charalampopoulos, D.; Khutoryanskiy, V. V., CLSM method for the dynamic observation of pH change within polymer matrices for oral delivery. *Biomacromolecules* **2013**, *14* (2), 387-393.
- 214. Ruozi, B.; Belletti, D.; Tombesi, A.; Tosi, G.; Bondioli, L.; Forni, F.; Vandelli, M. A., AFM, ESEM, TEM, and CLSM in liposomal characterization: a comparative study. *International Journal of Nanomedicine* **2011**, *6* (1), 557-563.
- 215. Tao, W.; Wang, J.; Zhou, Y.; Liu, Z.; Chen, H.; Zhao, Z.; Yan, H.; Liao, X., Acid/reduction dual-sensitive amphiphilic graft polyurethane with folic acid and detachable poly (ethylene glycol) as anticancer drug delivery carrier. *Colloids and Surfaces B: Biointerfaces* **2023**, 222, 113084.
- 216. Ajdary, M.; Moosavi, M. A.; Rahmati, M.; Falahati, M.; Mahboubi, M.; Mandegary, A.; Jangjoo, S.; Mohammadinejad, R.; Varma, R. S., Health concerns of various nanoparticles: A review of their in vitro and in vivo toxicity. *Nanomaterials* **2018**, *8* (9), 634.
- 217. Voigt, N.; Henrich-Noack, P.; Kockentiedt, S.; Hintz, W.; Tomas, J.; Sabel, B. A., Toxicity of polymeric nanoparticles in vivo and in vitro. *Journal of Nanoparticle Research* **2014**, *16*, 1-13.
- 218. Zielińska, A.; Carreiró, F.; Oliveira, A. M.; Neves, A.; Pires, B.; Venkatesh, D. N.; Durazzo, A.; Lucarini, M.; Eder, P.; Silva, A. M., Polymeric nanoparticles: production, characterization, toxicology and ecotoxicology. *Molecules* **2020**, *25* (16), 3731.
- 219. Shang, L.; Nienhaus, K.; Nienhaus, G. U., Engineered nanoparticles interacting with cells: size matters. *Journal of Nanobiotechnology* **2014**, *12* (1), 1-11.
- 220. Xu, Z.; Gu, W.; Huang, J.; Sui, H.; Zhou, Z.; Yang, Y.; Yan, Z.; Li, Y., In vitro and in vivo evaluation of actively targetable nanoparticles for paclitaxel delivery. *International Journal of Pharmaceutics* **2005**, *288* (2), 361-368.
- 221. Eliasof, S.; Lazarus, D.; Peters, C. G.; Case, R. I.; Cole, R. O.; Hwang, J.; Schluep, T.; Chao, J.; Lin, J.; Yen, Y., Correlating preclinical animal studies and human clinical trials of a

- multifunctional, polymeric nanoparticle. *Proceedings of the National Academy of Sciences* **2013**, 110 (37), 15127-15132.
- 222. Skotland, T.; Iversen, T.-G.; Sandvig, K., Development of nanoparticles for clinical use. Taylor & Francis: 2014; Vol. 9, pp 1295-1299.
- 223. Lee, H.; Hoang, B.; Fonge, H.; Reilly, R. M.; Allen, C., In vivo distribution of polymeric nanoparticles at the whole-body, tumor, and cellular levels. *Pharmaceutical Research* **2010**, *27*, 2343-2355.
- 224. Jain, A. K.; Swarnakar, N. K.; Das, M.; Godugu, C.; Singh, R. P.; Rao, P. R.; Jain, S., Augmented anticancer efficacy of doxorubicin-loaded polymeric nanoparticles after oral administration in a breast cancer induced animal model. *Molecular Pharmaceutics* **2011**, *8* (4), 1140-1151.
- 225. Huang, S.-Y.; Yeh, N.-T.; Wang, T.-H.; Hsu, T.-C.; Chin, H.-Y.; Tzang, B.-S.; Chiang, W.-H., Onion-like doxorubicin-carrying polymeric nanomicelles with tumor acidity-sensitive dePEGylation to expose positively-charged chitosan shell for enhanced cancer chemotherapy. *International Journal of Biological Macromolecules* **2023**, *227*, 925-937.
- 226. Wang, Y.; Zhang, L.; Zhang, X.; Wei, X.; Tang, Z.; Zhou, S., Precise Polymerization of a Highly Tumor Microenvironment-Responsive Nanoplatform for Strongly Enhanced Intracellular Drug Release. *ACS Applied Materials & Interfaces* **2016**, *8* (9), 5833-5846.
- 227. Yin, T.; Wang, Y.; Chu, X.; Fu, Y.; Wang, L.; Zhou, J.; Tang, X.; Liu, J.; Huo, M., Free adriamycin-loaded pH/reduction dual-responsive hyaluronic acid—adriamycin prodrug micelles for efficient cancer therapy. *ACS Applied Materials & Interfaces* **2018**, *10* (42), 35693-35704.
- 228. Zhu, A.; Miao, K.; Deng, Y.; Ke, H.; He, H.; Yang, T.; Guo, M.; Li, Y.; Guo, Z.; Wang, Y., Dually pH/reduction-responsive vesicles for ultrahigh-contrast fluorescence imaging and thermochemotherapy-synergized tumor ablation. *ACS Nano* **2015**, *9* (8), 7874-7885.
- 229. Yang, Z.; Guo, Q.; Cai, Y.; Zhu, X.; Zhu, C.; Li, Y.; Li, B., Poly (ethylene glycol)-sheddable reduction-sensitive polyurethane micelles for triggered intracellular drug delivery for osteosarcoma treatment. *Journal of Orthopaedic Translation* **2020**, *21*, 57-65.
- Weng, J.; Tong, H. H.; Chow, S. F., In vitro release study of the polymeric drug nanoparticles: development and validation of a novel method. *Pharmaceutics* **2020**, *12* (8), 732.
- 231. Kim, Y.; Park, E. J.; Kim, T. W.; Na, D. H., Recent progress in drug release testing methods of biopolymeric particulate system. *Pharmaceutics* **2021**, *13* (8), 1313.
- 232. Byeon, H. J.; Kim, I.; Choi, J. S.; Lee, E. S.; Shin, B. S.; Youn, Y. S., PEGylated apoptotic protein-loaded PLGA microspheres for cancer therapy. *International Journal of Nanomedicine* **2015**, *10* (1), 739-748.
- 233. Hirota, K.; Doty, A. C.; Ackermann, R.; Zhou, J.; Olsen, K. F.; Feng, M. R.; Wang, Y.; Choi, S.; Qu, W.; Schwendeman, A. S., Characterizing release mechanisms of leuprolide acetate-loaded PLGA microspheres for IVIVC development I: in vitro evaluation. *Journal of Controlled Release* 2016, 244 (1), 302-313.
- 234. Janagam, D. R.; Wang, L.; Ananthula, S.; Johnson, J. R.; Lowe, T. L., An accelerated release study to evaluate long-acting contraceptive levonorgestrel-containing in situ forming depot systems. *Pharmaceutics* **2016**, *8* (3), 28.
- 235. Wallenwein, C. M.; Nova, M. V.; Janas, C.; Jablonka, L.; Gao, G. F.; Thurn, M.; Albrecht, V.; Wiehe, A.; Wacker, M. G., A dialysis-based in vitro drug release assay to study dynamics of the drug-protein transfer of temoporfin liposomes. *European Journal of Pharmaceutics and Biopharmaceutics* **2019**, *143*, 44-50.
- 236. Park, S.; Kim, D.-H.; Kim, Y.; Park, J. H.; Lee, M.; Song, I.-S.; Shim, C.-K., Comparative in vitro release and clinical pharmacokinetics of leuprolide from Luphere 3M Depot, a 3-month release formulation of leuprolide acetate. *Drug Development and Industrial Pharmacy* **2017**, *43* (3), 441-447.

- 237. Chen, W.; Palazzo, A.; Hennink, W. E.; Kok, R. J., Effect of particle size on drug loading and release kinetics of gefitinib-loaded PLGA microspheres. *Molecular Pharmaceutics* **2017**, *14* (2), 459-467.
- 238. Lee, S.-W.; Yun, M.-H.; Jeong, S. W.; In, C.-H.; Kim, J.-Y.; Seo, M.-H.; Pai, C.-M.; Kim, S.-O., Development of docetaxel-loaded intravenous formulation, Nanoxel-PMTM using polymer-based delivery system. *Journal of Controlled Release* **2011**, *155* (2), 262-271.
- 239. Lee, K. S.; Chung, H. C.; Im, S. A.; Park, Y. H.; Kim, C. S.; Kim, S.-B.; Rha, S. Y.; Lee, M. Y.; Ro, J., Multicenter phase II trial of Genexol-PM, a Cremophor-free, polymeric micelle formulation of paclitaxel, in patients with metastatic breast cancer. *Breast Cancer Research and Treatment* 2008, 108, 241-250.
- 240. Madaan, A.; Singh, P.; Awasthi, A.; Verma, R.; Singh, A. T.; Jaggi, M.; Mishra, S. K.; Kulkarni, S.; Kulkarni, H., Efficiency and mechanism of intracellular paclitaxel delivery by novel nanopolymer-based tumor-targeted delivery system, Nanoxel TM. *Clinical and Translational Oncology* **2013**, *15*, 26-32.
- 241. Fujiwara, Y.; Mukai, H.; Saeki, T.; Ro, J.; Lin, Y.-C.; Nagai, S. E.; Lee, K. S.; Watanabe, J.; Ohtani, S.; Kim, S. B., A multi-national, randomised, open-label, parallel, phase III non-inferiority study comparing NK105 and paclitaxel in metastatic or recurrent breast cancer patients. *British Journal of Cancer* 2019, *120* (5), 475-480.
- 242. Kosaka, Y.; Saeki, T.; Takano, T.; Aruga, T.; Yamashita, T.; Masuda, N.; Koibuchi, Y.; Osaki, A.; Watanabe, J.; Suzuki, R., Multicenter randomized open-label phase II clinical study comparing outcomes of NK105 and paclitaxel in advanced or recurrent breast cancer. *International Journal of Nanomedicine* **2022**, *17*, 4567.
- 243. Hamaguchi, T.; Matsumura, Y.; Suzuki, M.; Shimizu, K.; Goda, R.; Nakamura, I.; Nakatomi, I.; Yokoyama, M.; Kataoka, K.; Kakizoe, T., NK105, a paclitaxel-incorporating micellar nanoparticle formulation, can extend in vivo antitumour activity and reduce the neurotoxicity of paclitaxel. *British Journal of Cancer* **2005**, *92* (7), 1240-1246.
- 244. Varela-Moreira, A.; Shi, Y.; Fens, M. H.; Lammers, T.; Hennink, W. E.; Schiffelers, R. M., Clinical application of polymeric micelles for the treatment of cancer. *Materials Chemistry Frontiers* **2017**, *I* (8), 1485-1501.
- 245. Matsumura, Y.; Hamaguchi, T.; Ura, T.; Muro, K.; Yamada, Y.; Shimada, Y.; Shirao, K.; Okusaka, T.; Ueno, H.; Ikeda, M., Phase I clinical trial and pharmacokinetic evaluation of NK911, a micelle-encapsulated doxorubicin. *British Journal of Cancer* **2004**, *91* (10), 1775-1781.
- 246. Tsukioka, Y.; Matsumura, Y.; Hamaguchi, T.; Koike, H.; Moriyasu, F.; Kakizoe, T., Pharmaceutical and biomedical differences between micellar doxorubicin (NK911) and liposomal doxorubicin (Doxil). *Japanese Journal of Cancer Research* **2002**, *93* (10), 1145-1153.
- 247. Harada, A.; Kataoka, K., Supramolecular assemblies of block copolymers in aqueous media as nanocontainers relevant to biological applications. *Progress in Polymer Scence* **2006**, *31* (11), 949-982.
- 248. Nishiyama, N.; Kataoka, K., Nanostructured devices based on block copolymer assemblies for drug delivery: designing structures for enhanced drug function. *Advances in Polymer Science* **2006**, *193* (Polymer Therapeutics II), 67-101.
- 249. Mikhail, A. S.; Allen, C., Block copolymer micelles for delivery of cancer therapy: Transport at the whole body, tissue and cellular levels. *Journal of Controlled Release* **2009**, *138* (3), 214-223.
- 250. Xiong, X.-B.; Falamarzian, A.; Garg, S. M.; Lavasanifar, A., Engineering of amphiphilic block copolymers for polymeric micellar drug and gene delivery. *Journal of Controlled Release* **2011**, 155 (2), 248-261.
- 251. Mura, S.; Nicolas, J.; Couvreur, P., Stimuli-responsive nanocarriers for drug delivery. *Nature Materials* **2013**, *12* (11), 991-1003.
- 252. Rijcken, C. J. F.; Soga, O.; Hennink, W. E.; van Nostrum, C. F., Triggered destabilization of polymeric micelles and vesicles by changing polymers polarity: An attractive tool for drug delivery. *Journal of Controlled Release* **2007**, *120* (3), 131-148.

- 253. Zhang, Q.; Ko, N. R.; Oh, J. K., Recent advances in stimuli-responsive degradable block copolymer micelles: synthesis and controlled drug delivery applications. *Chemical Communications* **2012**, *48* (61), 7542-7552.
- 254. Oh, J. K., Disassembly and tumor-targeting drug delivery of reduction-responsive degradable block copolymer nanoassemblies. *Polymer Chemistry* **2019**, *10* (13), 1554-1568.
- 255. Wang, Y.; Xu, H.; Zhang, X., Tuning the Amphiphilicity of Building Blocks: Controlled Self-Assembly and Disassembly for Functional Supramolecular Materials. *Advanced Materials* **2009**, 21 (28), 2849-2864.
- 256. Gohy, J. F.; Zhao, Y., Photo-responsive block copolymer micelles: design and behavior. *Chemical Society Reviews* **2013**, *42* (17), 7117-29.
- 257. Zhao, H.; Sterner, E. S.; Coughlin, E. B.; Theato, P., o-Nitrobenzyl Alcohol Derivatives: Opportunities in Polymer and Materials Science. *Macromolecules* **2012**, *45* (4), 1723-1736.
- 258. Zhao, Y., Light-Responsive Block Copolymer Micelles. *Macromolecules* **2012**, *45* (9), 3647-3657.
- 259. Delplace, V.; Nicolas, J., Degradable vinyl polymers for biomedical applications. *Nature Chemistry* **2015**, *7* (10), 771-784.
- 260. El-Sawy, H. S.; Al-Abd, A. M.; Ahmed, T. A.; El-Say, K. M.; Torchilin, V. P., Stimuli-Responsive Nano-Architecture Drug-Delivery Systems to Solid Tumor Micromilieu: Past, Present, and Future Perspectives. *ACS Nano* **2018**, *12* (11), 10636-10664.
- 261. Quintieri, G.; Gröschel, A. H., Naked micelles: well-defined polymer nanoparticles from photocleavable block copolymer micelles. *Polymer Chemistry* **2021**, *12* (10), 1429-1438.
- 262. Tannock, I. F.; Rotin, D., Acid pH in tumors and its potential for therapeutic exploitation. *Cancer Research* **1989**, *49* (16), 4373-4384.
- Watson, P.; Jones, A. T.; Stephens, D. J., Intracellular trafficking pathways and drug delivery: fluorescence imaging of living and fixed cells. *Advanced Drug Delivery Reviews* **2005**, *57* (1), 43-61.
- 264. Bazban-Shotorbani, S.; Hasani-Sadrabadi, M. M.; Karkhaneh, A.; Serpooshan, V.; Jacob, K. I.; Moshaverinia, A.; Mahmoudi, M., Revisiting structure-property relationship of pH-responsive polymers for drug delivery applications. *Journal of Controlled Release* **2017**, *253*, 46-63.
- 265. Binauld, S.; Stenzel, M. H., Acid-degradable polymers for drug delivery: a decade of innovation. *Chemocal Communications* **2013**, *49* (21), 2082-2102.
- 266. Kocak, G.; Tuncer, C.; Butun, V., pH-Responsive polymers. *Polymer Chemistry* **2017**, *8* (1), 144-176.
- 267. Qu, X.; Yang, Z., Benzoic-Imine-Based Physiological-pH-Responsive Materials for Biomedical Applications. *Chemistry -An Asian Journal* **2016**, *11* (19), 2633-2641.
- 268. Deirram, N.; Zhang, C.; Kermaniyan, S. S.; Johnston, A. P. R.; Such, G. K., pH-Responsive Polymer Nanoparticles for Drug Delivery. *Macromolecular Rapid Communications* **2019**, *40* (10), e1800917.
- 269. Sonawane, S. J.; Kalhapure, R. S.; Govender, T., Hydrazone linkages in pH responsive drug delivery systems. *European Journal of Pharmaceutical Sciences* **2017**, *99*, 45-65.
- 270. Gannimani, R.; Walvekar, P.; Naidu, V. R.; Aminabhavi, T. M.; Govender, T., Acetal containing polymers as pH-responsive nano-drug delivery systems. *Journal of Controlled Release* **2020**, *328*, 736-761.
- 271. Nichols, J. W.; Bae, Y. H., Odyssey of a cancer nanoparticle: From injection site to site of action. *Nano Today* **2012**, *7* (6), 606-618.
- 272. Bae, Y. H.; Park, K., Targeted drug delivery to tumors: Myths, reality and possibility. *Journal of Controlled Release* **2011**, *153* (3), 198-205.
- 273. Cabral, H.; Matsumoto, Y.; Mizuno, K.; Chen, Q.; Murakami, M.; Kimura, M.; Terada, Y.; Kano, M. R.; Miyazono, K.; Uesaka, M.; Nishiyama, N.; Kataoka, K., Accumulation of sub-100 nm polymeric micelles in poorly permeable tumors depends on size. *Nature Nanotechnology* **2011**, *6* (12), 815-823.

- 274. Dan, K.; Ghosh, S., One-Pot Synthesis of an Acid-Labile Amphiphilic Triblock Copolymer and its pH-Responsive Vesicular Assembly. *Angewandte Chemie International Edition* **2013**, *52* (28), 7300-7305.
- 275. Huang, F.; Cheng, R.; Meng, F.; Deng, C.; Zhong, Z., Micelles Based on Acid Degradable Poly(acetal urethane): Preparation, pH-Sensitivity, and Triggered Intracellular Drug Release. *Biomacromolecules* **2015**, *16* (7), 2228-2236.
- 276. Huang, X.; Du, F.; Cheng, J.; Dong, Y.; Liang, D.; Ji, S.; Lin, S.-S.; Li, Z., Acid-Sensitive Polymeric Micelles Based on Thermoresponsive Block Copolymers with Pendent Cyclic Orthoester Groups. *Macromolecules* **2009**, *42* (3), 783-790.
- 277. Qiao, Z.-Y.; Ji, R.; Huang, X.-N.; Du, F.-S.; Zhang, R.; Liang, D.-H.; Li, Z.-C., Polymersomes from Dual Responsive Block Copolymers: Drug Encapsulation by Heating and Acid-Triggered Release. *Biomacromolecules* **2013**, *14* (5), 1555-1563.
- 278. Gu, Y.; Zhong, Y.; Meng, F.; Cheng, R.; Deng, C.; Zhong, Z., Acetal-Linked Paclitaxel Prodrug Micellar Nanoparticles as a Versatile and Potent Platform for Cancer Therapy. *Biomacromolecules* **2013**, *14* (8), 2772-2780.
- 279. Son, I.; Lee, Y.; Baek, J.; Park, M.; Han, D.; Min, S. K.; Lee, D.; Kim, B. S., pH-Responsive Amphiphilic Polyether Micelles with Superior Stability for Smart Drug Delivery. *Biomacromolecules* **2021**, *22* (5), 2043-2056.
- 280. Moreno, A.; Lligadas, G.; Ronda, J. C.; Galia, M.; Cadiz, V., Orthogonally functionalizable polyacetals: a versatile platform for the design of acid sensitive amphiphilic copolymers. *Polymer Chemistry* **2019**, *10* (38), 5215-5227.
- 281. Myrgorodska, I.; Jenkinson-Finch, M.; Moreno-Tortolero, R. O.; Mann, S.; Gobbo, P., A Novel Acid-Degradable PEG Crosslinker for the Fabrication of pH-Responsive Soft Materials. *Macromolecular Rapid Communications* **2021**, *42* (12), e2100102.
- 282. Abtew, E.; Ezra, A. F.; Basu, A.; Domb, A. J., Biodegradable Poly(Acetonide Gluconic Acid) for Controlled Drug Delivery. *Biomacromolecules* **2019**, *20* (8), 2934-2941.
- 283. Wang, K.; Liu, Q.; Lu, G.; Zhang, Y.; Zhou, Y.; Chen, S.; Ma, Q.; Liu, G.; Zeng, Y., Acid-Labile Temperature-Responsive Homopolymers and a Diblock Copolymer Bearing the Pendent Acetal Group. *Macromolecules* **2021**, *54* (8), 3725-3734.
- 284. Cheng, R.; Wang, S.; Santos, H. A., Acid-labile chemical bonds-based nanoparticles for endosome escape and intracellular delivery. *Biomedical Technology* **2023**, *3* (1), 52-58.
- 285. Zalba, S.; Ten Hagen, T. L. M.; Burgui, C.; Garrido, M. J., Stealth nanoparticles in oncology: Facing the PEG dilemma. *Journal of Controlled Release* **2022**, *351*, 22-36.
- 286. Fang, Y.; Xue, J.; Gao, S.; Lu, A.; Yang, D.; Jiang, H.; He, Y.; Shi, K., Cleavable PEGylation: a strategy for overcoming the "PEG dilemma" in efficient drug delivery. *Drug Delivery* **2017**, *24* (sup1), 22-32.
- 287. Kong, L.; Campbell, F.; Kros, A., DePEGylation strategies to increase cancer nanomedicine efficacy. *Nanoscale Horizons* **2019**, *4* (2), 378-387.
- 288. Petrova, S.; Jager, E.; Konefal, R.; Jager, A.; Venturini, C. G.; Spevacek, J.; Pavlova, E.; Stepanek, P., Novel poly(ethylene oxide monomethyl ether)-b-poly(ε-caprolactone) diblock copolymers containing a pH-acid labile ketal group as a block linkage. *Polymer Chemistry* **2014**, *5* (12), 3884-3893.
- 289. Xiao, L.; Huang, L.; Moingeon, F.; Gauthier, M.; Yang, G., pH-Responsive Poly(Ethylene Glycol)-block-Polylactide Micelles for Tumor-Targeted Drug Delivery. *Biomacromolecules* **2017**, *18* (9), 2711-2722.
- 290. Worm, M.; Kang, B.; Dingels, C.; Wurm, F. R.; Frey, H., Acid-Labile Amphiphilic PEO-b-PPO-b-PEO Copolymers: Degradable Poloxamer Analogs. *Macromolecular Rapid Communications* **2016**, *37* (9), 775-780.
- 291. Wang, H.; He, J.; Zhang, M.; Tao, Y.; Li, F.; Tam, K. C.; Ni, P., Biocompatible and acidcleavable poly(ϵ -caprolactone)-acetal-poly(ethylene glycol)-acetal-poly(ϵ -caprolactone) triblock

- copolymers: synthesis, characterization and pH-triggered doxorubicin delivery. *Journal of Materials Chemistry B* **2013**, *I* (48), 6596-6607.
- 292. Jazani, A. M.; Oh, J. K., Synthesis of multiple stimuli-responsive degradable block copolymers via facile carbonyl imidazole-induced postpolymerization modification. *Polymer Chemistry* **2022**, *13* (31), 4557-4568.
- 293. Bawa, K. K.; Jazani, A. M.; Ye, Z.; Oh, J. K., Synthesis of degradable PLA-based diblock copolymers with dual acid/reduction-cleavable junction. *Polymers* **2020**, *194* (1), 122391.
- 294. Jazani, A. M.; Arezi, N.; Shetty, C.; Oh, J. K., Shell-Sheddable/Core-Degradable ABA Triblock Copolymer Nanoassemblies: Synthesis via RAFT and Concurrent ATRP/RAFT Polymerization and Drug Delivery Application. *Molecular Pharmaceutics* **2021**, *19* (6), 1786-1794.
- 295. Hao, Y.; He, J.; Li, S.; Liu, J.; Zhang, M.; Ni, P., Synthesis of an acid-cleavable and fluorescent amphiphilic block copolymer as a combined delivery vector of DNA and doxorubicin. *Journal of Materials Chemistry B* **2014**, *2* (27), 4237-4249.
- 296. Patil, S. S.; Wadgaonkar, P. P., Temperature and pH dual stimuli responsive PCL-b-PNIPAAm block copolymer assemblies and the cargo release studies. *Journal of Polymer Science Part A: Polymer Chemistry* **2017**, *55* (8), 1383-1396.
- 297. Moreno, A.; Ronda, J. C.; Cadiz, V.; Galia, M.; Lligadas, G.; Percec, V., pH-Responsive Micellar Nanoassemblies from Water-Soluble Telechelic Homopolymers Endcoding Acid-Labile Middle-Chain Groups in Their Hydrophobic Sequence-Defined Initiator Residue. *ACS Macro Letters* 2019, 8 (9), 1200-1208.
- 298. Zhu, F.; Yang, Q.; Zhuang, Y.; Zhang, Y.; Shao, Z.; Gong, B.; Shen, Y.-M., Self-assembled polymeric micelles based on Tetrahydropyran (THP) and THF linkage for pH-responsive drug delivery. *Polymers* **2014**, *55* (13), 2977-2985.
- 299. Huang, X.; Sevimli, S. I.; Bulmus, V., pH-labile sheddable block copolymers by RAFT polymerization: Synthesis and potential use as siRNA conjugates. *European Polymer Journal* **2013**, *49* (10), 2895-2905.
- 300. Lin, S.; Du, F.; Wang, Y.; Ji, S.; Liang, D.; Yu, L.; Li, Z., An Acid-Labile Block Copolymer of Poly(2-dimethylamino)ethyl methacrylate and Poly(ethylene glycol) as Potential Carrier for Intelligent Gene Delivery Systems. *Biomacromolecules* **2008**, *9* (1), 109-115.
- 301. Zeng, Z.; Wei, Z.; Ma, L.; Xu, Y.; Xing, Z.; Niu, H.; Wang, H.; Huang, W., pH-Responsive nanoparticles based on ibuprofen prodrug as drug carriers for inhibition of primary tumor growth and metastasis. *Journal of Materials Chemistry B* **2017**, *5* (33), 6860-6868.
- 302. Xu, M.; Zhang, C. Y.; Wu, J.; Zhou, H.; Bai, R.; Shen, Z.; Deng, F.; Liu, Y.; Liu, J., PEG-detachable polymeric micelles self-assembled from amphiphilic copolymers for tumor-acidity-triggered drug delivery and controlled release. *ACS Applied Materials & Interfaces* **2019**, *11* (6), 5701-5713.
- 303. Babikova, D.; Kalinova, R.; Momekova, D.; Ugrinova, I.; Momekov, G.; Dimitrov, I., Multifunctional Polymer Nanocarrier for Efficient Targeted Cellular and Subcellular Anticancer Drug Delivery. *ACS Biomaterials Science & Engineering* **2019**, *5* (5), 2271-2283.
- 304. He, L.; Jiang, Y.; Tu, C.; Li, G.; Zhu, B.; Jin, C.; Zhu, Q.; Yan, D.; Zhu, X., Self-assembled encapsulation systems with pH tunable release property based on reversible covalent bond. *Chemical Communications* **2010**, *46* (40), 7569-7571.
- 305. Sun, C.-Y.; Liu, Y.; Du, J.-Z.; Cao, Z.-T.; Xu, C.-F.; Wang, J., Facile Generation of TumorpH-Labile Linkage-Bridged Block Copolymers for Chemotherapeutic Delivery. *Angewandte Chemie International Edition* **2016**, *55* (3), 1010-1014.
- 306. Seidi, F.; Jenjob, R.; Crespy, D., Designing Smart Polymer Conjugates for Controlled Release of Payloads. *Chemical Reviews* **2018**, *118* (7), 3965-4036.
- 307. Jain, R.; Standley, S. M.; Frechet, J. M. J., Synthesis and degradation of pH-sensitive linear poly(amidoamine)s. *Macromolecules* **2007**, *40* (3), 452-457.

- 308. Paramonov, S. E.; Bachelder, E. M.; Beaudette, T. T.; Standley, S. M.; Lee, C. C.; Dashe, J.; Frechet, J. M. J., Fully Acid-Degradable Biocompatible Polyacetal Microparticles for Drug Delivery. *Bioconjugate Chemistry* **2008**, *19* (4), 911-919.
- 309. Louage, B.; van Steenbergen, M. J.; Nuhn, L.; Risseeuw, M. D. P.; Karalic, I.; Winne, J.; Van Calenbergh, S.; Hennink, W. E.; De Geest, B. G., Micellar Paclitaxel-Initiated RAFT Polymer Conjugates with Acid-Sensitive Behavior. *ACS Macro Letters* **2017**, *6* (3), 272-276.
- 310. Griset, A. P.; Walpole, J.; Liu, R.; Gaffey, A.; Colson, Y. L.; Grinstaff, M. W., Expansile Nanoparticles: Synthesis, Characterization, and in Vivo Efficacy of an Acid-Responsive Polymeric Drug Delivery System. *Journal of American Chemical Society* **2009**, *131* (7), 2469-2471.
- 311. Zhang, Q.; Ko, N. R.; Oh, J. K., Modulated morphologies and tunable thiol-responsive shedding of aqueous block copolymer aggregates. *RSC Advances* **2012**, *2* (21), 8079-8086.
- 312. Matyjaszewski, K.; Xia, J., Atom Transfer Radical Polymerization. *Chemical Reviews* **2001**, *101* (9), 2921-2990.
- 313. Matyjaszewski, K.; Davis, T. P., *Handbook of Radical Polymerization*. John Wiley & Sons Inc.: 2002.
- 314. Matyjaszewski, K.; Jakubowski, W.; Min, K.; Tang, W.; Huang, J.; Braunecker, W. A.; Tsarevsky, N. V., Diminishing catalyst concentration in atom transfer radical polymerization with reducing agents. *Proceedings of the National Academy of Sciences of the United States of America* **2006**, *103* (42), 15309-15314.
- 315. Shi, Y.; Lammers, T.; Storm, G.; Hennink, W. E., Physico-Chemical Strategies to Enhance Stability and Drug Retention of Polymeric Micelles for Tumor-Targeted Drug Delivery. *Macromolecular Bioscience* **2017**, *17* (1).
- 316. Zhuang, W. R.; Wang, Y.; Cui, P. F.; Xing, L.; Lee, J.; Kim, D.; Jiang, H. L.; Oh, Y. K., Applications of pi-pi stacking interactions in the design of drug-delivery systems. *Journal of Controlled Release* **2019**, *294* (1), 311-326.
- 317. Shi, Y.; van Steenbergen, M. J.; Teunissen, E. A.; Novo, L.; Gradmann, S.; Baldus, M.; van Nostrum, C. F.; Hennink, W. E., Pi-pi stacking increases the stability and loading capacity of thermosensitive polymeric micelles for chemotherapeutic drugs. *Biomacromolecules* **2013**, *14* (6), 1826-37.
- 318. Neto, L. J. d. L.; Ramos, A. G. B.; Freitas, T. S. d.; Barbosa, C. R. d. S.; de Sousa Júnior, D. L.; Siyadatpanah, A.; Nejat, M.; Wilairatana, P.; Coutinho, H. D. M.; da Cunha, F. A. B., Evaluation of benzaldehyde as an antibiotic modulator and its toxic effect against Drosophila melanogaster. *Molecules* **2021**, *26* (18), 5570.
- 319. Smyth, P.; Gibson, T. J.; Irvine, G.; Black, G.; Lavery, D.; Semsarilar, M.; Scott, C. J.; Themistou, E., pH-Responsive benzaldehyde-functionalized PEG-based polymeric nanoparticles for drug delivery: Effect of preparation method on morphology, dye encapsulation and attachment. *European Polymer Journal* **2020**, *124*, 109471.
- 320. Rong, G.; Wang, C.; Hu, J.; Li, Y.; Cheng, Y., Benzaldehyde-tethered fluorous tags for cytosolic delivery of bioactive peptides. *Journal of Controlled Release* **2022**, *351* (1), 703-712.
- 321. Bazban-Shotorbani, S.; Hasani-Sadrabadi, M. M.; Karkhaneh, A.; Serpooshan, V.; Jacob, K. I.; Moshaverinia, A.; Mahmoudi, M., Revisiting structure-property relationship of pH-responsive polymers for drug delivery applications. *Journal of Controlled Release* **2017**, *253*, 46-63.
- 322. Kamaly, N.; Yameen, B.; Wu, J.; Farokhzad, O. C., Degradable controlled-release polymers and polymeric nanoparticles: mechanisms of controlling drug release. *Chemical Reviews* **2016**, *116* (4), 2602-2663.
- 323. Song, J.; Hwang, E.; Lee, Y.; Palanikumar, L.; Choi, S.-H.; Ryu, J.-H.; Kim, B.-S., Tailorable degradation of pH-responsive all polyether micelles via copolymerisation with varying acetal groups. *Polymer Chemistry* **2019**, *10* (5), 582-592.
- 324. Rohani, N.; Hao, L.; Alexis, M. S.; Joughin, B. A.; Krismer, K.; Moufarrej, M. N.; Soltis, A. R.; Lauffenburger, D. A.; Yaffe, M. B.; Burge, C. B., Acidification of tumor at stromal

- boundaries drives transcriptome alterations associated with aggressive phenotypes. *Cancer Research* **2019**, *79* (8), 1952-1966.
- 325. Zhang, S.; Xu, J.; Chen, H.; Song, Z.; Wu, Y.; Dai, X.; Kong, J., Acid-Cleavable Unimolecular Micelles from Amphiphilic Star Copolymers for Triggered Release of Anticancer Drugs. *Macromolecular Bioscience* **2017**, *17* (3), 1600258.
- 326. Cao, H.; Chen, C.; Xie, D.; Chen, X.; Wang, P.; Wang, Y.; Song, H.; Wang, W., A hyperbranched amphiphilic acetal polymer for pH-sensitive drug delivery. *Polymer Chemistry* **2018**, *9* (2), 169-177.
- 327. Zhang, Q.; Ko, N. R.; Oh, J. K., Recent advances in stimuli-responsive degradable block copolymer micelles: synthesis and controlled drug delivery applications. *Chemical Communications* **2012**, *48* (61), 7542-7552.
- Wang, Z.; Pan, J.; Yuan, R.; Chen, M.; Guo, X.; Zhou, S., Shell-sheddable polymeric micelles alleviate oxidative stress and inflammation for enhanced ischemic stroke therapy. *Nano Letters* **2023**, *23* (14), 6544-6552.
- 329. Feng, J.; Wen, W.; Jia, Y.-G.; Liu, S.; Guo, J., pH-responsive micelles assembled by three-armed degradable block copolymers with a cholic acid core for drug controlled-release. *Polymers* **2019**, *11* (3), 511.
- 330. Andrade-Gagnon, B.; Oh, J. K., Recent advances in the synthesis and shell-sheddable disassembly of acid/glutathione-degradable block copolymer nanoassemblies for drug delivery. *Polymer Chemistry* **2024**, *15* (37), 3709-3735.
- 331. Bairagi, K.; Liu, J. T.; Thinphang-nga, A.; Oh, J. K., Synthesis and Dual-Acid/Light-Responsive Disassembly of Amphiphilic Block Copolymer Nanoassemblies Bearing Conjugated Benzoic Imine Pendants. *Macromolecules* **2023**, *56* (11), 4307-4317.
- 332. Gohy, J. F.; Zhao, Y., Photo-responsive block copolymer micelles: design and behavior. *Chemical Society Reviews* **2013**, *42* (17), 7117-29.
- 333. Liu, H.; Lu, H.-H.; Alp, Y.; Wu, R.; Thayumanavan, S., Structural determinants of stimuliresponsiveness in amphiphilic macromolecular nano-assemblies. *Progress in Polymer Science* **2024**, *148* (1), 101765.
- 334. Song, Y.; Ding, Y.; Dong, C. M., Stimuli-responsive polypeptide nanoassemblies: Recent progress and applications in cancer nanomedicine. *Wiley Interdisciplinary Reviews:*Nanomedicine & Nanobiotechnology **2022**, 14 (2), e1742.
- 335. Deirram, N.; Zhang, C.; Kermaniyan, S. S.; Johnston, A. P. R.; Such, G. K., pH-Responsive Polymer Nanoparticles for Drug Delivery. *Macromolecular Rapid Communications* **2019**, *40* (10), e1800917.
- 336. Dan, K.; Ghosh, S., One-Pot Synthesis of an Acid-Labile Amphiphilic Triblock Copolymer and its pH-Responsive Vesicular Assembly. *Angewandte Chemie International Edition* **2013**, *52* (28), 7300-7305.
- 337. Moreno, A.; Lligadas, G.; Ronda, J. C.; Galia, M.; Cadiz, V., Orthogonally functionalizable polyacetals: a versatile platform for the design of acid sensitive amphiphilic copolymers. *Polymer Chemistry* **2019**, *10* (38), 5215-5227.
- 338. Myrgorodska, I.; Jenkinson-Finch, M.; Moreno-Tortolero, R. O.; Mann, S.; Gobbo, P., A Novel Acid-Degradable PEG Crosslinker for the Fabrication of pH-Responsive Soft Materials. *Macromolecular Rapid Communications* **2021**, *42* (12), e2100102.
- 339. Cheng, R.; Wang, S.; Santos, H. A., Acid-labile chemical bonds-based nanoparticles for endosome escape and intracellular delivery. *Biomedical Technology* **2023**, *3*, 52-58.
- 340. Seidi, F.; Jenjob, R.; Crespy, D., Designing Smart Polymer Conjugates for Controlled Release of Payloads. *Chemical Reviews* **2018**, *118* (7), 3965-4036.
- 341. Griset, A. P.; Walpole, J.; Liu, R.; Gaffey, A.; Colson, Y. L.; Grinstaff, M. W., Expansile Nanoparticles: Synthesis, Characterization, and in Vivo Efficacy of an Acid-Responsive Polymeric Drug Delivery System. *Journal of American Chemical Society* **2009**, *131* (7), 2469-2471.

- 342. Liu, B.; Thayumanavan, S., Substituent Effects on the pH Sensitivity of Acetals and Ketals and Their Correlation with Encapsulation Stability in Polymeric Nanogels. *Journal of American Chemical Society* **2017**, *139* (6), 2306-2317.
- 343. Jazani, A. M.; Arezi, N.; Maruya-Li, K.; Jung, S.; Oh, J. K., Facile Strategies to Synthesize Dual Location Dual Acidic pH/Reduction-Responsive Degradable Block Copolymers Bearing Acetal/Disulfide Block Junctions and Disulfide Pendants. *ACS Omega* **2018**, *3* (8), 8980-8991.
- 344. Shetty, C.; Noronha, A.; Pontarelli, A.; Wilds, C. J.; Oh, J. K., Dual-Location Dual-Acid/Glutathione-Degradable Cationic Micelleplexes through Hydrophobic Modification for Enhanced Gene Silencing. *Molecular Pharmaceutics* **2020**, *17* (10), 3979-3989.
- 345. Moreno, A.; Ronda, J. C.; Cadiz, V.; Galia, M.; Lligadas, G.; Percec, V., pH-Responsive Micellar Nanoassemblies from Water-Soluble Telechelic Homopolymers Endcoding Acid-Labile Middle-Chain Groups in Their Hydrophobic Sequence-Defined Initiator Residue. *ACS Macro Letters* **2019**, *8* (9), 1200-1208.
- 346. Chen, M.; Zhong, M.; Johnson, J. A., Light-controlled radical polymerization: mechanisms, methods, and applications. *Chemical Reviews* **2016**, *116* (17), 10167-10211.
- 347. Aydogan, C.; Yilmaz, G.; Shegiwal, A.; Haddleton, D. M.; Yagci, Y., Photoinduced controlled/living polymerizations. *Angewandte Chemie* **2022**, *134* (23), e202117377.
- 348. Wu, C.; Corrigan, N.; Lim, C.-H.; Liu, W.; Miyake, G.; Boyer, C., Rational design of photocatalysts for controlled polymerization: effect of structures on photocatalytic activities. *Chemical Reviews* **2022**, *122* (6), 5476-5518.
- 349. Lissandrini, G.; Zeppilli, D.; Lorandi, F.; Matyjaszewski, K.; Isse, A. A.; Orian, L.; Fantin, M., Photo-RAFT Polymerization Under Microwatt Irradiation via Unimolecular Photoinduced Electron Transfer. *Angewandte Chemie International Edition* **2025**, *64* (19), e202424225.
- 350. Qiao, X.; Hao, Q.; Chen, M.; Shi, G.; He, Y.; Pang, X., Simple Full-Spectrum Heterogeneous Photocatalyst for Photo-induced Atom Transfer Radical Polymerization (ATRP) under UV/vis/NIR and its Application for the Preparation of Dual Mode Curing Injectable Photoluminescence Hydrogel. *ACS Applied Materials & Interfaces* **2022**, *14* (18), 21555-21563.
- 351. Allegrezza, M. L.; Konkolewicz, D., PET-RAFT polymerization: Mechanistic perspectives for future materials. *ACS Macro Letters* **2021**, *10* (4), 433-446.
- 352. Zhang, C.; Ye, G.; Wang, W.; Ding, X.; Feng, Y.; Wang, R., Thermal, pH, and Photo Multistimuli Responsive Block Copolymer Self-Assembly Nanoparticles for Drug Delivery Using Visible-Light-Induced PET-RAFT. ACS Applied Nano Materials 2024, 7 (1), 370-381.
- 353. Zhang, Z.; Yu, Y.; Boyer, C.; Wu, Z.; Wu, C., Design and synthesis of a new indazole-decorated raft agent for highly efficient PET-RAFT polymerization. *Macromolecules* **2024**, *57* (9), 4421-4429.
- 354. Mocny, P.; Lin, T.-C.; Parekh, R.; Zhao, Y.; Czarnota, M.; Urbańczyk, M.; Majidi, C.; Matyjaszewski, K., Selective and controlled grafting from PVDF-based materials by oxygentolerant green-light-mediated ATRP. *ACS Applied Materials & Interfaces* **2024**, *16* (18), 23932-23947.
- 355. He, J.; Zhang, W.; Lv, C.; Chen, R.; Wang, L.; Wang, Y.; Pan, X., Thermo-and pH-responsive star-like polymers synthesized by photoATRP. *Polymers* **2021**, *215* (1), 123345.
- 356. Jazani, A. M.; Schild, D. J.; Sobieski, J.; Hu, X.; Matyjaszewski, K., Visible Light-ATRP Driven by Tris (2-Pyridylmethyl) Amine (TPMA) Impurities in the Open Air. *Macromolecular Rapid Communications* **2023**, *44* (16), 2200855.

Appendix A

Supporting Information and Figures for Chapter 3

Figure A1. ¹³C NMR spectrum of BzAc-DOH in CDCl₃.

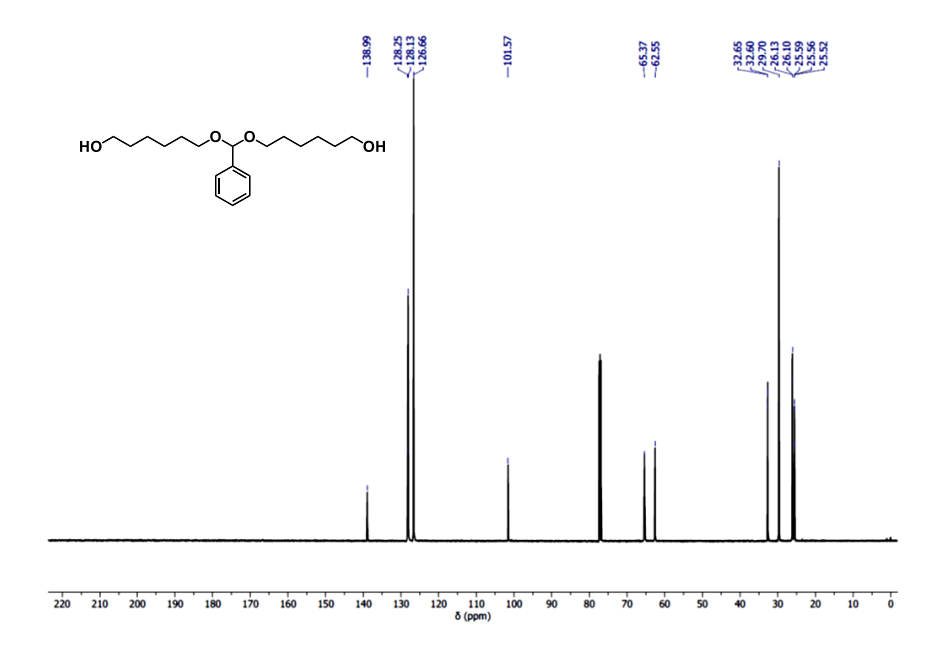


Figure A2. ¹³C NMR spectrum of CyPK-DOH in CDCl₃.

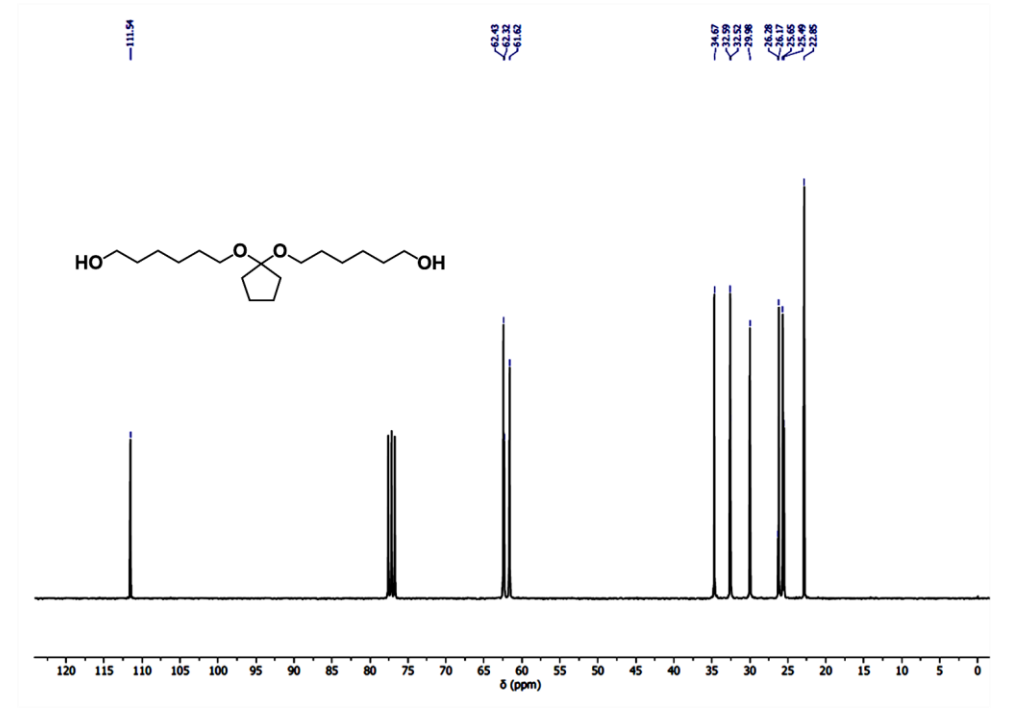
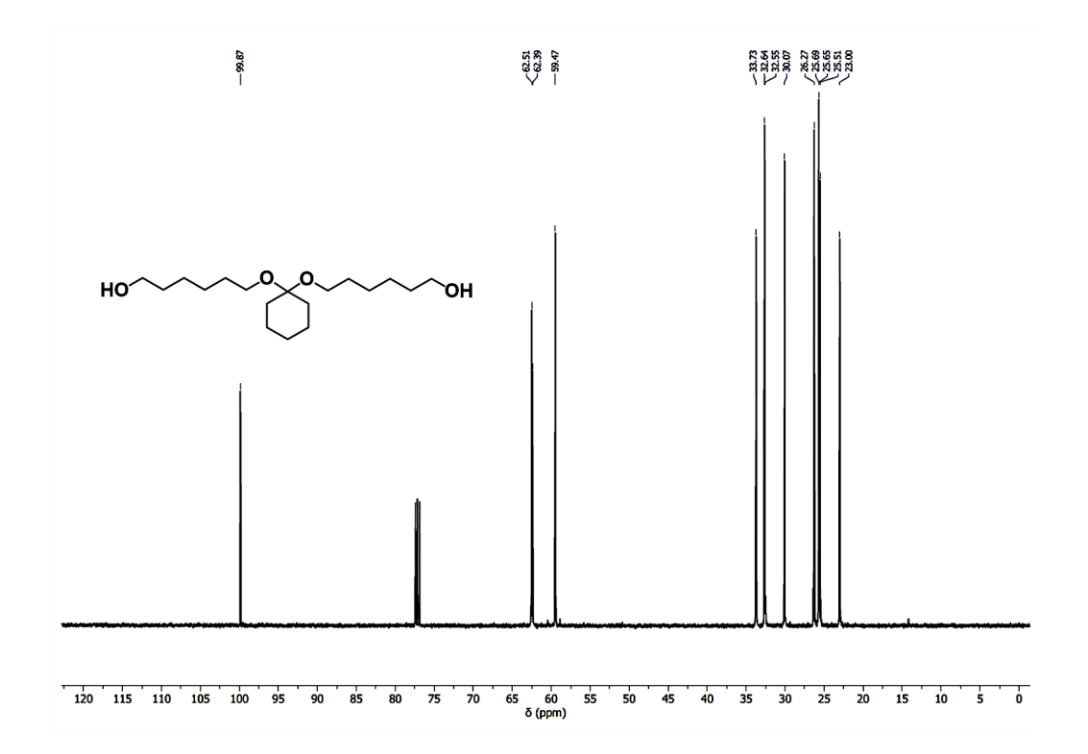
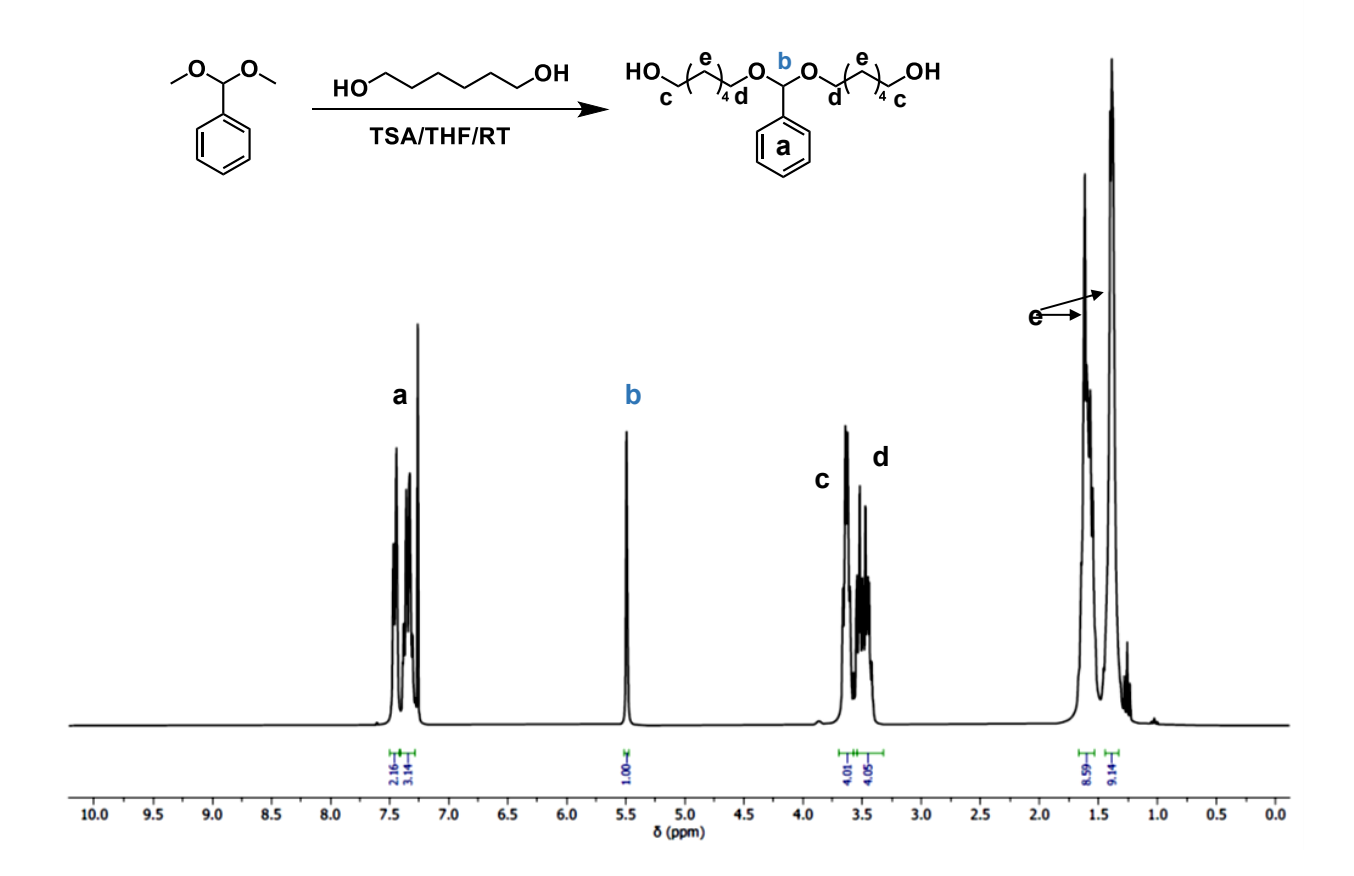


Figure A3. ¹³C NMR spectrum of CyHK-DOH in CDCl₃.



Synthesis of BzAc-DOH via transacetalization. In a 100 mL round bottom flask dried at 70 °C overnight, 1,6-hexanediol (18.6 g, 158 mmol) and p-toluenesulfonic acid monohydrate (TSA, 0.75 g, 4 mmol) were mixed with anhydrous THF (50 mL) containing 5 Å molecular sieves (25 g) dried in an oven at 180 °C for 5 hours. Benzaldehyde dimethyl acetal (6 g, 39 mmol) was added and the mixture was stirred at room temperature for 24 hours. After the removal of molecular sieves by filtration, the resulting mixture was quenched with Et₃N (1 mL). Solvent was removed by rotary evaporation and the residues were re-dissolved in ethyl acetate. Crude was extracted with a 2.5 % aqueous sodium bicarbonate solution (2 x 50 mL) and the organic layer was dried over magnesium sulfate. The product was collected as the second of the total two bands off a silica gel column using an eluent of 1/1 v/v hexane/ethyl acetate mixture, and then dried in vacuum oven for 24 hrs. Colorless oil residue with yield = 6.2 g (48%); R_f = 0.17 on (1/1 v/v hexane/ethyl acetate). ¹H NMR (CDCl₃, ppm): 7.46-7.30 (m, 5H, Ar-H), 5.50 (s, 1H, CH-O₂), 3.66-3.60 (q, 4H, CH₂-OH), 3.56-3.42 (m, 4H, CH₂-CH₂-O), 1.65-1.55 (m, 8H, CH₂), 1.40-1.38 (m, 8H, CH₂). ¹³C NMR (CDCl₃, ppm): 138.99, 128.25, 128.13, 126.66, 101.57, 65.37, 62.55, 32.65, 32.60, 29.70, 26.13, 26.10, 25.59, 25.56, 25.52.

Figure A4. Synthesis and ¹H NMR spectrum of BzAc-DOH in CDCl₃, synthesized by transacetalization of HDOH with benzaldehyde dimethyl acetal.



Synthesis of cyclic acetal. In a 100 mL round bottom flask dried at 70 °C overnight, ethylene glycol (4.9 g, 79 mmol) and TSA (0.37 g, 2 mmol) were mixed with anhydrous THF (50 mL) containing 5 Å molecular sieves (25 g) dried in an oven at 180 °C for 5 hours. Benzaldehyde dimethyl acetal (3 g, 20 mmol) was added and the mixture was stirred at room temperature for 24 hours. After the removal of molecular sieves by filtration, the resulting mixture was quenched with Et₃N (1 mL). Solvent was removed by rotary evaporation and the residues were redissolved in ethyl acetate. Crude was extracted with an aqueous 2.5% sodium bicarbonate solution (2 x 50 mL) and the organic layer was dried with magnesium sulfate. The product was collected as the second of the total two bands off a silica gel column using an eluent of 4/1 v/v hexane/ethyl acetate mixture, and then dried in vacuum oven for 24 hrs. Colorless oil residue with yield = 1.0 g (35%); $R_f = 0.5$ on (1/1 v/v hexane/ethyl acetate). ¹H NMR (CDCl₃, ppm): 7.47-7.37 (m, 5H, Ar-H), 5.82 (s, 1H, CH-O₂), 4.15-4.04 (m, 4H, O-CH₂-CH₂-O).

Figure A5. ¹H NMR spectrum in CDCl₃ of a cyclic acetal, synthesized by the reaction of benzaldehyde with glycol.

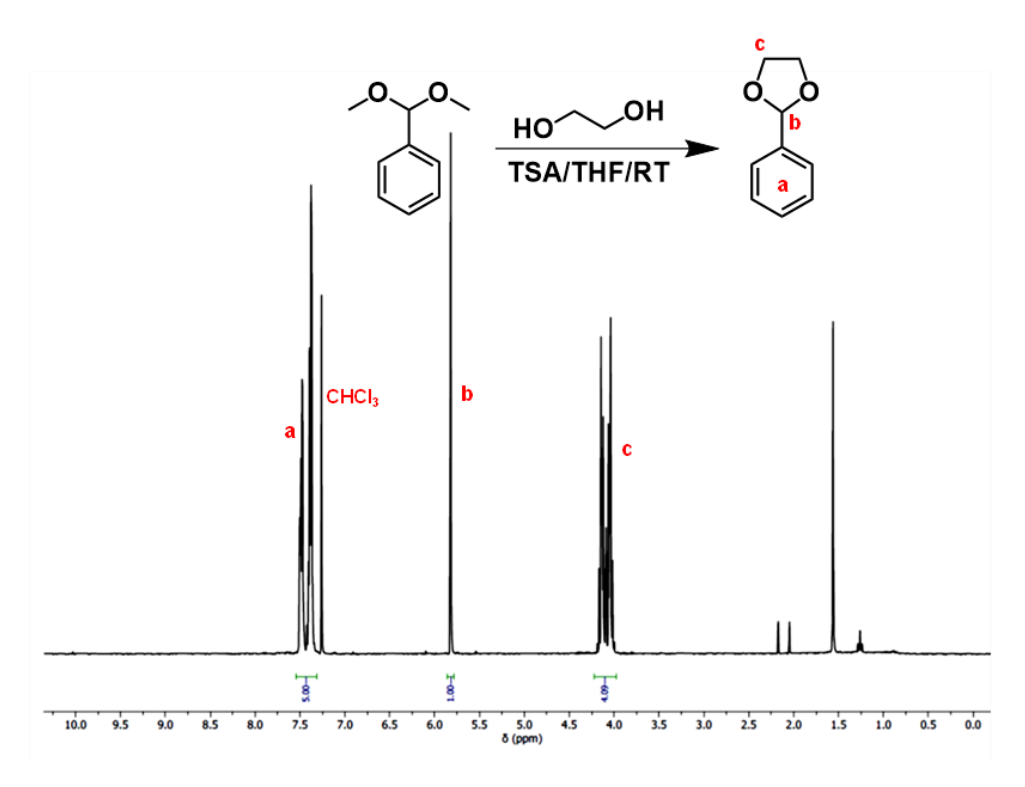


Figure A6. Our approach with two steps to synthesize benzaldehyde hydroxyethyl acetal (BzAA-DHEOH) in the presence of TSA at room temperature in anhydrous THF.

Materials. Benzaldehyde (\geq 99%), trimethyl orthoformate (99%), p-toluenesulfonic acid monohydrate (PTS, \geq 98.5%), triethylamine (Et₃N, \geq 99.5%) were purchased from Sigma-Aldrich. 2-Hydroxyethylacetate was synthesized according to other literature (J. Org. Chem. 1996, 61, 4469-4471)

Synthesis

Benzaldehyde dimethyl acetal (BzAc-DMA). Prior to the synthesis of BzAc-DMA, benzoic acid impurities in benzaldehyde commercial bottles were removed by washing with aqueous sodium bicarbonate solution (2.5 w/w %) two times. Next, benzaldehyde (3.0 g, 0.028 mol) was mixed to the solution of trimethyl orthoformate (30.0 g, 0.28 mol) and PTS (0.16 g, 0.85 mmol) in methanol (50 mL), and the reaction was stirred overnight. After evaporation of the solvent, the residues were dissolved in DCM and washed by sodium bicarbonate solution. The product was collected after rotary evaporation, yielding 3.87 g (90%). H-NMR (CDCl₃, ppm): 7.45 (d, 1H, -(CH)₂CH(CH)₂-), 7.35 (m, 4H, -(CH)₂CH(CH)₂-), 5.40 (s, 1H, CH₃OCHC(CH)₂-), 3.33 (s, 6H, CH₃OCH-).

Benzene acetal diacetate (BzAc-DEAc). 2-Hydroxyethylacetate (7.1 g, 0.068 mol) dissolved in anhydrous THF (150 mL) was mixed with PTS (0.10 g, 0.53 mmol), molecular sieves (5 Å, 1.6 mm pellet, dried at 120 °C for 3 h, 30 g), and BzAc-DMA (1.6 g, 10 mmol). The resulting mixture was stirred overnight at room temperature and then quenched by the addition of Et₃N (1 mL). After removing molecular sieves by filtration and solvents by rotary evaporation, the residues were dissolved in DCM (200 mL) and washed by sodium bicarbonate aqueous solution (2.5 w/w %) two times. After the solvent was evaporated, the product was purified by silica gel column chromatography (1/4 v/v EA/HE). The product was collected as the second of the total

three bands off a silica gel column, yielding 0.93 g (25%). $R_f = 0.37$ on silica (2/3 v/v EA/HE). ¹H-NMR (CDCl₃, ppm): 7.45 (d, 1H, -(CH)₂CH(CH)₂-), 7.35 (m, 4H, (CH)₂CH(CH)₂), 5.66 (s, 1H, -CH₂OCHC(CH)₂-), 4.25 (t, 2H, CH₃C(O)OCH₂-), 3.70 (t, 2H, -OCH₂CH₂OCH-), 2.06 (s, 6H, CH₃C(O)OCH₂-).

Benzene acetal diol (BzAc-DHEOH). An aqueous solution of NaOH (6 mM, 55 mL) was added to the mixture of BzAc-DEAc (1.8 g, 50.8 mmol) in methanol (35 mL). The reaction mixture was stirred overnight at room temperature and then extracted with DCM two times. The organic layers were evaporated and dried in vacuum oven at room temperature for 12 hrs, yielding pale-yellow oil 0.86 g (80 %). H-NMR (CDCl₃, ppm): 7.45 (d, 1H, -(CH)₂CH(CH)₂-), 7.35 (m, 4H, (CH)₂CH(CH)₂), 5.66 (s, 1H, -CH₂OCHC(CH)₂-), 3.75 (m, 2H, HOCH₂-), 3.65 (t, 2H, -CH₂CH₂OCH-). CDCl₃, ppm): 61.8, 67.8, 102.6, 126.6, 128.4, 128.8, 137.8.

Figure A7. ¹H NMR spectrum of BzAc-DMA in CDCl₃.

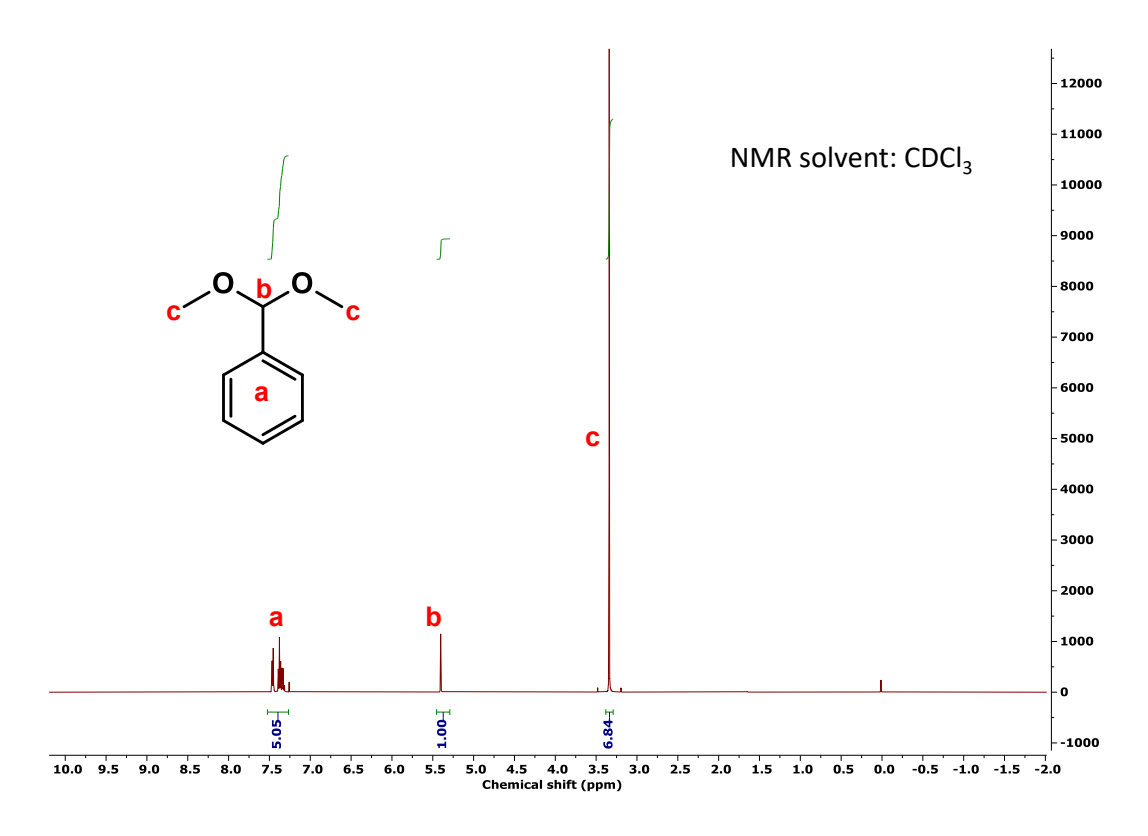


Figure A8. ¹H NMR spectrum of BzAc-DEAc in CDCl₃.

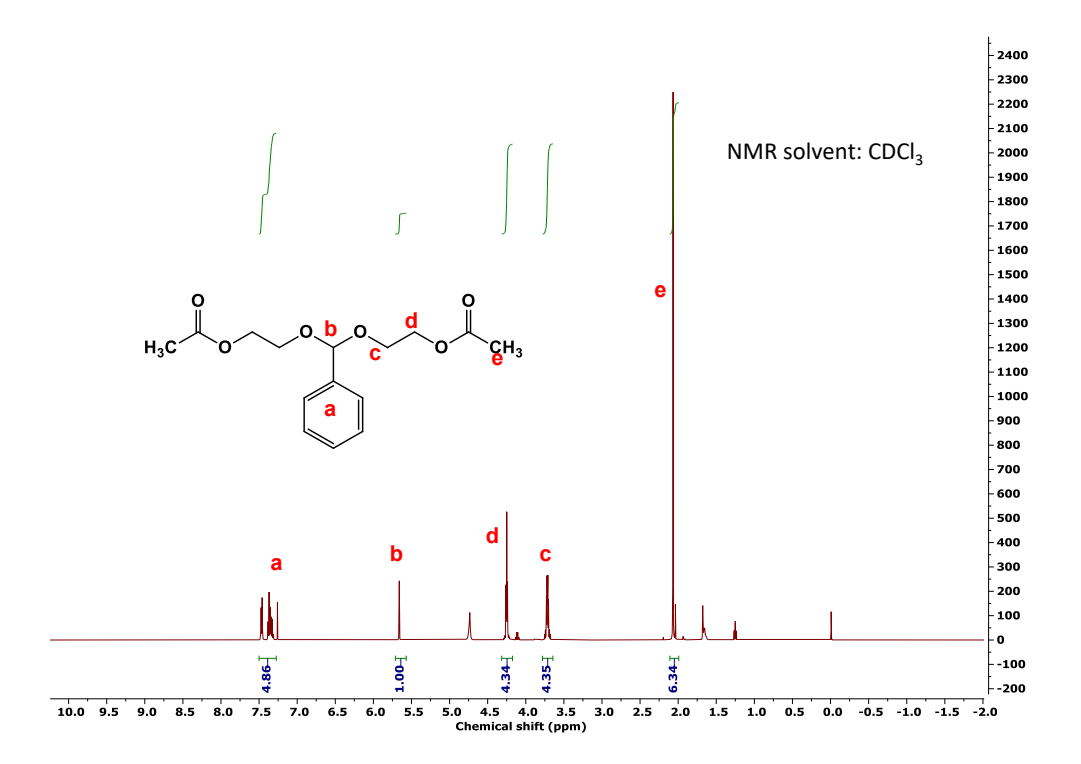


Figure A9. ¹H NMR spectrum of BzAc-DHEOH in CDCl₃.

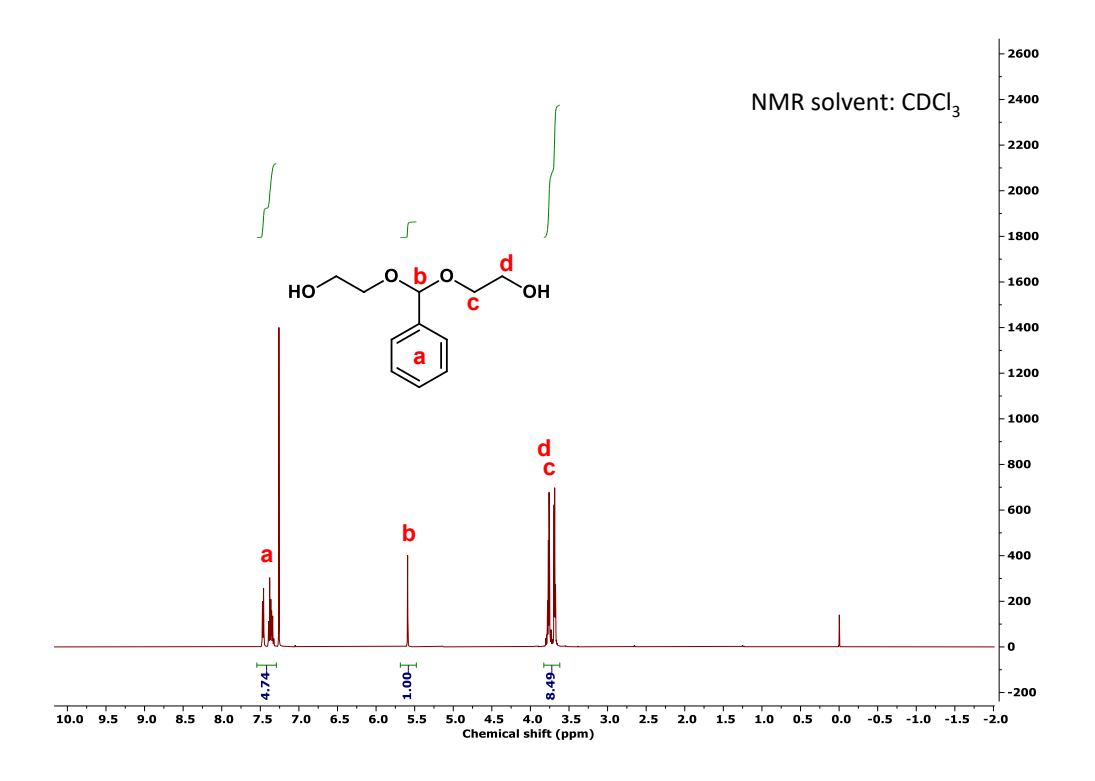


Figure A10. Overlaid ${}^{1}H$ NMR spectra in CDCl₃ of BzAc-DOH incubated at pD = 6.5.

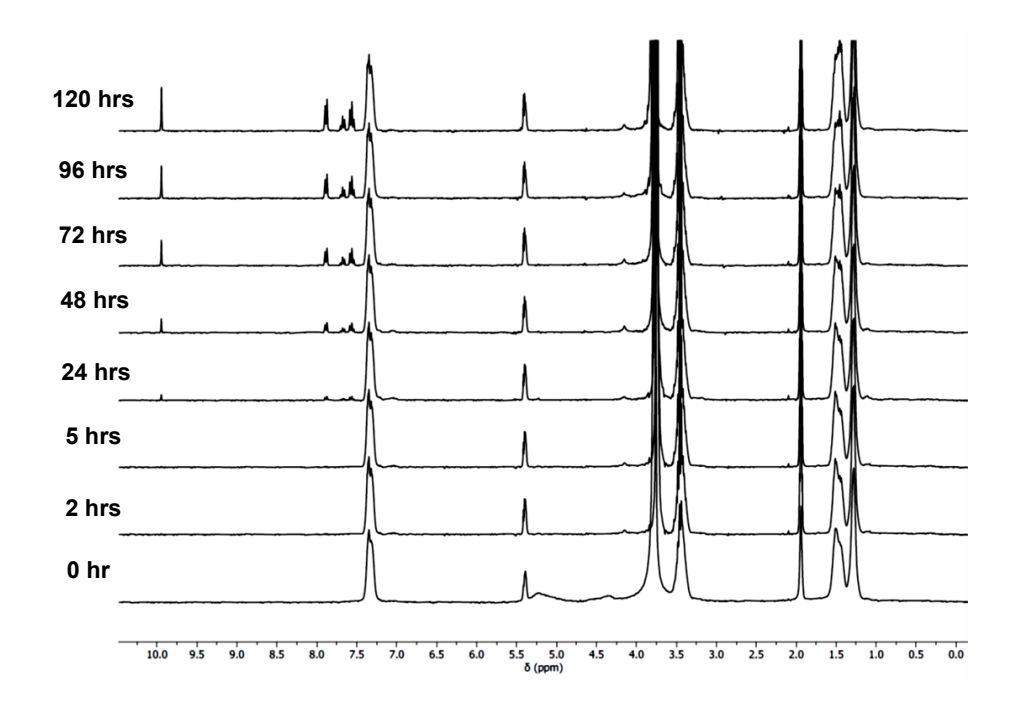


Figure A11. Overlaid ${}^{1}H$ NMR spectra in CDCl₃ of BzAc-DOH incubated at pD = 7.4.

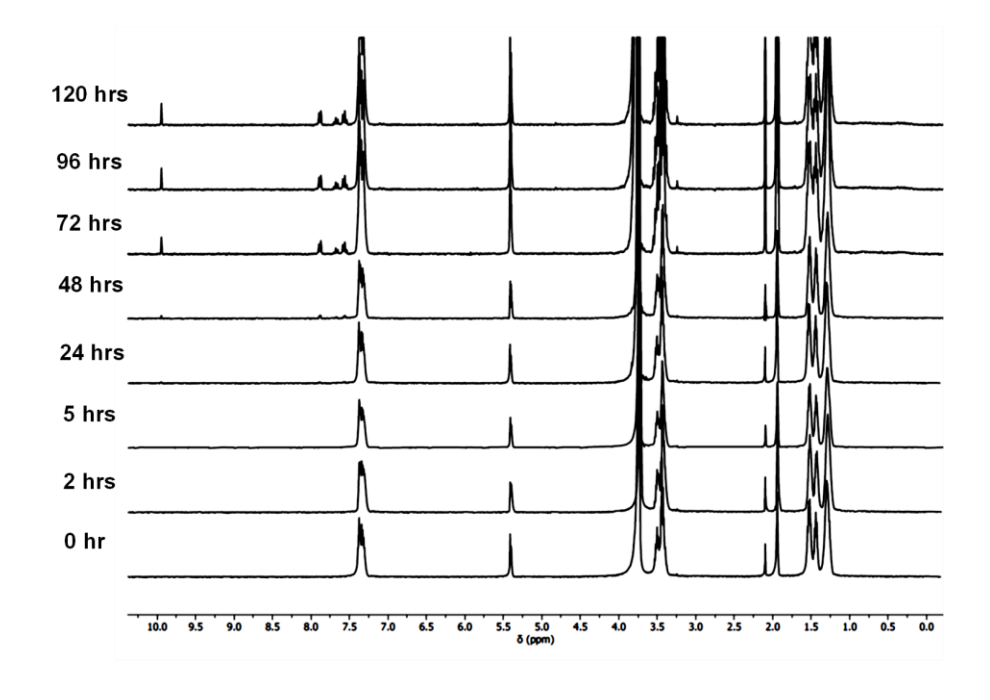


Figure A12. Overlaid ${}^{1}H$ NMR spectra in CDCl₃ of CyPK-DOH incubated at pD = 6.5.

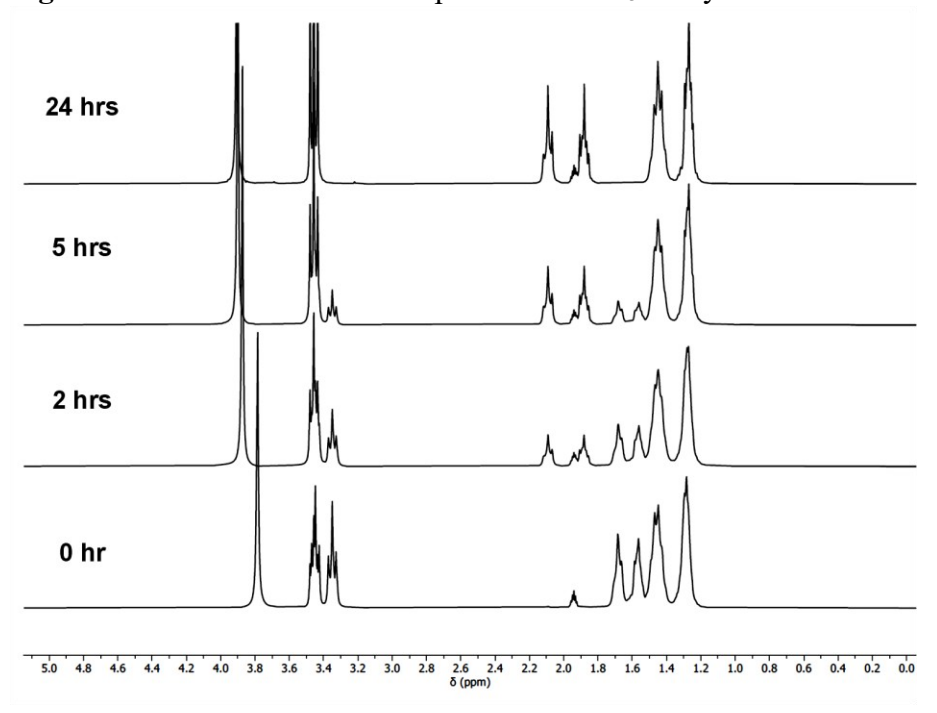


Figure A13. Overlaid ${}^{1}H$ NMR spectra in CDCl₃ of CyPK-DOH incubated at pD = 7.4.

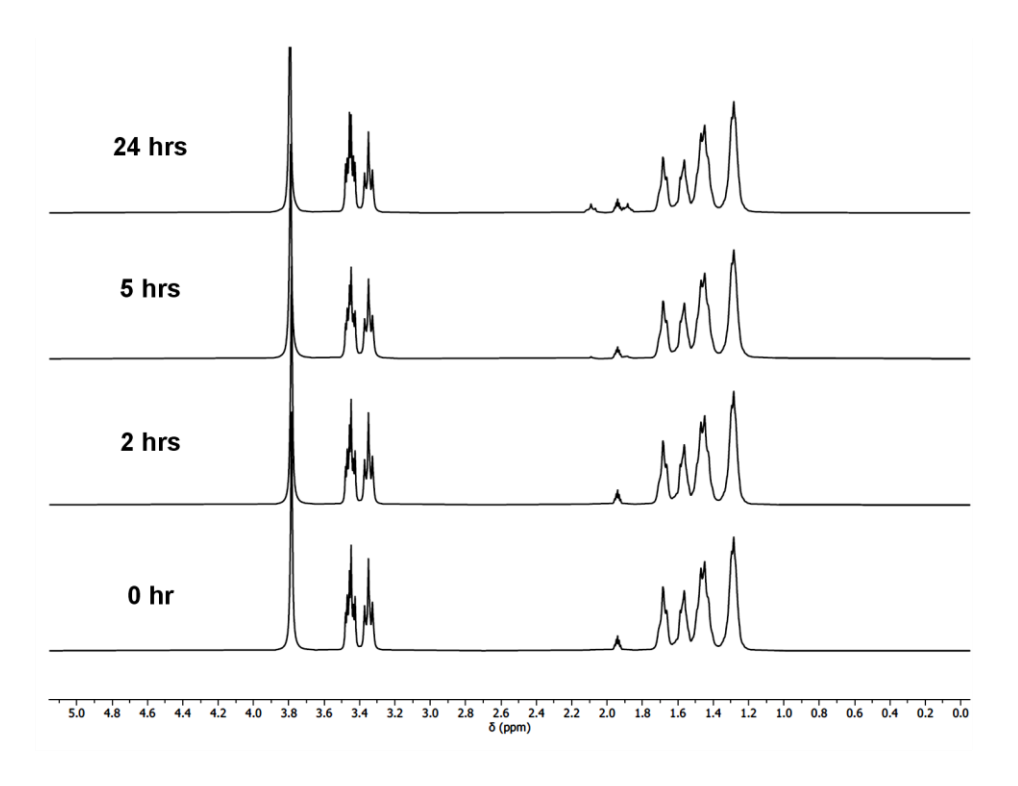


Figure A14 Overlaid ${}^{1}H$ NMR spectra in CDCl₃ of CyHK-DOH incubated at pD = 6.5.

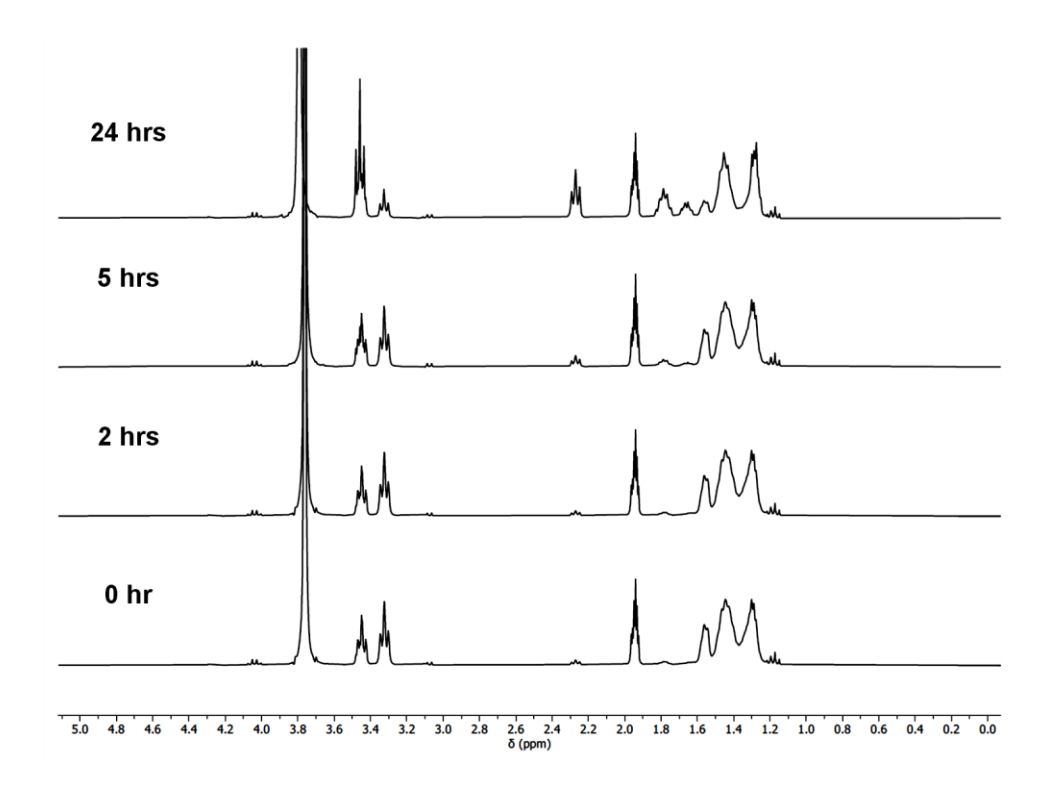


Figure A15. Overlaid ¹H NMR spectra in CDCl₃ of CyHK-DOH incubated at pD = 7.4.

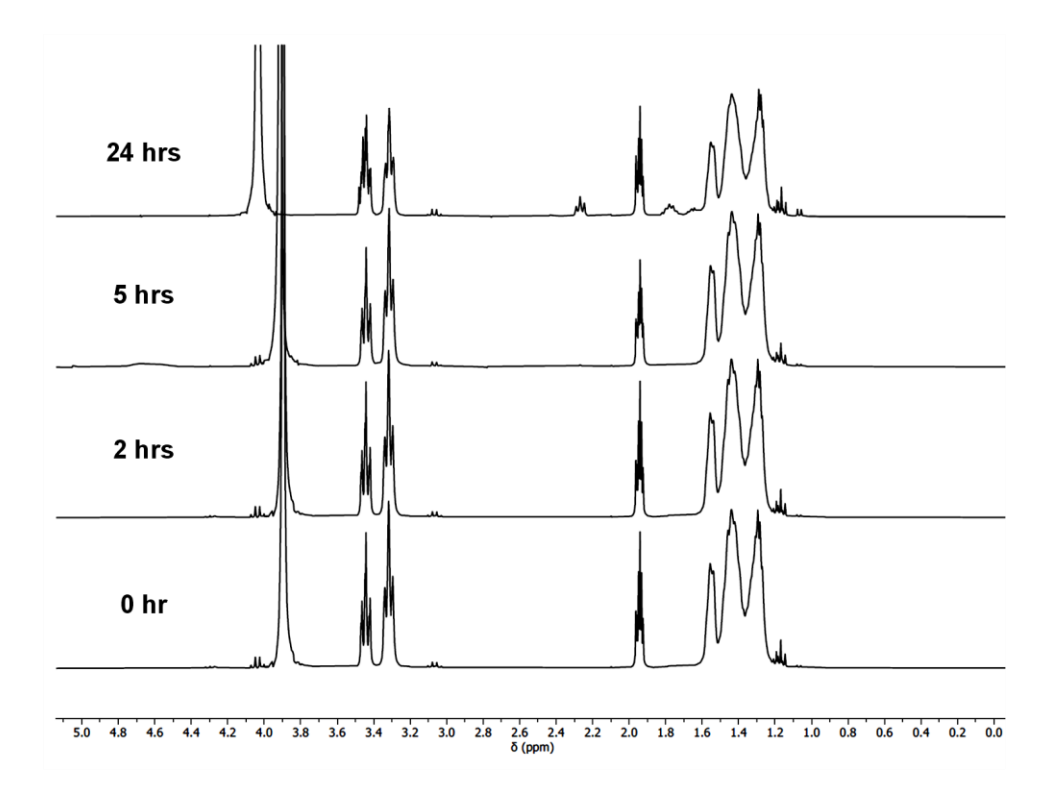


Figure A16. ¹H NMR spectrum of PEG-BzAc-OH in CDCl₃.

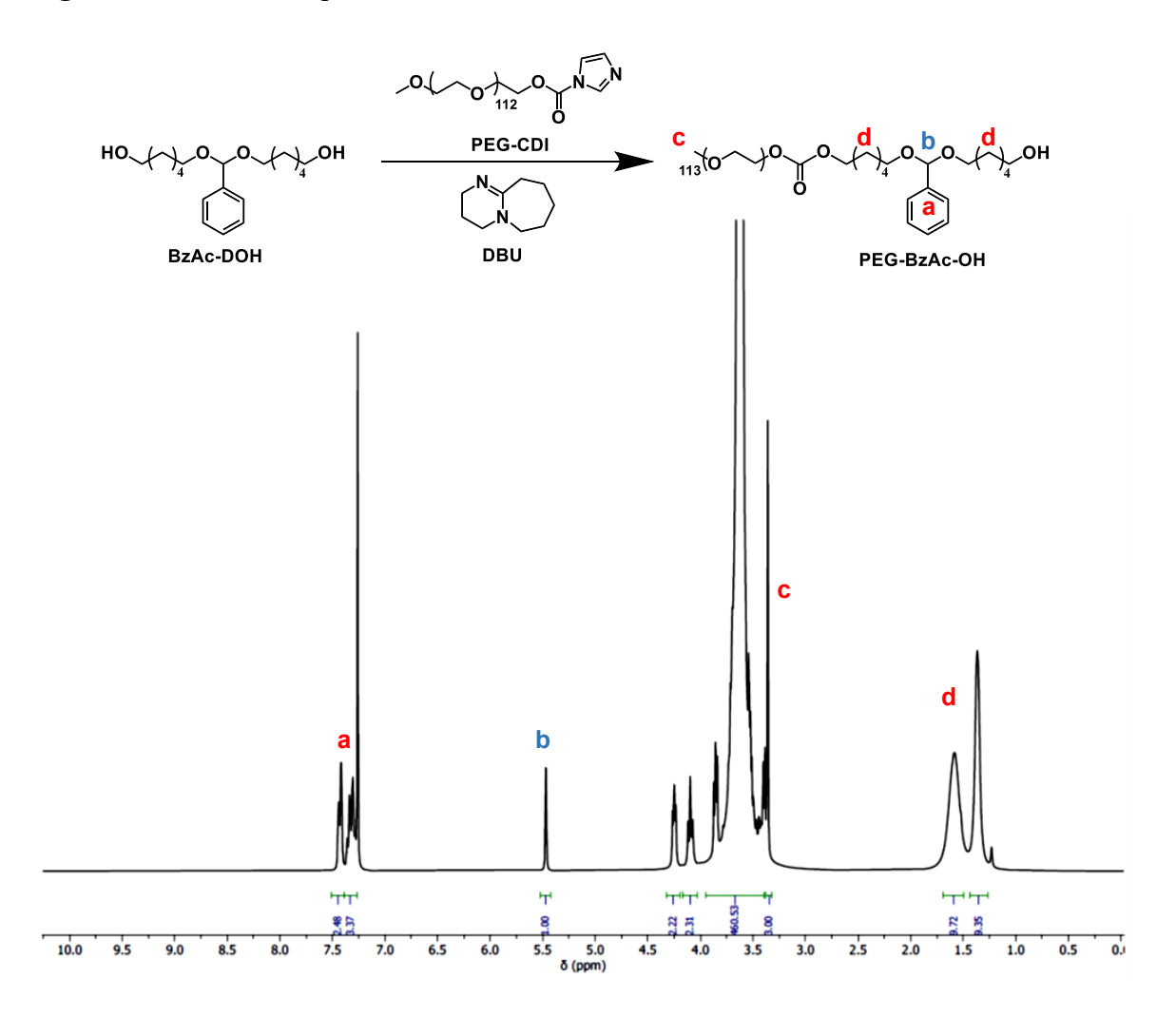


Figure A17. ¹H NMR spectrum of PEG-BzAc-Br in CDCl₃.

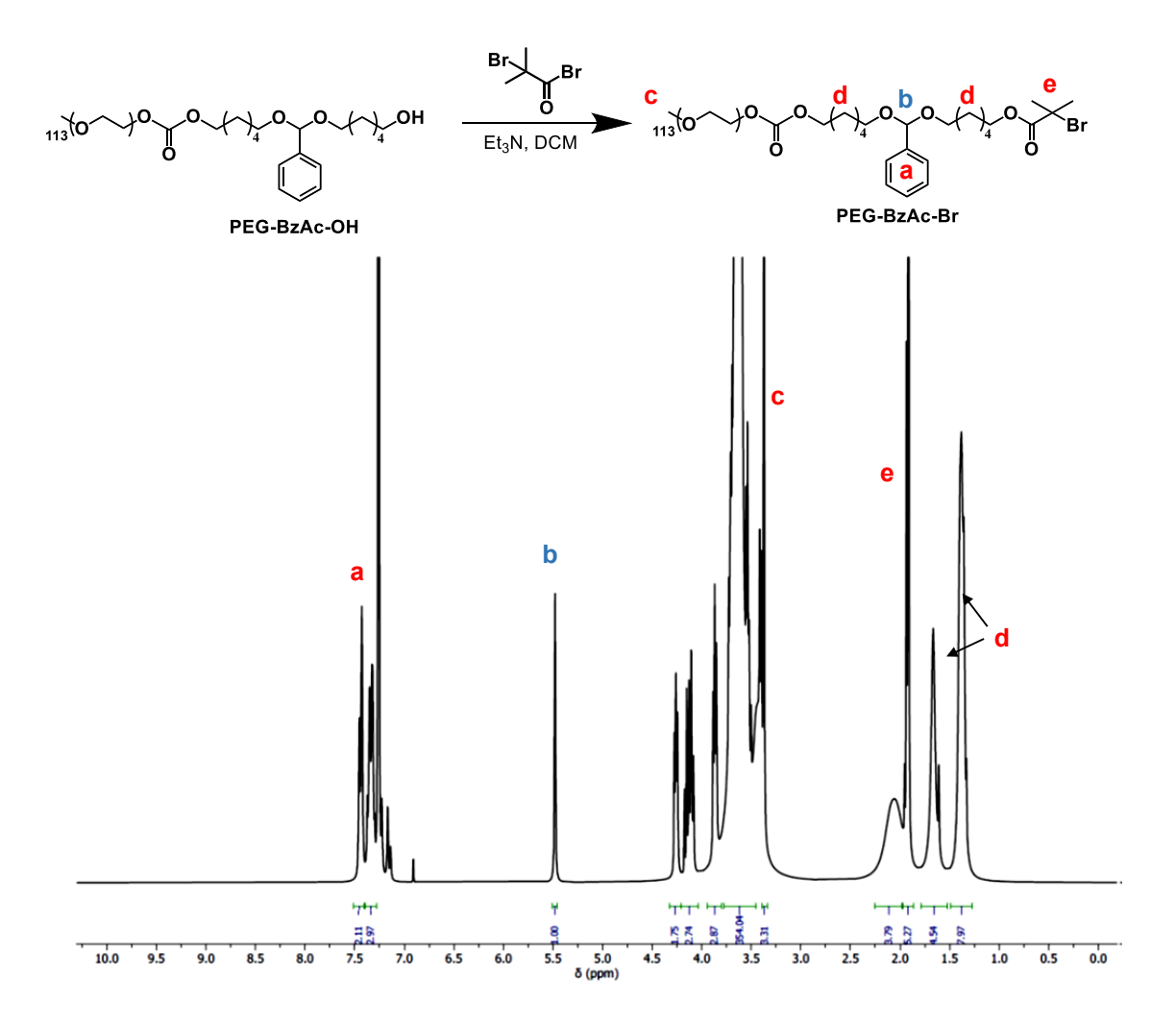


Figure A18. Overlaid ¹H NMR spectra in CDCl₃ of PEG-BzAc-Br incubated at pD = 7.4.

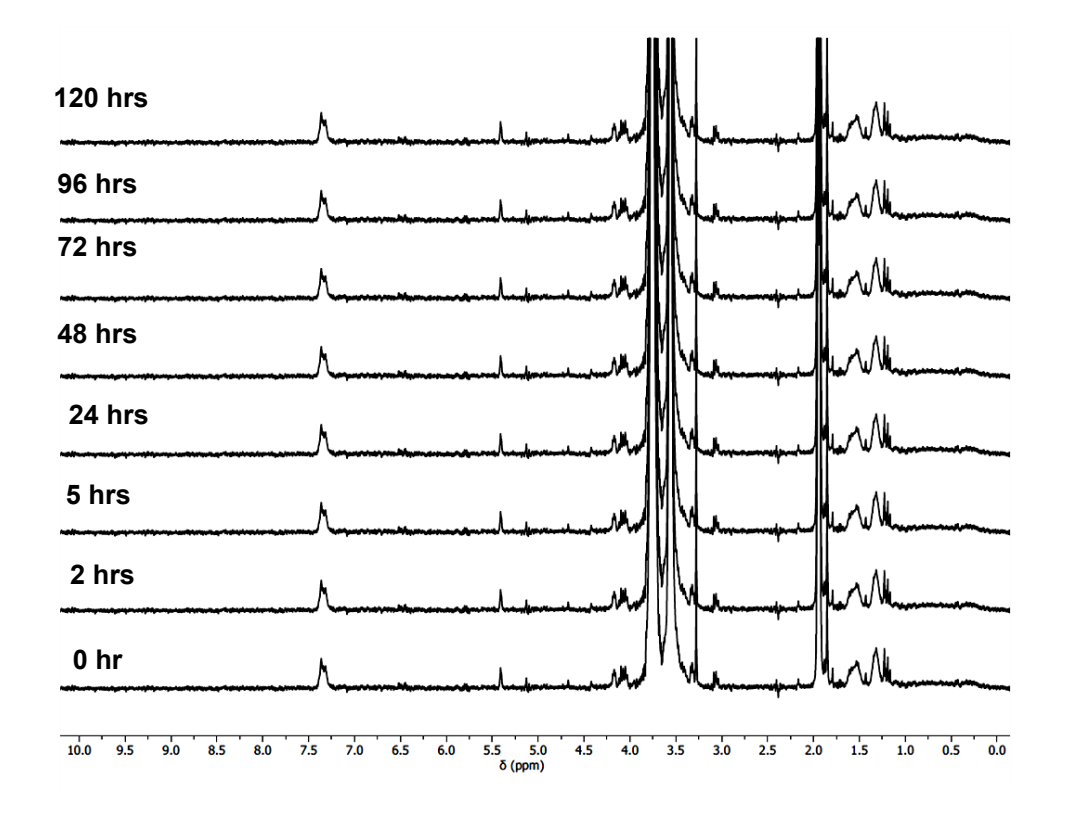


Figure A19. Overlaid ¹H NMR spectra in CDCl₃ of PEG-BzAc-Br incubated at pD = 6.5.

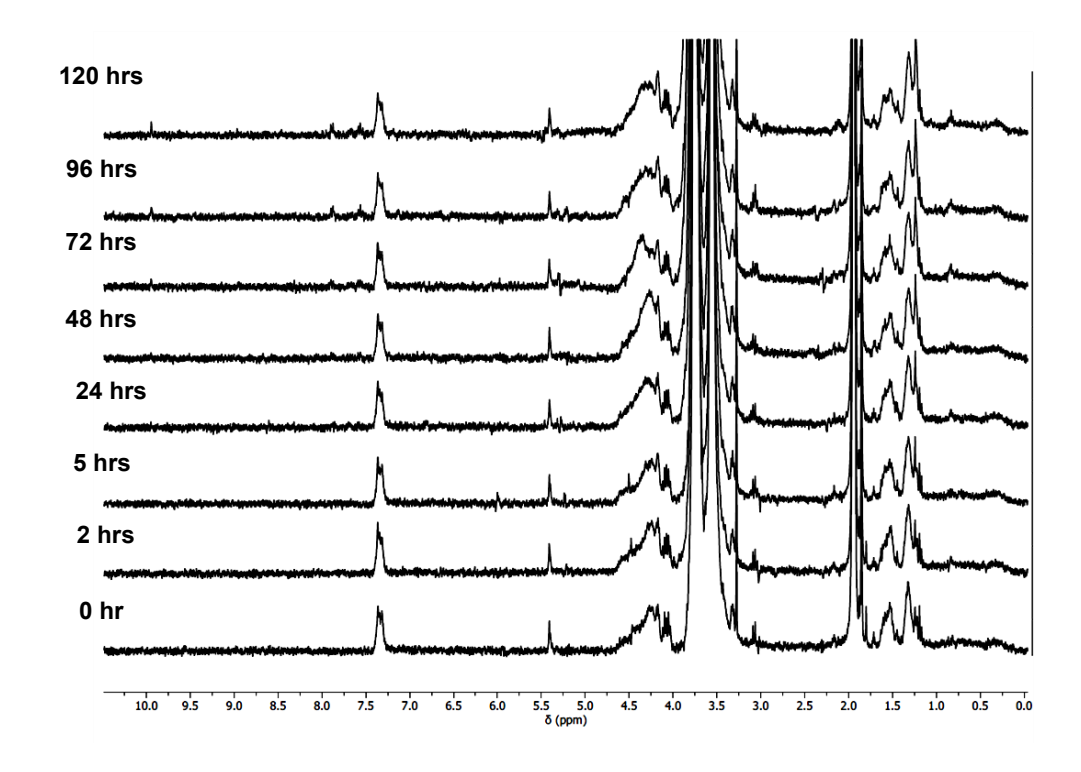


Figure A20. Overlaid ${}^{1}H$ NMR spectra in CDCl₃ of PEG-BzAc-Br incubated at pD = 5.0.

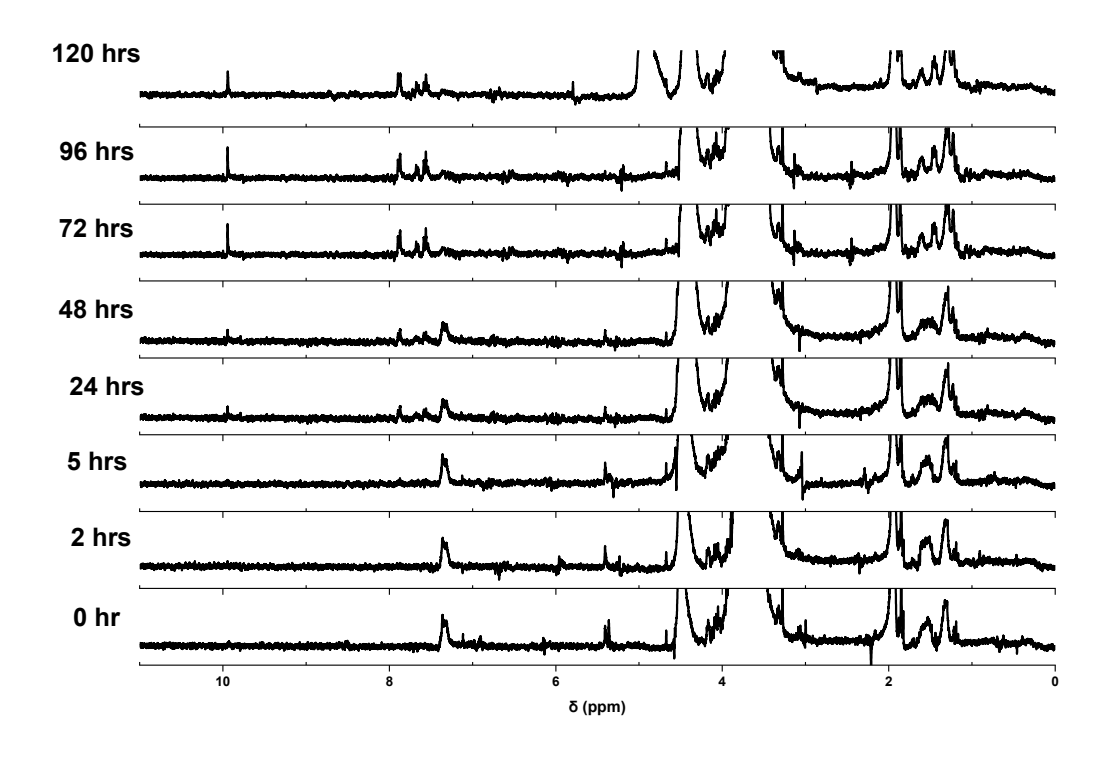


Figure A21. Schematic illustration of acid-catalyzed hydrolysis and evolution of %hydrolysis at pD = 5.0, 6.8, and 7.4 for PEG-BzAc-Br dissolved in a $3/1 \text{ v/v} \text{ CD}_3\text{CN/PB-D}_2\text{O}$ mixtures.

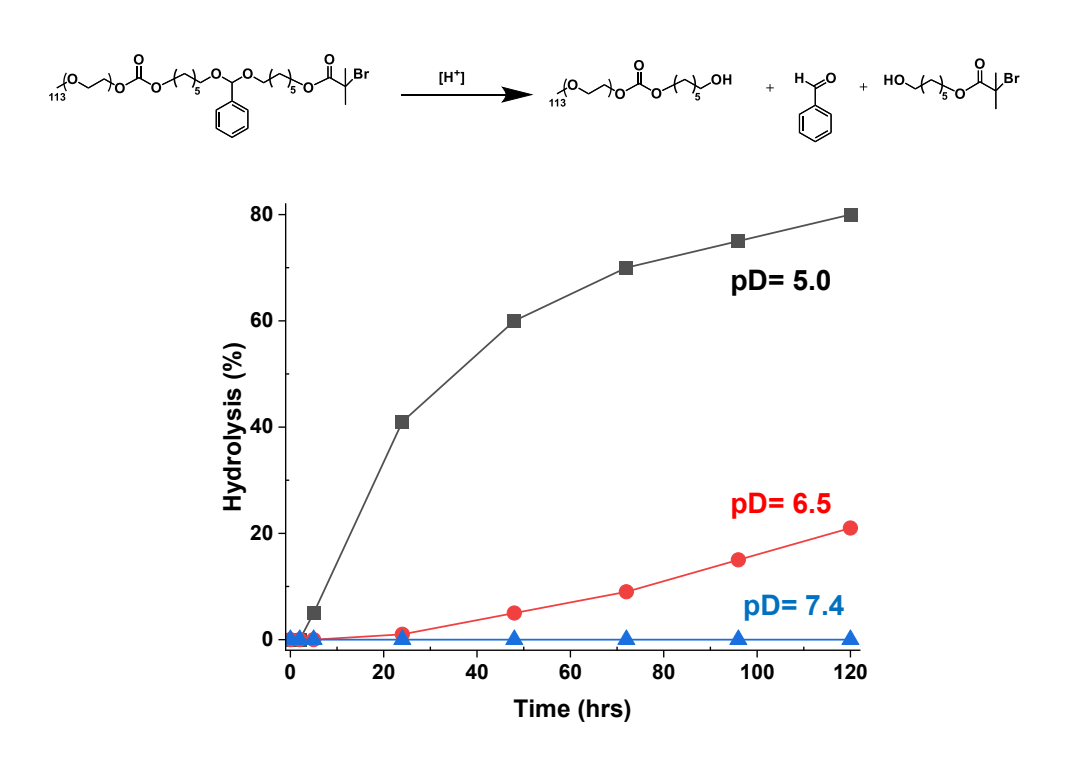


Figure A22. Fluorescence spectra of NR in the mixtures with various amounts of PEG-BzAc-PBM in aqueous solutions.

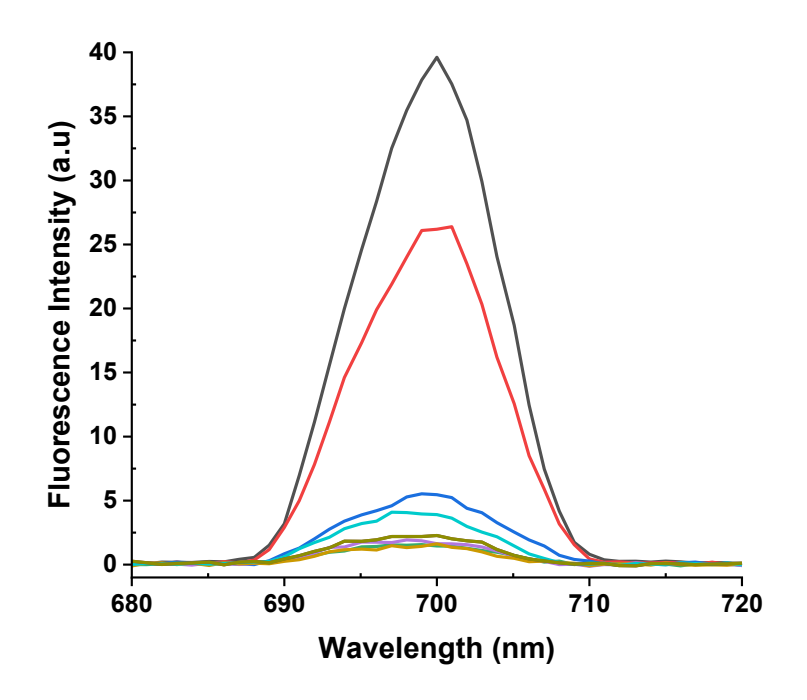


Figure A23. TEM images with different magnifications.

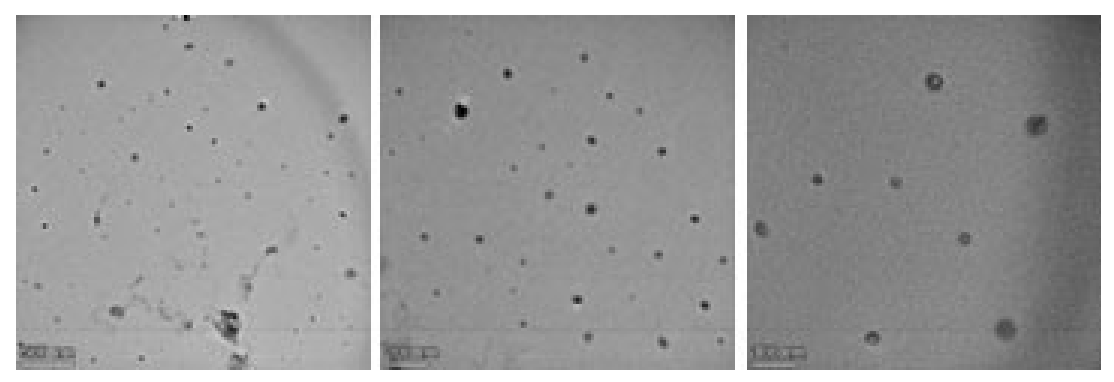
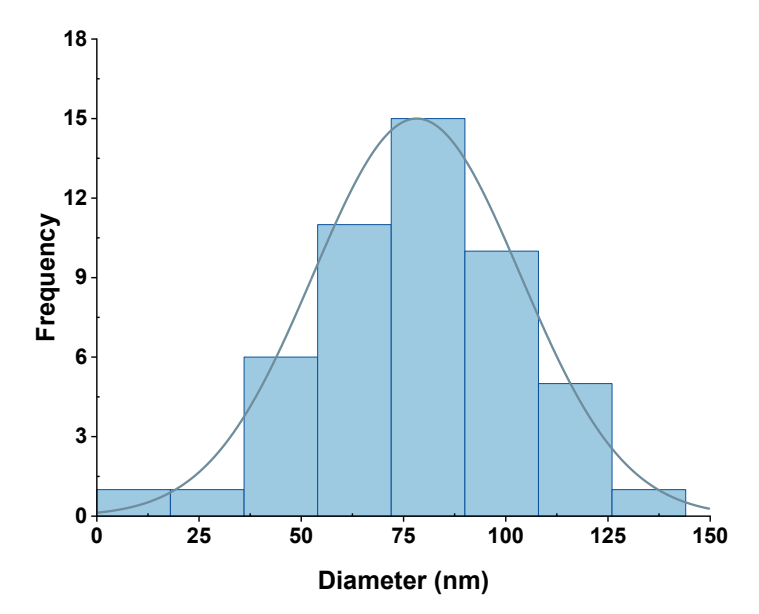


Figure A24. TEM analysis with size distribution of nanoassemblies in dried state.



Appendix B

Supporting Information and Figures for Chapter 4

Figure B1. Overlaid ¹H NMR of PEG-BzAc-PCIMA (PBPM-50 & PBPM-200) in CDCl₃.

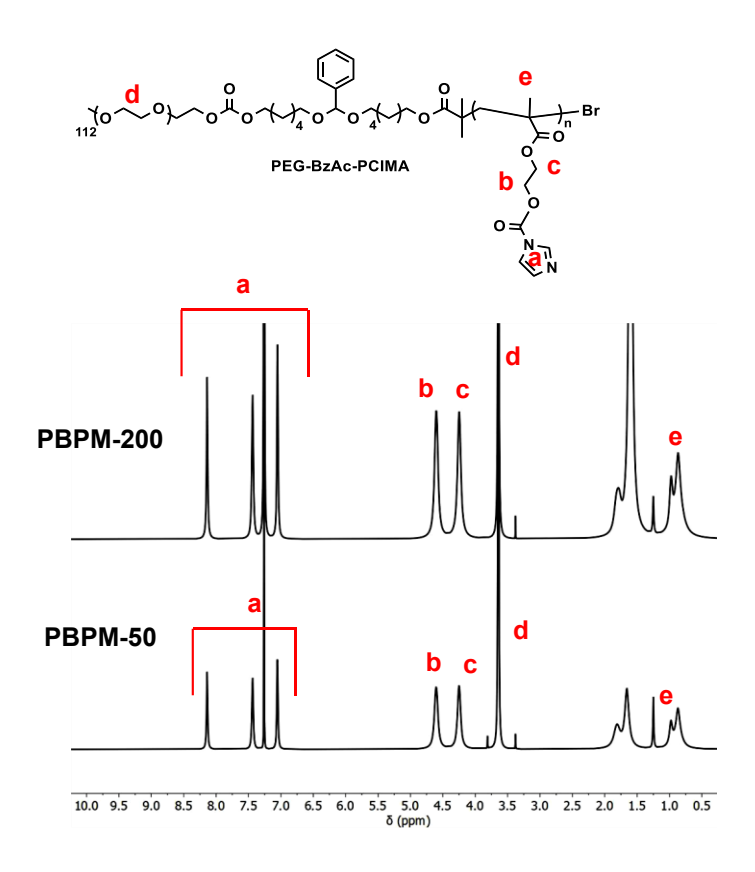


Figure B2. Overlaid GPC diagrams of PEG-BzAc-PCIMA ABPs, compared with that of PEG-BzAc-Br macroinitiator.

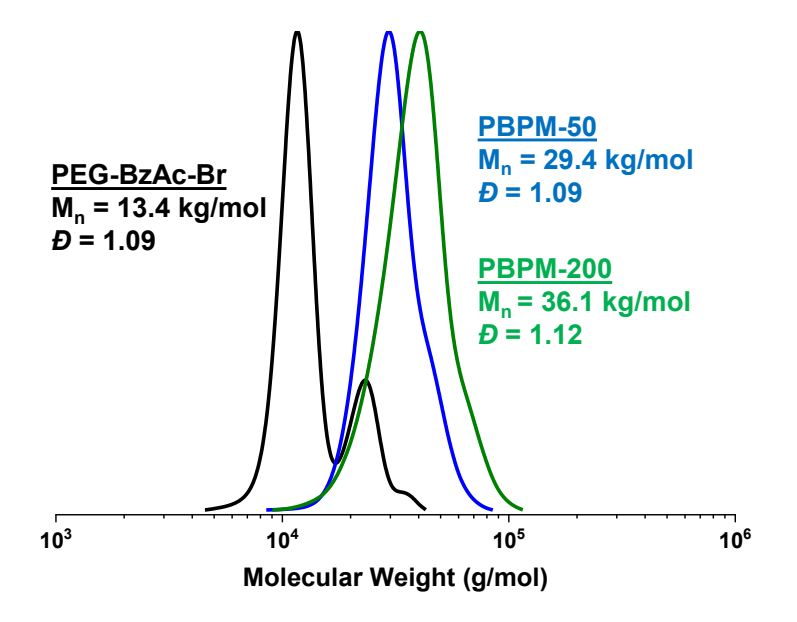


Figure B3. First-order kinetics over polymerization time (a) molecular weight and its distribution over conversion (b) and overlaid GPC trace of kinetics (c) for ATRP of CIMA in the presence of PEG-BzAc-Br. Conditions for ATRP: $[CIMA]_0/[PEG-BzAc-Br]_0/[Cu(II)Br_2/TPMA]_0/[TPMA]_0 = 100/1/0.2/0.5$ in anisole at 40 °C, BM/anisole = 0.40 wt/wt.

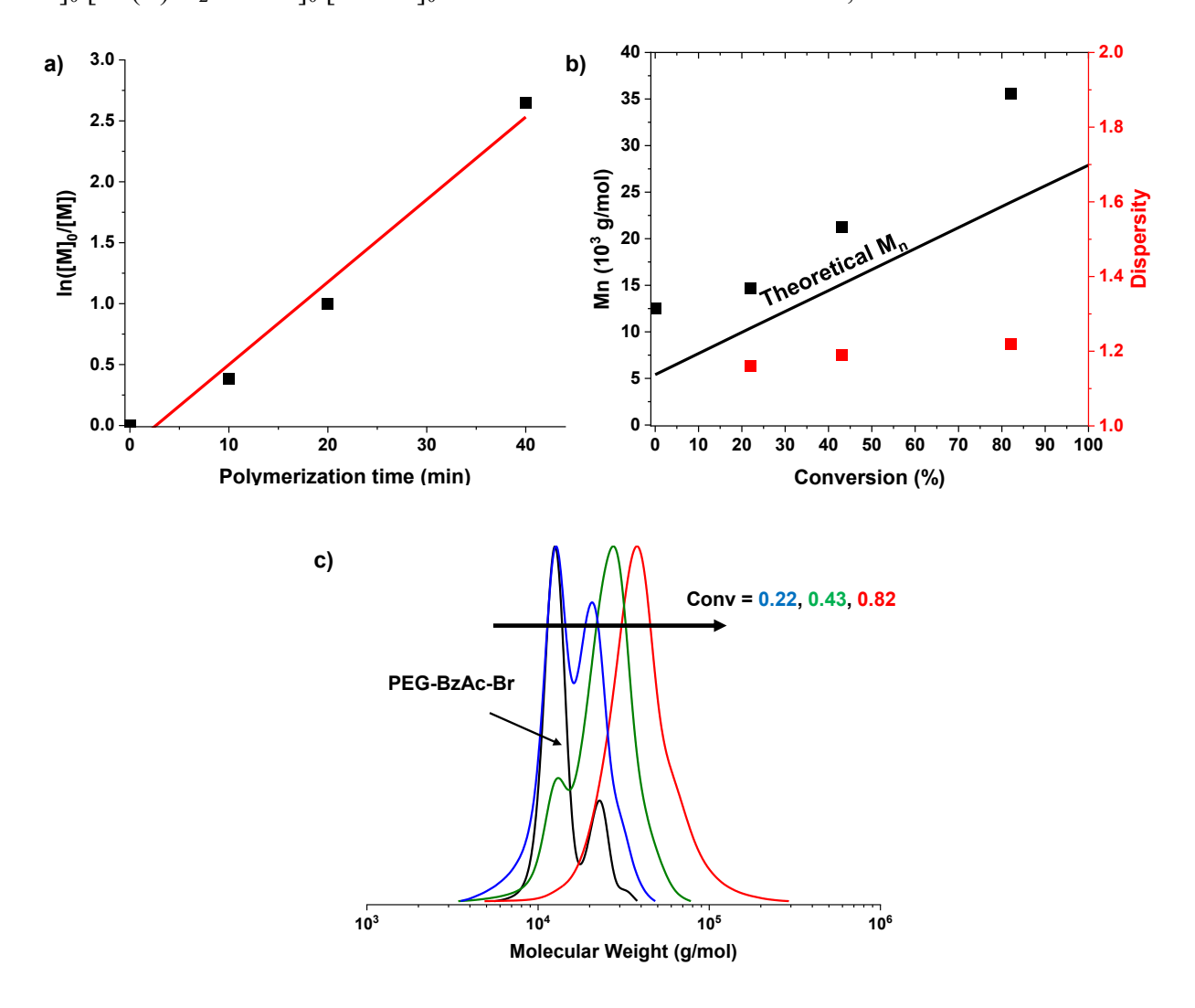


Figure B4. Overlaid ¹H NMR spectra of degradation of PEG-BzAc-PBzI to its corresponding BzA, PEG-OH and HO-Am-Br species bearing terminal hydroxyl groups

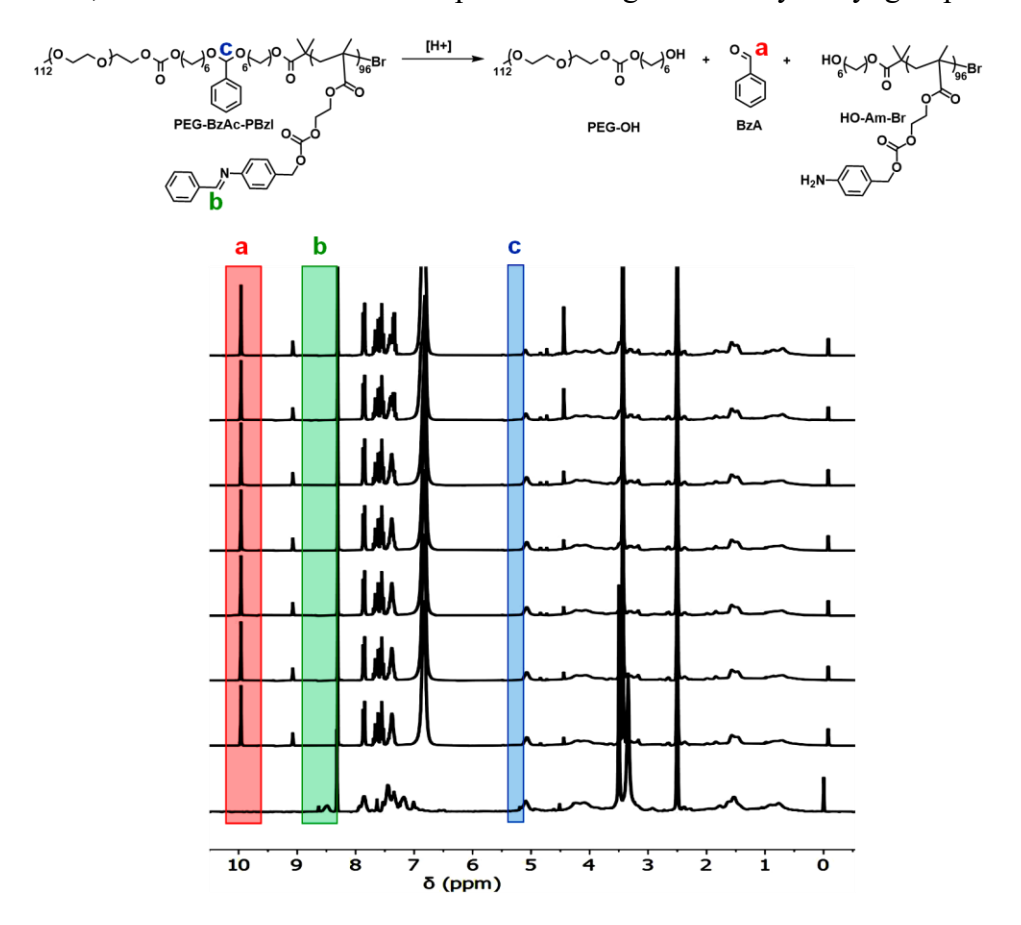


Figure B5. Overlaid ${}^{1}H$ NMR spectra in CD₃CN/PB-D₂O mixtures of PEG-BzAc-Br incubated at pD = 5.0.

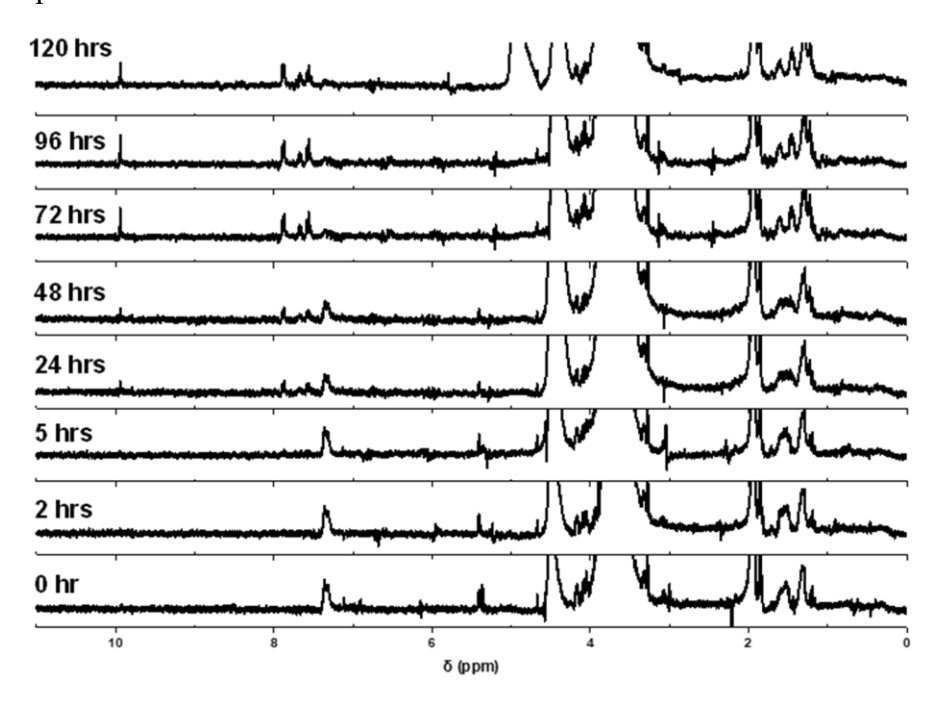


Figure B6. Overlaid 1H NMR spectra in CD₃CN/PB-D₂O mixtures of PEG-BzAc-Br incubated at pD = 6.5.

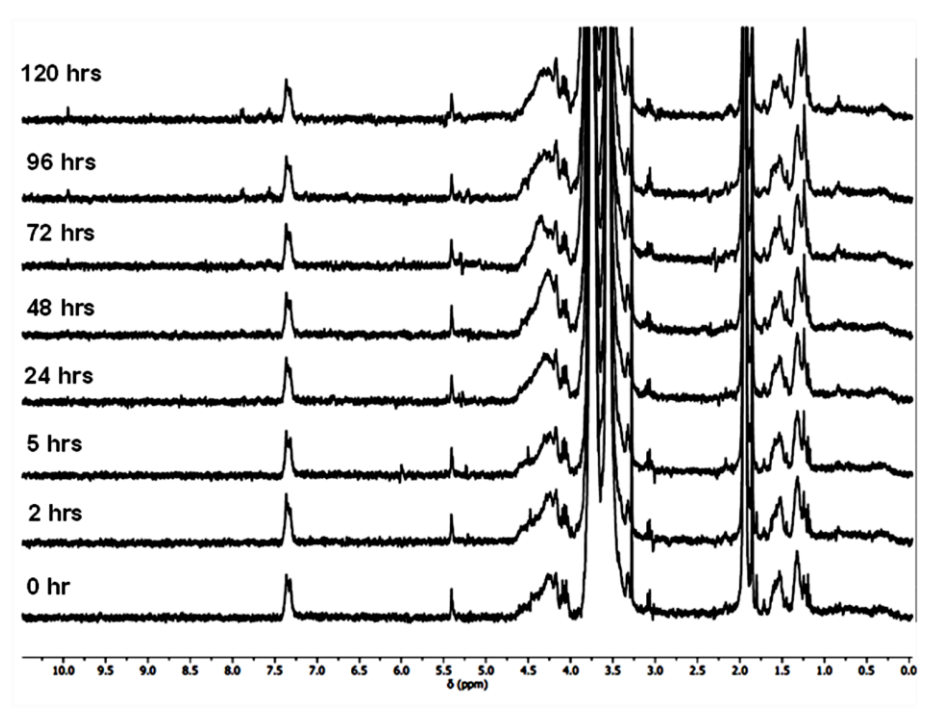


Figure B7. Overlaid ${}^{1}H$ NMR spectra in CD₃CN/PB-D₂O mixtures of PEG-BzAc-Br incubated at pD = 7.4.

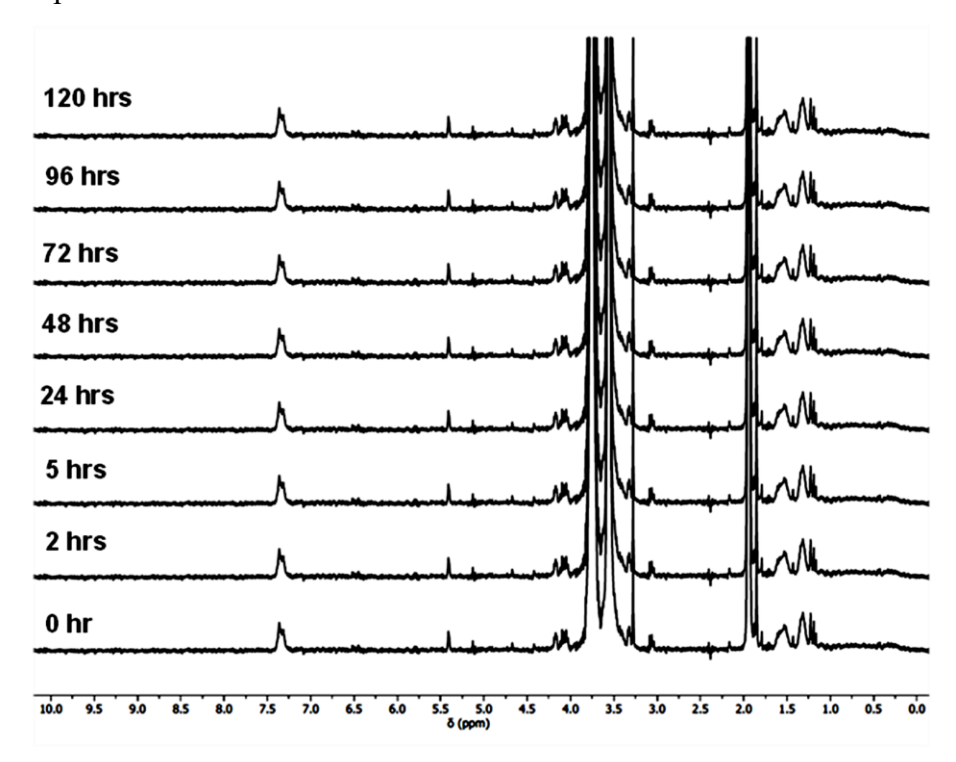


Figure B8. Overlaid ¹H NMR spectra in CD₃CN/PB-D₂O mixtures of BzI-OH incubated at pD = 5.0.

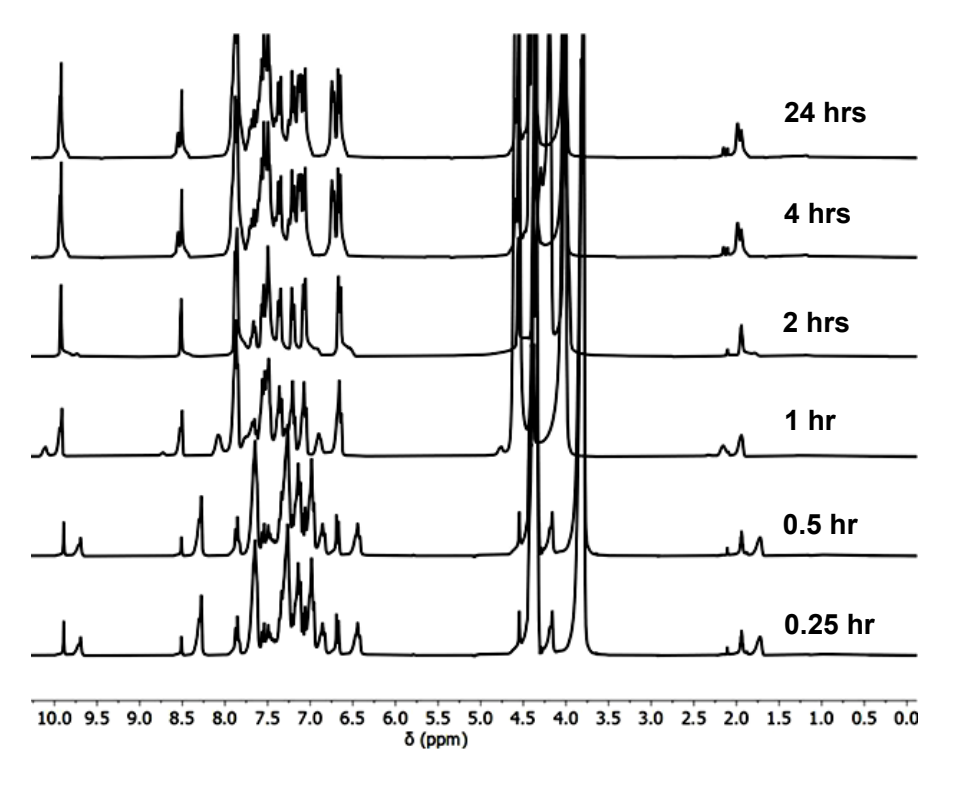


Figure B9. Overlaid ¹H NMR spectra in CD₃CN/PB-D₂O mixtures of BzI-OH incubated at pD = 6.5.

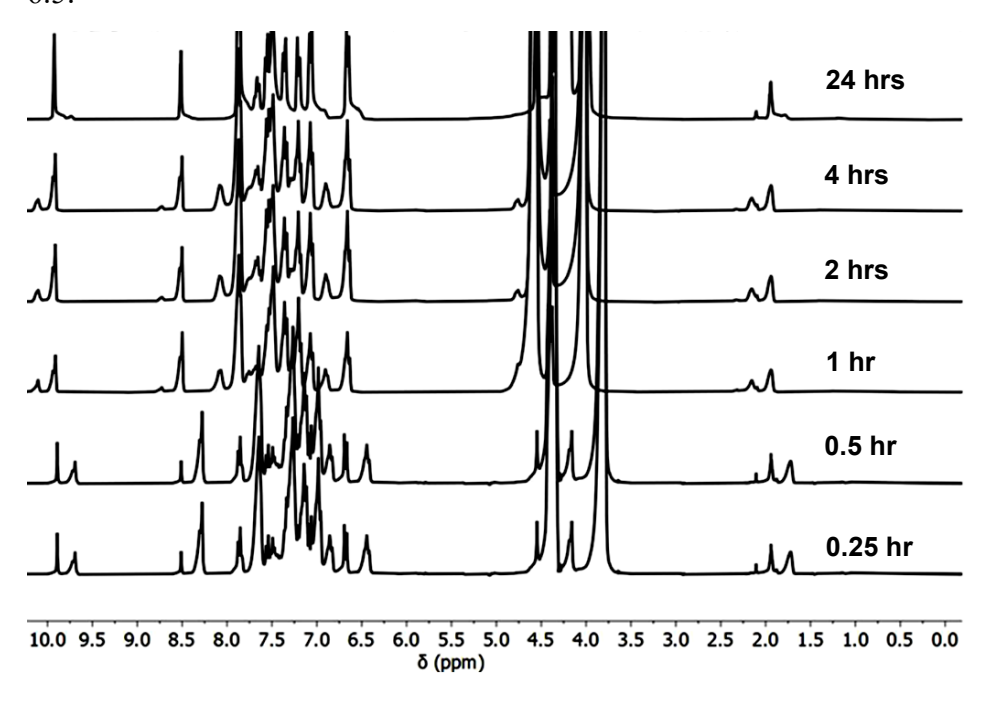


Figure B10. Overlaid ¹H NMR spectra in CD₃CN/PB-D₂O mixtures of BzI-OH incubated at pD = 7.4.

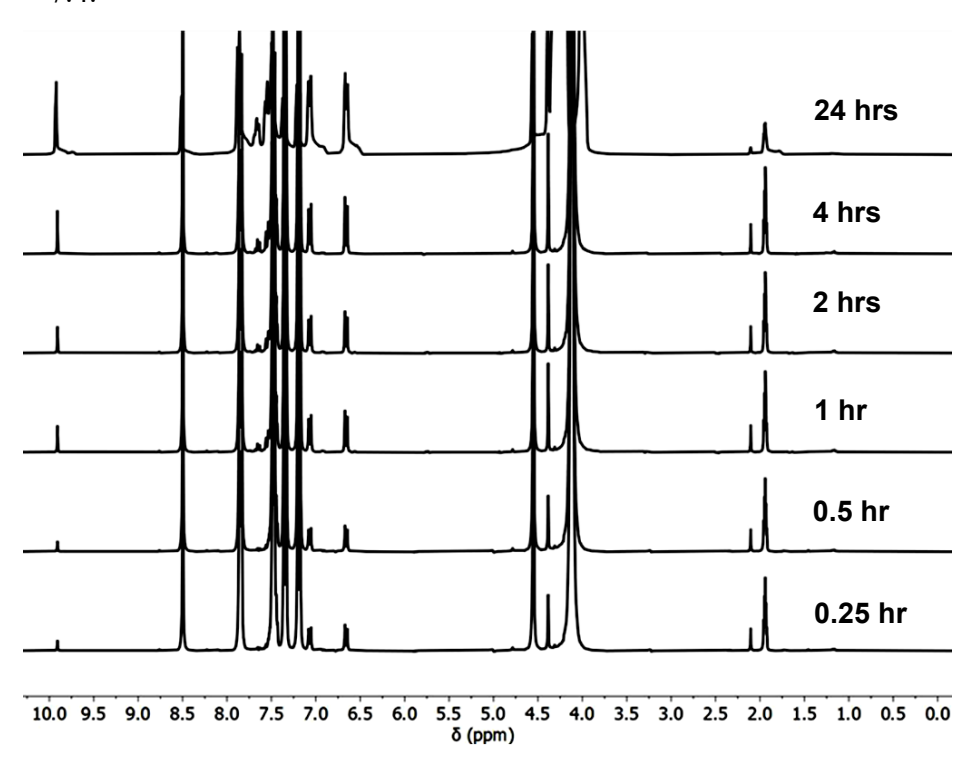


Figure B11. Overlaid fluorescence spectra of NR in the mixtures with various amounts of PEG-BzAc-PBzI in aqueous solutions.

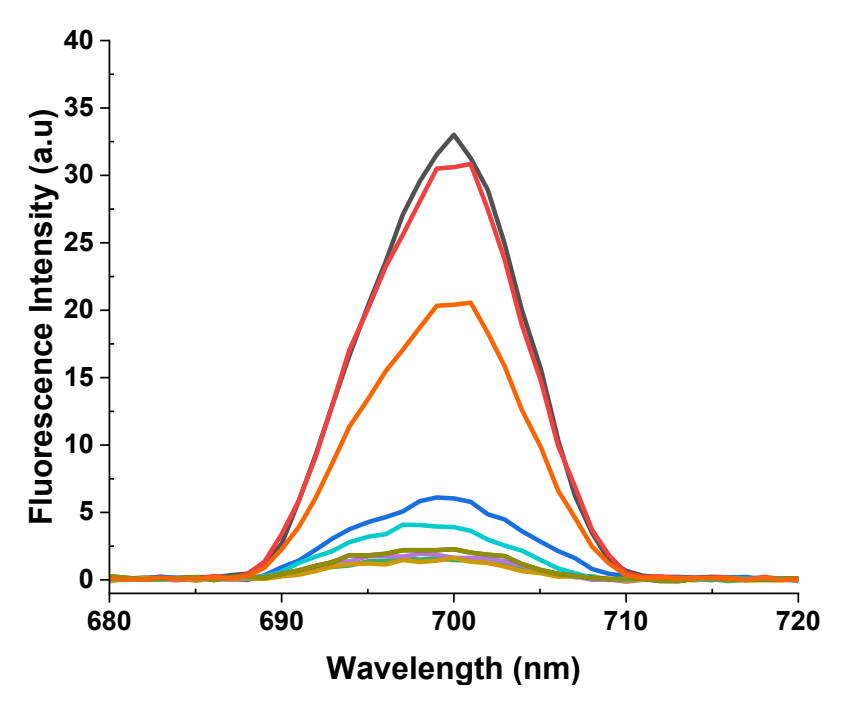


Figure B12. Overlaid DLS plots of aqueous micellization disassembly at pH = 5 (a) and pH = 6.5 (b).

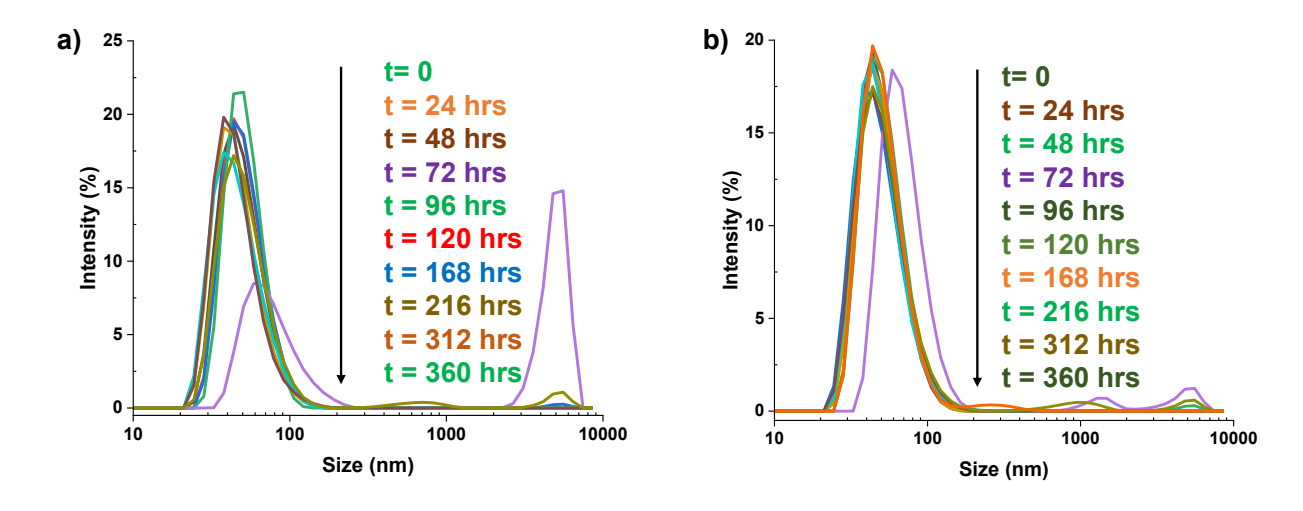


Figure B13. Overlaid UV-Vis spectra of Cur at different concentrations (a) and correlation curve (b) to determine molar absorptivity for quantitative cumulative Cur release.

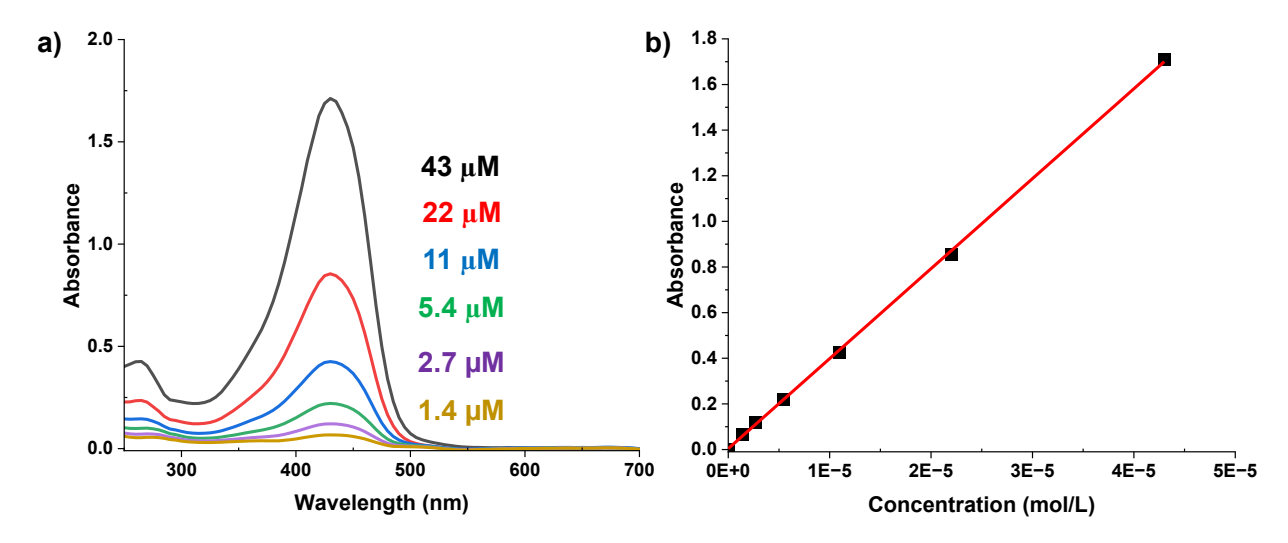


Figure B14. Overlaid UV-Vis spectra of stock Cur and Cur-loaded micelles to determine EE% and LC% (a), and correlation plot between LC% and EE% of Cur-loaded micelles (b).

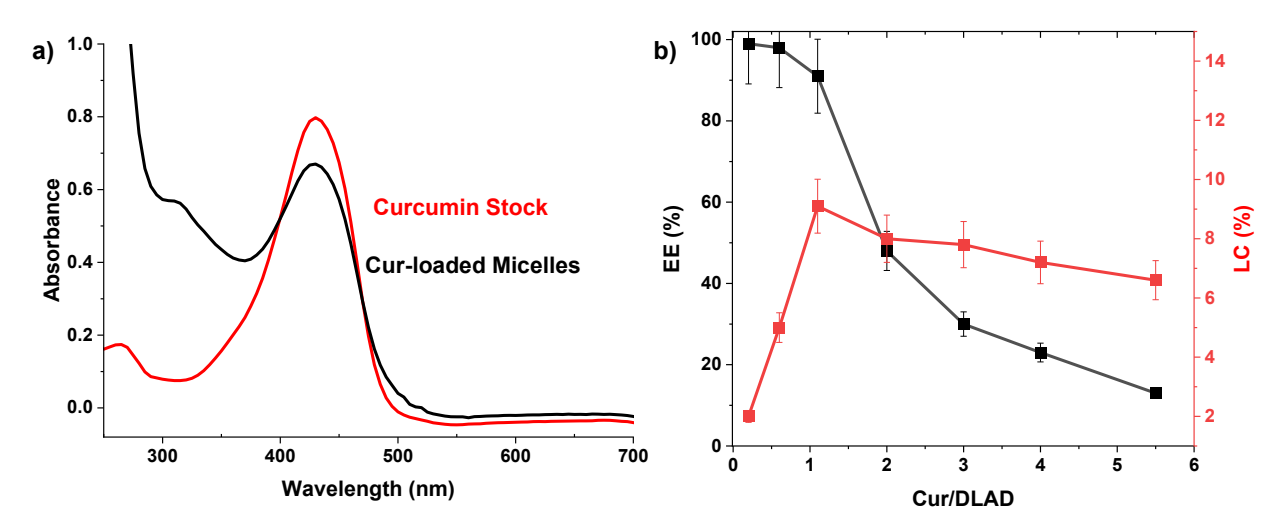


Figure B15. Overlaid UV-Vis spectra of release of Cur at different time points at pH = 5.0 (a), pH = 6.5 (b), and pH = 7.4 (c).

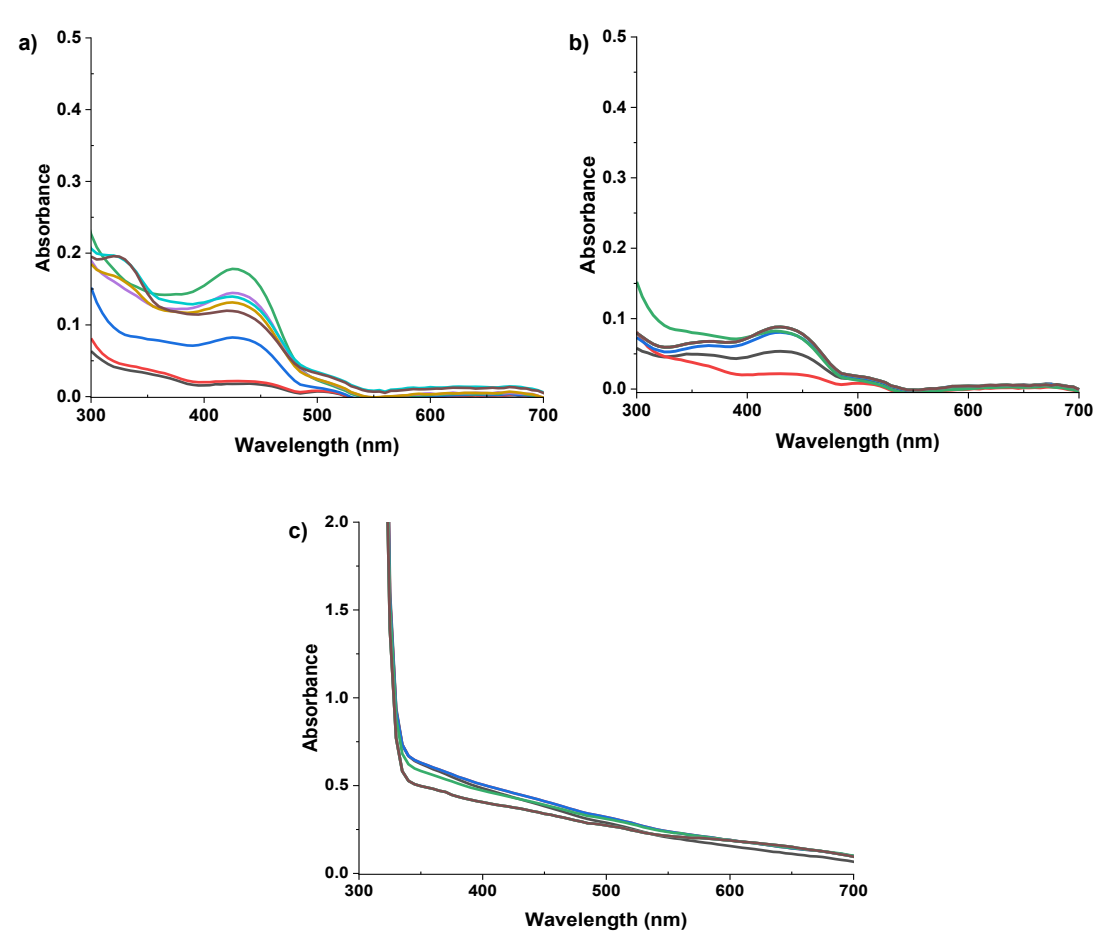


Table B1. Characteristics as well as EE% and DL% for the encapsulation of Cur in DLAD nanoassemblies.

Cur/DLAD wt/wt ratio	Concentration (mg/mL)	LL (%)	LE (%)
2/1	34.4	2.0	99
6/1	11.5	5.0	98
11/1	6.3	9.1	91
20/1	3.4	8.0	48
30/1	2.3	7.8	30
40/1	1.7	7.2	23
55/1	1.3	6.6	13

Appendix C

Supporting Information and Figures for Chapter 5

Figure C1. For ATRP-1, ¹H NMR spectrum of PBM-BzAc-PBM in CDCl₃.

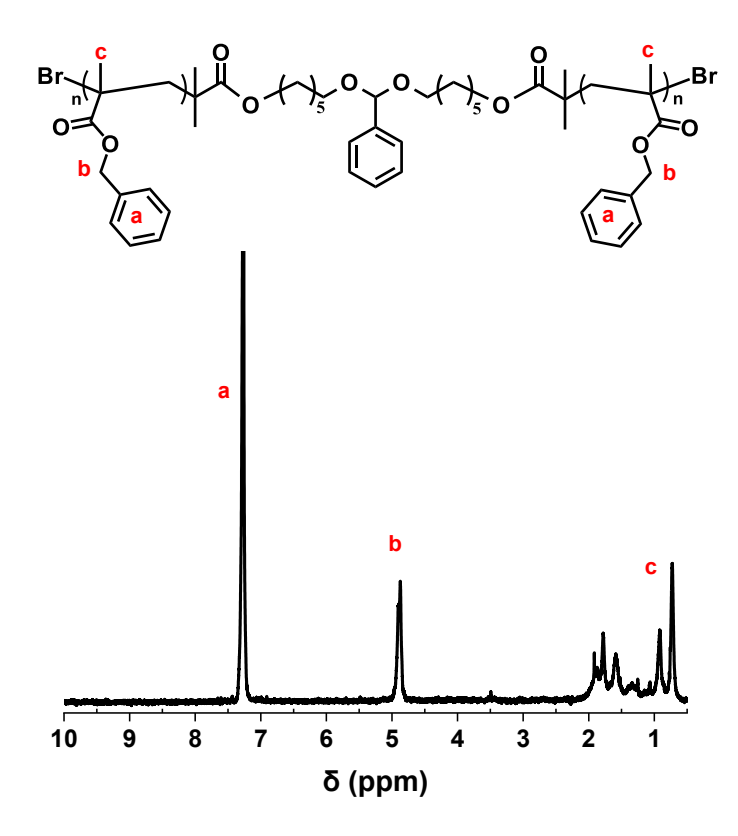


Figure C2. For ATRP-2, synthesis for ATRP initiated with BzAc-DBr (a), ¹H NMR spectrum in CDCl₃ (b), and overlaid GPC diagrams before and after treatment with HCl (acid) in DMF (c).

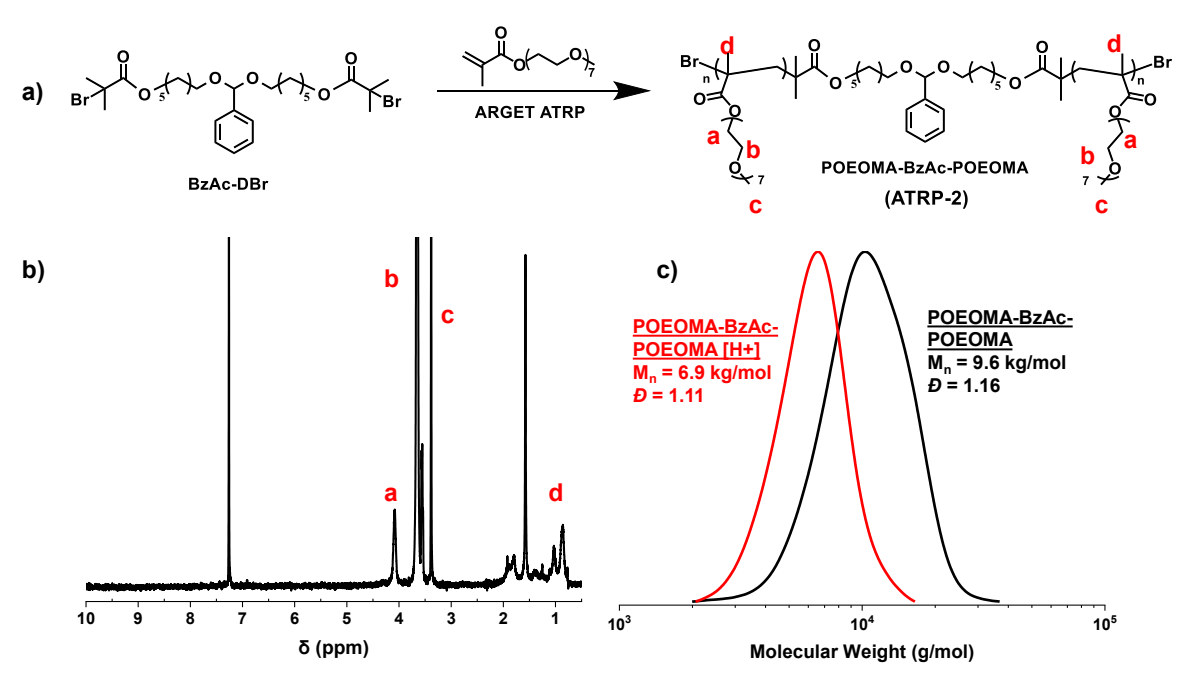


Figure C3. For ATRP-1, first-order kinetics over polymerization time (a) and molecular weight and its distribution over conversion (b) for ATRP of BM in the presence of BzAc-DBr. Conditions for ATRP: $[BM]_0/[BzAc-DBr]_0/[Cu(II)Br_2/TPMA]_0/[TPMA]_0/[Sn(EH)_2]_0 = 50/1/0.05/0.15/0.4$ in anisole at 40 °C, BM/anisole = 0.25 wt/wt.

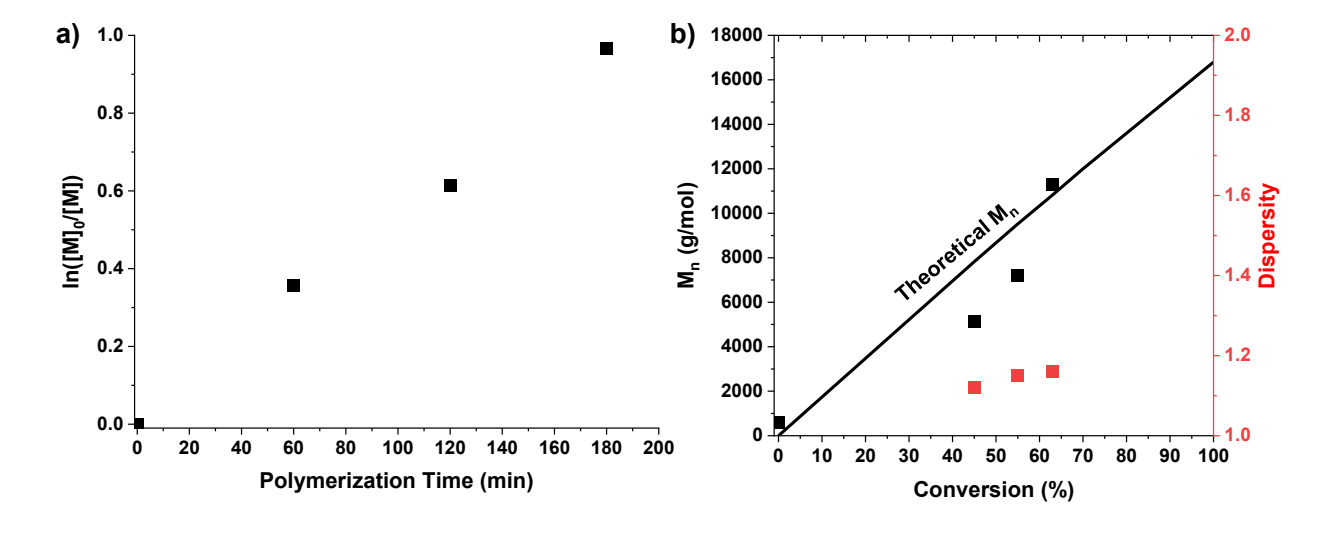


Figure C4. For ATRP-2, first-order kinetics over polymerization time (a) and molecular weight and its distribution over conversion (b) for ATRP of OEOMA in the presence of BzAc-DBr. Conditions for ATRP: $[OEOMA]_0/[BzAc-DBr]_0/[Cu(II)Br_2/TPMA]_0/[TPMA]_0/[Sn(EH)_2]_0 = 50/1/0.05/0.15/0.4$ in anisole at 40 °C, OEOMA/anisole = 0.25 wt/wt.

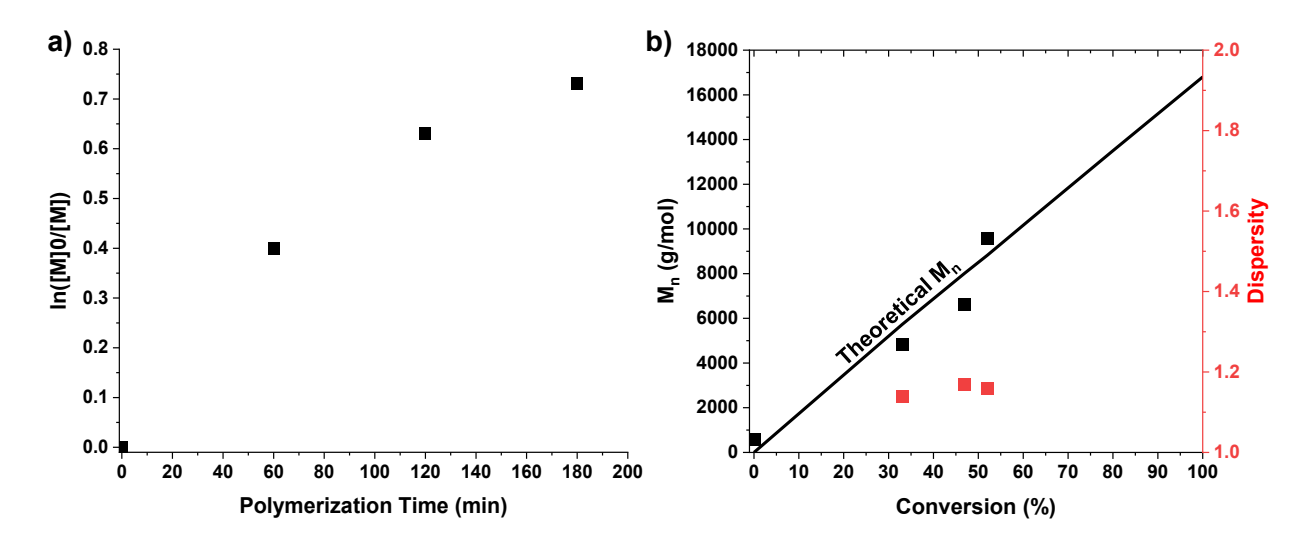


Figure C5. For ATRP-3, acid-catalyzed degradation of PBM-BzAc-PBM (a) and its overlaid GPC diagrams before and after treatment with HCl (acid) in DMF (b) for AGET ATRP of BM in the presence of BzAc-DBr. Conditions for ATRP: $[BM]_0/[BzAc-DBr]_0/[Cu(II)Br_2/TPMA]_0/[TPMA]_0/[Sn(EH)_2]_0 = 50/1/0.2/0.5/0.4$ in anisole at 40 °C, BM/anisole = 0.40 wt/wt.

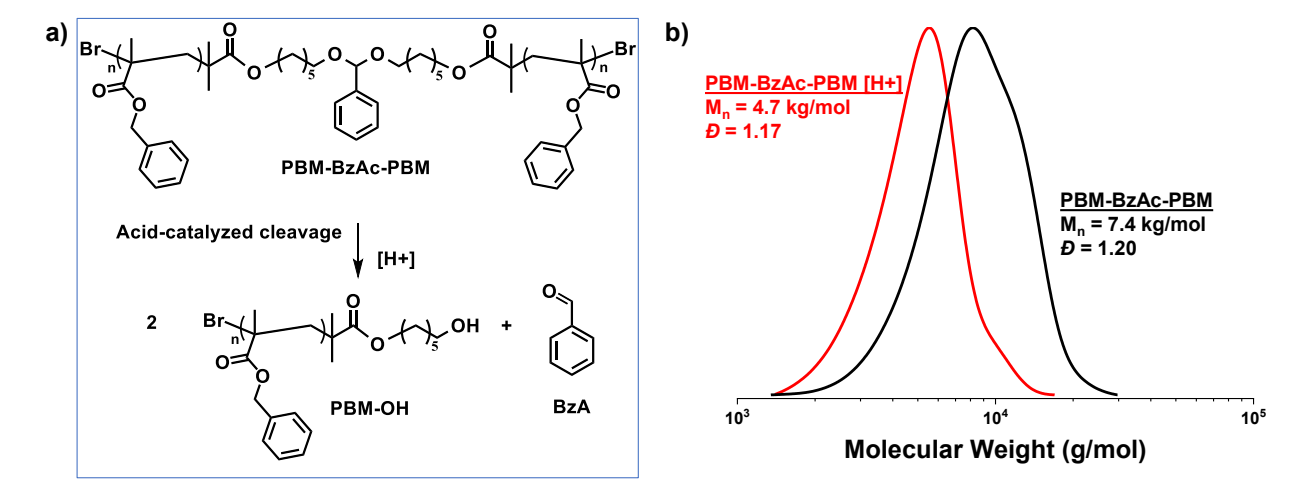


Figure C6. For ATRP-4, synthesis by ATRP of OEOMA in the presence of BzAc-DBr and acid-responsive degradation upon the cleavage of BzAc groups of PBM-BzAc-PBM (a) and its overlaid GPC diagrams before and after treatment with HCl (acid) in DMF (b). Conditions for ATRP: $[OEOMA]_0/[BzAc-DBr]_0/[Cu(II)Br_2/TPMA]_0/[TPMA]_0/[Sn(EH)_2]_0 = 50/1/0.2/0.5/0.4$ in anisole at 40 °C, OEOMA/anisole = 0.40 wt/wt.

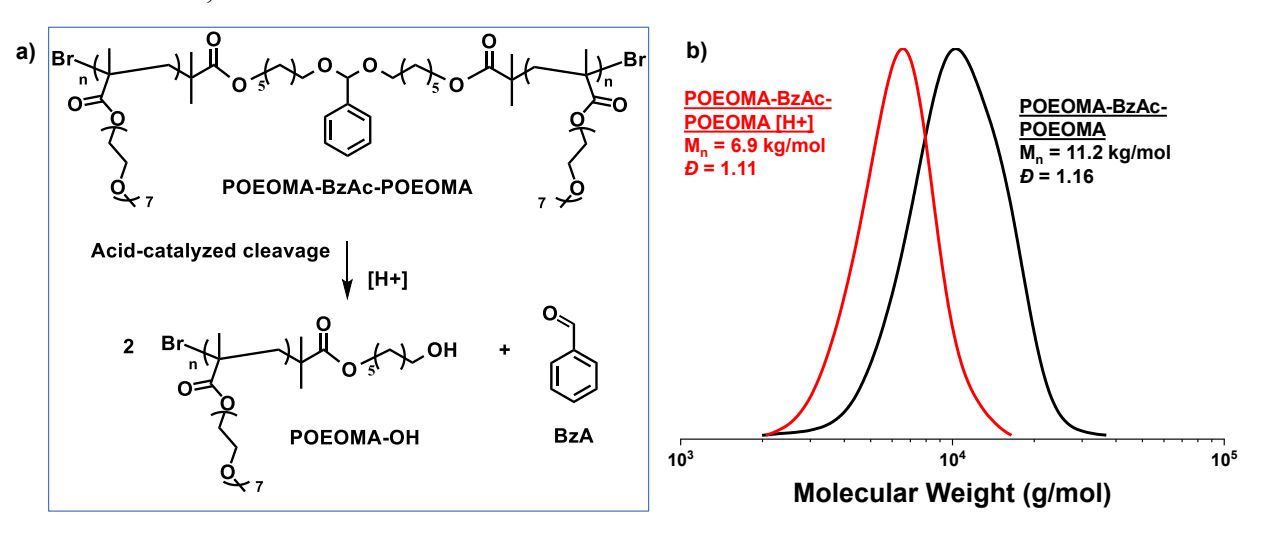


Figure C7. For ATRP-5, ¹H NMR spectrum of PBM-CyHK-PBM in CDCl₃.

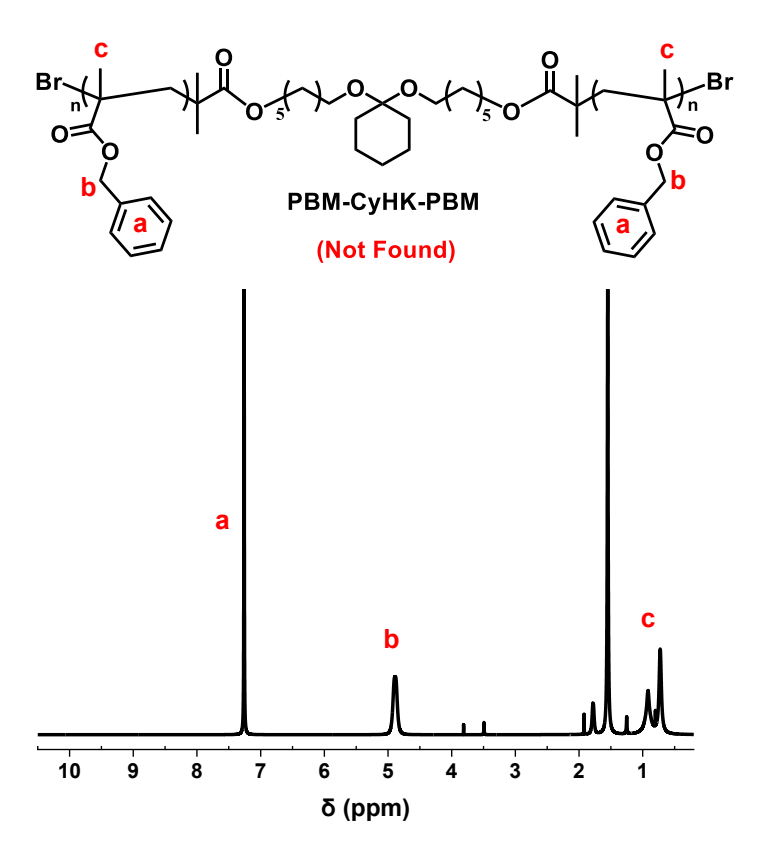


Figure C8. For ATRP-6, overlaid GPC diagrams before and after treatment with HCl (acid) in DMF.

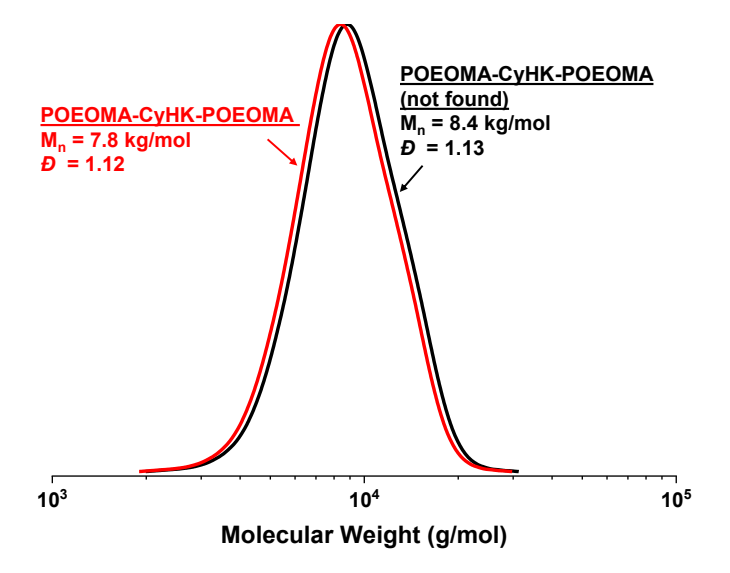


Figure C9. For ATRP 5, proposed pathway for premature degradation of CyHK linkage during ATRP and acid-catalyzed degradation of the synthesized PBM.

Figure C10. For ROP-2, 1 H NMR spectrum in DMSO-d₆ for PLA formed by ROP of LA initiated with CyHK-DOH. Conditions for ROP: $[LA]_0/[CyHK-DOH]_0/[Sn(EH)_2]_0 = 70/1/0.4$ in toluene at 120 °C, LA/toluene = 0.4/1 wt/wt. X denotes residual toluene.

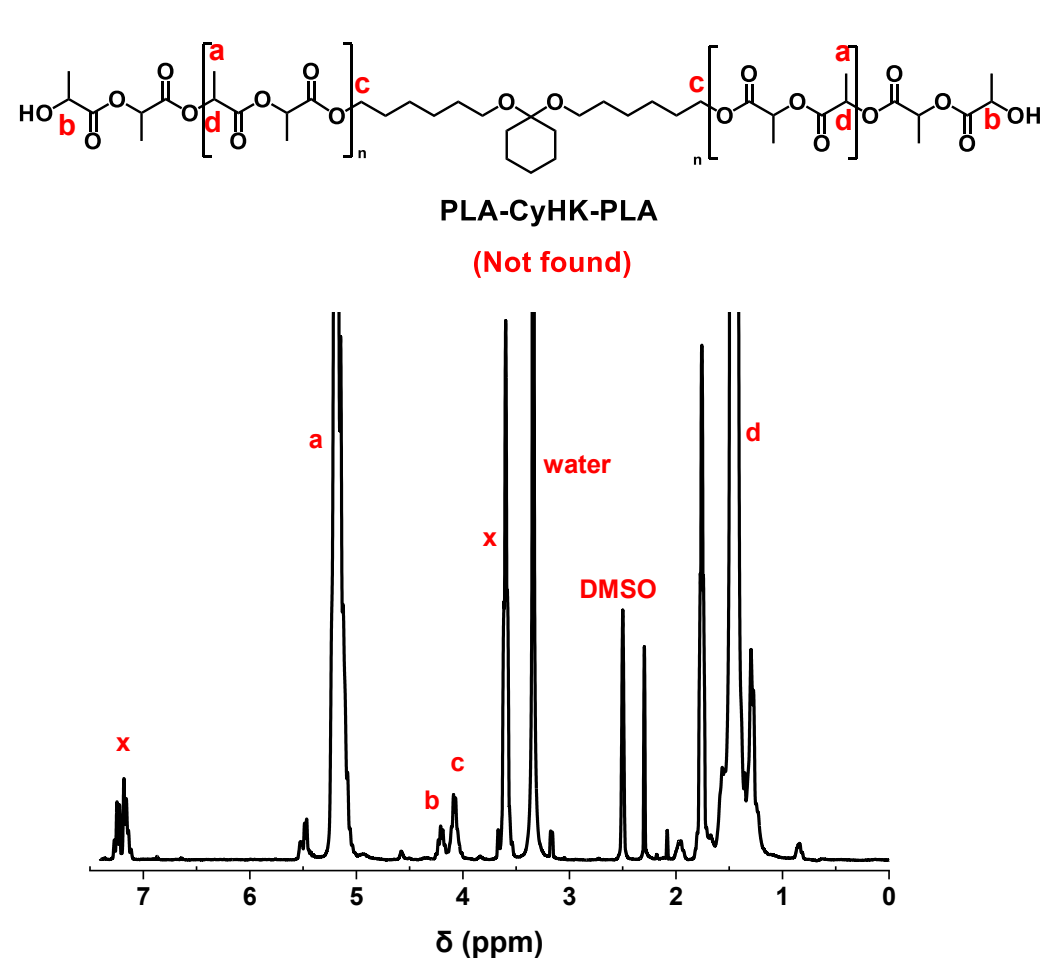


Figure C11. For ROP-2, proposed pathway for premature degradation of CyHK linkage during ROP and acid-catalyzed degradation of the synthesized PLA.

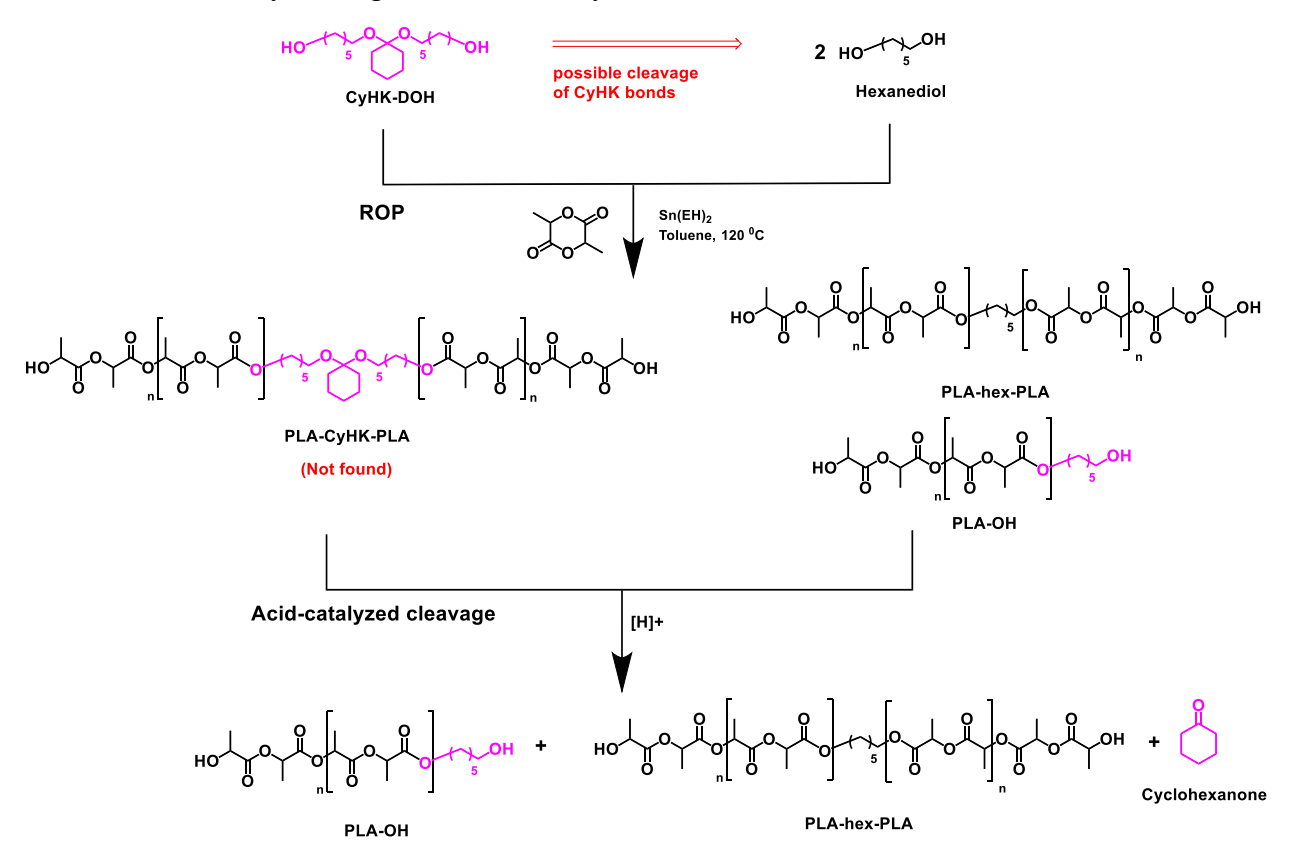


Table C1. Recipes for ATRP of BM or OEOMA initiated with BzAc-DBr or CyHK-DBr in anisole.

Recipe	Monomer	DBr	Monomer (mmol)	DBr (µmol)	Cu(II)[TPMA]Br (µmol)	TPMA (μmol)	Sn(EH) ₂ (μmol)
ATRP-1	BM	BzAc-DBr	11.6	23.2	5.81	17.4	46.5
ATRP-2	OEOMA	BzAc-DBr	7.3	140	3.67	11	29.3
ATRP-3	BM	BzAc-DBr	12.5	25	25	62.4	49.9
ATRP-4	OEOMA	BzAc-DBr	6.7	130	13.3	33.3	26.7
ATRP-5	BM	CyHK-DBr	11.9	23.9	5.96	17.8	47.6
ATRP-6	OEOMA	CyHK-DBr	9	18	4.5	13.5	36

Table C2. Recipes for ROP of LA initiated with BzAc-DOH or CyHK-DOH in toluene.

Recipe	Monomer	DOH	Monomer (mmol)	DOH (µmol)	Sn(EH) ₂ (µmol)
ROP-1	LA	BzAc-DOH	43.8	630	100
ROP-2	LA	CyHK-DOH	43.8	600	100

Publications

- Andrade-Gagnon, Brandon; Casillas-Popova, Sofia Nieves; Oh, Jung Kwon. Stability of Acetals/Ketals under Controlled Radical and Ring Opening Polymerization. *Macromolecular Rapid Communications*, 2025, e00399
- 2. **Andrade-Gagnon, Brandon**; Oh, Jung Kwon. Recent Advances in Synthesis and Shell-Sheddable Disassembly of Acid/Glutathione-Degradable Block Copolymer Nanoassemblies for Drug Delivery. *Polymer Chemistry*, 2024, 15, 3709-3735
- 3. Casillas-Popova, Sofia Nieves; Lokuge, Nishadi; **Andrade-Gagnon, Brandon**; Chowdhury, Farhan; Skinner, Cameron; Oh, Jung Kwon. pH-Responsive Degradable Electro-Spun Nanofibers Crosslinked via Boronic Ester Chemistry for Smart Wound Dressings. *Macromolecular Bioscience*, 2024, 24, 2400217.
- 4. **Andrade-Gagnon, Brandon**; Casillas-Popova, Sofia Nieves; Jazani, Arman Moini; Oh, Jung Kwon. Rational Design, Synthesis, and Acid-Responsive Disassembly of Shell-Sheddable Block Copolymer Labeled with Benzaldehyde Acetal Junction. *Macromolecular Rapid Communications*, 2023, 45, 2400097

Oral and Poster Presentations

- 1. **Brandon Andrade-Gagnon.** Dual Location Acid-Degradable Amphiphilic Block Copolymers for Drug Delivery. Macromolecular Science and Engineering Division (MSED) of Canadian Chemistry Conference & Exhibition (CSC), Winnipeg, Manitoba, Canada, June 7, 2024. (**Oral**)
- 2. **Brandon Andrade-Gagnon.** Substituent Effects on pH Sensitivity of Acid-Degradable Shell-Sheddable Nanoassemblies for Enhanced Drug Delivery. Polymeric Nanoparticles for Drug Delivery (PoND) Research Days, Victoria, BC, Canada, June 8-10, 2023. (**Oral**)
- 3. **Brandon Andrade-Gagnon.** Dual Location Acid-Degradable Amphiphilic Block Copolymers for Drug Delivery. Polymeric Nanoparticles for Drug Delivery (PoND) Research Days, Edmonton, Alberta, Canada, August 21-25, 2022. (**Poster**)